CORA Cork Open Research Archive
Cartlann Taighde Oscailte Chorcaí

Title	Development and characterisation of macro-disc and micro-band electrodes for electrochemical sensing applications
Authors	Madden, Julia
Publication date	2022
Original Citation	Madden, J. 2022. Development and characterisation of macro-disc and micro-band electrodes for electrochemical sensing applications. PhD Thesis, University College Cork.
Type of publication	Doctoral thesis
Rights	© 2022, Julia Madden. - https://creativecommons.org/licenses/by-nc-nd/4.0/
Download date	2024-03-29 13:11:47
Item downloaded from	https://hdl.handle.net/10468/14471

UCC
University College Cork, Ireland
Coláiste na hOllscoile Corcaigh

Ollscoil na hÉireann, Corcaigh

National University of Ireland, Cork

Development and characterisation of macro-disc and micro-band electrodes for electrochemical sensing applications

Thesis presented by

Julia Madden

[0000-0002-4988-2062]

for the degree of

Doctor of Philosophy

University College Cork

Dept. of Science and Engineering

&

Tyndall National Institute

Head of School/Department: Fathima Gunning

Supervisors: Dr. Paul Galvin, Professor Michael Thompson and Dr. Alan O' Riordan

2022

Declaration

This is to certify that the work I am submitting is my own and has not been submitted for another degree, either at University College Cork or elsewhere. All external references and sources are clearly acknowledged and identified within the contents. I have read and understood the regulations of University College Cork concerning plagiarism and intellectual property.

_____

Julia Madden 2022

Abstract

The aim of this PhD thesis was to investigate potential next generation sensor platforms for electrochemical biosensor developments, specifically towards health monitoring applications. With increasing interest in the integration of miniaturised electrodes with minimally invasive and wearable devices, this thesis sought to explore electrodes fabricated using three different technologies for the construction of electrochemical biosensors: Silicon microfabrication, Laser scribing, and dispense printing.

The first experimental section aimed to investigate the use of a single ultramicroband electrode fabricated on silicon for mediator-free glucose monitoring in bio-fluid environments. Six ultramicroband electrodes, a counter electrode and reference electrode were fabricated using standard microfabrication methods i.e. lithography and etching techniques. Glucose oxidase was selected as a model enzyme to attach onto a platinum-modified gold microband electrode by electropolymerisation with an o-phenylenediamine/ß-cyclodextrin layer. The resulting microband biosensor demonstrated on-chip glucose detection in buffer based media. When applied to foetal bovine serum the sensor displayed a reduced sensitivity. The second experimental section explores the use of laser-scribed graphitic carbon for flexible sensing applications. A facile fabrication method was assessed involving electrodeposition of platinum followed by two casting steps to functionalise electrodes. This study examined the chronoamperometric response of the enzymatic lactate sensor whilst the flexible polyimide substrates were fixed at a curvature (K) of 0.14 mm^{-1}. No noticeable change in signal response was observed in comparison to calibrations obtained with a flat substrate (K=0 mm^{-1}), suggesting potential opportunities for sensor attachment or integration with oral-care products such as mouth swabs and mouth guards. Both laser scribed graphitic carbon and Ag/AgCl modified-laser scribed graphitic carbon were examined as reference electrodes for chronoamperometric lactate measurements. This device was applied for measuring lactate concentrations in artificial saliva and diluted sterile human serum. Finally, this study investigates the potential for a low cost additive printing tool to enable the fabrication of electrochemical sensor devices. To do this, electrodes were designed and printed onto polyimide substrates. Reproducibility between electrode dimensions was assessed using 3D microscopy. Standard electrochemical characterisation techniques were employed to study the reproducibility between electrode electrochemical response. Functionality was

also assessed whilst electrodes were fixed were fixed at a curvature (K) of 0.14 mm^{-1}. Finally, a simple casting approach was applied to the dispense printed working electrode to construct a lactate biosensor for a proof of concept electrochemical sensor demonstration.

Acknowledgements

This research was supported in part by grants from Science Foundation Ireland (Grant numbers 18-ECSEL/3499 and 12/RC/2289-P2), and from EC ECSEL Programme (Grant number ECSEL 2017-2-783132).

Firstly, I would like to express my gratitude to my supervisor Dr. Paul Galvin for giving me the opportunity to pursue a PhD in Tyndall with the Life science Interface group. I will be forever grateful for the experience I acquired during my time in Tyndall. Thank you for your guidance and support over the years. I would also like to thank my co-supervisors Dr. Alan O' Riordan and Professor Michael Thompson for their help, advice and encouragement at various phases of the adventure. Alan thank you for welcoming me in to the nanotechnology group for a period of the PhD, the support provided by the group was excellent. Mike, I am grateful for my trip to the University of Toronto and it was a pleasure to have you in Tyndall for a period of time during the PhD.

In addition to the support from my supervisors, I would like to express my gratitude to Dr. Sofia Teixeira who has been an incredible mentor to me during the latter phase of the PhD. Thank you for taking me under your wing, the shared learnings in the lab were both helpful and enjoyable. I would also like to thank Dr. Colm Barrett for the electrochemistry training and coaching. I would also like to extend my gratitude to Dr. Daniela Iacopino and Eoghan Vaughan for their collaboration and support during the final year. It was a pleasure to work with both of you.

A big thank you to all of the Life science interface group old and new. Firstly to the LSI lab manager Eileen Hurley, from day one you have been a treasure, always making the effort to keep the lab safe, help out with risk assessments, checking in as you passed by and always available to answer a question. Conor, thank you for letting me join in on your group meetings and for introducing me to the world of Microneedles. Andrea, what can I say, a long journey since day one for us both, thank you for your energy, positivity, support, friendship and most of all for introducing me to porcini linguine. Lisa Helen, the time we had you in LSI was amazing, I am grateful for our continued friendship since you left, thank you for introducing me to the world of hiking and for our weekend of mountaineering skills in Glengariff, it has been a great way to disconnect. Suzanne, thank

you for your sense of humour, all of the laughs in the office and of course the best dinner party. Ryan, you brought joy to the office and labs every day, it was great to have you around during the post-covid phase especially. Thank you to Fjodor for passing on your PCB printing knowledge. Thank you to Yuan for your 3-D printing expertise. I would also like to thank Eamonn and Frank for their collaboration and teamwork during the Position II project.

To the Tyndall gang, Caoimhe, thank you for the sons of anarchy nights and coming to see the backstreet boys and the spice girls with me. Fiona, thank you for also joining in on the spice girls fun, the walks, the gym .sessions after long days in the lab and most especially our pull-ups phase. Ian, thank you for your sense of humour, your help with all of my electrochemistry questions, joining me for lunch time runs and for completing my first half marathon with me. Also I am super grateful to your sister Sharon for all of the lockdown yoga and helping me to finally master the headstand. Niamh, I'm delighted to have gotten to know you during your time in Tyndall, your drive was always inspiring, thank you for the lab singing, nights out, chats and runs. A big thank you also to Louise, you were always there for the chats and support during your time in Tyndall. I would also like to thank Vulsat for our trips to the river lee and extended conversations on health and well-being. Thank you to Gokhan for the lunch time chats and morning coffees especially during the post-covid phase.

I would like to express my gratitude to some of the extended Tyndall employees Donal O' Sullivan, Dan O' Connell, Krimo Khalfi, Dr. Pierre Lovera, Finbarr Waldron, all of the IT staff members, Dr. Lynette Keeney and Dr. Eric Moore for their support throughout my time in Tyndall.

For those outside of Tyndall, I would like to thank Marian and Naomi for our yearly visit to one of three counties. Lisa for rare, but great catch ups over a cuppa. Laura thank you for the voice notes of encouragement and mini adventures. Valerie, thank you for the support, the shared interest in the gym and general well-being, hikes, the laughs, and the philosophical conversations. Magz, thank you for the belly laughs. Forever grateful for your outlook on life and general sense of humour.

I would also like to thank Baptiste for your love, support and patience especially over the last year. Thank you for all of the little things, sourdough pancakes, syriniki, cold morning sea dips, and most of all for your impeccable cooking skills.

Finally, a big thank you to the Madden family. To my brothers Liam and Patrick, thank you for always helping me to switch off and enjoy the downtime when I come home for the weekends. Thank you to my little niece Sinead for bringing new light to my eyes. Lastly, I would like to thank my parents, Josephine and Gerard for their never-ending encouragement and love.

“If you wish to make an apple pie from scratch, you must first invent the universe.”
Carl Sagan, Cosmos

Chapter 1 Introduction

Enzymatic biosensors are an important diagnostic tool for diabetes management. Perhaps, the most famous enzymatic biosensor is the glucose finger prick sensor used for self-glucose monitoring. Advances in biosensor technology have since seen the glucose biosensors move from a single reading in a blood sample to devices that can monitor glucose concentrations continuously. The continuous glucose monitoring systems market was valued at approximately $8 billion in 2021 and is expected to grow to $15 billion by 2030.[1] Although this is a well-established market, research continues to further advance and innovate glucose biosensors, especially since the future of glucose monitors are not limited to diabetic patients. Glucose monitoring is also becoming popular with athletes.[2,3]Another enzymatic biosensor desirable for diagnostics in sport science is the lactate sensor. L-lactate is a key biomarker used in clinical diagnostics to assess for health conditions and diseases such as liver disease, organ failure and sepsis.[4–6] Lactate concentrations in blood can also be used to evaluate an athlete's lactate threshold which can be used as an endurance indicator.[7–9]

When developing enzymatic sensors, fast and accurate detection of biomarkers is crucial, whether for healthcare or sport science applications. Electrochemical biosensors are an attractive alternative to invasive clinical diagnostic methods requiring large equipment, trained professionals and lengthy procedures. Electrodes can be fabricated on both rigid and flexible materials such as silicon, ceramics and polymers, and can then be modified to enable sensing of specific targets. The range of substrates available for electrochemical sensors allows them to be adapted towards numerous applications, including point-of-care (POC) devices.

This thesis aims to investigate three separate sensor platforms, firstly, an on-chip ultra microband electrode is studied and modified for electrochemical glucose sensing and tested using foetal bovine serum. Silicon fabrication methods produce robust devices with the possibility of multiple small footprint sensors on-chip. Although silicon fabrication is an expensive fabrication method its compatibility with mass production is desirable. Secondly, larger macro-disc electrodes fabricated on polyimide substrates using direct laser scribing methods are assessed for their potential as flexible electrochemical lactate sensors. These offer a cost effective alternative to silicon devices. Furthermore, the lightweight and flexible nature of thin film polymer substrates such as polyimide makes them attractive for wearable sensing applications. The ability to fabricate electrodes on bendable substrates using conductive inks has become a topic of interest in recent years.

The last chapter of this thesis explores the possibility for using an emerging low cost PCB additive printing tool, to fabricate macro disc electrodes for electrochemical sensing applications.

In chapter 1, a framework for the thesis is provided. Firstly electrochemistry fundamentals are discussed. This is followed by an overview of electrochemical glucose and lactate biosensors. Specific examples of enzymatic glucose biosensors and enzymatic lactate biosensors based on platinum electrodeposited materials, o-phenylenediamine and chitosan are detailed. Immobilisation techniques to attach glucose oxidase (GOx) or lactate oxidase (LOx) to electrodes are also described. Finally, silicon fabrication methods, laser scribing, and additive printing technologies are introduced, including recent examples of electrochemical sensors constructed from each.

1.1 Fundamental Concepts of Electrochemistry

Electrochemistry is the branch of chemistry that is concerned with processes that occur at an electrode/electrolyte interface, primarily the transfer of electrons.[10] It has proven to be an important research field for the development of fuel cells, batteries, and electrochemical biosensors.[11] Electrochemistry methods have enabled the advancement of electroplating technologies for application to electronic devices, commercial appliances and car components. In addition, electrochemical techniques can help to determine the corrosion resistance properties of materials.[12] This thesis is concerned with the application of electrochemistry for glucose and lactate sensing applications. Prior to introducing the electrochemical biosensor, the first section of the introduction will focus on electrochemistry fundamentals.

1.1.1 Components of an Electrochemical Cell

An electrochemical cell can contain a two, three or four-electrode configuration. Most commonly, a three-electrode configuration is employed containing a working electrode (WE), counter electrode (CE) and reference electrode (RE). These electrodes are interfaced with a solution of interest commonly referred to as an electrolyte solution. Each of the electrodes are connected to a potentiostat, a device that facilitates the control of the applied potential and the measurement of the current generated by electrochemical reactions occurring at the electrode/electrolyte interface. An electrochemical cell can be placed in a Faraday cage to minimise electromagnetic noise interferences. The

potentiostat is connected to a computer to acquire data. Figure 1.1 shows a schematic representation of the experimental set-up of an electrochemical cell used to conduct electrochemical measurements.

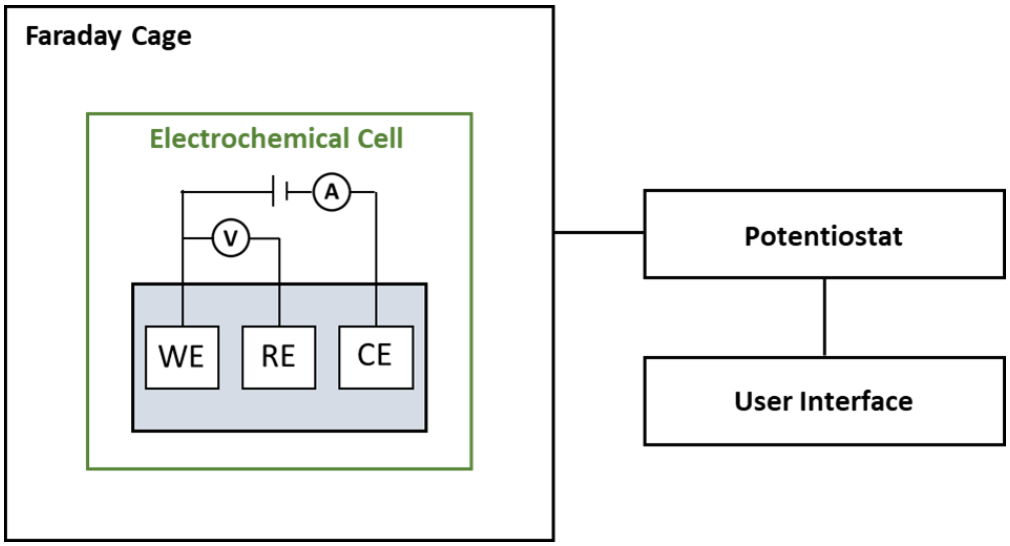

Figure 1.1: *Schematic diagram of a standard three-electrode electrochemical cell within a Faraday cage, connected to a potentiostat and to a computer. WE, RE and CE are the working, the reference and the counter electrodes, respectively.*

1.1.1.1 *Working Electrode*

The WE is the electrode in the electrochemical cell where the measured reaction or reactions take place. WE materials must be conductive, hence, the most common examples include the noble metals gold and platinum and non-metals such as carbon. The surface of the WE should be clean and have a known reproducible surface area. Depending on the final application, different WE designs and geometries can be selected.

1.1.1.2 *Counter Electrode*

The CE, also referred to as an auxiliary electrode operates to supply or sink electrons for the WE. The CE is typically made from conductive inert materials such as platinum, gold and carbon and is normally larger than the WE. Current flow between the CE and WE prevents current flowing through the reference electrode, which, would polarize the RE leading to a shift in potential. The potentiostat adjusts the voltage to maintain a potential difference between the WE and the RE, and the current travelling between the WE and the CE is measured.

1.1.1.3 *Reference Electrode*

The RE enables a steady and accurate measurement of the WE potential. A RE should be a non-polarisable electrode, meaning, the potential does not change despite the application of current.[13] The reaction governing the RE must also be reversible so that the potential can be calculated from the Nernst equation.[14] The standard hydrogen electrode (SHE) also known as the normal hydrogen electrode (NHE) is the conventional reference electrode against which standard electrode potentials are measured and has a standard potential, E^0, of 0 V. The standard cell potential, E^0 is the potential of a cell under standard conditions. Under standard conditions the concentration of each species in solution is 1 M and the partial pressure of each species in gaseous form is 1 atm. and the temperature is 25 °C. Other REs have also been developed that do not require the need for constant bubbling of hydrogen such as the saturated calomel electrode and the silver/silver chloride electrode.[15] The calomel electrode contains mercury which can be unsafe if broken. The Ag/AgCl RE contains a silver wire, coated with silver chloride that is contained within a saturated potassium chloride solution. Ag/AgCl is an inexpensive electrode and does not contain toxic components. The controlling redox reaction of the Ag/AgCl, KCL (saturated) RE has a standard potential of 0.197 V vs SHE at 25 °C.

$$AgCl + e^- \rightleftharpoons Ag + Cl^-, E^o_{Ag|AgCl} = 0.197\ \text{V vs. SHE} \quad (1)$$

With $E^0_{Ag|AgCl}$ being the standard potential of the electrode. The potential of the electrode under non-standard condition can be calculated using the Nernst eqtions:

$$E_{Ag|AgCl} = E^0_{Ag|AgCl} + \frac{RT}{nF}\ln([Cl^-]) \quad (2)$$

One shortcoming of conventional reference electrodes are that they require a specific volume of fluid (a few millilitres) during measurements. With the advancement of electrochemical sensors for portable, point of care, wearable and in-vivo applications, analysis of smaller volumes is desirable. As a result, miniaturised REs have been fabricated on-chip or on-device as appropriate.[16,17] Ag/AgCl electrodes have been produced on-chip; however, to continue to function they require repeated depositions of the silver chloride material. Another approach has been the use of a pseudo-reference or quasi reference electrode such as platinum and silver or laser scribed graphene. These electrodes are not an ideal non-polarisable electrode and are subject to potential drift, hence, they require calibration against a conventional RE, whereby the potential of the

pseudo-electrode versus that of a reference electrode is measured. A redox couple can also be used as a reference to measure and correct for a shift in potential. Quasi-reference electrodes can be used as long as they are calibrated within the solution or matrix of interest i.e. the solution that the electrochemical measurements will be carried out in.

1.1.2 Electron Transfer

Examples of electrochemical reactions include the electrodeposition of materials onto electrodes,[18] the formation of oxide layers,[19] the removal of materials from electrodes,[20] generation of charged species,[21] and the conversion of species from a liquid to a gas.[22] During an electrochemical reaction either the oxidation (loss of electrons) or reduction (gain of electrons) occurs. If one segment of an electron transfer reaction is oxidised then the other part is reduced. A simplified electrochemical reaction can be described by the following equation:

$$O + ne^- \rightleftharpoons R \quad (3)$$

Where O is the oxidised form of a redox species in solution, n is the number of electrons (e^-) transferred and R is the reduced form of the redox species. The electrode at which the reduction reaction occurs, is named the cathode. When an oxidation reaction occurs at the electrode, it is called the anode. For the transfer of electrons to occur, the energy level of the electrode needs to match the energy level of the species within the electrolyte solution. When a negative potential is applied to the cell, the electrode raises the energy of the electron. If this is sufficient to reach the lowest unoccupied molecular orbital (LUMO) of the electrolyte, then the electron will be transferred to the electrolyte. When a species gains an electron this reaction is referred to as a reduction reaction. The electrode can also be driven to a positive potential, reducing the energy of the electrode. If the energy of the electrode is reduced enough to match the highest occupied molecular orbital (HOMO) of the solution species, then an electron can be transferred from the species in solution to the electrode surface. The loss of electrons from an electroactive species in solution is referred to as an oxidation reaction. Faradaic and Non-faradaic processes

During electrochemical measurements, the charge transfer occurring at the electrode/solution interface generates a Faradaic current. These reactions obey Faraday's law:[23]

$$Q = nNF \quad (4)$$

Where Q is the electric charge (Coulombs, C), n is the number of electrons involved, N is the number of moles (mol) and F is Faraday's constant (96485 C/mol). Hence, these electrochemical reactions are referred to as faradaic processes. However, not all measurements obtained using a potentiostat arise from faradaic processes. Adsorption or desorption at the electrode surface can result in current contributions attributed to changes at the electrode/electrolyte interface. These are referred to as non-faradaic processes since they are not governed by Faraday's law.

If we consider an electrochemical cell where non-faradaic currents exist, once a potential is applied, an electric field is created resulting in a build-up of charge at the electrode-solution interface. This behaviour obeys the following equation:

$$\frac{Q}{E} = C \qquad (5)$$

Where Q is charge (Coulombs, C), E is the potential applied (Volts, V) and C is the Capacitance (Farads, F). This accumulation of charge results in the formation of an interfacial layer known as an electrical double layer consisting of one layer of charge from the electrode and an opposing layer of charge from the solution. A number of models for the double layer have been described in the literature, the Helmholtz, the Gouy and Chapman and the Stern. [24–26] The most common model is the Stern model which combines Helmholtz and Gouy-Chapman as displayed in Figure 1.2.[10] The first region of the double layer known as the Inner Helmholtz plane (IHP), which is made up of specifically adsorbed species and solvent molecules. The second region is known as the outer Helmholtz plane (OHP), and contains non-specifically adsorbed solvated ions that are attracted to the electrode via coulombic forces. Outside the OHP is a layer of non-specifically adsorbed species making up the outer diffuse layer, which extends into the bulk solution. This double layer results in the formation of charging currents, also known as capacitive currents, which, during an electrochemical measurement, can form part of the background current and is not related to the electrochemical reaction taking place. Capacitive currents can be negligible, however, in instances where fast scan rates are required and when trying to measure low concentrations (mM-nM), they can have a significant impact on measurements and should be accounted for.

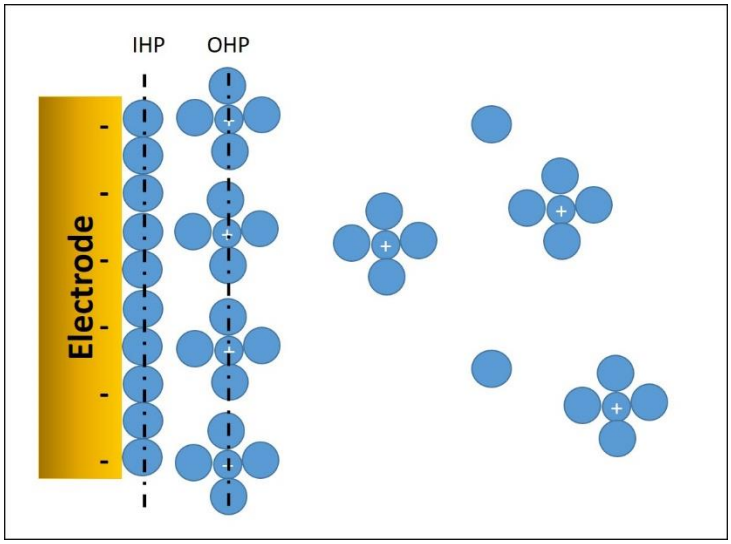

Figure 1.2: *Simplified model of the double-layer region with specifically adsorbed anions and solvent molecules in the inner layer, and solvated cations in the diffuse layer. IHP and OHP are the inner and outer Helmholtz planes, respectively.*

1.1.3 What affects a faradaic current response?

An electrochemical response is predominantly influenced by the kinetics of an electrochemical reaction and the mass transport between the bulk solution and the interfacial region as shown in Figure 1.3, which also depicts other smaller influencing processes such as adsorption and desorption. The slowest process will determine the rate of electrochemical reactions. When mass transport effects are insignificant, the Butler-Volmer equation can be used to determine currents arising from an overpotential.[27] An overpotential is the difference between the standard potential of the reaction and the potential required to initiate a reaction.

$$i = i_o[e^{\frac{-\alpha\eta F}{RT}} - e^{\frac{(1-\alpha)\eta f}{RT}}] \quad (6)$$

where:

- $\mathbf{i_o}$ is the exchange current (A)
- α is the transfer coefficient, estimated to be 0.5, a dimensionless value between 0 and 1.
- η is the overpotential (V)

- f = F/RT, where F is Faraday's constant (C), R is the gas constant (J mol^{-1} K^{-1}) and T is temperature (K).

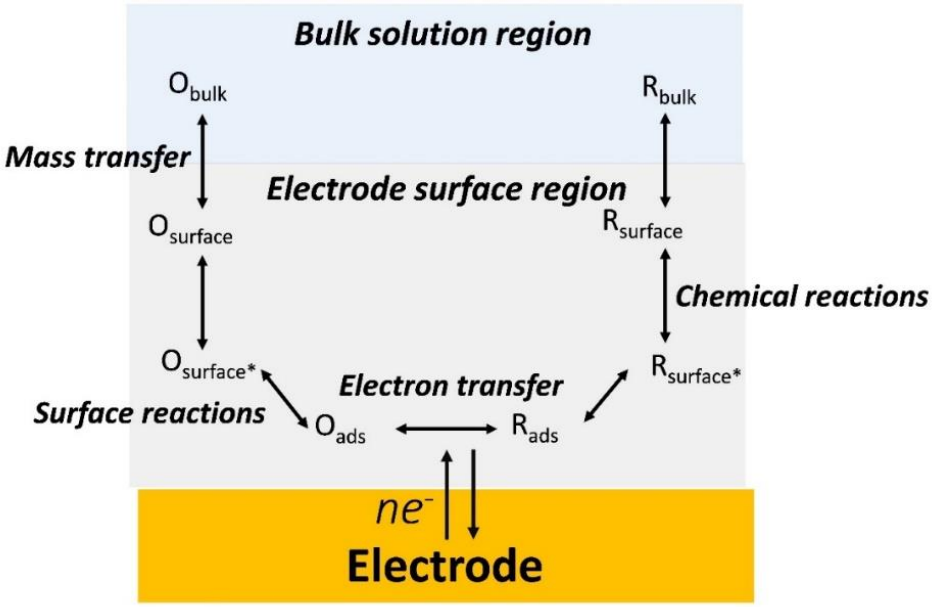

Figure 1.3: *The electron kinetics and mass transfer pathways that can be involved in a redox reaction at the electrode surface.*

1.1.3.1 *Mass Transfer*

Following the oxidation or reduction of a species, additional species need to travel from the bulk solution to the interfacial region. Similarly, after an electrochemical reaction has occurred, a species needs to move away from the electrode. The rate of mass transfer can be slower than the rate of electron transfer; hence, mass transfer influences faradaic currents. Mass transport of a species from the bulk solution can occur via convection, migration and diffusion. Each transfer type described below:

Migration

Migration is the movement of charged species when influenced by an electric field. During electrochemistry experiments, the supporting electrolyte compresses the potential potential drop at the electrode-solution interface to within a very short distance of the electrode surface. Thus the potential gradient throughout the remainder of the solution is approximately zero and hence mass transport due to migration can be considered negligible.

Convection

Convection movement occurs when forces in the bulk solution such as temperature changes and mechanical stirring result in the movement of species in the bulk solution.

Diffusion

Diffusion is the spontaneous movement of molecules as a result of a concentration gradient. During electrochemical reactions, after a species has been consumed at the electrode surface, redox molecules then move from the bulk solution (region of high concentration) to the electrode surface (region of low concentration).

The flux of species can be calculated by the Nernst-Planck equation:

$$J_i(x) = -D_i \frac{\delta C_i(x)}{\delta x} - \frac{z_i F}{RT} D_i C_i \frac{\delta \phi(x)}{\delta x} + C_i v(x) \qquad (7)$$

where:

- $J_i(x)$ is the total flux of species i (mol s-1 cm-2) at a distance x from the surface
- D_i is the diffusion coefficient (cm2 s-1)
- $\frac{\delta C_i(x)}{\delta x}$ is the concentration gradient at distance x
- z_i is the charge
- Ci is the concentration (mol cm-3) of species i
- $v(x)$ is velocity of a unit volume of solution moving in a one dimensional direction
- $(x)\ \delta$ is the potential gradient.

Each portion of the equation accounts for one of the mass transfer modes mentioned: $-D_i \frac{\boldsymbol{\delta C_i(x)}}{\boldsymbol{\delta x}}$ relates to diffusion, $\frac{z_i F}{RT} D_i C_i \frac{\delta \phi(x)}{\delta x}$ relates to migration and $C_i v(x)$ relates to convection.

Excess inert electrolyte can reduce migration effects. Removing mass transport effects can be appropriate for experimentation. Natural convection can be eliminated by fixing the temperature of a room/experimental set-up. Conducting measurements in static

solutions helps to avoid mechanical convection. Without migration and convection mass transport is limited by diffusion.

1.1.4 Electrochemical Techniques to Study Reactions

1.1.4.1 *Voltammetry*

Voltammetric techniques are commonly used to study electrochemical reactions. Voltammetry involves applying a potential and monitoring the corresponding current over time. During a cyclic voltammetry, the potential is swept at a specific scan speed to a fixed potential and is then swept back to the original potential at the same scan speed. Figure 1.4 A shows a potential profile and Figure 1.4 B displays a CV in ferrocene monocarboxylic acid at 50 mV/s at a macro-band electrode. Another technique that can be applied is linear sweep voltammetry, where the potential is not reversed after reaching the maximum E_{max}.

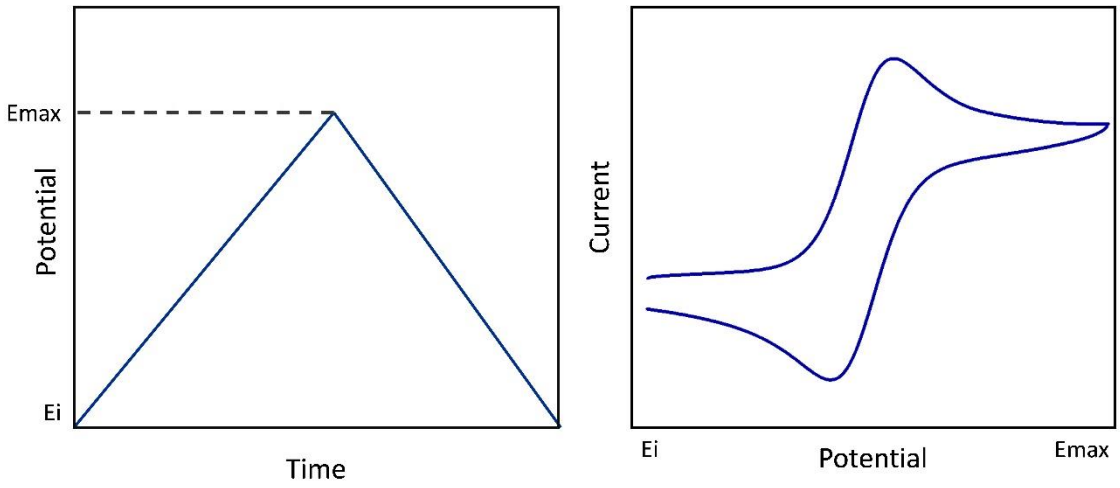

Figure 1.4: *(A) Schematic of a potential-time wave form for a CV where a potential is swept from an initial potential (Ei) to a maximum potential (Emax) (B) the current response observed during cyclic voltammetry for a reversible redox couple.*

Cyclic voltammetry (CV) is regularly used to assess oxidation and reduction processes of a molecular species. It can be applied to determine if a reaction is reversible based on the ratio of the anodic and cathodic peak currents. If a ratio of 1 exists, the reaction is reversible. Peak separation values (ΔEp) can also be useful towards understanding the reversibility of the reaction using the Nernst Equations. For a one electron transfer process, a peak separation of 0.059 V at 25°C ($\frac{2.302RT}{F}$) is indicative of a fully reversible reaction. The peak current i_p can also be used to determine the concentration of a species.

Since i_p can be related to the concentration of the molecular species present according to the Randles-Sevcik equation:[28]

$$i_p = 0.446nFAC\left(\frac{nFvD_o}{RT}\right)^{1/2} \quad (8)$$

Where v is scan rate, C is the concentration of the solution and A is the surface area this equation can be used for reversible redox reactions that are limited by diffusional mass transport.

1.1.4.2 *EIS*

Electrochemical impedance spectroscopy (EIS) can be used to measure the impedance of an electrochemical cell. Resistive and capacitive charges in the system can be measured from the Nyquist plot, by fitting the data to a Randles equivalent circuit. Ohms law describes the resistance R in an electrical circuit

$$R = E/I \quad (9)$$

where E is the circuit potential and I is the current. This relationship applies to ideal resistors that are (1) circuits that follow ohms law for all currents and voltages, (2) where the resistance is independent of frequency and (3) the alternating current and voltage signals through a resistor are in phase with each other. Since an electrochemical system does not have these characteristics, impedance is used to determine a circuit's resistance to current flow. Impedimetric measurements involve applying a small sinusoidal excitation signal to the WE and measuring the response of the system. For the purpose of this thesis, EIS was used to assess changes to the electrode surface following surface modifications.

1.1.4.3 *Chronoamperometry*

Chronoamperometry involves applying a fixed potential to the WE and measuring the corresponding current over time. When the potential of the WE is adjusted from a value where no faradaic processes occur, to a value where a redox reaction takes place, in an unstirred or static solution, the net concentration of electroactive species at the electrode surface will decrease close to zero. Electrochemical species are either oxidised or reduced causing a flow of current. The reaction results in a concentration gradient initiating the diffusion of electrochemical species from the bulk solution to the electrode surface. A flow of faradaic current is maintained as species continue to reach the electrode surface.

The Cottrell equation can be used to calculate the current associated with a diffusion-controlled process over time:

$$i(t) = \frac{nFAD^{\frac{1}{2}}C^*}{\pi^{\frac{1}{2}}t^{\frac{1}{2}}} \quad (10)$$

where:

- t (s) is the time
- A (cm^2) is the area of the electrode
- C* is the bulk concentration of the solution.

As a chronoamperometric measurement continues, the depleted species near the electrode surface diffuse out from the electrode forming a diffusion layer. This diffusion layer expands slowing down the arrival of electrochemical species to the electrode surface. Hence, fewer oxidation or reduction reactions take place resulting in decreased currents over time. At a planar electrode the current is expected to eventually reach zero over time; however, practically this is not the case, as after a period of time (30-100s) natural convection effects are observed. At spherical electrodes, radial diffusion contributions occur resulting in steady state currents. The time taken to reach steady currents is a function of the electrode dimension.[29] As electrode size decreases radial diffusion dominates. [30]

1.1.5 Electroanalysis at various electrode sizes

Electrodes used in electrochemical analysis can be fabricated as macro, micro, ultra-micro and nano electrodes. In the present work, both macro and ultra-microelectrodes were used for the construction of electrochemical biosensors. A macro-electrode has dimensions in the millimetre range, a microelectrode has critical dimensions in the micrometre range and nano-electrodes refer to electrodes with critical dimensions ≤ 100 nm.[31] Macro electrodes are advantageous when developing biosensors for the first time since they are easy to handle, and provide a larger surface area for material and biomolecule attachment. In addition to this, macro electrode fabrication is cost effective and timely in comparison to microelectrode fabrication methods. However, at macro electrodes, diffusion of species in solution to the electrode is limited by mass transport

unless low scan speeds such as 10 mV/s are used; this scan speed is not always practical for experimentation. Figure 1.5 A displays a schematic representation of the diffusion behaviour at a planar macro electrode, a typical CV from a macro electrode is displayed in Figure 1.5 B. On the other hand, ultramicroelectrodes (UMEs) demonstrate steady-state behaviour at higher scan speeds because of enhanced mass transport via radial diffusion to the electrode as displayed in Figure 1.5 C. Figure 1.5 D shows a typical CV obtained at an ultra-microelectrode. UMEs have been defined as electrodes with at least one critical dimension of less than 25 µm.[32] Scan speeds do not affect steady state currents, however they are affected by electrode geometry. Steady state current i_{ss} can be determined using the following equation:[33]

$$i_{ss} = nFAD_o m_o C \qquad (11)$$

where:

- m_o is the mass transfer coefficient and is dependent on the geometry of the electrode.

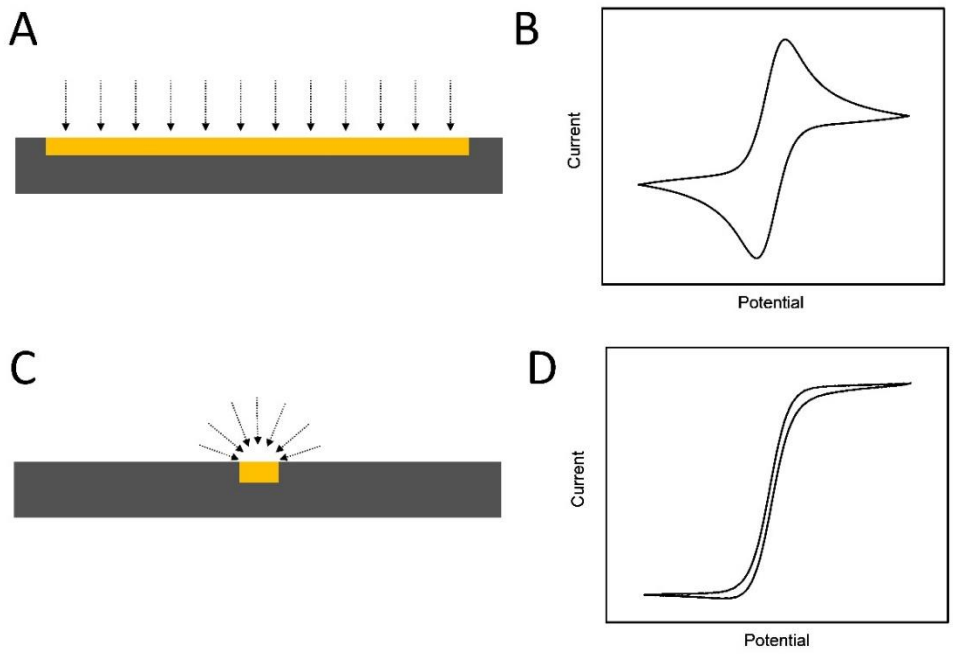

Figure 1.5: *Schematic representation of (A) a macro electrode whereby planar diffusion of analyte to the electrode surface occurs (B) diffusion limited CV response for to a Fc/Fc+ redox couple at a macroelectrode (C) a schematic representation of radial diffusion behaviour to an ultramicroelectrode and (D) a steady state CV response to a Fc/Fc+ redox couple at an ultramicroelectrode.*

UMEs use less material and power, they exhibit improved detection limits, are less affected by capacitance, and require smaller volumes of test solution for analysis. Another advantage of microelectrodes is that they produce smaller currents than macro-electrodes with a greater signal to noise ratio.

1.2 Glucose and lactate electrochemical biosensors

1.2.1 An overview

Three separate electrochemical sensor platforms are examined within this study for either glucose or lactate sensing applications. This section of the introduction aims to deliver a background to enzymatic glucose biosensors and enzymatic lactate biosensors constructed from glucose oxidase (GOx) and lactate oxidase (LOx) respectively. A brief history of both enzymatic electrochemical biosensors is provided, highlighting key achievements and challenges met during their evolution. Electrode modification steps that have been applied to construct both biosensor types are described with a specific focus on materials relevant to this thesis i.e. platinum, o-phenylenediamine and chitosan.

A biosensor is defined as an analytical device that can convert a biological response into a measurable electronic signal. Typically, biosensors are composed of (1) A biomolecule that binds or interacts with an analyte of interest (examples of bioreceptors include DNA, cells, microorganisms, antibodies and enzymes), (2) A transducer element that converts the reaction at the bio-recognition site into a measurable signal and (3) A reader that can process the signal into a readable format.[34,35] For an electrochemical biosensor, the transducer element is a combination of the bio-receptor and the electrode materials at the electrode interface. Examples of Bio-receptors and types of electrical interfaces are shown in Figure 1.6.

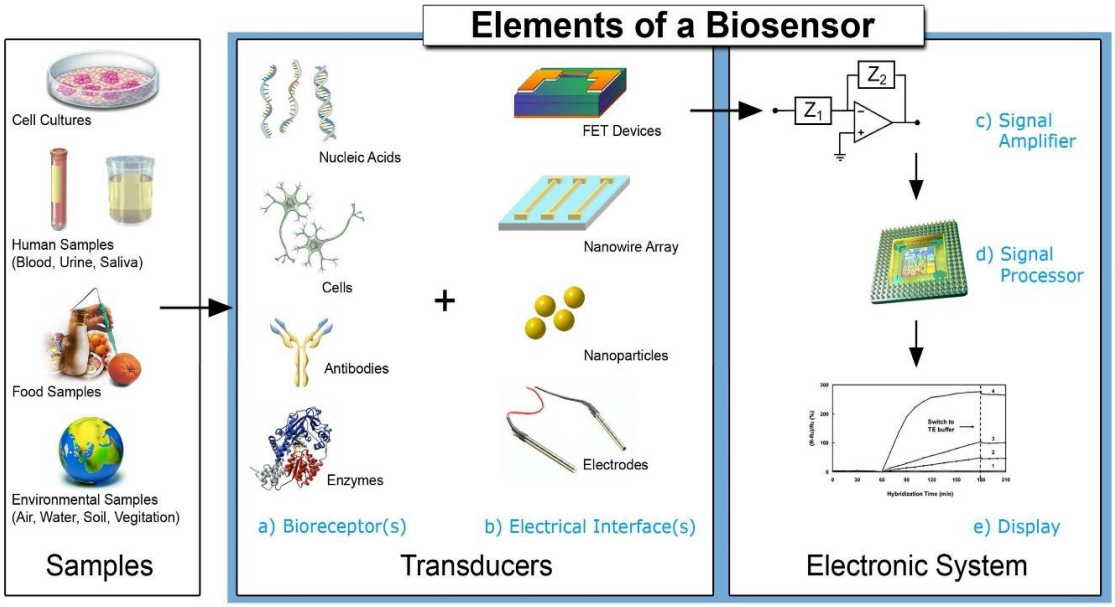

Figure 1.6: *Components of a Biosensor. (Taken from [34])*

Electrochemical biosensors have been popular since the introduction of the first GOx based electrode by Clark and Lyons in 1962.[36] In that example, GOx was entrapped within a semipermeable membrane fabricated on an oxygen electrode. This work was a major milestone that led to the commercialisation of the first glucose analyser from yellow springs instrument (YSI). In the YSI glucose analyser "23A YSI analyser" GO_X was entrapped between two different membranes (polycarbonate and cellulose acetate), polycarbonate functioned to reduce interference effects by blocking larger molecules such as enzymes and proteins present in whole blood from reaching the GOx layer, meaning that glucose oxidation could take place. H_2O_2 produced as a result of glucose oxidation could then pass through the cellulose acetate layer facilitating amperometric detection of H_2O_2 at the platinum electrode according to the following reactions:

$$Glucose + O_2 \rightarrow Gluconic\ acid + H_2O_2 \quad (12)$$

$$H_2O_2 \rightarrow O_2 + 2H^+ + 2e^- \quad (13)$$

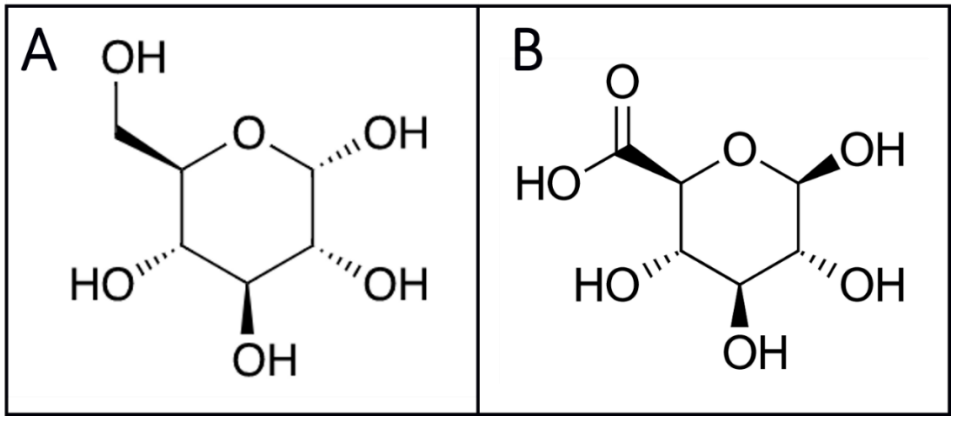

Figure 1.7: *Chemical structure of (A) Glucose and (B) Gluconic acid*

At operating potentials required for H_2O_2 sensing, electroactive species such as acetaminophen, uric acid and ascorbic acid can interfere with electrochemical measurements. Incorporating permselective membranes such as o-phenylenediamine and Nafion is one method employed to prevent this.[37,38] Permselective coatings are constructed so that The requirement for oxygen is also a challenge since limited dissolved oxygen levels in biological fluids can result in inaccurate measurements. The inclusion of diffusion limiting membranes has been one approach employed as it can alter the diffusion behaviour of both glucose and oxygen at the electrode.[39] Challenges associated with first generation glucose biosensors led to the use of redox couples or mediators, owing to their ability to move electrons from the redox centre of the enzyme to the electrode. In 1984, an amperometric glucose sensor was reported by Cass *et al.,* whereby mediator molecules alongside GOx were shown to facilitate sensor operation at reduced potentials, enhance selectivity and were unaffected by dissolved oxygen levels in the solutions of interest. This sensor type became classified as the second generation glucose sensor and was the basis for the first commercial miniaturized, screen printed disposable test strip.[40]

Mediator solubility, toxicity challenges as well as operational constraints with disposable test strips limits the potential applications of second-generation biosensors for wearable and in-vivo applications. This has led to a third generation of glucose sensor. Third generation glucose biosensors operate based on direct electron transfer between the enzyme and the electrode. DET based sensors are assembled with a view to decreasing the electron transfer distance between the active centre of the enzyme and the electrode surface. Although many research articles have claimed to achieve DET between glucose

oxidase and the electrode surface this remains a topic of debate with mixed reports. Third generation sensors offer a number of potential advantages, firstly, sensor performance is not affected by oxygen fluctuations. Furthermore, they can operate at lower oxidation potentials. However, they suffer from decreased electron transfer rates by comparison to first and second generation sensors. In spite of significant research utilising nanostructures for DET based detection, these methods have not yet been realised as part of commercial glucose sensors which continue to function from first and second generation sensing approaches.[41] The thick protein layer covering the active enzyme can be a challenge for DET based methods as this can inhibit electron transfer through the redox centre of the enzyme to the electrode. Figure 1.8 shows a schematic representation of all three generations of glucose sensor.[42]

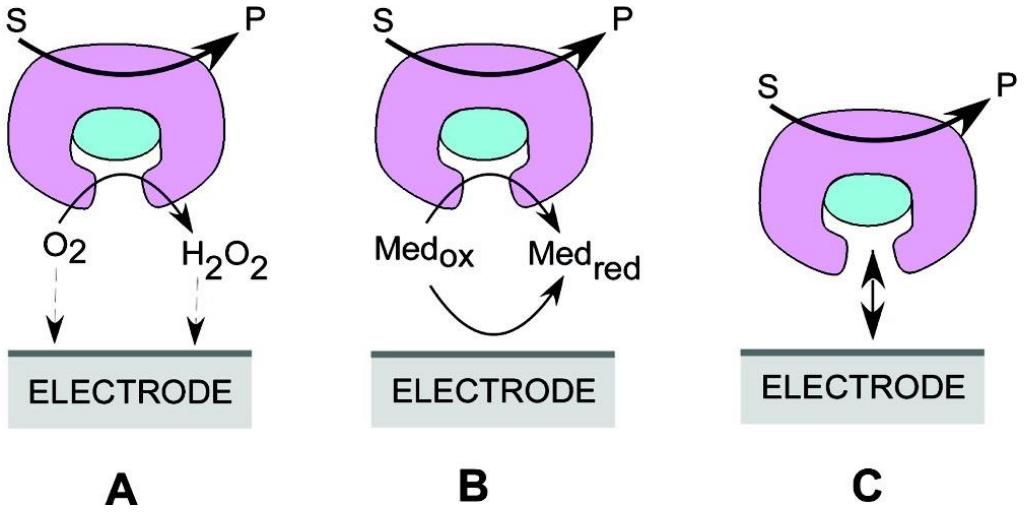

Figure 1.8: *Three generations of amperometric glucose sensors using (A) oxygen as a natural co-factor (B) artificial redox mediators and (C) direct electron transfer between GOx and electrode. (Taken from* [42])

Advances in the development of glucose biosensors has paved the way for other targets such as lactate, which has followed a similar research story to the glucose biosensor. L-lactate biosensors using the enzyme lactate oxidase (LOx) were reported soon after early studies on glucose biosensors.[43,44] In 1982, Matsunga *et al.* reported a lactate sensor whereby LOx was immobilised on a porous acetyl cellulose membrane and subsequently attached to a Pt electrode. In 1984, Clark *et al.* reported an L-Lactate sensor using the Glucose *YSI 23 A* sensor probe. GOx was replaced by LOx within the cellulose acetate and polycarbonate membranes (see Figure 1.10). Hydrogen peroxide sensing took place at the Pt WE produced from the oxidation of L-lactate through the reaction listed below:[45,46]

$$L - Lactate + LOx \rightarrow Pyruvate + LOx_{red} \quad (14)$$

$$LOx_{red} + O_2 \rightarrow LOx_{ox} + H_2O_2 \quad (15)$$

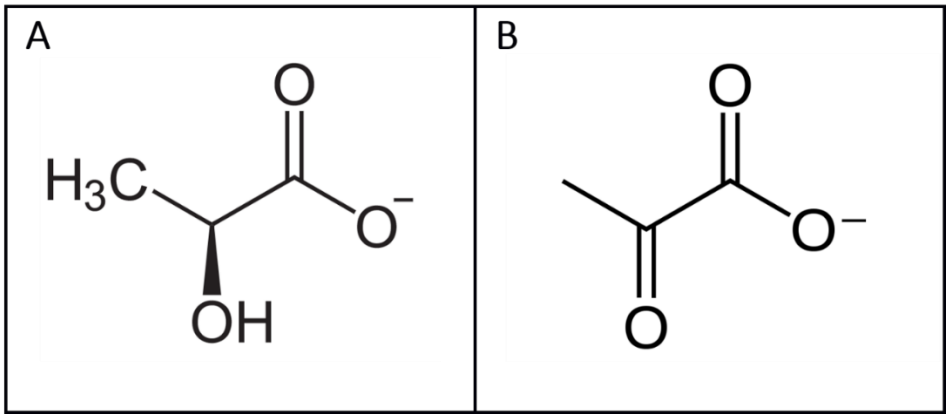

Figure 1.9: *Chemical structure of (A) Lactate and (B) Pyruvate*

This work led to commercial blood lactate analysers such as the YSI 2300, the Biosens Analyzer and Abbotts portable i-STAT.[47] Similar to first generation GOx based biosensors, fluctuating oxygen concentrations in biological media led to variations in sensor response. The need for high operating potentials resulted in the oxidation of electroactive species that can co-exist in blood.[48] Redox molecules and polymer based mediators have been incorporated into lactate biosensor construction to alleviate challenges associated with the first generation of lactate sensors.[44, 46]

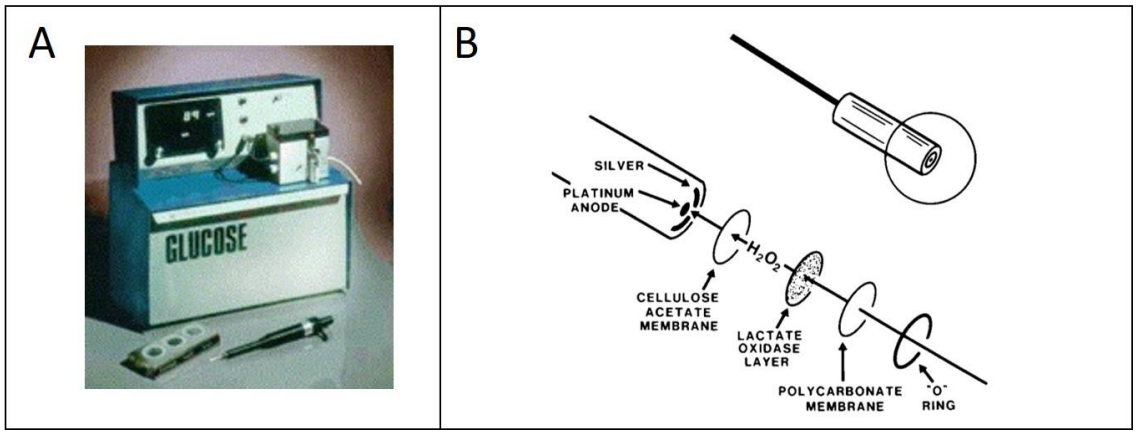

Figure 1.10: *(A) YSI 23 A,[40] (B) The sensor probe with LOx immobilised between a membrane of cellulose acetate and polycarbonate for use with the YSI 23A analyser.*[45]

Many commercial portable lactate analysers determine lactate concentrations in whole blood from an electrochemical lactate-oxidase mediated reaction. The Lactate Pro for example, operates with test strips that contain lactate oxidase and ferricyanide.[50–54] In the

last decade, both glucose and lactate biosensor research has shifted from POC developments towards in-vivo, minimally invasive and non-invasive applications using other bio-fluids such as skin, interstitial fluid, saliva, tears and sweat. Table 1 provides typical concentrations ranges of glucose and lactate in various bio-fluids for a healthy individual at rest.

Table 1: *Physiological glucose and lactate concentration ranges in various bio-fluids for a healthy individual at rest.*

Bio-fluid	Lactate (mM)	Glucose (mM)	Ref.
Blood	0.5–2 mM	3.6 − 7.5 mM	[55,56]
Interstitial fluid	0.5–2 mM	3.9–6.6	[47,57]
Saliva	1.9–2.2 mM	0.23 to 0.38 mM	[58,59]
Tears	1–5 mM	0.1–0.5 mM	[60,61]
Sweat	5–10's mM	0.02–0.11 mM	[62,63]

Electrochemical glucose sensors have reached major milestones with the release of CGM's capable of monitoring glucose concentrations in skin interstitial fluid for 7 to 14 days. As of April 2022, a commercial continuous lactate monitor is not available on the market; however, it has featured as a prospective future bio-wearable.[64] A number of challenges remain for lactate sensor development specifically for wearable and monitoring applications. Long-term stability, selectivity, biocompatibility and resilience during applied stresses are examples of areas that require improvement for the success of flexible sensor platforms. The next section will focus on reports of electrode modifications and functionalisation techniques applied to electrode structures for the construction of glucose and lactate sensors on both rigid and flexible platforms.

1.2.2 Electrode modifications

1.2.2.1 *Platinum electrodeposits and their application in glucose and lactate biosensors*

Pt microelectrodes, Pt wires, and platinum nanoparticles have been widely used in amperometric glucose and lactate sensors as a catalyst for the oxidation of H_2O_2.[65–67] As an alternative to using planar Pt electrodes, Pt nanoparticles can be electrodeposited onto electrode surfaces to enhance sensor performance.[68] Pt NPs can increase the electrode surface area resulting in an increased current. . Gu *et al.* reported a droplet-based

microfluidic electrochemical sensor using platinum black modified Pt micro-electrode. The micro-electrode was formed using a single 1 cm Pt wire with a 100 micro-meter diameter which are embedded in 100 micro-meter deep electrode channels in the micro-fluidic device. The platinum-black electrodeposition was carried out at -0.1 V for 10 minutes. A schematic of the set-up for the microfluidic electrochemical biosensor is shown in Figure 1.11 A and B. The current measured at the bare Pt and the Pt-Black modified electrode in response to a 5 mM glucose concentration in 1 mg/L GOx acetate buffer solution is shown in Figure 1.11 C. A clear increase in signal response is seen at the Pt-Black electrodeposition. As the solution was passed through the microfluidic channels the current response to 'flowing droplets' of the solution was measured (see Figure 1.11 D), Pt-Black modified electrodes were found to have a current response 10.2 times higher than the Pt electrodes.[65]

Increasing the conductive surface area with nanoparticles also provides a larger area to support enzyme immobilization. Lourenço *et al.* reported the construction of glucose biosensor on carbon fibre electrodes using a platinum electrodeposition step followed by GOx enzyme attachment. The authors first studied both galvanostatic and potentiostatic Pt electrodeposition methods by measuring the amperometric H_2O_2 response at various depositions. Compared to the unmodified carbon fibres, galvanostatic depositions

demonstrated a 30 to 60-fold increase in sensitivity for H_2O_2 sensing. Potentiostatic depositions to the carbon fibres showed a 200-fold increase in sensor sensitivity to H_2O_2.

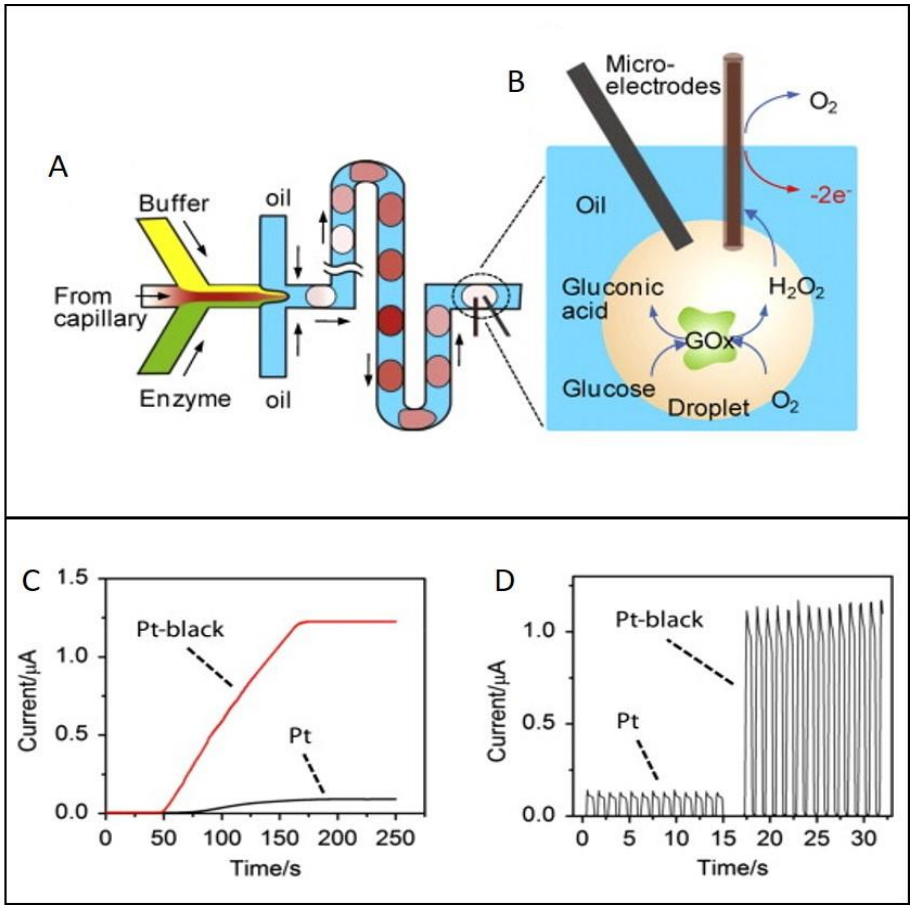

Figure 1.11: *(A) Schematic of the microfluidic electrochemical sensor and the electrochemical detection mechanism in a droplet containing glucose and GOx (C) i-t curve of 10.0 mM glucose solution at bare Pt and Pt-black microelectrode (D) Current response of 5 mM glucose on Pt and Pt-black microelectrodes in flowing droplets.*[65]

Both Pt modifications were found to display improved analytical performance in comparison to the unmodified carbon surface. Potentiostatic depositions proved to be the more favourable for H_2O_2 sensing since this allows high current efficiency, which remains constant during the deposition by contrast during the galvantostatic method current efficiency decreases over time. A potential of -0.2 V was applied for 10 seconds vs. Ag/AgCl RE. GOx was subsequently cross-linked with glutaraldehyde onto the platinised surface. To prevent the oxidation of electroactive species m-phenylenediamine (10 mM solution) was electrodeposited onto the WE using CV for 20 minutes. The resulting biosensor demonstrated in-vitro glucose detection from 0 to 4 mM before being applied for ex-vivo analysis in brain slices. Whilst the sensor did not measure exact glucose

concentrations, the sensor was capable of detecting changes to glucose levels in the brain.[69] Faruk *et al*. reported the use of platinum electrodepositions onto a laser scribed graphene electrode for the fabrication of both a glucose biosensor and uric acid sensor (see Figure 1.12). In that study, platinum NPs were anchored to pyrenebutanoic acid, succinimide ester (PBSE) via electrodepositions. PBSE was initially cast on the electrode surface to form carboxylic functional groups. Electrochemical platinum depositions were performed by cycling the potential from -0.2 V to 0.75 V in a solution containing 0.002 M K_2PtCl_4 and a 0.06 M H_2SO_4. GOx was immobilised on the electrode surface followed by the application of a Nafion membrane. The resulting glucose biosensor demonstrated detection over a linear range of 5 µM to 3200 µM and was found to have a sensitivity of 12.74 µA/mM/cm^2.[70]

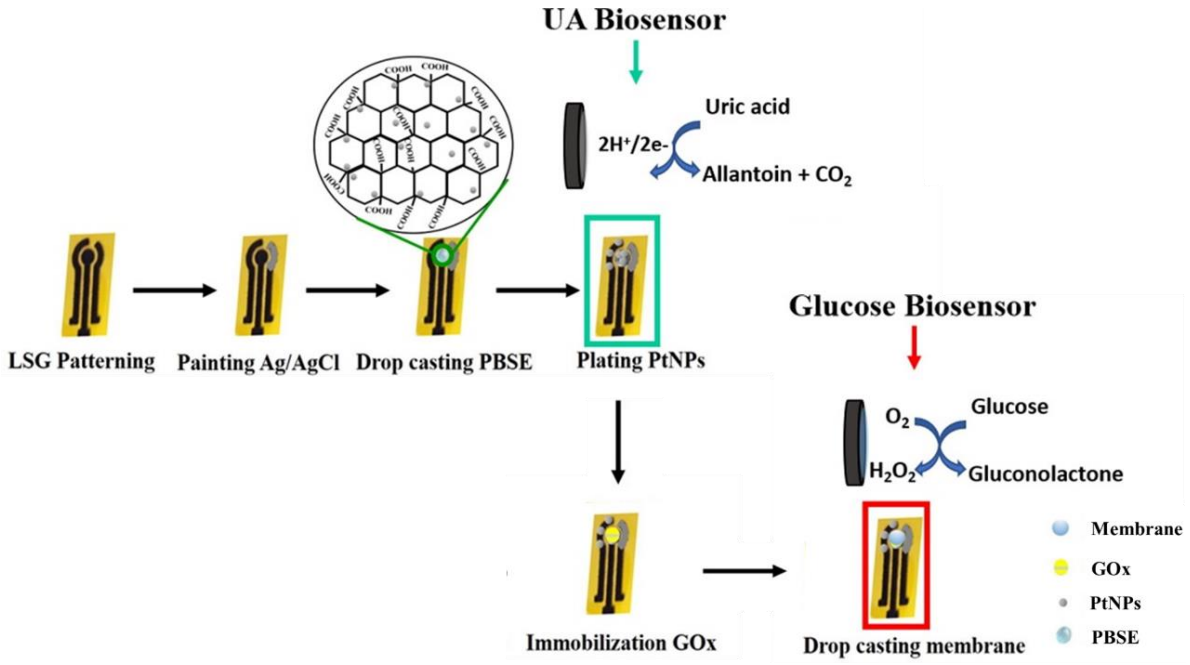

Figure 1.12: *Schematic of uric acid and glucose sensor fabrication process, for the uric acid sensor PBSE is dropcasted followed by a PtNP electrodeposition, for the glucose sensor, the same process is followed with the inclusion of GOx immobilisation and the application of a nafion membrane.*[70]

Platinum has also been incorporated as part of a nanocomposite material for the detection of lactate. Neampet *et al.* reported a nanocomposite material composed of platinum, polyaniline and Ti_3C_2 deposited on a carbon screen-printed electrode for H_2O_2 and lactate sensing. MXenes are 2D transition metal carbide and nitride materials that have become increasingly popular because of their biocompatibility, chemical stability and electrical conductivity.[71] The electrode fabrication steps are outlined in the schematic in Figure

1.13. It was found that the platinum/polyaniline/MXene modified electrode had a current signal 180 times higher than the unmodified carbon screen-printed electrode in response to H_2O_2. The resulting biosensor demonstrated amperometric lactate detection at 0.3 V in a linear range of 0.005 mM to 5 mM. The sensor was applied to spiked milk samples demonstrating successful lactate detection for four lactate concentrations.[72] In another report by Anusha *et al.* the inclusion of a platinum electrodeposition to a ZnO, Chitosan (CS) and GOx based biosensor resulted in a sensitivity one order of magnitude higher than the ZnO/CS/GOx layer without the Pt electrodeposition. The authors attributed the enhanced sensitivity to the increased electro-active surface area and hence the enhanced electron transfer properties of the electrode.

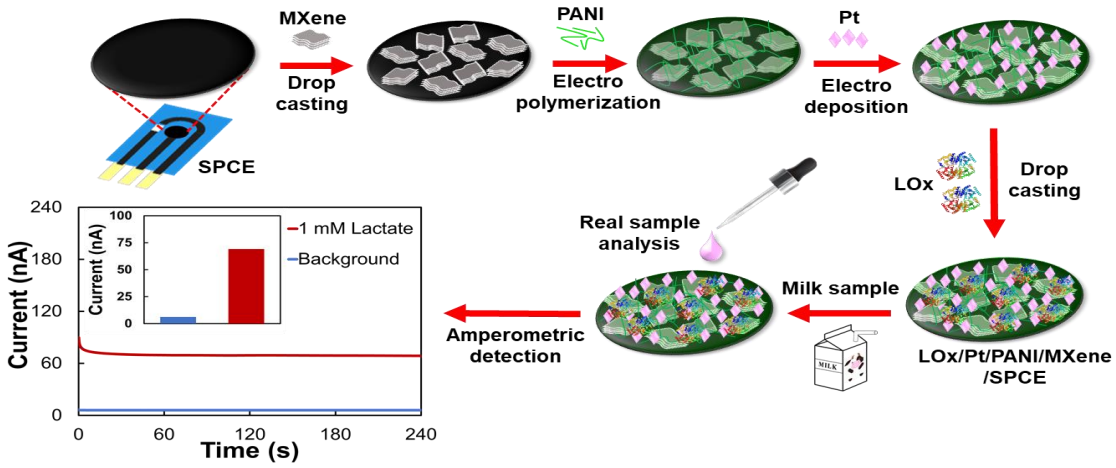

Figure 1.13: *Schematic representation of the fabrication process of the Pt/PANI/MXene biosensors on a carbon SPE, inset graph shows an amperometric response in a background solution containing 0 mM lactate and a 1 mM lactate solution.*[72]

Chen *et al.* also reported an enhanced sensitivity to H_2O_2 when Pt microspheres were electrodeposited onto a carbon nanotube electrode on a fabric based sensor. The resulting biosensor demonstrated a sensitivity of 288.86 μA mM^{-1} cm^{-2} for 0 to 5 mM glucose concentrations. It is clear that Pt offers benefits for H_2O_2 sensing and hence glucose oxidase or lactate oxidase based sensors. However, we know this is not without challenges as indicated in the overview section. Platinum is more costly than carbon based materials and is affected by interfering species at oxidising potentials required for both GOx and LOx based glucose and lactate sensors. The use of permselective coatings and diffusion limiting membranes should be considered when operating at higher potentials for the oxidation of H_2O_2. Whilst Pt offers enhanced sensitivity, this can be reduced when applying coatings for interference rejection and diffusion limiting membranes. Whilst

platinum is a costly material by contrast to carbons, it has been widely used in biosensor technologies, is biocompatible and can be electrodeposited onto electrodes in a manner that will offer a higher surface area for enzyme attachment.[73]

1.2.2.2 *Enzyme attachment techniques for glucose and lactate based biosensors*

Enzyme attachment or immobilisation close to the electrode surface is an important step in assembling an electrochemical biosensor. Figure 1.14 shows a simple schematic of chemical and physical immobilization methods to attach enzymes to electrodes. A number of detailed reviews on enzyme immobilization strategies and their advancement can be found elsewhere.[74–77] This section of the introduction will give examples of some recent studies using either physical adsorption, physical entrapment or chemical linking methods for the immobilisation of GOx or LOx enzymes to construct glucose and lactate sensors respectively.

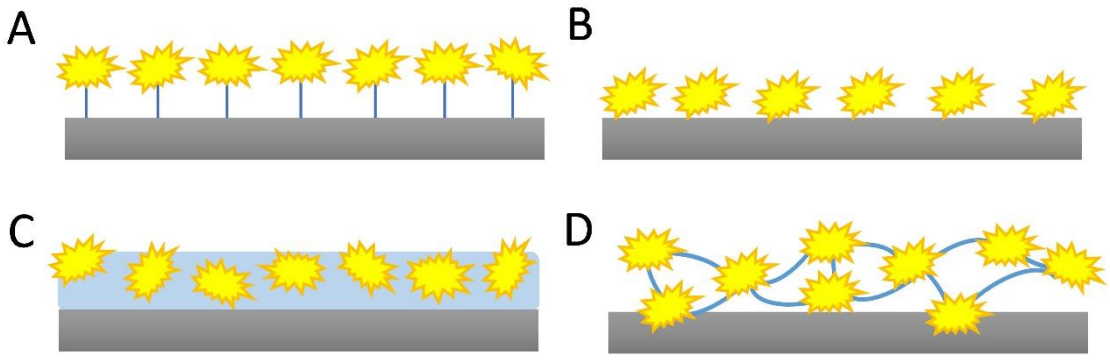

Figure 1.14: *Schematic of four commonly used enzyme attachment methods (A) Covalent bonding (B) Physical adsorption and (C) Physical encapsulation or entrapment and (D) Crosslinking.(adapted from,[67,68])*

Yu *et al.* recently reported a flexible glucose and lactate electrochemical sensor whereby GOx was cross-linked to WE 1 and LOx was crosslinked to WE 2 using poly (ethylene glycol) diglycidyl ether (PEDGE). In brief, two Au WEs were modified with Au nanostructures via electrochemical deposition. The modified WEs were placed in 0.1 M β-cysteamine solution for 24 h, after cleaning. The glucose sensor was prepared by drop casting a solution containing GOx/BSA/PEGDE onto one WE. The second WE was modified by casting a LOx/BSA/PEGDE solution. A schematic of the flexible sensor and the modification process is displayed in Figure 1.15. The dual biosensor achieved an LOD of 7 µM and 54 µM respectively. A linear range of 1 mM to 25 mM and 25 µM to 250 µM was found for glucose and lactate respectively. The biosensor revealed good stability

with no decrease in sensor sensitivity after 4 weeks of storage. Lastly, the flexible biosensor demonstrated good recovery values for both glucose and lactate detection in human sweat samples.

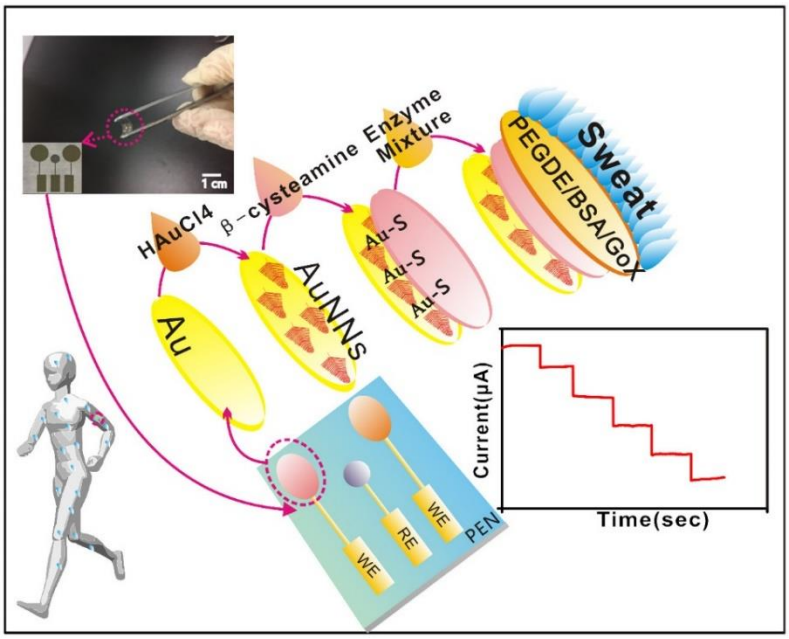

Figure 1.15: *Schematic representation of the WE modification process to one of the WEs on the flexible polyethylene naphthalate (PEN) substrate for glucose detection, inset photograph shows an image of the sensor being bent and a magnified image of the sensor.*[69]

Physical adsorption is a versatile immobilization method achieved via interactions between the enzyme and the enzyme carrier material or the electrode surface. Adsorption can occur as a result of van der Waals weak electrostatic forces that attract neutral molecules to one another, hydrogen bonding and ionic interactions.[77] Physical adsorption techniques can suffer from the weaker bonds, although, it has been reported that these methods do not disturb the enzyme active sites.[78] Physical adsorption strategies include immersion and drop casting. For drop casting, enzyme solutions are commonly applied directly to the WE and allowed to dry at room temperature: alternatively electrodes can be immersed in enzyme solutions. In both instances, after a given amount of time, electrodes are rinsed to remove any un-adsorbed enzyme.[79]

Wang *et al.* have fabricated a stretchable textile based electrochemical biosensor for lactate detection which involves a combination immobilisation strategy involving physical adsorption and the use of an approach sometimes referred to as “sandwiching”. Prussian blue was electrodeposited onto the stretchable gold fibres followed by drop-casting LOx onto the surface. After drying at room temperature, a chitosan membrane

was cast onto the fibres again allowing them to dry at room temperature. A schematic of the textile material and the layers used to construct the WE are shown in Figure 1.16. A and B. The counter and reference electrode modifications can be seen in Figure 1.16 C and D. The final biosensor revealed a sensitivity of 19.13 μA/mM/cm^2 over a concentration range of 0 to 5 mM and 2.9 μA/mM cm^2 over a concentration range of 10 to 30 mM. The textile biosensor was also studied using amperometry in artificial sweat revealing a sensitivity of 14.6 μA/mM/cm^2 for concentrations between 0 to 5 mM and a sensitivity of 2.5 μA/mM/cm^2 for the concentration range of 0 to 30 mM. Short term stability studies detailed a decrease in signal by 29 % after 6 days of storage at 4 °C.[80]

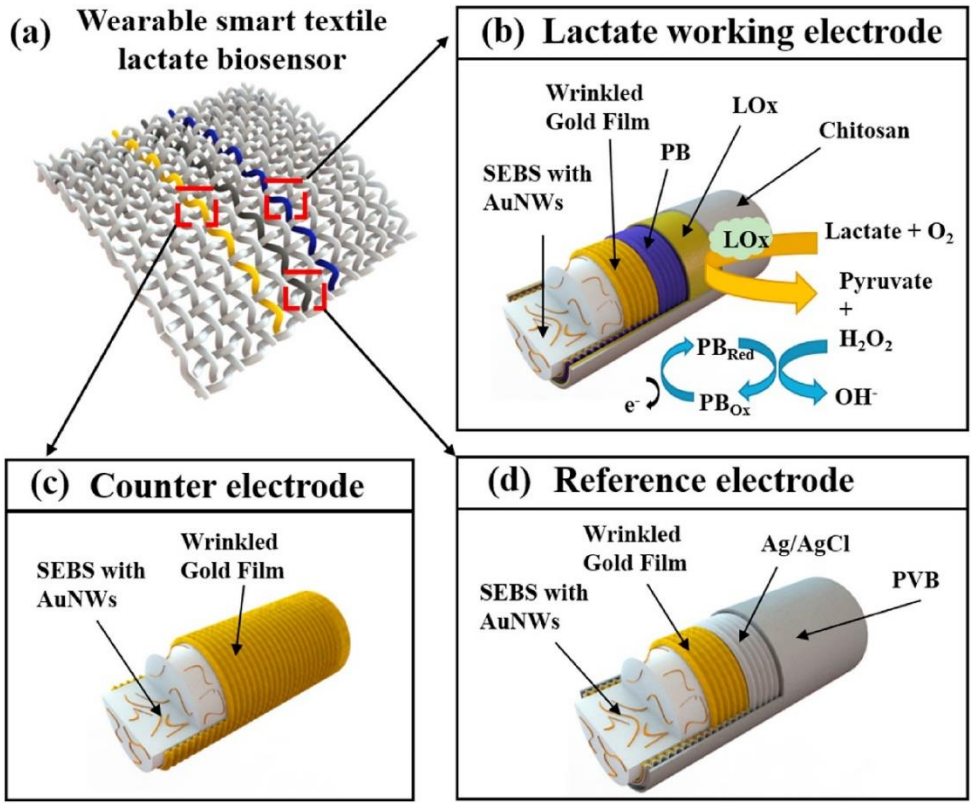

Figure 1.16: *Schematic representation of the textile electrochemical biosensor depicting the WE, RE and CE, (B) the layers used to fabricate the lactate sensor including mechanism for lactate detection at Prussian blue (C) the gold film modified textile (CE) (D) the PVB/Ag/AgCl/Gold film modified textile (RE).*[71]

Physical entrapment as the name suggests involves entrapping the enzyme within a solid matrix such as a polymeric membrane. Entrapment methods are efficient and can facilitate the deposition of a mixture of mediator, enzyme and polymer onto an electrode surface. In a recent report by Park *et al*. a multi-parametric sensor was fabricated to measure conductivity, pH, and the concentrations of both lactate and glucose (see Figure 1.17).[81]

Entrapment methods were used for both LOx and GOx attachment. The lactate sensor was assembled via electropolymerisation of LOx with polypyrrole (PPy) onto a prussian blue modified Au WE. Polypyrolle was selected for LOx in order to increase the linear range for lactate detection. A constant potential of 0.8 V was applied vs. the pseudo Ag/AgCl RE in a solution containing 4 mM of the PPy monomer mixed with 600 U/ml of enzyme in 0.1 M PBS for 4 minutes. The lactate biosensor demonstrated linear detection from 1-5 mM. Poor repeatability was observed when successive calibrations were conducted on the same sensor. The authors attributed this to the detachment of LOx from the sand-like structure of the PPy layer. For the glucose sensor, electropolymerisation of GOx was carried out at a constant potential of +0.55 V vs. the pseudo Ag/AgCl RE for 2 minutes in a solution containing 10 mM o-phenylenediamine (o-PD), 5 mM sodium sulphate and 1600 U/mL of GOx in a 0.1 M PBS solution. Glucose sensing was achieved over a linear range of 0-4 mM. Unlike the lactate sensor, the glucose sensor showed no decrease in chronoamperometric current after the third calibration on

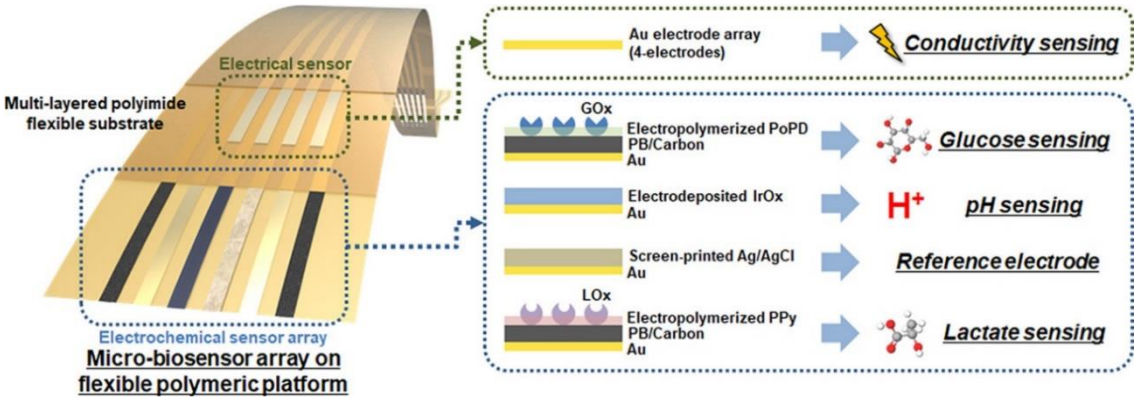

Figure 1.17: *Schematic representation of a microscale biosensor fabricated on polyimide. A number of WEs were fabricated on the polyimide substrate and modified for pH, Glucose and Lactate sensing. Electropolymerisation methods were used to entrap GOx at one WE in o-PD and LOx at a separate WE in polypyrrole.*[72]

the same biosensor indicating a more robust immobilization of the GOx enzyme. The sensors demonstrated functionality in a hydrogel phantom (agarose and PBS) constructed with properties similar to a healthy liver in the outer regions of the phantom and with properties similar to cancerous liver at the centre of the phantom.

1.2.2.3 *O-phenylenediamine and its use in glucose based biosensors*

Anodic depositions of o-Phenylenediamine can form a non-conducting coating at the electrode surface.[82]o-Phenylenediamine (o-PD) was first used as a non-conducting

polymer for the entrapment of GOx at a Pt transducer in 1990.[83] Since then it has been been widely studied for the construction of enzymatic biosensors targeting glucose, lactate, glutamate and alcohol.[84–88] For example in 2014, Turkmen *et al.* reported the use of o-phenylenediamine for GOx entrapment during electropolymerisation. The Pt WE was firstly modified with polyvinylferrocenium perchlorate ($PVF^{+}ClO_4^{-}$) via electro-precipitation. This was followed by a platinum electrodeposition step. Lastly, a solution containing 5 mM o-PD and 1 mg/ml of GOx prepared in an acetate buffer (0.1M, pH 5.4) was deposited at a constant potential of +0.7 V for 15 minutes. The resulting biosensor had a linear range of 0.06mM to 9.64 mM, an LOD of 0.018 mM and a sensitivity of 17.40 μA mM^{-1} cm^{-2}. Sensor stability was found to decrease by 26 % after 30 days of storage.[89] o-Phenylenediamine has also been used as a final coating layer covering the immobilized GOx; for example Li *et al.* reported a glucose sensor constructed on a Pt-Ir wire within tubing made from polyetheretherketone (PEEK). Electrodeposition of GOx was carried out at 1.3 V for 1 hour followed by a 15 minute electrodeposition at 0.7 V vs. Ag/AgCl in a 50 mM o-PD solution made up in 0.1 M PBS. The 'fine pointed' electrochemical biosensor demonstrated glucose detection within a linear range of 1.4 mM to 21 mM, with an LOD of 0.1 mM and a sensitivity of 2.55 μA/cm^2/mM.[90] One drawback of this device was that sensor stability measurements were found to decrease by 20 to 30 % during a second week of measurements. In some instances the deposition of the o-PD layer is carried out directly to the bare electrode prior to enzyme immobilization, here, o-PD is not used to entrap the biomolecule but solely for interference rejection at the transducer.[87,91]

Whilst o-PD offers a method for physically entrapping glucose oxidase at the electrode surface, many reports have detailed reduced signals after 2 weeks of storage. Despite this, the material has shown promise during intermittent monitoring measurements described by Kim *et al.* In that study, LOx was entrapped during electropolymerisation in o-PD at 0.55 V for 1 minute. The final biosensor demonstrated stable currents in response to a 0.5 mM lactate concentration measurement carried out every 10 minutes for up to 2 hours (Figure 1.18).[92]

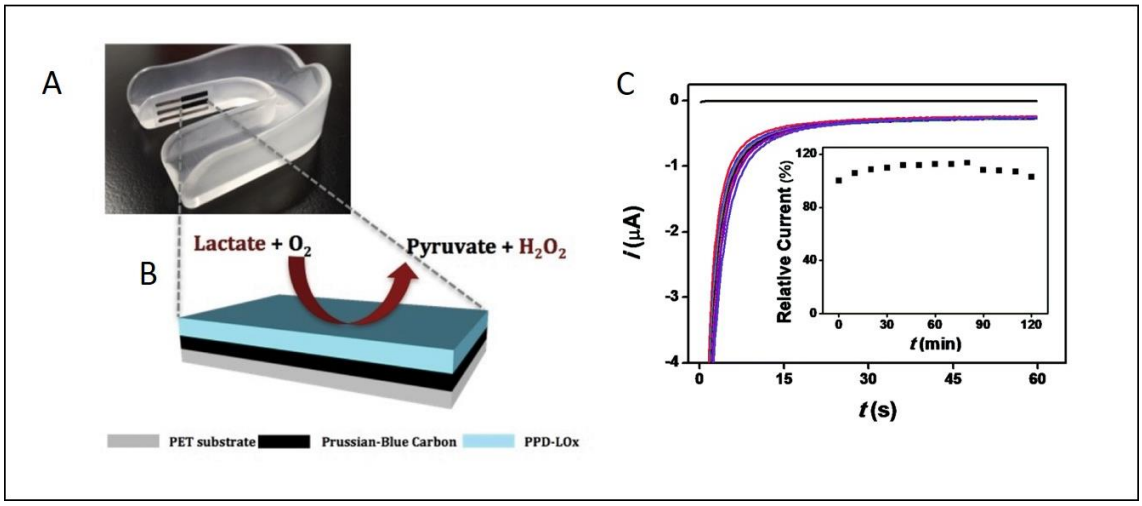

Figure 1.18: *Photograph of a mouthguard with the three-electrode configuration fabricated on PET attached, (B) the layers used to assemble the lactate biosensors and the reaction occurring at the electrode (C) i-t curves in a 0.5 mM lactate concentration ran every 10 minutes over a 2 hour period.* [81]

1.2.2.4 *Chitosan based glucose and lactate biosensors*

Chitosan (CS), a natural polyaminosacharide, is frequently used in the formation of electrochemical biosensors as it provides a healthy microenvironment for biomolecule immobilisation. CS has excellent film-forming abilities, good adhesion behaviour, is biocompatible and has a high water permeability.[93] CS electrodepositions are a rapid method of forming stable hydrogel coatings onto the surface of an electrode. Figure 1.19 shows a schematic of the CS electrodeposition process. Electrodeposition of chitosan occurs by application of a reduction potential, which results in a local change in pH. The

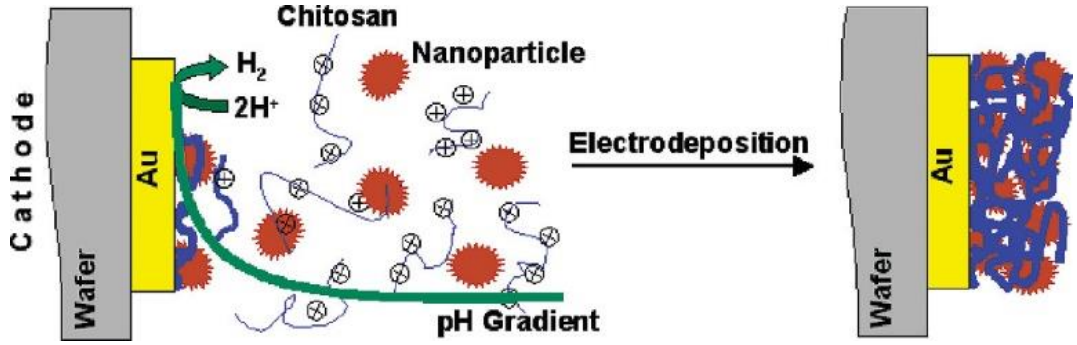

Figure 1.19: *Schematic of chitosan electrodeposition. Polarisation of the cathode results in a local pH change. Chitosan chains in the vicinity of the cathode electrode become insoluble as a result of the higher pH. Nanoparticles present in the CS solution also become entrapped during the electrodeposition.*[83]

reduction of H^+ to H_2 at the electrode surface leads to a change in CS solubility, where CS becomes insoluble and coats the electrode surface.[94]

Some reports have included an enzyme in the chitosan mixture during electrodeposition. Zeng *et al.* report an electrodeposition of a chitosan GOx mixture onto an Au NP modified electrode at -0.1V for 300 seconds.[95] Sensor signal was found to decrease by 5 % after 2 weeks of storage and 10 % after 30 days. Redox molecules and conductive nanomaterials have been integrated in this one-step electrodeposition process to produce bio-nanocomposite films with improved sensor performance.[96,97] For example, Luo *et al.* reported a one-step electrodeposition process in a solution mixture of ferrocene-grafted chitosan, single walled CNTs and GOx onto monolithic 3-D graphene, Figure 1.20 shows a schematic of the modification process. The resulting biosensor demonstrated a wide linear range (5.0 μM–19.8 mM), an LOD of 1.2 μM and excellent reproducibility with an RSD of 3.2 %. After storage for 7 days, 91.6 % of the original current response was retained.[98] One drawback noted with electrodepositions is the use of a high voltage which can result in loss of enzyme activity.

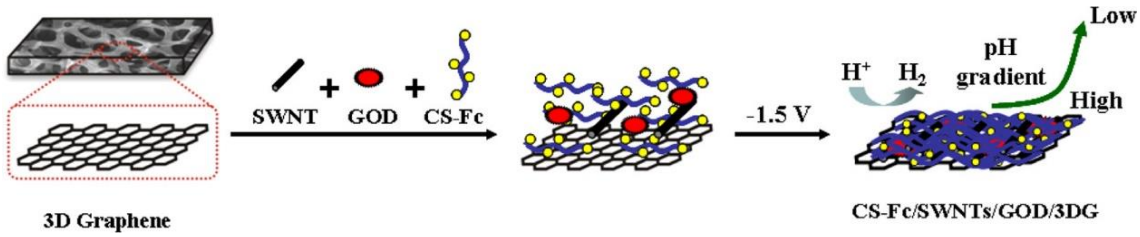

Figure 1.20: *Schematic representation of the fabrication of a glucose sensor on three-dimensional graphene by a one-step chitosan electrodeposition process.*[87]

Chitosan can also be used to produce hydrogels which can be drop casted as a coating membrane to electrode surfaces.[99,100] Work carried out by Payne *et al.* described drop casting methods to apply chitosan onto a transducer surface. Briefly, CS was mixed with both CNTs and LOx, the mixture was applied to the WE electrode and was left to dry over-night at 35 °C. Chitosan optimisation experiments showed that a low concentration of 0.1 % did not enable sufficient enzyme immobilization, at 0.6 % a linear range up to 20 mM was observed and at a higher concentration of 1 % the sensor sensitivity was found to decrease.[101] Another report by Silva *et al.* detailed the use of chitosan for the development of an enzymatic lactate sensor. A number of CS concentrations were assessed from 0 to 2 %. The inclusion of the CS layer resulted in an increase in current response with a 0.6 wt % CS concentration demonstrating optimum sensor performance.

This study also investigated three different layering processes. One where CS was drop casted on the transducer surface and allowed to dry at room temperature prior to enzyme immobilisation, another where CS was cast after enzyme immobilisation, and one where CS was applied before and after enzyme immobilisation. In the latter two a reduction in current was observed which the authors attributed to the loss of LOx activity as a result of the pH of the CS solution. The final biosensor was found to have good reproducibility with an RSD of less than 7% and a limit of detection of 0.75 μM. The biosensor also demonstrated good repeatability for nine consecutive measurements. After 50 days of storage at 4 °C, the biosensor retained its original sensitivity,[102] each enzyme attachment method comes with advantages and disadvantages. Crosslinking methods are desirable due to their strong chemical binding resulting in biosensors with improved operational stability. However, crosslinking can lead to a loss in enzyme activity. Adsorption methods have been reported to retain enzyme activity, however, they can result in poor stability owing to the reversible nature of the bonds. Entrapment techniques are efficient, for example electro-polymerisation steps can take just 10 minutes by comparison to adsorption and crosslinking techniques where enzyme remains on the electrode surface for a number of hours before rinsing.

1.3 Electrode fabrication

Various fabrication techniques and processing steps have led to highly innovative electrochemical biosensors on microneedles,[103] contact lenses,[104] point of care flexible skin wearables,[105] pacifiers,[106] and more. The previous section focused on construction techniques for the formation of lactate and glucose biosensors specifically using the enzymes GOx and LOx. This section aims to present a number of electrode fabrication techniques to provide a background to the fabrication of electrodes used within this thesis. A description of the fabrication methods along with recent examples of electrochemical biosensors assembled on these electrodes will be covered.

1.3.1.1 *Silicon microfabrication*

Integrated electronic devices fabricated on silicon were first integrated with membranes for electrochemical analysis in the 1970s with the introduction of ion sensitive field effect transistors.[107] Conventional silicon fabrication methods have since been successful in creating micro and nano-electrodes on silicon substrates for various electrochemical sensor and biosensor applications.[108] Point of care sensors, chips integrated with micro-

fluidics, neurochemical probes and implantable devices are all examples of electrochemical sensor devices realised as a result of silicon micro-fabrication technologies.[109–114] Silicon fabrication offers benefits such as scalable production, reproducibility, customisable structures and multiplexing opportunities. Figure 1.21 (a) shows a schematic of the silicon fabrication process. Broadly speaking, the fabrication steps include photolithography, deposition and etching. Starting with a silicon wafer that has a blanket insulation layer, micro and nano features as small as 100 nm can be achieved using UV lithography steps. A photoresist (PR) is deposited on the wafer in order to "write" the desired microelectrode pattern. Exposed photoresist is removed, and deposition techniques such as sputter coating, electron beam evaporation and chemical vapour deposition can be used to deposit the metal.[115] This is followed by a lift-off process which removes the remaining photoresist and metal. Another adjustment to this fabrication process is to deposit the metallic layer prior to the photoresist (see Figure 1.21 (b)). Electrode gaps can then be patterned using UV lithography. This is followed by an etch to remove exposed photoresist.[116] Finally, if required, a passivation or insulating layer is deposited to expose only the micro or nano electrodes.

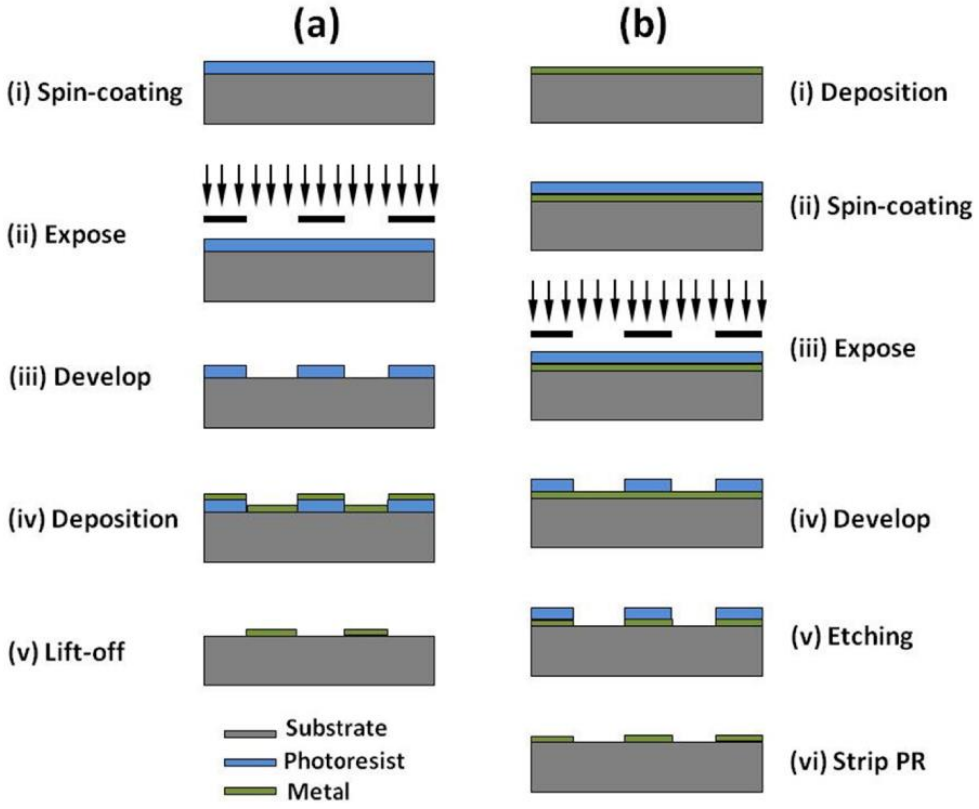

Figure 1.21: *Silicon fabrication process for constructing electrodes. (reproduced from [106])*

A recent example of an ultraminiaturised glucose sensor fabricated using photolithography and microfabrication methods on a 100 nm thick silicon wafer was reported by Ribet *et al.*.[117] The microsensor had a three-electrode configuration consisting of a platinum WE and CE and an iridium RE. The RE was modified via CV in a 0.1 M PBS solution, to produce an oxidised iridium pseudo-reference. The WE was modified using a three-step drop-casting process: 1. GOx + BSA + glutaraldehyde 2. Polyurethane and 3. Nafion (5 wt %). Polyurethane was used to adjust the diffusion of oxygen and glucose to the electrode in order to increase the linear range. Variation in polyurethane thickness across sensors led to variations in sensor performance such as linear range and sensitivity. In a follow on study, Ribet *et al.* fabricated a CGM device by combining two components: a miniaturised electrochemical sensor on silicon (see Figure 1.22 A) and a silicon microneedle (see Figure 1.22 B). Here, the glucose sensor was assembled using a high-precision liquid dispenser (Ultimus V, Nordson EFD). The microneedle electrochemical sensor device was applied for in-vivo amperometric measurements in a human forearm for comparison to blood glucose measurements. The device demonstrated in-situ minimally delayed (10-12 minutes) minimally invasive glucose monitoring in human skin.[118] Silicon fabrication methods are expensive, involve a number of fabrication and processing steps and hence can take a number of days to obtain a batch of sensors. Alternative fabrication techniques such as laser scribing and additive printing provide a

more cost effective means to producing electrochemical sensors and can be used to modify other materials particularly polymers such as Polyimide.

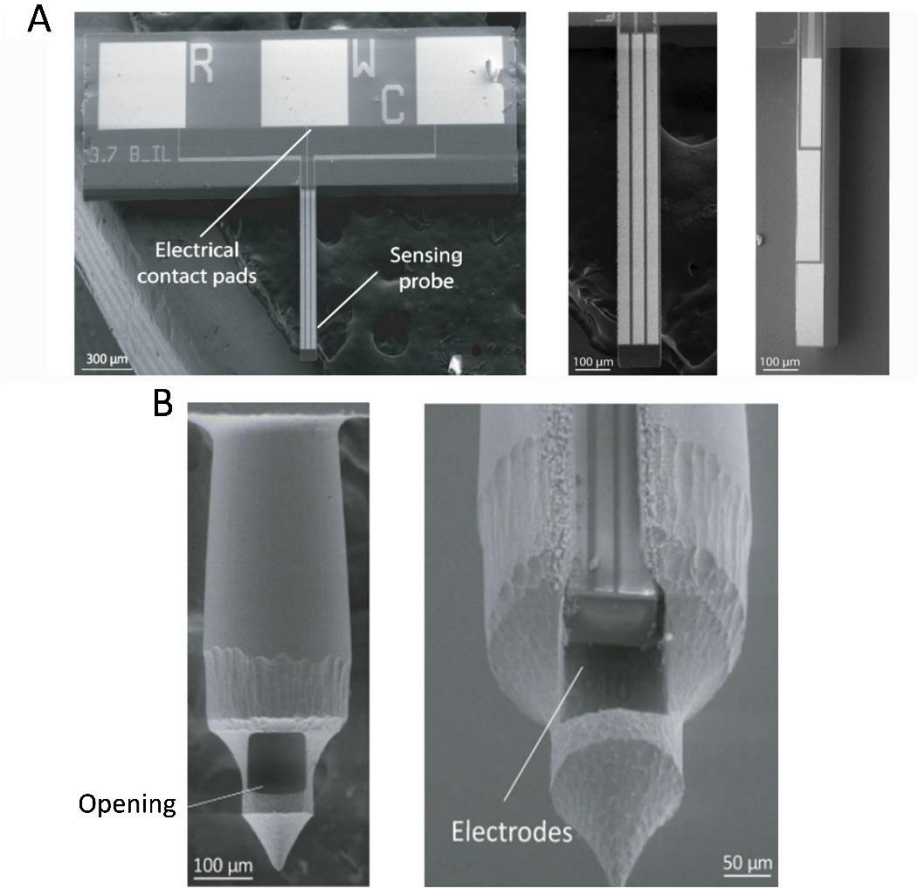

Figure 1.22: *(A) SEM of the T-shaped sensor, a magnified view of the parallel three electrode configuration and second version with a type with vertical three-electrode configuration (B) The silicon microneedle and an image of the three-electrode sensor within the lumen of the microneedle.*[108]

1.3.1.2 *Flexible electrochemical Biosensors*

1.3.1.2.1 Laser scribed graphene

Graphene fabrication techniques such as chemical vapour deposition, photolithography and laser ablation involve high temperature low-pressure requirements in addition to numerous processing steps. [119–121] Laser scribed graphene (LSG) also referred to as laser induced graphene, has been reported as an alternative to costly and complex graphene fabrication methods offering high-yield, mask-free, precise and cost-effective production. LSG has been fabricated on various substrates including polyimide (PI), wood, cloth,

potato skin and coconut shells.[122] Specifically for PI substrates, the formation of LSG is said to result from atomic rearrangements and photodissociative bond breaking caused by laser irradiation.[123] LSG is composed of a 3-D porous architecture rich in edge planes. The conductive and electrocatalyic properties of LSG has led to an interest in the materials use in electrochemical biosensors. Marques *et al.* reported a CO_2 laser cutting machine used to produce the dual electrode setup with silver conductive ink being applied to the connection tracks. One WE was modified for amoxicillin sensing and the second was modified for sensing ascorbic acid (see Figure 1.23). The amoxicillin sensor was modified via a PEDOT electropolymerisation of Eriochrome Black T. The biosensor demonstrated a linear response between 50 nM to 100 µM and an LOD of 11.98 nM. The ascorbic acid sensor was constructed by electropolymerisation of pyrrole in the presence of ascorbic acid in an electrolyte solution of $LiClO_4$. The resulting sensor displayed a linear response from 1.5 mM to 4 mM. Both electrodes demonstrated ascorbic acid and amoxicillin detection in water samples obtained from a well.[124]

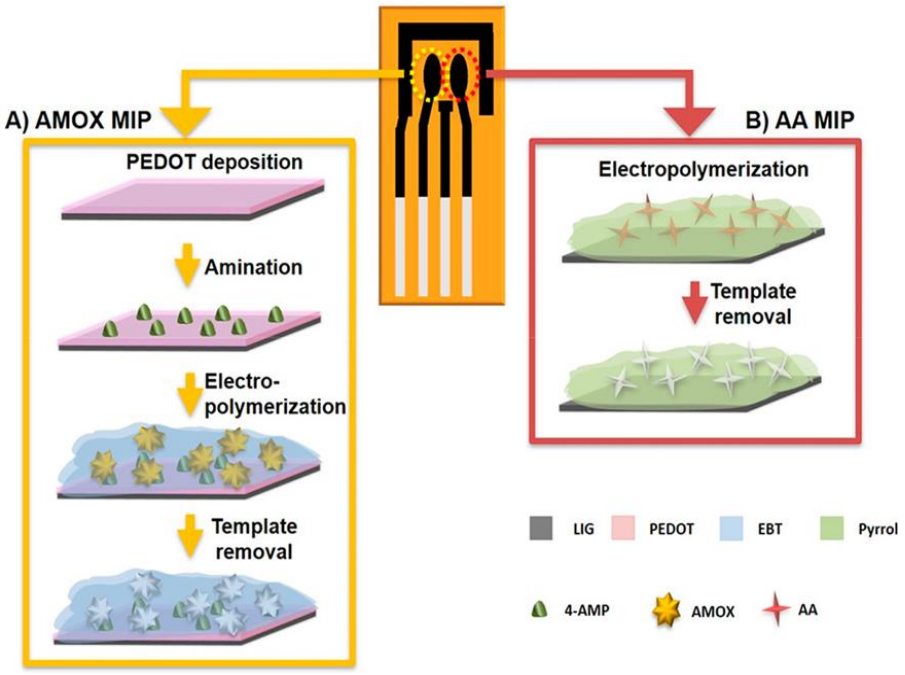

Figure 1.23: *Schematic representation of the dual-LIG device and MIPs fabrication workflow: (A) AMOX MIP fabrication comprises PEDOT deposition and amination steps followed by electropolymerisation around AMOX molecules and template removal. (B) AA MIP fabrication comprises the electropolymerisation step around AA molecules and template removal.*[124]

Raquel *et al.* reported another interesting application for LSG as an impedimetric immunosensor for the detection of *S. enterica* in food. A CO_2 laser was used to fabricate laser induced graphene electrodes onto polyimide films see Figure 1.24. A passivation (lacquer) was applied to the connection tracks to ensure that only the WE area was exposed. The WE was modified with Salmonella antibodies using EDC/NHS chemistry. The immunosensor demonstrated detection of salmonella in chicken broth samples with a linear range of 25 CFU mL^{-1} to 105 CFU mL^{-1} and an LOD of 13 ± 7 CFU mL^{-1}.[125]

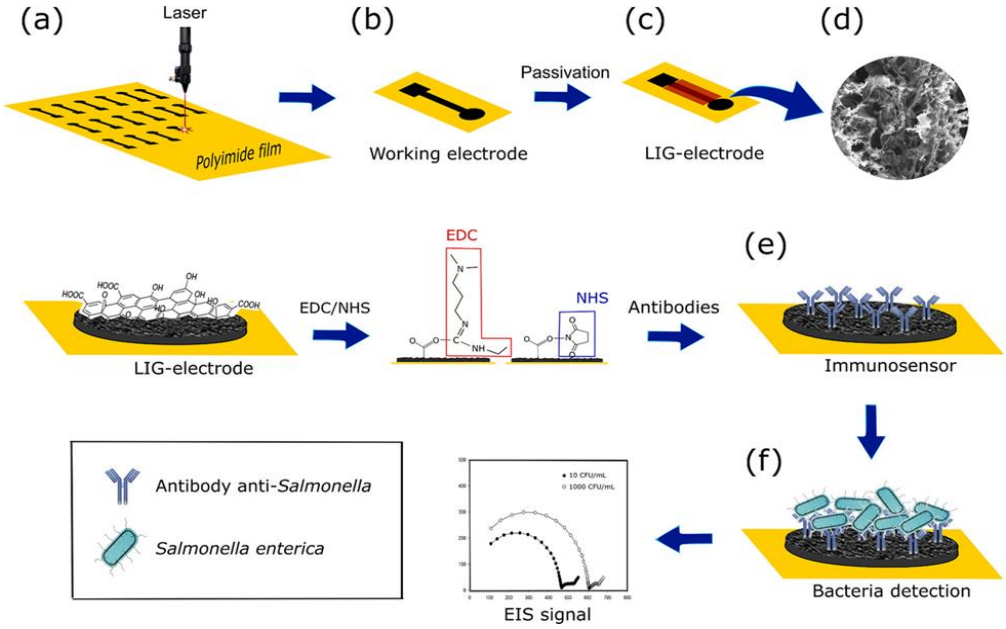

Figure 1.24: *Fabrication, biofunctionalization, and sensing scheme for the LIG based salmonella immunosensor.* [124]

Figure 1.25 displays a schematic of the materials involved in the construction of a wearable flexible sensor designed and constructed to measure lactate in sweat.[126] LSG electrodes were fabricated using a CO_2 laser (WE, RE and CE) on polyimide. The LSG was reinforced with a conductive binder poly (3, 4-ethylenedioxythiophene) (PEDOT). Prussian blue was anodically deposited onto the WE for 200 seconds. This was followed by drop casting a BSA/LOx mixture onto the WE. The RE was formed by painting Ag/AgCl ink onto the RE electrode using a stencil. Lastly, all three electrodes were encapsulated with a polycarbonate diffusion membrane. Since lactate levels in sweat can go up to 25 mM or higher, the PC layer was applied to increase the linear range for lactate detection.[127] The non-invasive lactate sensor was studied using amperometry. Lactate measurements were demonstrated in artificial sweat over a linear range of 0 to 18 mM. A sensitivity of 2.23 µA mM^{-1} was determined for the flexible lactate biosensor.

The three examples provided so far, described LSG electrodes fabricated using a CO_2 laser, alternative laser cutters such as UV visible and visible lasers have also demonstrated scribing of polyimide substrates.[128] Visible laser scribing provides a low cost alternative to expensive CO_2 lasers. Previous work in Tyndall has reported the use of a low cost laser for visible laser scribing of LSG electrodes.[129] In that study, polyimide was irradiated with a 450 nm laser under ambient conditions in a one-step process. The LSG electrodes consisted of highly porous 3D structures rich in defects and edge planes. The electrodes demonstrated lower ΔEp values 60.7 mV in $[Fe(CN)_6]^{3-/4-}$ in comparison with another visible scribed electrode (85.6 mV) and one fabricated by IR illumination (85.6 mV). LSG electrode performance was studied using CV and DPV for the detection of ascorbic acid, dopamine and uric acid. In this thesis, the low cost laser was used to produce a three-electrode configuration on PI for electrochemical characterisation and modification towards the construction of a flexible enzymatic lactate sensor. The results will be presented in chapter 3.

Figure 1.25: *Schematic of a flexible lactate sweat sensor fabricated on LSG.*[125]

1.3.1.2.2 Additive manufacturing techniques for electrode fabrication

As previously mentioned, another low cost fabrication technique of interest to the electrochemical sensor field is additive printing. This technology offers alternative fabrication and prototyping possibilities to the electrochemical biosensor research field. Similar to LSG fabrication, additive printing is an efficient and autonomous method of

producing electrodes. Additive printing can be used to fabricate electrodes from Au, Pt, C and Ag. Some attractive benefits of additive printing methods include the ability to customise electrodes, reduce costs owing to the requirement for less equipment and less material waste in contrast to typical microfabrication methods.[130,131]

In work carried out by Lopez Marzo *et al.,* a 3D-printed graphene/polylactic (PLA) electrode was fabricated using a fused deposition modelling (FDM) extrusion printer. Figure 1.26 shows a schematic representation of the sensor construction process. After printing, the graphene/PLA electrode was activated in dimethylformamide using both chemical and electrochemical processes. The electrodes were modified via two incubation steps, firstly with AuNPs followed by incubation with horseradish peroxidase (HRP). AuNPs improved the heterogeneous electron transfer, whilst HRP enabled an efficient DET for H_2O_2.[132] This report indicates the potential for the application of FDM printers to fabricate low cost electrochemical biosensors on demand.

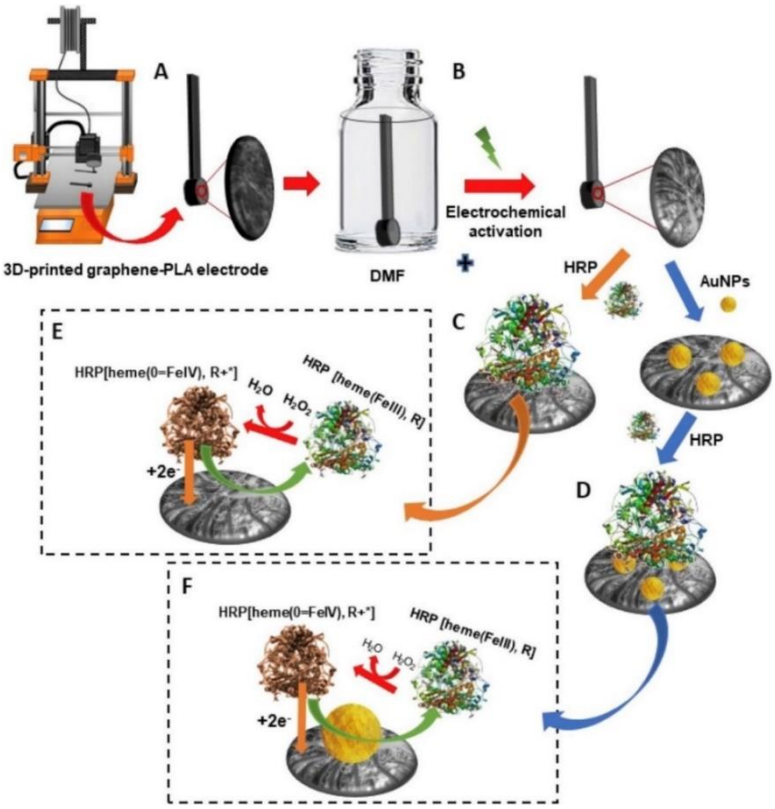

***Figure 1.26**: Schematic of the fabrication process for the 3D graphene-PLA biosensor (A) 3D-printer construction of the electrode; (B) DMF activation followed by electrochemical activation, (C) HRP enzyme modification of 3D-printed electrode and (D) AuNP and HRP enzyme modification of the 3D-printed electrode. (E) and (F) are corresponding mechanisms of H2O2 detection.*[130]

3-D printing has also contributed to the fabrication of electrochemical cell holders that can be tailored to the sensor depending on the final application.[133] An example of a recent study reported by Alachkar *et al.* described the use of a stereolithography 3D printer to fabricate a microfluidic device with openings for pencil graphite electrodes. The constructed microsyringe sensor device was used for amperometric measurements in artificial cerebrospinal fluid for dopamine concentrations.[134] The potential for printing of both the electrochemical sensor and the packaging or electrochemical cell holder component during the same printing process is an exciting possibility for biosensor research. Crapnell *et al*. recently reported an electrochemical cell and electrodes (WE, CE and RE) that were printed in a continuous manner removing the need to assemble the electrochemical cell and electrodes after printing. A dual extrusion printer (see Figure 1.27 A) was employed to print the electrochemical cell from PLA filament and each of the electrodes were printed using a conductive carbon black/PLA paste.[135] Figure 1.27 B-D shows the 3D printed cell with the carbon electrodes. The WE was electrochemically

activated in 50 mM NaOH by applying a potential of +1.4 V for 200 seconds followed by a potential of -1 V for 200 seconds. CV was applied to demonstrate the oxidation of both ascorbic acid and acetaminophen from solutions containing effervescent tablets.

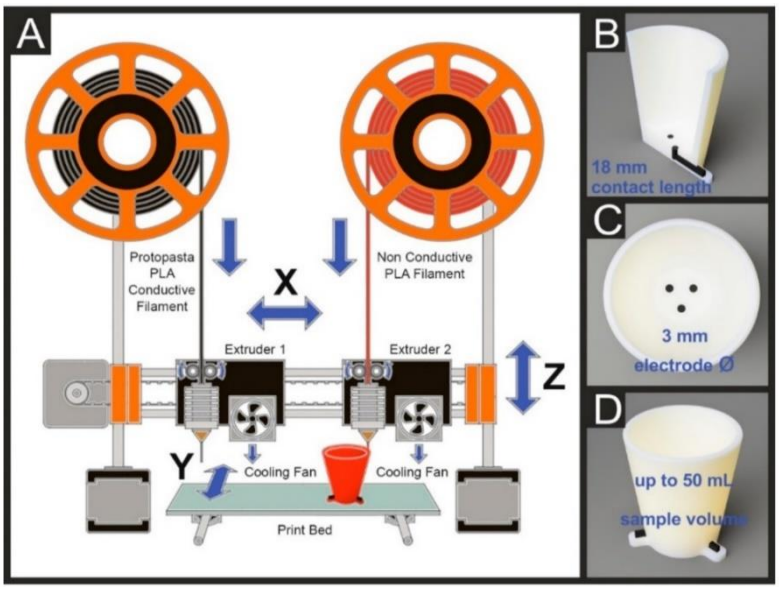

Figure 1.27: *(A) Schematic of the FFF printing of the AM all-in-one cell, the dual extruders 1 and 2 can be seen, one filled with conductive carbon black/PLA and the other loaded with non-conductive PLA. (B) CAD cut view of the printed cell (C) Top view of the cell showing the three electrodes (D) Side view of the cell, the connection points for the electrodes can be seen, designed to easily attach to standard crocodile clips.*[133]

In addition to standard printing on substrates, more complex structures have been produced for electrochemical sensor based research. A "ConceptLaser" printer was used to print metallic helical structures using the selective laser melting (SLM) technique. This involved the use of a high-energy laser beam that can fuse the steel particles as they are deposited in powder form under the instruction of the design. The helical spirals were then electroplated with gold (see Figure 1.28 A) and used in voltammetric studies for the detection of ascorbic acid and uric acid (see Figure 1.28 B). Helical sensor performance revealed an enhanced electrocatalytic performance when compared to the conventional GCE.[136]

The benefits of additive printing in the electrochemical sensor field are evident. Additive printing offers simplicity as a fabrication process and an ability to produce complex electrode designs in an efficient manner. Some limitations exist in this field, the compatibility between the selected ink and the printer of choice must be considered since printers often have a specification to which they operate. There is a limited number of

commercial conductive inks available. When using conductive polymer based inks the need for post-cleaning steps should be investigated to ensure that the polymer component of conductive inks are not limiting electron transfer. Furthermore, many of the high spec printers offering high resolution prints are not feasible for academic research owing to costs.

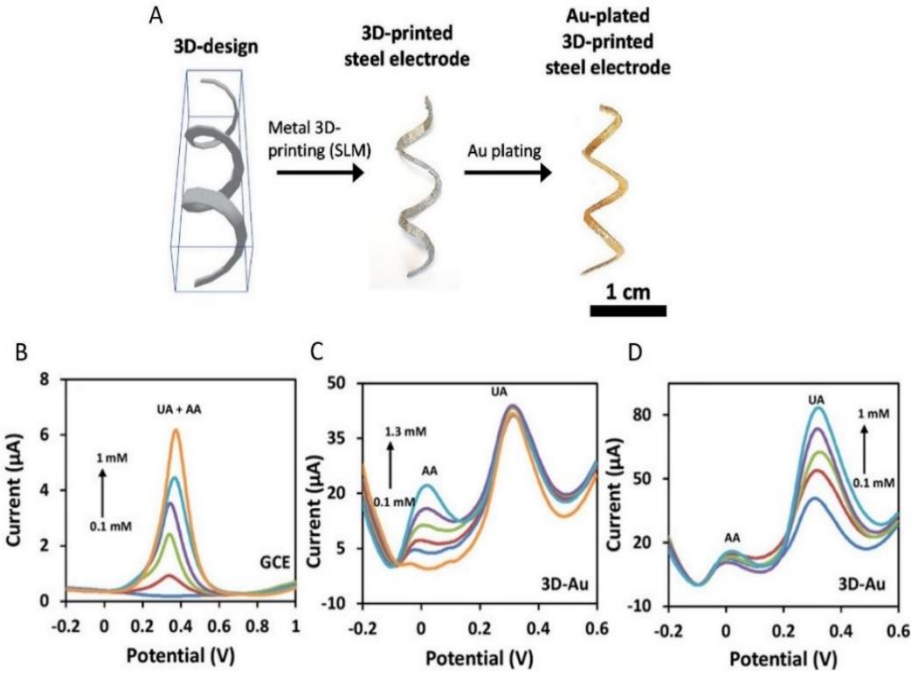

Figure 1.28: *(A) Schematic of the metal 3D-printed electrode fabrication and modification and (B) DPV profile of different concentration of UA with increasing concentration of AA in 0.1 M PBS (pH 7.2) on GCE. (C) DPV profile of 0.1 mM UA with different concentrations of AA in 0.1 M PBS (pH 7.2) on 3D-printed Au electrode. (D) DPV profile of 0.1 mM AA with different concentration of UA in 0.1 M PBS (pH 7.2) on the 3D-printed Au electrode.*[134]

The field of electrochemical biosensors has seen significant developments over the last number of decades; we have observed the construction of electrochemical sensors on low-cost polymer or paper based sensor devices, wearable technologies for both skin and skin interstitial fluid detection and the arrival of the commercial continuous glucose monitoring devices. With continuous advances in fabrication techniques, additional opportunities exist to explore and attempt to further progress sensor platforms. The focus of this PhD work was to develop and study electrochemical sensors constructed on electrodes fabricated using three separate electrode fabrication technologies: silicon microfabrication, laser scribing polyimide substrates with graphene and additive printing of electrodes on polyimide.

1.4 Scope and Organisation of Thesis

Chapter 2 describes the fabrication, characterisation and modification of gold microband electrodes on silicon using standard microfabrication methods, i.e., lithography and etching techniques. Understanding the electrochemical behaviour of miniaturized electrodes on devices is becoming increasingly important as advances continue towards integrating microelectrodes on wearable, surgical, and other medical devices. A two-step electrodeposition process was carried out using the on-chip platinum reference and gold counter electrodes, entrapping GOx onto a platinum-modified, gold microband electrode with an o-phenylenediamine and ß-cyclodextrin mixture. The on-chip single microband glucose sensor was examined in buffer and serum solutions using an on-chip CE and RE. Chapter 3 describes the fabrication of a flexible lactate sensor using a low cost visible laser-scribing fabrication process with a 450 nm laser. The laser-scribed graphite was functionalized via electrodeposition of platinum, followed by two drop-casting steps with chitosan and LOx. Sensor performance was examined in diluted human serum and artificial saliva. The resulting flexible biosensor was 'bent' at a curvature, K of 0.14 mm^{-1} to demonstrate aerometric lactate measurements in a 'bent' configuration. Chapter 4 describes the fabrication and characterization of gold electrodes onto flexible polyimide films using a low-cost dispense printer and commercial gold polymer inks produced from a gold and thermoplastic resin mixture. Polyimide was chosen as the substrate owing to the increased interest in flexible, wearable and low cost solutions for electrochemical sensor devices. The design selected was chosen on the basis of creating a three electrode sensor. A low cost PCB printer was examined as a sensor fabrication tool by assessing the reproducibility between fabricated electrodes from a geometrical and electrochemical analysis perspective. Finally, Chapter 5 provides a summary of the main results of this thesis and explores how the biosensors presented in this study could be further advanced for future electrochemical analysis applications.

1.5 References

(1) GlobalData Healthcare. *The continuous glucose monitors market grows rapidly due to fast customer adoption*. The continuous glucose monitors market grows rapidly due to fast customer adoption. https://www.medicaldevice-network.com/comment/continuous-glucose-monitors-market-customer-adoption/.

(2) Clavel, P.; Tiollier, E.; Leduc, C.; Fabre, M.; Lacome, M.; Buchheit, M. Concurrent Validity of a Continuous Glucose-Monitoring System at Rest and During and Following a High-Intensity Interval Training Session. *International Journal of Sports Physiology and Performance* **2022**, *17* (4), 627–633. https://doi.org/10.1123/ijspp.2021-0222.

(3) Holzer, R.; Bloch, W.; Brinkmann, C. Continuous Glucose Monitoring in Healthy Adults—Possible Applications in Health Care, Wellness, and Sports. *Sensors* **2022**, *22* (5), 2030. https://doi.org/10.3390/s22052030.

(4) Bakker, J.; Nijsten, M. W.; Jansen, T. C. Clinical Use of Lactate Monitoring in Critically Ill Patients. *Ann Intensive Care* **2013**, *3* (1), 12. https://doi.org/10.1186/2110-5820-3-12.

(5) Bakker, J.; Gris, P.; Coffernils, M.; Kahn, R. J.; Vincent, J.-L. Serial Blood Lactate Levels Can Predict the Development of Multiple Organ Failure Following Septic Shock. *The American Journal of Surgery* **1996**, *171* (2), 221–226. https://doi.org/10.1016/S0002-9610(97)89552-9.

(6) Bellomo, R. Bench-to-Bedside Review: Lactate and the Kidney. *Crit Care* **2002**, *6* (4), 322. https://doi.org/10.1186/cc1518.

(7) Beneke, R.; Leithäuser, R. M.; Ochentel, O. Blood Lactate Diagnostics in Exercise Testing and Training. *International Journal of Sports Physiology and Performance* **2011**, *6* (1), 8–24. https://doi.org/10.1123/ijspp.6.1.8.

(8) Faude, O.; Kindermann, W.; Meyer, T. Lactate Threshold Concepts: How Valid Are They? *Sports Medicine* **2009**, *39* (6), 469–490. https://doi.org/10.2165/00007256-200939060-00003.

(9) Goodwin, M. L.; Harris, J. E.; Hernández, A.; Gladden, L. B. Blood Lactate Measurements and Analysis during Exercise: A Guide for Clinicians. *J Diabetes Sci Technol* **2007**, *1* (4), 558–569. https://doi.org/10.1177/193229680700100414.

(10) Bard, A. J.; Faulkner, L. R. Ch Introduction and Overview of Electrode Processes. In *Electrochemical Methods: Fundamentals and Applications*; Wiley: New York, 2001; pp 1–43.

(11) Scherer, G. G. Fuel Cell Fuel Cell Types Fuel Cell Types and Their Electrochemistry Fuel Cell Electrochemistry. In *Encyclopedia of Sustainability Science and Technology*; Meyers, R. A., Ed.; Springer New York: New York, NY, 2012; pp 3872–3886. https://doi.org/10.1007/978-1-4419-0851-3_132.

(12) Crow, D. R. *Principles and Applications of Electrochemistry*.

(13) Bard, A. J.; Faulkner, L. R. Ch Introduction and Overview of Electrode Processes. In *Electrochemical Methods: Fundamentals and Applications*; Wiley: New York, 2001; pp 87–136.

(14) Smith, T. J.; Stevenson, K. J. Reference Electrodes. In *Handbook of Electrochemistry*; 2007; pp 73–110.

(15) Brett, C. M. A.; Brett, A. M. O. *Electroanalysis*; Oxford chemistry primers; Oxford Universisty Press: Oxford ; New York, 1998.

(16) Dawson, K.; Wahl, A.; Barry, S.; Barrett, C.; Sassiat, N.; Quinn, A. J.; O'Riordan, A. Fully Integrated On-Chip Nano-Electrochemical Devices for Electroanalytical

Applications. *Electrochimica Acta* **2014**, *115*, 239–246. https://doi.org/10.1016/j.electacta.2013.10.144.

(17) Zhao, Z.; Tu, H.; Kim, E. G. R.; Sloane, B. F.; Xu, Y. A Flexible Ag/AgCl Micro Reference Electrode Based on a Parylene Tube Structure. *Sensors and Actuators B: Chemical* **2017**, *247*, 92–97. https://doi.org/10.1016/j.snb.2017.02.135.

(18) Nagle, L. C.; Wahl, A.; Ogourstov, V.; Seymour, I.; Barry, F.; Rohan, J. F.; Mac Loughlin, R. Electrochemical Discrimination of Salbutamol from Its Excipients in VentolinTM at Nanoporous Gold Microdisc Arrays. *Sensors* **2021**, *21* (12), 3975. https://doi.org/10.3390/s21123975.

(19) Therese, G. H. A.; Kamath, P. V. Electrochemical Synthesis of Metal Oxides and Hydroxides. *Chem. Mater.* **2000**, *12* (5), 1195–1204. https://doi.org/10.1021/cm990447a.

(20) Benke, G.; Gnot, W. The Electrochemical Dissolution of Platinum. *Hydrometallurgy* **2002**, *64* (3), 205–218. https://doi.org/10.1016/S0304-386X(02)00044-0.

(21) Bao, D.; Millare, B.; Xia, W.; Steyer, B. G.; Gerasimenko, A. A.; Ferreira, A.; Contreras, A.; Vullev, V. I. Electrochemical Oxidation of Ferrocene: A Strong Dependence on the Concentration of the Supporting Electrolyte for Nonpolar Solvents. *J. Phys. Chem. A* **2009**, *113* (7), 1259–1267. https://doi.org/10.1021/jp809105f.

(22) Carmo, M.; Fritz, D. L.; Mergel, J.; Stolten, D. A Comprehensive Review on PEM Water Electrolysis. *International Journal of Hydrogen Energy* **2013**, *38* (12), 4901–4934. https://doi.org/10.1016/j.ijhydene.2013.01.151.

(23) Ciobanu, M.; Wilburn, J.; Krim, M. L.; Cliffel, D. E. Part 1 Fundamentals. In *Handbook of Electrochemistry*; Elsevier, 2007; pp 3–11.

(24) Koryta, J.; Dvořák, J.; Kavan, L. *Principles of Electrochemistry*, 2nd ed.; Wiley: Chichester ; New York, 1993.

(25) Reddy, A. K. N.; Bockris, J. O., Gamboa-Aldeco, Maria E. *Modern Electrochemistry*; Plenum Press: New York, 1998.

(26) Oldham, K. B. A Gouy–Chapman–Stern Model of the Double Layer at a (Metal)/(Ionic Liquid) Interface. *Journal of Electroanalytical Chemistry* **2008**, *613* (2), 131–138. https://doi.org/10.1016/j.jelechem.2007.10.017.

(27) Bard, A. J.; Faulkner, L. R. Ch Introduction and Overview of Electrode Processes. In *Electrochemical Methods: Fundamentals and Applications*; Wiley: New York, 2001; pp 44–86.

(28) Elgrishi, N.; Rountree, K. J.; McCarthy, B. D.; Rountree, E. S.; Eisenhart, T. T.; Dempsey, J. L. A Practical Beginner's Guide to Cyclic Voltammetry. *J. Chem. Educ.* **2018**, *95* (2), 197–206. https://doi.org/10.1021/acs.jchemed.7b00361.

(29) *Handbook of Electrochemistry*, 1st ed.; Zoski, C. G., Ed.; Elsevier: Amsterdam ; Boston, 2007.

(30) Wang, J. *Analytical Electrochemistry: Wang/Analytical Electrochemistry, Third Edition*; John Wiley & Sons, Inc.: Hoboken, NJ, USA, 2006. https://doi.org/10.1002/0471790303.

(31) Forster, R. J.; Keyes, T. E. Part 6 Ultramicroelectrodes. In *Handbook of Electrochemistry*; Elsevier, 2007; pp 155–171.

(32) Fletcher, B. L.; Fern, J. T.; Rhodes, K.; McKnight, T. E.; Fowlkes, J. D.; Retterer, S. T.; Keffer, D. J.; Simpson, M. L.; Doktycz, M. J. Effects of Ultramicroelectrode Dimensions on the Electropolymerization of Polypyrrole. *Journal of Applied Physics* **2009**, *105* (12), 124312. https://doi.org/10.1063/1.3152633.

(33) Bard, A. J.; Faulkner, L. R. Ch 5 Basic Potential Step Methods. In *Electrochemical Methods: Fundamentals and Applications*; Wiley: New York, 2001; pp 156–225.
(34) Grieshaber, D.; MacKenzie, R.; Vörös, J.; Reimhult, E. Electrochemical Biosensors - Sensor Principles and Architectures. *Sensors* **2008**, *8* (3), 1400–1458. https://doi.org/10.3390/s80314000.
(35) Palchetti, I.; Mascini, M. Biosensor Technology: A Brief History. In *Sensors and Microsystems*; Malcovati, P., Baschirotto, A., d'Amico, A., Natale, C., Eds.; Lecture Notes in Electrical Engineering; Springer Netherlands: Dordrecht, 2010; Vol. 54, pp 15–23. https://doi.org/10.1007/978-90-481-3606-3_2.
(36) Clark, L. C.; Lyons, C. ELECTRODE SYSTEMS FOR CONTINUOUS MONITORING IN CARDIOVASCULAR SURGERY. *Annals of the New York Academy of Sciences* **2006**, *102* (1), 29–45. https://doi.org/10.1111/j.1749-6632.1962.tb13623.x.
(37) McAteer, K.; O'Neill, R. D. Strategies for Decreasing Ascorbate Interference at Glucose Oxidase-Modified Poly(o-Phenylenediamine)-Coated Electrodes. *Analyst* **1996**, *121* (6), 773. https://doi.org/10.1039/an9962100773.
(38) Scholten, K.; Meng, E. A Review of Implantable Biosensors for Closed-Loop Glucose Control and Other Drug Delivery Applications. *International Journal of Pharmaceutics* **2018**, *544* (2), 319–334. https://doi.org/10.1016/j.ijpharm.2018.02.022.
(39) Matsumoto, T.; Ohashi, A.; Ito, N.; Fujiwara, H.; Matsumoto, T. A Long-Term Lifetime Amperometric Glucose Sensor with a Perfluorocarbon Polymer Coating. *Biosensors and Bioelectronics* **2001**, *16* (4–5), 271–276. https://doi.org/10.1016/S0956-5663(01)00139-7.
(40) Newman, J. D.; Turner, A. P. F. Home Blood Glucose Biosensors: A Commercial Perspective. *Biosensors and Bioelectronics* **2005**, *20* (12), 2435–2453. https://doi.org/10.1016/j.bios.2004.11.012.
(41) Teymourian, H.; Barfidokht, A.; Wang, J. Electrochemical Glucose Sensors in Diabetes Management: An Updated Review (2010–2020). *Chem. Soc. Rev.* **2020**, *49* (21), 7671–7709. https://doi.org/10.1039/D0CS00304B.
(42) Wang, J. Electrochemical Glucose Biosensors. *Chem. Rev.* **2008**, *108* (2), 814–825. https://doi.org/10.1021/cr068123a.
(43) Matsunaga, T.; Karube, I.; Teraoka, N.; Suzuki, S. Determination of Cell Numbers of Lactic Acid Producing Bacteria by Lactate Sensor. *European J. Appl. Microbiol. Biotechnol.* **1982**, *16* (2–3), 157–160. https://doi.org/10.1007/BF00500746.
(44) Palleschi, G.; Turner, A. P. F. Amperometric Tetrathiafulvalene-Mediated Lactate Electrode Using Lactate Oxidase Absorbed on Carbon Foil. *Analytica Chimica Acta* **1990**, *234*, 459–463. https://doi.org/10.1016/S0003-2670(00)83591-6.
(45) Clark, L. C.; Noyes, L. K.; Grooms, T. A.; Moore, M. S. Rapid Micromeasurement of Lactate in Whole Blood: *Critical Care Medicine* **1984**, *12* (5), 461–464. https://doi.org/10.1097/00003246-198405000-00011.
(46) Romero, M. R.; Ahumada, F.; Garay, F.; Baruzzi, A. M. Amperometric Biosensor for Direct Blood Lactate Detection. *Anal. Chem.* **2010**, *82* (13), 5568–5572. https://doi.org/10.1021/ac1004426.
(47) Alam, F.; RoyChoudhury, S.; Jalal, A. H.; Umasankar, Y.; Forouzanfar, S.; Akter, N.; Bhansali, S.; Pala, N. Lactate Biosensing: The Emerging Point-of-Care and Personal Health Monitoring. *Biosensors and Bioelectronics* **2018**, *117*, 818–829. https://doi.org/10.1016/j.bios.2018.06.054.
(48) Cass, A. E. G.; Davis, Graham.; Francis, G. D.; Hill, H. A. O.; Aston, W. J.; Higgins, I. John.; Plotkin, E. V.; Scott, L. D. L.; Turner, A. P. F. Ferrocene-

Mediated Enzyme Electrode for Amperometric Determination of Glucose. *Anal. Chem.* **1984**, *56* (4), 667–671. https://doi.org/10.1021/ac00268a018.

(49) Rathee, K.; Dhull, V.; Dhull, R.; Singh, S. Biosensors Based on Electrochemical Lactate Detection: A Comprehensive Review. *Biochemistry and Biophysics Reports* **2016**, *5*, 35–54. https://doi.org/10.1016/j.bbrep.2015.11.010.

(50) van Oldruitenborgh-Oosterbaan, M. M. S.; van den Broek, E. T. W.; Spierenburg, A. J. Evaluation of the Usefulness of the Portable Device Lactate Pro for Measurement of Lactate Concentrations in Equine Whole Blood. *J VET Diagn Invest* **2008**, *20* (1), 83–85. https://doi.org/10.1177/104063870802000117.

(51) Halpin, G.; Herdman, K.; Dempsey, E. Electrochemical Investigations into Enzymatic Polymerisation of 1,10-Phenanthroline-5,6-Dione as a Redox Mediator for Lactate Sensing. *Sensors and Actuators Reports* **2021**, *3*, 100032. https://doi.org/10.1016/j.snr.2021.100032.

(52) Pereira, A. C.; Kisner, A.; Tarley, C. R. T.; Kubota, L. T. Development of a Carbon Paste Electrode for Lactate Detection Based on Meldola's Blue Adsorbed on Silica Gel Modified with Niobium Oxide and Lactate Oxidase. *Electroanalysis* **2011**, *23* (6), 1470–1477. https://doi.org/10.1002/elan.201000709.

(53) Marzouk, S. A. M.; Cosofret, V. V.; Buck, R. P.; Yang, H.; Cascio, W. E.; Hassan, S. S. M. A Conducting Salt-Based Amperometric Biosensor for Measurement of Extracellular Lactate Accumulation in Ischemic Myocardium. *Anal. Chem.* **1997**, *69* (14), 2646–2652. https://doi.org/10.1021/ac970020s.

(54) Hiraka, K.; Kojima, K.; Tsugawa, W.; Asano, R.; Ikebukuro, K.; Sode, K. Rational Engineering of Aerococcus Viridans L-Lactate Oxidase for the Mediator Modification to Achieve Quasi-Direct Electron Transfer Type Lactate Sensor. *Biosensors and Bioelectronics* **2020**, *151*, 111974. https://doi.org/10.1016/j.bios.2019.111974.

(55) Sardesai, N. P.; Ganesana, M.; Karimi, A.; Leiter, J. C.; Andreescu, S. Platinum-Doped Ceria Based Biosensor for *in Vitro* and *in Vivo* Monitoring of Lactate during Hypoxia. *Anal. Chem.* **2015**, *87* (5), 2996–3003. https://doi.org/10.1021/ac5047455.

(56) Balasubramanian, P.; Annalakshmi, M.; Chen, S.-M.; Chen, T.-W. Ultrasensitive Non-Enzymatic Electrochemical Sensing of Glucose in Noninvasive Samples Using Interconnected Nanosheets-like NiMnO3 as a Promising Electrocatalyst. *Sensors and Actuators B: Chemical* **2019**, *299*, 126974. https://doi.org/10.1016/j.snb.2019.126974.

(57) Juvenile Diabetes Research Foundation Continuous Glucose Monitoring Study Group. Variation of Interstitial Glucose Measurements Assessed by Continuous Glucose Monitors in Healthy, Nondiabetic Individuals. *Diabetes Care* **2010**, *33* (6), 1297–1299. https://doi.org/10.2337/dc09-1971.

(58) Schabmueller, C. G. J.; Loppow, D.; Piechotta, G.; Schütze, B.; Albers, J.; Hintsche, R. Micromachined Sensor for Lactate Monitoring in Saliva. *Biosensors and Bioelectronics* **2006**, *21* (9), 1770–1776. https://doi.org/10.1016/j.bios.2005.09.015.

(59) Gupta, S.; Sandhu, S. V.; Bansal, H.; Sharma, D. Comparison of Salivary and Serum Glucose Levels in Diabetic Patients. *J Diabetes Sci Technol* **2015**, *9* (1), 91–96. https://doi.org/10.1177/1932296814552673.

(60) Lin, C.-E.; Hiraka, K.; Matloff, D.; Johns, J.; Deng, A.; Sode, K.; La Belle, J. Development toward a Novel Integrated Tear Lactate Sensor Using Schirmer Test Strip and Engineered Lactate Oxidase. *Sensors and Actuators B: Chemical* **2018**, *270*, 525–529. https://doi.org/10.1016/j.snb.2018.05.061.

(61) Bruen, D.; Delaney, C.; Florea, L.; Diamond, D. Glucose Sensing for Diabetes Monitoring: Recent Developments. *Sensors* **2017**, *17* (8), 1866. https://doi.org/10.3390/s17081866.

(62) Heikenfeld, J.; Jajack, A.; Feldman, B.; Granger, S. W.; Gaitonde, S.; Begtrup, G.; Katchman, B. A. Accessing Analytes in Biofluids for Peripheral Biochemical Monitoring. *Nat Biotechnol* **2019**, *37* (4), 407–419. https://doi.org/10.1038/s41587-019-0040-3.

(63) Lee, H.; Song, C.; Hong, Y. S.; Kim, M. S.; Cho, H. R.; Kang, T.; Shin, K.; Choi, S. H.; Hyeon, T.; Kim, D.-H. Wearable/Disposable Sweat-Based Glucose Monitoring Device with Multistage Transdermal Drug Delivery Module. *Sci. Adv.* **2017**, *3* (3), e1601314. https://doi.org/10.1126/sciadv.1601314.

(64) Abbott. *ABBOTT ANNOUNCES FUTURE OF BIOWEARABLES AT CONSUMER ELECTRONICS SHOW*. PRESS RELEASES. https://abbott.mediaroom.com/2022-01-06-Abbott-Announces-Future-of-Biowearables-at-Consumer-Electronics-Show.

(65) Gu, S.; Lu, Y.; Ding, Y.; Li, L.; Song, H.; Wang, J.; Wu, Q. A Droplet-Based Microfluidic Electrochemical Sensor Using Platinum-Black Microelectrode and Its Application in High Sensitive Glucose Sensing. *Biosensors and Bioelectronics* **2014**, *55*, 106–112. https://doi.org/10.1016/j.bios.2013.12.002.

(66) Harrison, D. Jed.; Turner, R. F. B.; Baltes, H. P. Characterization of Perfluorosulfonic Acid Polymer Coated Enzyme Electrodes and a Miniaturized Integrated Potentiostat for Glucose Analysis in Whole Blood. *Anal. Chem.* **1988**, *60* (19), 2002–2007. https://doi.org/10.1021/ac00170a003.

(67) Yang, Z.; Cao, Y.; Li, J.; Jian, Z.; Zhang, Y.; Hu, X. Platinum Nanoparticles Functionalized Nitrogen Doped Graphene Platform for Sensitive Electrochemical Glucose Biosensing. *Analytica Chimica Acta* **2015**, *871*, 35–42. https://doi.org/10.1016/j.aca.2015.02.029.

(68) Gamero, M.; Pariente, F.; Lorenzo, E.; Alonso, C. Nanostructured Rough Gold Electrodes for the Development of Lactate Oxidase-Based Biosensors. *Biosensors and Bioelectronics* **2010**, *25* (9), 2038–2044. https://doi.org/10.1016/j.bios.2010.01.032.

(69) Lourenço, C. F.; Caetano, M.; Ledo, A.; Barbosa, R. M. Platinized Carbon Fiber-Based Glucose Microbiosensor Designed for Metabolic Studies in Brain Slices. *Bioelectrochemistry* **2019**, *130*, 107325. https://doi.org/10.1016/j.bioelechem.2019.06.010.

(70) Faruk Hossain, M.; Slaughter, G. Flexible Electrochemical Uric Acid and Glucose Biosensor. *Bioelectrochemistry* **2021**, *141*, 107870. https://doi.org/10.1016/j.bioelechem.2021.107870.

(71) Pei, Y.; Zhang, X.; Hui, Z.; Zhou, J.; Huang, X.; Sun, G.; Huang, W. Ti3C2TX MXene for Sensing Applications: Recent Progress, Design Principles, and Future Perspectives. *ACS Nano* **2021**, *15* (3), 3996–4017. https://doi.org/10.1021/acsnano.1c00248.

(72) Neampet, S.; Ruecha, N.; Qin, J.; Wonsawat, W.; Chailapakul, O.; Rodthongkum, N. A Nanocomposite Prepared from Platinum Particles, Polyaniline and a Ti3C2 MXene for Amperometric Sensing of Hydrogen Peroxide and Lactate. *Microchim Acta* **2019**, *186* (12), 752. https://doi.org/10.1007/s00604-019-3845-3.

(73) Yu, H.; Yu, J.; Li, L.; Zhang, Y.; Xin, S.; Ni, X.; Sun, Y.; Song, K. Recent Progress of the Practical Applications of the Platinum Nanoparticle-Based Electrochemistry Biosensors. *Front. Chem.* **2021**, *9*, 677876. https://doi.org/10.3389/fchem.2021.677876.

(74) Wahab, R. A.; Elias, N.; Abdullah, F.; Ghoshal, S. K. On the Taught New Tricks of Enzymes Immobilization: An All-Inclusive Overview. *Reactive and Functional Polymers* **2020**, *152*, 104613. https://doi.org/10.1016/j.reactfunctpolym.2020.104613.

(75) Hanefeld, U.; Cao, L.; Magner, E. Enzyme Immobilisation: Fundamentals and Application. *Chem. Soc. Rev.* **2013**, *42* (15), 6211. https://doi.org/10.1039/c3cs90042h.

(76) Homaei, A. A.; Sariri, R.; Vianello, F.; Stevanato, R. Enzyme Immobilization: An Update. *J Chem Biol* **2013**, *6* (4), 185–205. https://doi.org/10.1007/s12154-013-0102-9.

(77) Sassolas, A.; Blum, L. J.; Leca-Bouvier, B. D. Immobilization Strategies to Develop Enzymatic Biosensors. *Biotechnology Advances* **2012**, *30* (3), 489–511. https://doi.org/10.1016/j.biotechadv.2011.09.003.

(78) Jesionowski, T.; Zdarta, J.; Krajewska, B. Enzyme Immobilization by Adsorption: A Review. *Adsorption* **2014**, *20* (5–6), 801–821. https://doi.org/10.1007/s10450-014-9623-y.

(79) Mohamad, N. R.; Marzuki, N. H. C.; Buang, N. A.; Huyop, F.; Wahab, R. A. An Overview of Technologies for Immobilization of Enzymes and Surface Analysis Techniques for Immobilized Enzymes. *Biotechnology & Biotechnological Equipment* **2015**, *29* (2), 205–220. https://doi.org/10.1080/13102818.2015.1008192.

(80) Wang, R.; Zhai, Q.; An, T.; Gong, S.; Cheng, W. Stretchable Gold Fiber-Based Wearable Textile Electrochemical Biosensor for Lactate Monitoring in Sweat. *Talanta* **2021**, *222*, 121484. https://doi.org/10.1016/j.talanta.2020.121484.

(81) Park, J.; Sempionatto, J. R.; Kim, J.; Jeong, Y.; Gu, J.; Wang, J.; Park, I. Microscale Biosensor Array Based on Flexible Polymeric Platform toward Lab-on-a-Needle: Real-Time Multiparameter Biomedical Assays on Curved Needle Surfaces. *ACS Sens.* **2020**, *5* (5), 1363–1373. https://doi.org/10.1021/acssensors.0c00078.

(82) Myler, S.; Eaton, S.; Higson, S. P. J. Poly(o-Phenylenediamine) Ultra-Thin Polymer-Film Composite Membranes for Enzyme Electrodes. *Analytica Chimica Acta* **1997**, *357* (1–2), 55–61. https://doi.org/10.1016/S0003-2670(97)00558-8.

(83) Malitesta, Cosimino.; Palmisano, Francesco.; Torsi, Luisa.; Zambonin, P. Giorgio. Glucose Fast-Response Amperometric Sensor Based on Glucose Oxidase Immobilized in an Electropolymerized Poly(o-Phenylenediamine) Film. *Anal. Chem.* **1990**, *62* (24), 2735–2740. https://doi.org/10.1021/ac00223a016.

(84) Rhemrev-Boom, M. M.; Jonker, M. A.; Venema, K.; Tiessen, R.; Korf, J.; Jobst, G. On-Line Continuous Monitoring of Glucose or Lactate by Ultraslow Microdialysis Combined with a Flow-through Nanoliter Biosensor Based on Poly(m-Phenylenediamine) Ultra-Thin Polymer Membrane as Enzyme Electrode. *Analyst* **2001**, *126* (7), 1073–1079. https://doi.org/10.1039/b100452m.

(85) Dempsey, E. Electropolymerised O-Phenylenediamine Film as Means of Immobilising Lactate Oxidase for a L-Lactate Biosensor. *Talanta* **1993**, *40* (3), 445–451. https://doi.org/10.1016/0039-9140(93)80257-R.

(86) Lobo-Castañón, M. J.; Miranda-Ordieres, A. J.; Tuñón-Blanco, P. A Bienzyme-Poly-(o-Phenylenediamine)-Modified Carbon Paste Electrode for the Amperometric Detection of l-Lactate. *Analytica Chimica Acta* **1997**, *346* (2), 165–174. https://doi.org/10.1016/S0003-2670(97)00115-3.

(87) Ganesana, M.; Trikantzopoulos, E.; Maniar, Y.; Lee, S. T.; Venton, B. J. Development of a Novel Micro Biosensor for in Vivo Monitoring of Glutamate

Release in the Brain. *Biosensors and Bioelectronics* **2019**, *130*, 103–109. https://doi.org/10.1016/j.bios.2019.01.049.

(88) Carelli, D.; Centonze, D.; De Giglio, A.; Quinto, M.; Zambonin, P. G. An Interference-Free First Generation Alcohol Biosensor Based on a Gold Electrode Modified by an Overoxidised Non-Conducting Polypyrrole Film. *Analytica Chimica Acta* **2006**, *565* (1), 27–35. https://doi.org/10.1016/j.aca.2006.02.023.

(89) Turkmen, E.; Bas, S. Z.; Gulce, H.; Yildiz, S. Glucose Biosensor Based on Immobilization of Glucose Oxidase in Electropolymerized Poly(o-Phenylenediamine) Film on Platinum Nanoparticles-Polyvinylferrocenium Modified Electrode. *Electrochimica Acta* **2014**, *123*, 93–102. https://doi.org/10.1016/j.electacta.2013.12.189.

(90) Li, J.; Koinkar, P.; Fuchiwaki, Y.; Yasuzawa, M. A Fine Pointed Glucose Oxidase Immobilized Electrode for Low-Invasive Amperometric Glucose Monitoring. *Biosensors and Bioelectronics* **2016**, *86*, 90–94. https://doi.org/10.1016/j.bios.2016.06.037.

(91) Vaddiraju, S.; Burgess, D. J.; Jain, F. C.; Papadimitrakopoulos, F. The Role of H2O2 Outer Diffusion on the Performance of Implantable Glucose Sensors. *Biosensors and Bioelectronics* **2009**, *24* (6), 1557–1562. https://doi.org/10.1016/j.bios.2008.08.015.

(92) Kim, J.; Valdés-Ramírez, G.; Bandodkar, A. J.; Jia, W.; Martinez, A. G.; Ramírez, J.; Mercier, P.; Wang, J. Non-Invasive Mouthguard Biosensor for Continuous Salivary Monitoring of Metabolites. *Analyst* **2014**, *139* (7), 1632–1636. https://doi.org/10.1039/C3AN02359A.

(93) Feng, D.; Wang, F.; Chen, Z. Electrochemical Glucose Sensor Based on One-Step Construction of Gold Nanoparticle–Chitosan Composite Film. *Sensors and Actuators B: Chemical* **2009**, *138* (2), 539–544. https://doi.org/10.1016/j.snb.2009.02.048.

(94) Wu, L.-Q.; Lee, K.; Wang, X.; English, D. S.; Losert, W.; Payne, G. F. Chitosan-Mediated and Spatially Selective Electrodeposition of Nanoscale Particles. *Langmuir* **2005**, *21* (8), 3641–3646. https://doi.org/10.1021/la047420c.

(95) Zeng, X.; Li, X.; Xing, L.; Liu, X.; Luo, S.; Wei, W.; Kong, B.; Li, Y. Electrodeposition of Chitosan–Ionic Liquid–Glucose Oxidase Biocomposite onto Nano-Gold Electrode for Amperometric Glucose Sensing. *Biosensors and Bioelectronics* **2009**, *24* (9), 2898–2903. https://doi.org/10.1016/j.bios.2009.02.027.

(96) Luo, X.-L.; Xu, J.-J.; Du, Y.; Chen, H.-Y. A Glucose Biosensor Based on Chitosan–Glucose Oxidase–Gold Nanoparticles Biocomposite Formed by One-Step Electrodeposition. *Analytical Biochemistry* **2004**, *334* (2), 284–289. https://doi.org/10.1016/j.ab.2004.07.005.

(97) Qiu, J.-D.; Wang, R.; Liang, R.-P.; Xia, X.-H. Electrochemically Deposited Nanocomposite Film of CS-Fc/Au NPs/GOx for Glucose Biosensor Application. *Biosensors and Bioelectronics* **2009**, *24* (9), 2920–2925. https://doi.org/10.1016/j.bios.2009.02.029.

(98) Liu, J.; Wang, X.; Wang, T.; Li, D.; Xi, F.; Wang, J.; Wang, E. Functionalization of Monolithic and Porous Three-Dimensional Graphene by One-Step Chitosan Electrodeposition for Enzymatic Biosensor. *ACS Appl. Mater. Interfaces* **2014**, *6* (22), 19997–20002. https://doi.org/10.1021/am505547f.

(99) Talarico, D.; Arduini, F.; Amine, A.; Cacciotti, I.; Moscone, D.; Palleschi, G. Screen-Printed Electrode Modified with Carbon Black and Chitosan: A Novel

Platform for Acetylcholinesterase Biosensor Development. *Anal Bioanal Chem* **2016**, *408* (26), 7299–7309. https://doi.org/10.1007/s00216-016-9604-y.

(100) Zhang, Y.; Li, Y.; Wu, W.; Jiang, Y.; Hu, B. Chitosan Coated on the Layers' Glucose Oxidase Immobilized on Cysteamine/Au Electrode for Use as Glucose Biosensor. *Biosensors and Bioelectronics* **2014**, *60*, 271–276. https://doi.org/10.1016/j.bios.2014.04.035.

(101) Payne, M. E.; Zamarayeva, A.; Pister, V. I.; Yamamoto, N. A. D.; Arias, A. C. Printed, Flexible Lactate Sensors: Design Considerations Before Performing On-Body Measurements. *Sci Rep* **2019**, *9* (1), 13720. https://doi.org/10.1038/s41598-019-49689-7.

(102) Cunha-Silva, H.; Arcos-Martinez, M. J. Dual Range Lactate Oxidase-Based Screen Printed Amperometric Biosensor for Analysis of Lactate in Diversified Samples. *Talanta* **2018**, *188*, 779–787. https://doi.org/10.1016/j.talanta.2018.06.054.

(103) Madden, J.; O'Mahony, C.; Thompson, M.; O'Riordan, A.; Galvin, P. Biosensing in Dermal Interstitial Fluid Using Microneedle Based Electrochemical Devices. *Sensing and Bio-Sensing Research* **2020**, *29*, 100348. https://doi.org/10.1016/j.sbsr.2020.100348.

(104) Donora, M.; Vásquez Quintero, A.; De Smet, H.; Underwood, I. Spatiotemporal Electrochemical Sensing in a Smart Contact Lens. *Sensors and Actuators B: Chemical* **2020**, *303*, 127203. https://doi.org/10.1016/j.snb.2019.127203.

(105) Ashley, B. K.; Brown, M. S.; Park, Y.; Kuan, S.; Koh, A. Skin-Inspired, Open Mesh Electrochemical Sensors for Lactate and Oxygen Monitoring. *Biosensors and Bioelectronics* **2019**, *132*, 343–351. https://doi.org/10.1016/j.bios.2019.02.041.

(106) García-Carmona, L.; Martín, A.; Sempionatto, J. R.; Moreto, J. R.; González, M. C.; Wang, J.; Escarpa, A. Pacifier Biosensor: Toward Noninvasive Saliva Biomarker Monitoring. *Anal. Chem.* **2019**, *91* (21), 13883–13891. https://doi.org/10.1021/acs.analchem.9b03379.

(107) *Fundamentals and Applications of Chemical Sensors*; Schuetzle, D., Hammerle, R., Eds.; ACS Symposium Series; American Chemical Society: Washington, DC, 1986; Vol. 309. https://doi.org/10.1021/bk-1986-0309.

(108) Feeney, R.; Kounaves, S. P. Microfabricated Ultramicroelectrode Arrays: Developments, Advances, and Applications in Environmental Analysis. *Electroanalysis* **2000**, *12* (9), 677–684. https://doi.org/10.1002/1521-4109(200005)12:9<677::AID-ELAN677>3.0.CO;2-4.

(109) Vasylieva, N.; Marinesco, S.; Barbier, D.; Sabac, A. Silicon/SU8 Multi-Electrode Micro-Needle for in Vivo Neurochemical Monitoring. *Biosensors and Bioelectronics* **2015**, *72*, 148–155. https://doi.org/10.1016/j.bios.2015.05.004.

(110) Forouzanfar, S.; Alam, F.; Khakpour, I.; Baboukani, A. R.; Pala, N.; Wang, C. Highly Sensitive Lactic Acid Biosensors Based on Photoresist Derived Carbon. *IEEE Sensors J.* **2020**, *20* (16), 8965–8972. https://doi.org/10.1109/JSEN.2020.2988383.

(111) Dornhof, J.; Kieninger, J.; Muralidharan, H.; Maurer, J.; Urban, G. A.; Weltin, A. Microfluidic Organ-on-Chip System for Multi-Analyte Monitoring of Metabolites in 3D Cell Cultures. *Lab Chip* **2022**, *22* (2), 225–239. https://doi.org/10.1039/D1LC00689D.

(112) Frebel, H.; Chemnitius, G. C.; Cammann, K.; Kakerow, R.; Rospert, M.; Mokwa, W. Multianalyte Sensor for the Simultaneous Determination of Glucose, L-Lactate and Uric Acid Based on a Microelectrode Array. *Sensors and Actuators B: Chemical* **1997**, *43* (1–3), 87–93. https://doi.org/10.1016/S0925-4005(97)00133-0.

(113) Ahmadi, M. M.; Jullien, G. A. A Wireless-Implantable Microsystem for Continuous Blood Glucose Monitoring. *IEEE Trans. Biomed. Circuits Syst.* **2009**, *3* (3), 169–180. https://doi.org/10.1109/TBCAS.2009.2016844.
(114) Liao, Z.; Wang, J.; Zhang, P.; Zhang, Y.; Miao, Y.; Gao, S.; Deng, Y.; Geng, L. Recent Advances in Microfluidic Chip Integrated Electronic Biosensors for Multiplexed Detection. *Biosensors and Bioelectronics* **2018**, *121*, 272–280. https://doi.org/10.1016/j.bios.2018.08.061.
(115) Hierlemann, A.; Brand, O.; Hagleitner, C.; Baltes, H. Microfabrication Techniques for Chemical/Biosensors. *Proc. IEEE* **2003**, *91* (6), 839–863. https://doi.org/10.1109/JPROC.2003.813583.
(116) Voldman, J.; Gray, M. L.; Schmidt, M. A. Microfabrication in Biology and Medicine. *Annu. Rev. Biomed. Eng.* **1999**, *1* (1), 401–425. https://doi.org/10.1146/annurev.bioeng.1.1.401.
(117) Ribet, F.; Stemme, G.; Roxhed, N. Ultra-Miniaturization of a Planar Amperometric Sensor Targeting Continuous Intradermal Glucose Monitoring. *Biosensors and Bioelectronics* **2017**, *90*, 577–583. https://doi.org/10.1016/j.bios.2016.10.007.
(118) Ribet, F.; Stemme, G.; Roxhed, N. Real-Time Intradermal Continuous Glucose Monitoring Using a Minimally Invasive Microneedle-Based System. *Biomed Microdevices* **2018**, *20* (4), 101. https://doi.org/10.1007/s10544-018-0349-6.
(119) Wei, D.; Liu, Y.; Wang, Y.; Zhang, H.; Huang, L.; Yu, G. Synthesis of N-Doped Graphene by Chemical Vapor Deposition and Its Electrical Properties. *Nano Lett.* **2009**, *9* (5), 1752–1758. https://doi.org/10.1021/nl803279t.
(120) El-Kady, M. F.; Strong, V.; Dubin, S.; Kaner, R. B. Laser Scribing of High-Performance and Flexible Graphene-Based Electrochemical Capacitors. *Science* **2012**, *335* (6074), 1326–1330. https://doi.org/10.1126/science.1216744.
(121) Wu, Z.-S.; Parvez, K.; Feng, X.; Müllen, K. Photolithographic Fabrication of High-Performance All-Solid-State Graphene-Based Planar Micro-Supercapacitors with Different Interdigital Fingers. *J. Mater. Chem. A* **2014**, *2* (22), 8288. https://doi.org/10.1039/c4ta00958d.
(122) Lahcen, A. A.; Rauf, S.; Beduk, T.; Durmus, C.; Aljedaibi, A.; Timur, S.; Alshareef, H. N.; Amine, A.; Wolfbeis, O. S.; Salama, K. N. Electrochemical Sensors and Biosensors Using Laser-Derived Graphene: A Comprehensive Review. *Biosensors and Bioelectronics* **2020**, *168*, 112565. https://doi.org/10.1016/j.bios.2020.112565.
(123) Lin, J.; Peng, Z.; Liu, Y.; Ruiz-Zepeda, F.; Ye, R.; Samuel, E. L. G.; Yacaman, M. J.; Yakobson, B. I.; Tour, J. M. Laser-Induced Porous Graphene Films from Commercial Polymers. *Nat Commun* **2014**, *5* (1), 5714. https://doi.org/10.1038/ncomms6714.
(124) Marques, A. C.; Cardoso, A. R.; Martins, R.; Sales, M. G. F.; Fortunato, E. Laser-Induced Graphene-Based Platforms for Dual Biorecognition of Molecules. *ACS Appl. Nano Mater.* **2020**, *3* (3), 2795–2803. https://doi.org/10.1021/acsanm.0c00117.
(125) Soares, R. R. A.; Hjort, R. G.; Pola, C. C.; Parate, K.; Reis, E. L.; Soares, N. F. F.; McLamore, E. S.; Claussen, J. C.; Gomes, C. L. Laser-Induced Graphene Electrochemical Immunosensors for Rapid and Label-Free Monitoring of *Salmonella Enterica* in Chicken Broth. *ACS Sens.* **2020**, *5* (7), 1900–1911. https://doi.org/10.1021/acssensors.9b02345.
(126) Meng, L.; Turner, A. P. F.; Mak, W. C. Conducting Polymer-Reinforced Laser-Irradiated Graphene as a Heterostructured 3D Transducer for Flexible Skin Patch

Biosensors. *ACS Appl. Mater. Interfaces* **2021**, *13* (45), 54456–54465. https://doi.org/10.1021/acsami.1c13164.

(127) Xuan, X.; Pérez-Ràfols, C.; Chen, C.; Cuartero, M.; Crespo, G. A. Lactate Biosensing for Reliable On-Body Sweat Analysis. *ACS Sens.* **2021**, *6* (7), 2763–2771. https://doi.org/10.1021/acssensors.1c01009.

(128) Chen, Y.; Long, J.; Zhou, S.; Shi, D.; Huang, Y.; Chen, X.; Gao, J.; Zhao, N.; Wong, C. UV Laser-Induced Polyimide-to-Graphene Conversion: Modeling, Fabrication, and Application. *Small Methods* **2019**, *3* (10), 1900208. https://doi.org/10.1002/smtd.201900208.

(129) Vaughan, E.; Larrigy, C.; Burke, M.; Sygellou, L.; Quinn, A. J.; Galiotis, C.; Iacopino, D. Visible Laser Scribing Fabrication of Porous Graphitic Carbon Electrodes: Morphologies, Electrochemical Properties, and Applications as Disposable Sensor Platforms. *ACS Appl. Electron. Mater.* **2020**, *2* (10), 3279–3288. https://doi.org/10.1021/acsaelm.0c00612.

(130) Hamzah, H. H.; Shafiee, S. A.; Abdalla, A.; Patel, B. A. 3D Printable Conductive Materials for the Fabrication of Electrochemical Sensors: A Mini Review. *Electrochemistry Communications* **2018**, *96*, 27–31. https://doi.org/10.1016/j.elecom.2018.09.006.

(131) Cardoso, R. M.; Kalinke, C.; Rocha, R. G.; dos Santos, P. L.; Rocha, D. P.; Oliveira, P. R.; Janegitz, B. C.; Bonacin, J. A.; Richter, E. M.; Munoz, R. A. A. Additive-Manufactured (3D-Printed) Electrochemical Sensors: A Critical Review. *Analytica Chimica Acta* **2020**, *1118*, 73–91. https://doi.org/10.1016/j.aca.2020.03.028.

(132) López Marzo, A. M.; Mayorga-Martinez, C. C.; Pumera, M. 3D-Printed Graphene Direct Electron Transfer Enzyme Biosensors. *Biosensors and Bioelectronics* **2020**, *151*, 111980. https://doi.org/10.1016/j.bios.2019.111980.

(133) Rocha, D. S.; Duarte, L. C.; Silva-Neto, H. A.; Chagas, C. L. S.; Santana, M. H. P.; Antoniosi Filho, N. R.; Coltro, W. K. T. Sandpaper-Based Electrochemical Devices Assembled on a Reusable 3D-Printed Holder to Detect Date Rape Drug in Beverages. *Talanta* **2021**, *232*, 122408. https://doi.org/10.1016/j.talanta.2021.122408.

(134) Alachkar, A.; Alhassan, S.; Senel, M. Lab-In-A-Syringe: A Novel Electrochemical Biosensor for On-Site and Real-Time Monitoring of Dopamine in Freely Behaving Mice. *ACS Sens.* **2022**, *7* (1), 331–337. https://doi.org/10.1021/acssensors.1c02525.

(135) Crapnell, R. D.; Bernalte, E.; Ferrari, A. G.-M.; Whittingham, M. J.; Williams, R. J.; Hurst, N. J.; Banks, C. E. All-in-One Single-Print Additively Manufactured Electroanalytical Sensing Platforms. *ACS Meas. Au* **2021**, acsmeasuresciau.1c00046. https://doi.org/10.1021/acsmeasuresciau.1c00046.

(136) Ho, E. H. Z.; Ambrosi, A.; Pumera, M. Additive Manufacturing of Electrochemical Interfaces: Simultaneous Detection of Biomarkers. *Applied Materials Today* **2018**, *12*, 43–50. https://doi.org/10.1016/j.apmt.2018.03.008.

Chapter 2 Modification of single microband electrodes towards on-chip glucose sensing

2.1 Introduction

Electrochemical glucose sensor developments continue to progress in a number of application fields including; point-of-care diagnostics,[1] both wearable and implantable glucose monitoring devices,[2,3] animal health diagnostics,[4] cell-culture monitoring,[5] in addition to monitoring within the food and drinks industry. [6,7] While methods such as Cyclic Voltammetry,[8] Differential Pulse Voltammetry,[9] and Square Wave Voltammetry[10] have been used for electrochemical detection of glucose, amperometric electrochemical glucose sensors have been extensively studied because of their simple, fast and sensitive nature.[11–13] Enzymatic detection mechanisms are desirable in electrochemical sensor developments as they yield high specificity to the biological recognition element in addition to obtaining high sensitivity, good selectivity and low detection limits.[14] As discussed in the introductory chapter, significant advances in both micro and nanofabrication techniques has facilitated the fabrication of structures with controllable dimensions in the ultramicro to nanoscale. Miniaturised electrodes can offer a number of advantages for electrochemical biosensor developments, such as lower detection limits, higher signal to noise ratio as well as their ability to achieve steady-state currents resulting from radial diffusion to the electrode surface.[15,16] Ultramicroelectrodes (UMEs) have been developed for applications such as heavy metal detection,[17] glucose,[18] DNA,[19] bacteria,[20] and virus detection.[21] Previous work in our group has demonstrated mediated glucose detection on nano-electrodes fabricated on a chip platform similar to that described here.[22] In that study, unmodified gold electrodes were used to detect increasing glucose concentrations in a solution containing an external redox reagent (ferrocene monocarboxylic acid) with glucose oxidase (GOx) free in solution to demonstrate mediated glucose detection in buffer based solutions. In this chapter*, we eliminate the need for the external solution of mediator and enzyme. Removal of redox mediators can simplify device fabrication in addition to reducing biosensor fabrication costs.[23] We exploit the enhanced mass transport to ultra-microelectrodes, i.e. radial diffusion, to undertake reagent-less enzymatic-based glucose detection. A two-step electrodeposition process at the single band was carried out using the on-chip Pt RE and Au CE to produce a nano-dendritic platinum-black (Pt-B) coating followed by an electrodeposition of a

* This work has been published in 'On-Chip Glucose Detection Based on Glucose Oxidase Immobilized on a Platinum-Modified, Gold Microband Electrode.' *Biosensors* **2021**, 11 (8), 249. https://doi.org/10.3390/bios11080249.

mixture containing o-PD, β-cyclodextrin and the enzyme GOx. In addition to providing an increased surface area for electron transfer, it is well known that Pt-B has a catalytic affinity to H_2O_2,[24,25] which is important as a basis for first generation electrochemical glucose sensors such as this one. The use of o-PD has been well documented for the immobilization of glucose oxidase onto electrodes.[26–28] The permselective o-PD layer has been shown to prevent interfering species such as uric acid and ascorbic acid from reaching the electrode.[29,30] o-PD has previously been used to immobilize GOx on to electrodes for diagnostic, wearable, and in vivo-based biosensors.[31–33] Here, we demonstrate the amperometric deposition of a mixture of both ß-cyclodextrin and o-phenylenediamine (o-PD) for glucose oxidase immobilization onto an ultramicroband electrode. By using the on-chip RE and CE electrodes, lower sample volumes are required for depositions and hence a lower number of units of enzyme are required during the modification stages in comparison to the volumes needed with an external RE and CE set-up. Harley *et al.* have demonstrated that sulphonated β-cyclodextrin, when incorporated with an electro-polymer layer, can mitigate against L-ascorbic acid interference, this is said to be a result of 7–11–SO_3^- charges on the sulphonated β-cyclodextrin.[34,35] The resulting enzymatic based microband biosensor exhibited a linear response to clinically relevant glucose concentrations (2.5-15 mM) using both linear sweep voltammetry and chronoamperometric measurements. The device was capable of measuring in small sample volumes without the need for external counter and reference electrodes. On-chip chronoamperometric detection was carried out in foetal bovine serum (FBS) to assess sensor performance in a biological matrix. A reduction in sensitivity was evident within 100% of serum samples; nevertheless, the sensor achieved linear glucose detection when spiking the solution with 2-12 mM additions.

2.2 Experimental work

2.2.1 Materials

Phosphate buffered saline (PBS) (140 mM NaCl, 10 mM phosphate buffer, and 3 mM KCl), ferrocene monocarboxylic acid (FcCOOH), o-phenylenediamine (o-PD), β-cyclodextrin sulphated sodium salt, D-(+)-glucose, sodium sulphate, sodium phosphate monobasic, sodium phosphate dibasic, chloroplatanic acid hexahydrate, lead acetate trihydrate, sulphuric acid, hydrogen peroxide, D-(-)-fructose, D-(+)-mannose, L-ascorbic acid, salicylic acid and uric acid were all sourced from Sigma Aldrich. Glucose oxidase

(GOx, E.C. 1.1.3.4) from *Aspergillus niger* was purchased from Sekisui Diagnostics Ltd (UK). Foetal bovine serum was purchased from Thermofisher. All solutions were prepared with double distilled 18.2 MΩ deionized water which was obtained using an ELGA Pure Lab Ultra system.

2.2.2 Chip Fabrication

Single microband working electrodes, interconnection tracks, peripheral contact pads, a gold counter electrode and platinum pseudo-reference electrode were all fabricated on-chip using a combination of electron beam and photolithography processes as reported previously.[36–38] Fabrication† was carried out on 4-inch silicon wafers bearing a thermally grown 300 nm silicon dioxide layer. The chip was designed to fit a microSD port for connection with external electronics. Optical lithography and metal evaporations of titanium (10 nm) and gold (50 nm) using a Temescal FC-2000 E-beam were used to form the single microbands (55 µm x 1 µm x 60 nm). Each chip contained six microband electrodes (WE) spaced 940 µm apart. The second stage of fabrication again involved an optical lithographic and metal deposition (Ti 10 nm/Au 100 nm) process to create the interconnection tracks and the counter (90 µm x 7 mm) electrode. Alignment to the as-deposited wafer level alignment marks was used to define the MicroSD pinout, interconnection tracks and the counter and reference electrodes. The counter and reference electrodes were fabricated parallel to the working electrodes, to ensure equidistance from each working electrode. A final optical lithography, metal deposition and lift-off process was carried out to define the platinum reference electrode. A final deposition of 500 nm of silicon nitride (Si_3N_4) was blanket deposited by plasma-enhanced chemical vapour deposition to insulate the interconnection tracks. Photolithography and reactive ion etching were utilised to open 45 µm x 100 µm windows in the insulating layer directly over the working electrodes, as well as openings for the peripheral contact pads and the on-chip counter and reference electrodes. Each 4-inch wafer yields 28 chips (9.78 mm x 17.52 mm). An electrochemical cell was machined using a Bridgeport Hardinge VMC 480 CNC machine, to allow electrochemical analysis in small sample volumes of approximately 50 µl-5 ml (see Figure 2.1 A). The cell consisted of an aluminium base that was milled to mount and hold the chip. A PTFE Teflon lid was milled

† Chip fabrication was carried out by Mr. Dan O'Connell of Tyndall's CFF

to contain a well, which was sealed with an O-Ring (Polymax Ltd.). The O-ring prevented the solution from contacting the connection pins and contact pads. The O-ring inner diameter selected was 7 mm and had a cross section of 1.6 mm to ensure that each of the WEs, the CE and RE were exposed (see Figure 2.1 B) to the solution of interest. The lid also contained openings for spring-loaded pins (Coda Systems Ltd. PM4J Plain Radius

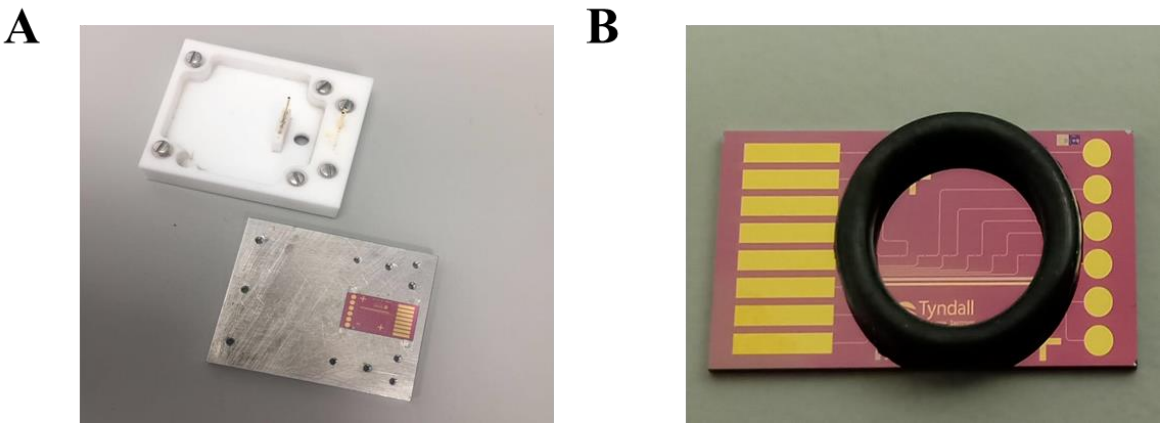

Figure 2.1: *A: The electrochemical cell comprised of a PTFE Teflon lid with a well, to interface the solution with the chip potentiostat, and an aluminium base to house the chip. B: An image of the chip with the O-ring positioned over the area of the chip exposed to the solution of interest.*

Microprobes) which facilitated the connection between the chip and the potentiostat.

2.2.3 Characterisation of chip and working microband electrode

2.2.3.1 *Electrochemical Analysis at Microband Electrodes*

Electrochemical experiments were carried out using an AutoLab potentionstat PGSTAT302N electrochemical workstation (Metrohm Ltd.) controlled by the AutoLab NOVA software. All experiments were performed at room temperature using a Faraday Cage (Metrohm Ltd.). All electrochemical measurements were conducted with the on-chip CE and RE unless otherwise stated. The single microband electrodes were characterised using CV and electrochemical impedance spectroscopy (EIS) in a 10 mM PBS solution (pH = 7.4) containing 1 mM FcCOOH. CV was performed by cycling the potential from -200 mV to 500 mV versus the on-chip platinum pseudo-reference electrode at a scan rate of 50 mVs^{-1}. Impedance measurements were conducted at a potential of 200 mV over a frequency range of 100 mHz to 100 kHz. The amplitude of the alternating voltage was 5 mV. EIS was used to characterise and measure the charge transfer processes occurring at the electrode-solution interface. The on-chip counter electrode (90 µm x 7 mm) was used as a macro-working electrode to demonstrate the

diffusion behaviour at a gold macroband electrode in comparison to the single gold microband. CV was performed by cycling the potential from 0 mV to 600 mV at a scan rate of 50 mVs^{-1} in 1 mM FcCOOH. Here, an Ag/AgCl (3 M KCl) electrode (Gamry Ltd.) and a platinum wire (Gamry Ltd.) were employed as the reference and counter electrodes. As this study presents an on-chip first generation electrochemical glucose detection approach, the final biosensor surface was also evaluated in the presence of H_2O_2 (0.5 mM to 2.5 mM) using Linear sweep voltammetry (LSV), the chosen LSV potential parameters were 0V to 0.4 V at a scan rate of 50 mVs^{-1}.

2.2.3.2 *Surface characterisation of electrode materials*

Prior to use, the microband electrodes were optically imaged using an Olympus camera and calibrated epifluorescence microscope Model BX51 TRF SN 5M18343. The chip, contact pads, and single microbands were examined to ensure that the WEs, the RE and CE were exposed in addition to confirming that no visual defects were present on the chip prior to measurements. Scanning electron microscopy (SEM) images were obtained using Zeiss Supra 40 SEM. Atomic force microscopy images (AFM) were acquired with a Veeco Dimension 3100 atomic force microscope, in tapping mode using commercial Olympus probes (Oxford Instruments Asylum Research, High Wycombe, UK). An area of 5 µm x 5 µm was investigated at a scan rate of 0.7 Hz. Background plane subtraction was applied to the images. X-ray photoelectron spectroscopy (XPS) measurements were performed at the University of Limerick using a Kratos AXIS ultra spectrometer equipped with a mono Al Kα X-ray gun. Survey and high-resolution scans were recorded with a 1 eV and 0.05 eV resolution, respectively. The geometry of the single microband electrodes were not suited to the resolution needed i.e. the electrode area was too small for the 50 μm^2 spot size (see appendices section A.1). In order to confirm the composition of electrodeposited materials, modifications were carried out on the gold counter macro electrode (90 µm x 7 mm). Firstly, platinum-black (Pt-B) was electrodeposited using amperometry from a solution containing 15 mM hexachloroplatanic acid and 2.1 mM lead acetate in deionised water at -0.5 V for 10 seconds. Electro-polymerisation of the o-PD-β-cyclodextrin-GOx layer was carried out using amperometry at 0.5 V in a mixture containing 5 mM *o*-PD, 2.5 mM sulphonated-β-cyclodextrin, 5 mM sodium sulphate and 10 mg/ml of GOx in a 50 mM phosphate buffer (PB) solution (pH 7.4) for 1200 seconds.

2.2.3.3 *Microband functionalisation for Glucose detection*

Prior to use, chips were exposed to a mixed solvent clean process (acetone, isopropyl alcohol and DI water) for 15 minutes and dried under a stream of nitrogen. On-chip electrodepositions were performed using the pre-fabricated chip holder. Pt-B was electrodeposited using amperometry from a solution containing 15 mM hexachloroplatanic acid and 2.1 mM lead acetate in deionised water at -0.75 V for 10 seconds. Electro-polymerisation of the o-PD-β-cyclodextrin-GOx layer was carried out using amperometry at 0.35 V in a mixture containing 5 mM *o*-PD, 2.5 mM sulphonated-β-cyclodextrin, 5 mM sodium sulphate and 10 mg/ml of GOx in a 50 mM phosphate buffer (PB) solution (pH 7.4) for 1200 seconds. The potential for on-chip electrodepositions was adjusted owing to the potential shift occurring when moving from an Ag/AgCl RE to a Pt pseudo RE. Deposition time and electrolyte concentrations were chosen based on previous work within our group.[35] Following electrodeposition, the chips were rinsed with phosphate buffer (PB) to remove any unbound enzyme and were subsequently stored in 50 mM PB solution (pH 7.4) at 4°C when not in use.

2.2.4 Glucose detection

2.2.4.1 *Glucose detection in phosphate buffers*

Glucose stock solutions were prepared using D-(+)-glucose in 50 mM PB (pH 7.4). Pre-determined aliquots were employed for chronoamperometric measurements. As-modified electrodes were exposed to aliquots of PB containing glucose concentrations within physiologically relevant levels (2.5 mM to 15 mM) by dropping 50 µl aliquots onto the chip and allowing 45 seconds prior to running a measurement. Both linear sweep voltammetry (LSV) and chronoamperometry were utilised to measure the response of glucose additions at the o-PD/β-cyclodextrin/GOx electrode surface in 50 mM PB (pH 7.4) against the on chip RE and CE. The LSV potential parameters were 0 V to 0.4 V (versus Pt) with a 50 mVs^{-1} scan rate. For chronoamperometry measurements, a voltage of 0 V was applied as a conditioning step for 5 seconds followed by application of a 0.25 V for 45 seconds. Following each measurement, the solution was removed, and the next concentration was directly added to the well. All data were background subtracted using the values for the phosphate buffer baseline (the blank). After a time of 40 seconds, the mean current from 30 data points (obtained over 5 seconds) was measured from

background subtracted data for each concentration, this was done for n = 3 bands from three separate chips. Interference testing in phosphate buffers

Interfering species at the upper end of typical physiological concentrations were prepared to evaluate the selectivity of the o-PD/β-cyclodextrin/GOx UME to a 2.5 mM glucose concentration. Stock solutions of uric acid (UA), L-ascorbic acid (AA), salicylic acid, D-(-)-fructose and D-(+)-mannose were prepared in 50 mM PB (pH 7.4). As-modified electrodes were exposed to aliquots of PB containing only 2.5 mM glucose, as well as aliquots containing 2.5 mM glucose spiked with each individual interfering species, by dropping 50 µl aliquots onto the chip and allowing 45 seconds prior to running a chronoamperometric scan. Chronoamperometry was carried out at an applied voltage of 0.25 V. The current was sampled by averaging 30 data points after a time of 30 seconds (obtained over 5 seconds).

2.2.4.2 *Glucose detection in foetal bovine serum spiked with known glucose concentrations*

Aliquots of foetal bovine serum were prepared to contain known concentrations of glucose (2-12 mM) in order to assess the sensor in a more complex biological fluid at physiologically relevant glucose concentrations. Chronoamperometry was applied at 0 V for 5 seconds followed by 0.25 V for 70 seconds. The current was sampled by averaging 30 data points after a time of 50 seconds. A freestyle neo one glucometer and test strips (Abbott) were used to confirm the glucose concentrations in un-spiked foetal bovine serum.

2.3 Results and Discussion

2.3.1 Device characterisation

Prior to measurements, as described in the methodology, chips were separated from the wafer, cleaned and inspected using optical microscopy. Each chip contains six separate working electrodes, a gold counter electrode and a platinum pseudo-reference electrode (see Figure 2.3 (A)). Figure 2.3 (B) shows a microscopy image of a fully passivated single microband electrode. The passivation window (dark rectangular region) exposed the working electrode, which has a length of 45 µm.

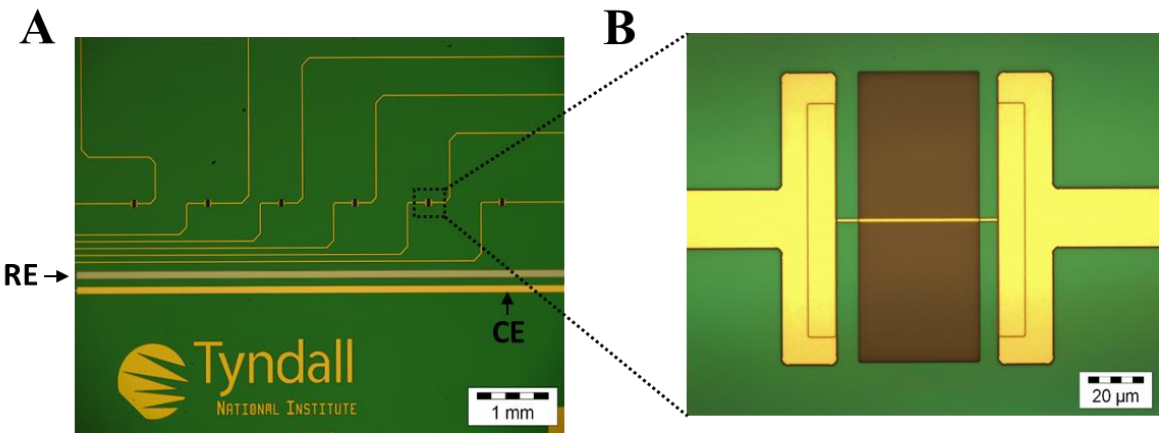

Figure 2.3: *A: Optical microscopy image showing the on-chip platinum and counter reference electrodes as well as the 6 working electrodes (2.5x) B: Zoom on a single microband working electrode and the dark passivation window (50x).*

A CV in 0.1 M H_2SO_4 (3 scans were obtained the middle scan is presented) can be seen in Figure 2.2, an oxidation peak is visible at 0.9 V representing the formation of the gold oxide layers (Au_2O_3). A reduction peak is seen at 0.29 V as a result of the removal of the gold oxide layers.[39] The microband area was determined using the charge associated with the reduction of gold oxide which is proportional to the active surface area. This was calculated to be 7.5×10^{-7} cm^2. This is higher than the geometric surface area determined using the dimensions (5×10^{-7} cm^2) This method takes into account the surface roughness unlike the use of the dimensional measurements.

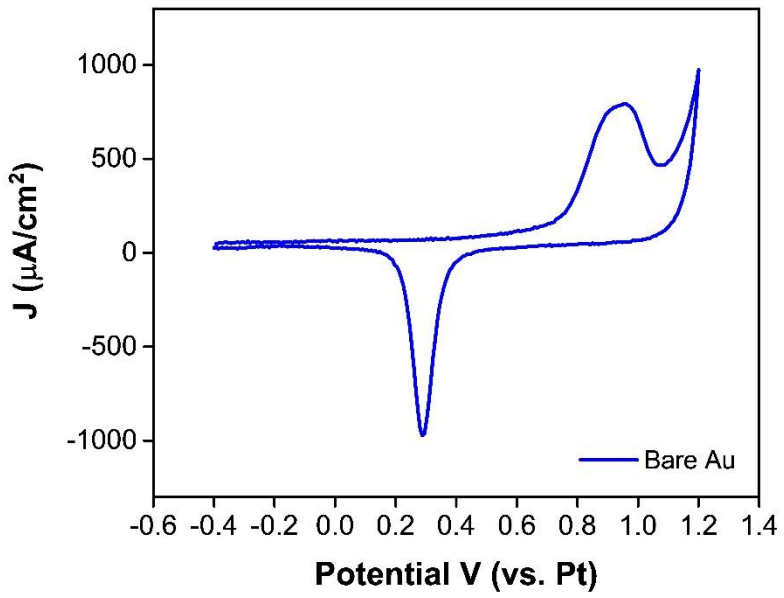

Figure 2.2: *Cyclic voltammogram obtained in 0.1 M H_2SO_4 at a scan rate of 50 mVs^{-1}.*

CV was also carried out in the electroactive probe FcCOOH at the microband electrode (see Figure 2.4). CVs exhibited quasi steady-state behaviour resulting from radial diffusion to the microband electrode. The single microband showed excellent intra-chip reproducibility with an RSD less than 0.1 % between both the oxidation and reduction currents (n = 5). This also demonstrated that the on-chip CE and RE were functional for electrochemical measurements. The lower inset graph of Figure 2.4 displays a CV carried out on a macro-Au band electrode (dimensions 90 µm × 7 mm) under the same conditions (50 mVs^{-1} scan rate) versus Ag/AgCl. The resulting graph displays a peak shaped CV behaviour, depicting planar diffusion to the larger band electrode. Data was normalised to current density using the approximate geometric area of both electrodes (macro-electrode: 6.3 × 10^{-3} cm^2, microelectrode: 5 × 10^{-7} cm^2). Dimensions were confirmed using the SEM (see Figure 2.5) AFM (see inset of Figure 2.4), and the fabrication designs. (macro-electrode: 90 µm × 7 mm, microband electrode: 90 nm × 1 µm × 45 µm). Higher current densities were observed at the microband electrode as a result of radial diffusion.

Band shaped microelectrodes have the characteristics of macroelectrodes and microelectrodes since they are macroscopic in one dimension and microscopic in the other, offering higher sensitivity with increased current output. The magnitude of the current varies directly with the electrode length. The microband presented in this work is

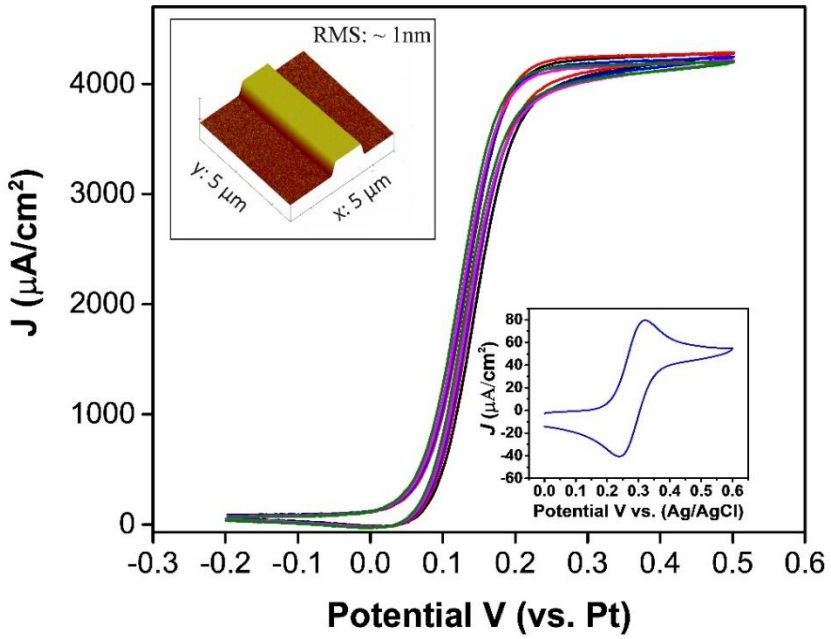

Figure 2.5: *Cyclic voltammogram obtained in 1 mM FcCOOH for n = 5 electrodes (RSD < 0.1%), Bottom inset: voltammogram obtained at a macro-Au band electrode, top inset figure depicts a 3D atomic force microscopy image of a 5 µm × 5 µm area at a scan rate of 0.7 Hz (Background plane subtraction was applied to the image.*

not a true microelectrode since one of the dimensions is not microscopic (45 microns in length). A quasi-steady-state current is achieved at long times since the current changes very slowly with time. [40,41]

$$I_{qss} = \frac{2\pi nFD_O Ac^*}{w\ln(\frac{64D_O t}{w^2})} \qquad (1)$$

Where n is the number of electrons transferred, A is the geometric area of the electrode, c^* is the bulk concentration and w is the width of the band. The electrochemical surface area was also measured using the steady state current from Figure 2.4 and inserting into the equation above. This was measured to be 4×10^{-7} cm^2. This area was lower than that measured using the gold oxide reduction peak, this may be attributed to ferrocene reacting quickly at the gold microband, in addition it is not taking surface roughness into account.

2.3.1.1 *Electrode modifications*

Figure 2.6 shows an image of the chip with a microscopy image of the single microband electrode, and a schematic of the deposition process carried out to functionalise the microband for glucose sensing. Two primary materials of choice were explored for biosensor fabrication: Pt-B and o-PD. The Pt-B electrodeposition results in an enhanced surface area for enzyme deposition. Furthermore, as previously mentioned, platinum is commonly studied for the oxidation of hydrogen peroxide.[42]

A typical amperometric i-t curve for the Pt-B electrodeposition is shown in Figure 2.7 with the inset showing a microscopy image (100x) of the Pt-B deposition completely covering the Au microband.constant potential of 0.35 V was applied for 20 minutes at the Pt-B modified surface. Figure 2.8 shows a typical amperometric i-t curve for the o-PD/β-cyclodextrin/GOx electrodeposition.

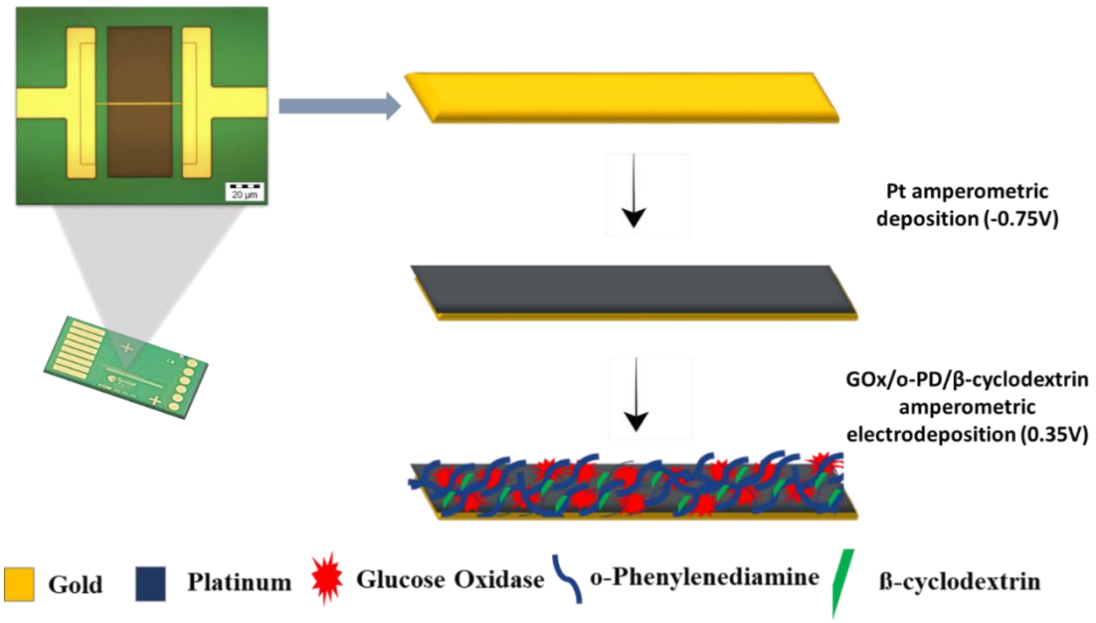

Figure 2.6: *Schematic of electrodeposition process carried out on the microband electrodes.*

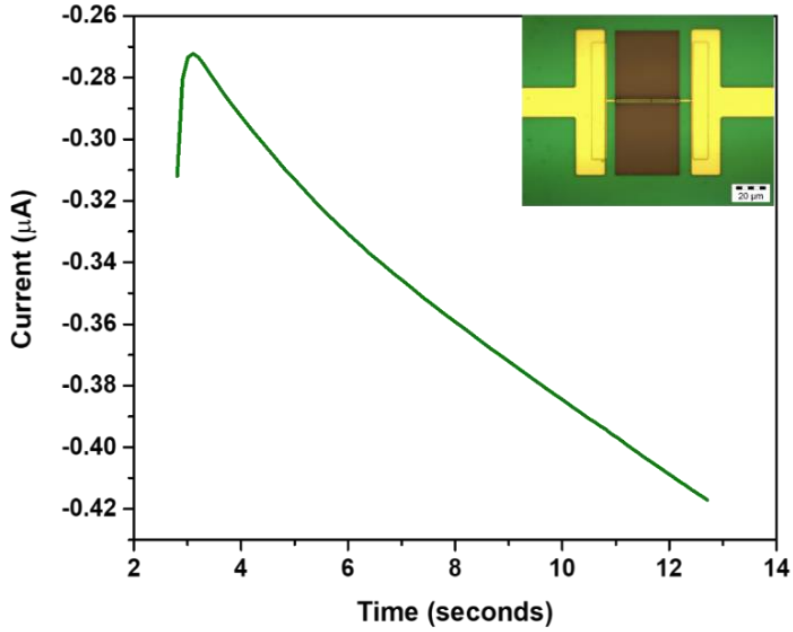

Figure 2.7: *Typical i-t graph depicting the electrodeposition carried out at -0.75 V versus the on chip platinum pseudo-reference in 15 mM H_2PtCl_6 and 2.5 mM Pb ($C_6H_6O_4$), inset image showing an optical microscopy image of the Pt-B deposition on the gold microband electrode.*

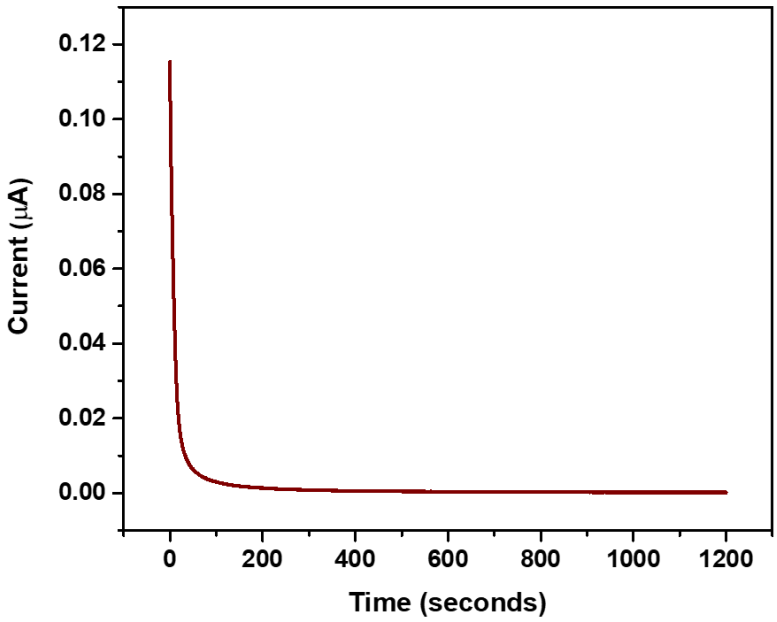

Figure 2.8: *Typical electrodeposition chronoamperometric scan carried out at 0.35 V for 1200 seconds versus the on-chip platinum electrode.*

2.3.1.2 *Potentiometric and Impedimetric Characterisation*

Cyclic voltammetry was carried out in a 1 mM FcCOOH redox probe following each electrodeposition step in order to electrochemically characterise the modified electrode surface. Following the Pt-B deposition, an increased surface area of the Pt-B conductive layer was confirmed by the increase in the magnitude of the oxidation current at 0.2V of 3 nA (see Figure 2.9). Following the o-PD/β-cyclodextrin/GOx deposition, a decrease in the magnitude of the current could be seen; the oxidation and reduction of the redox probe were no longer visible indicating the successful deposition of a non-conducting semi-permeable o-PD/β-cyclodextrin/GOx layer.[43]

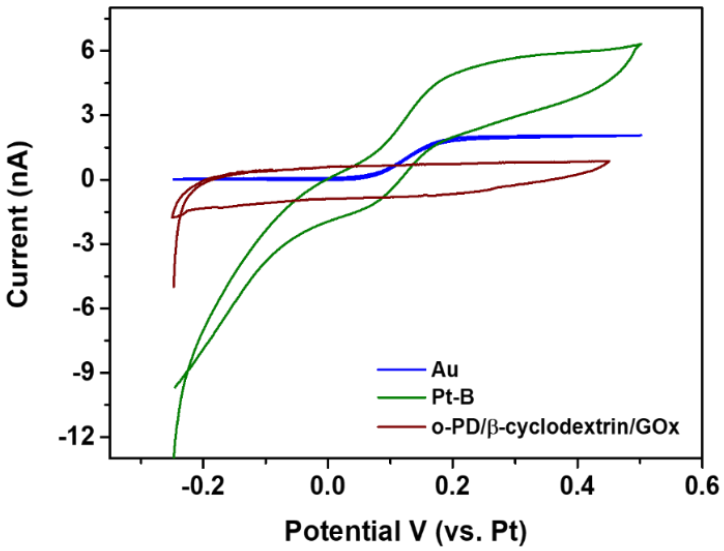

Figure 2.9: *Comparison of CV in 1 mM FcCOOH in 10 mM PBS, on a bare gold (green), platinum-black modified (blue) and o-PD/β-cyclodextrin/GOx modified (red).*

EIS was used to assess the change in the electrode surface behaviour in 1 mM FcCOOH. This change is indicated through a measured change in the impedance. Resistive and capacitive charges in the system can be measured from the Nyquist plot, by fitting the data with a Randles equivalent circuit (discussed in the Introduction chapter). The R_{ct} reflects the transfer of electrons during redox reactions and can be used as a method to measure changes occurring at the surface of the electrode.[44] Nyquist plots can include a semi-circular region and a linear part. At higher frequencies, the semi-circular region corresponds to the electron transfer limited process, and the diameter is equivalent to the

R_{ct}. The linear part at lower frequencies corresponds to the diffusion process.[45] Figure 2.10 shows the Nyquist plot obtained at each surface modification. For both the fabricated gold band and a Pt-B modified band, an electrochemical circle fit was used to determine the R_{ct}. The R_{ct} decreased from 217 MΩ at the bare Au surface to 151 MΩ following the introduction of an enhanced surface area Pt-B electrodeposition. Following o-PD/β-cyclodextrin/GOx deposition, under the same parameters, a full semi-circle was not visible for an electrochemical circle fit; however, data indicates a clear change in the surface behaviour with an increase in R_{ct} between the Pt-B surface layer and the o-PD/β-

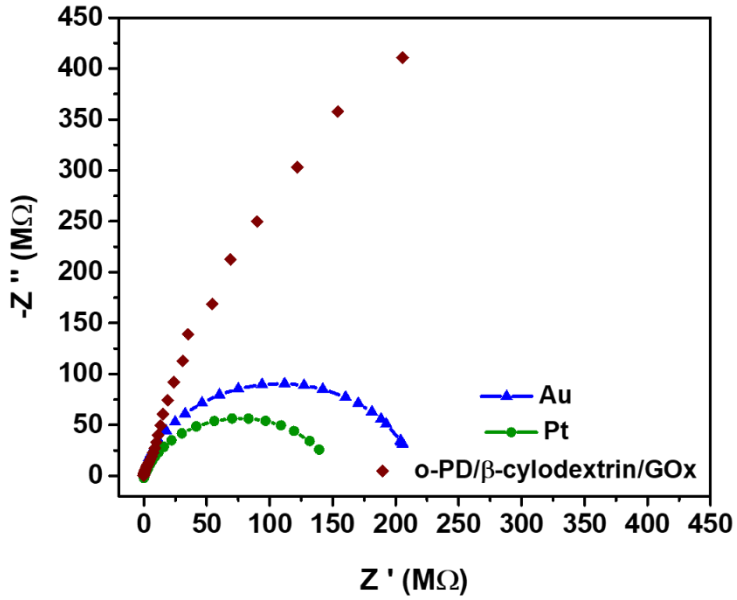

Figure 2.10: *Nyquist plots obtained in 1 mM FcCOOH in 10 mM PBS, on a bare gold (green) [R_{ct} 204 MΩ], platinum black modified (blue) and o-PD/β-cyclodextrin/GOx modified (red) [unfitted data].*

cyclodextrin/GOx modification. No diffusion-controlled effect was observed in the EIS spectrum. All CV data supported the results of EIS studies.

2.3.1.3 *Electroanalysis in H_2O_2*

In this study, glucose was quantified from enzymatically produced hydrogen peroxide; for this reason, LSV was carried out in H_2O_2 to evaluate the change in signal response between the Pt-B modification and the o-PD/ß-cyclodextrin/GOx layer. Figure 2.11 displays cyclic voltammograms carried out in a 1 mM solution of H_2O_2 in 0.01 M PBS (pH 7.4) at the Pt-B modified surface and the o-PD/β-cyclodextrin/GOx modified surface.

As expected, a decrease in the oxidation current (8 nA) was seen following the o-PD/β-cyclodextrin/GOx electrodeposition.

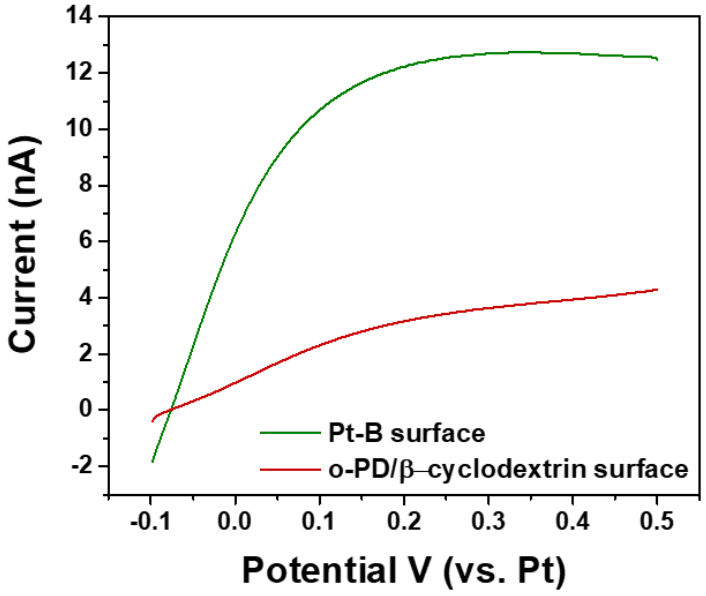

Figure 2.11: *CV in 1 mM H_2O_2 at the Pt-B modified band (green) and at the o-PD/β-cyclodextrin/GOx modified band (red).*

Whilst it is expected that H_2O_2 can permeate o-PD modification layers, we confirmed this utilising LSV in various concentrations of H_2O_2.[46] An increase in faradaic current was observed with increasing concentrations, ranging from 0.5 mM to 2.5 mM of H_2O_2 (see Figure 2.12). Current was converted to current density using an estimated geometric area of the microband after sensor preparation (1.35×10^{-6} cm^2), which was determined using dimensional information (3 µm × 45 µm); (the width after Pt electrodepositions was approximated using AFM). These results show that the H_2O_2 molecule can penetrate through the modification layer to reach the underlying Pt-B surface and undergo electrochemical oxidation. A plot of peak current density versus H_2O_2 concentration is presented in Figure 2.13, the plot exhibits good linearity (R^2=0.99) indicating that the sensor response to H_2O_2 is linear within this concentration range. The oxidation of hydrogen peroxide at the o-PD modified platinum electrode can be explained via the following reaction:

$$H_2O_2 \overset{Pt}{\rightarrow} O_2 + 2H^+ + 2e^- \qquad (2)$$

The theoretical limit of detection (LOD) was determined to be 17 µM using the blank method: $3S_b/m$, where S_b is the standard deviation of the blank and m is the slope of the line. A sensor sensitivity of 2882 µA mM^{-1} cm^{-2} was determined from the slope of the line.

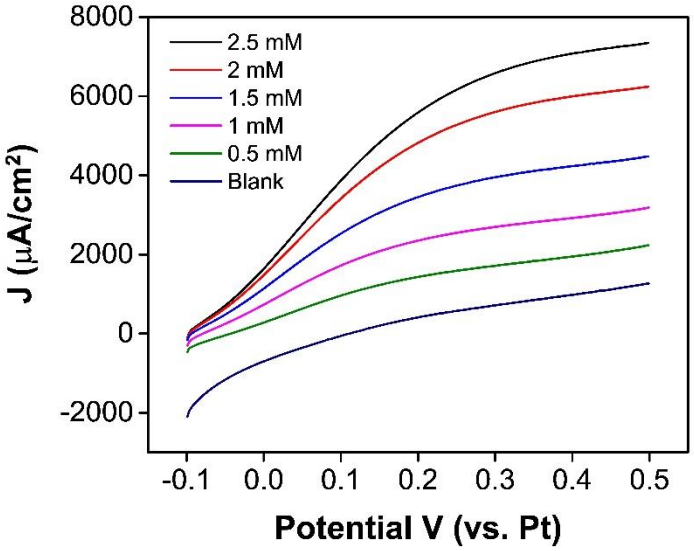

Figure 2.12: *Cyclic Voltammogram obtained in increasing concentrations of H_2O_2 at the o-PD/β-cyclodextrin surface.*

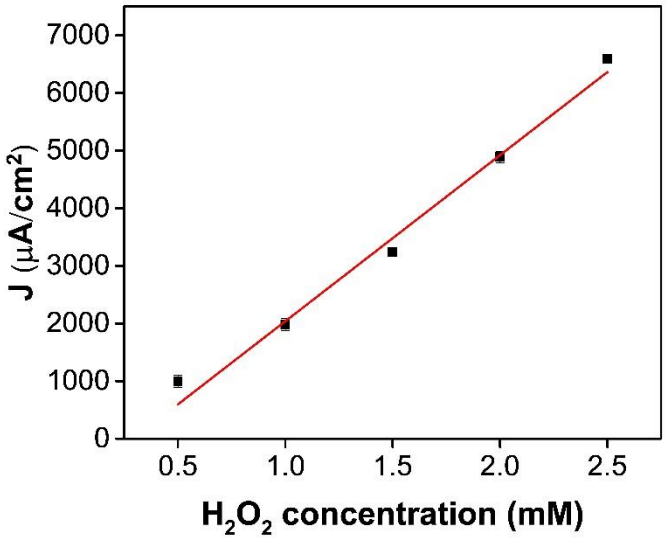

Figure 2.13: *Corresponding calibration obtained from background subtracted data at 0.25 V.*

Scanning electron microscopy images confirmed the presence of a nanodentritic Pt-B coating on to the 1 µm band electrode with a clear change in surface morphology (see Figure 2.15 (1-3). Following the o-PD/β-cyclodextrin/GOx deposition subtle changes to dendrite morphology were visible with SEM (Figure 2.15 (3)), with dendrites appearing

slightly wider than the Pt-B electrodeposited surface. As detailed in the experimental section, compositional analysis was conducted on electrode modifications prepared on a macro planar band electrode. All XPS measurements were conducted in the absence of the GOx enzyme. Figure 2.14 clearly shows the introduction of a platinum peak Pt 4f (green) post Pt-B deposition. The Au 4f peak intensity (blue) was no longer visible, as XPS probes the upper 10 nm of the surface.

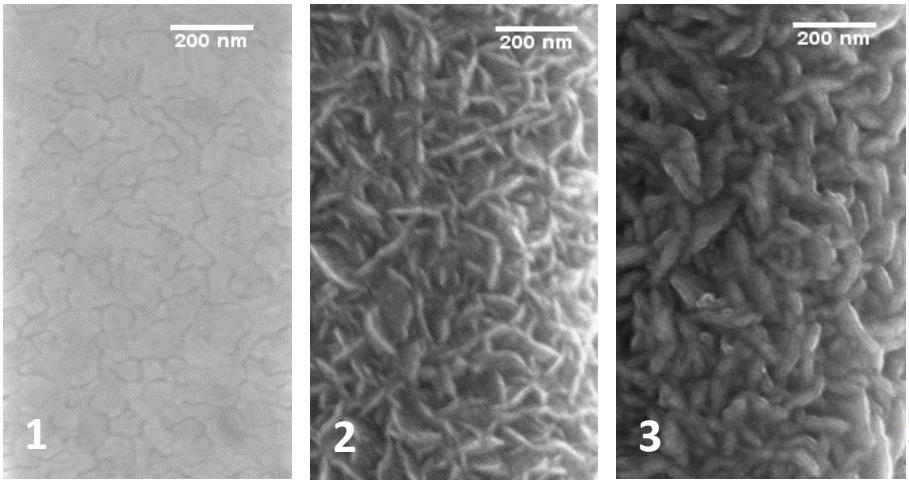

Figure 2.15: *Scanning electron microscopy images taken at (1) clean gold electrode surface (2) Pt-B modified electrode surface and (3) o-PD/GOx/β-cyclodextrin mixture surface.*

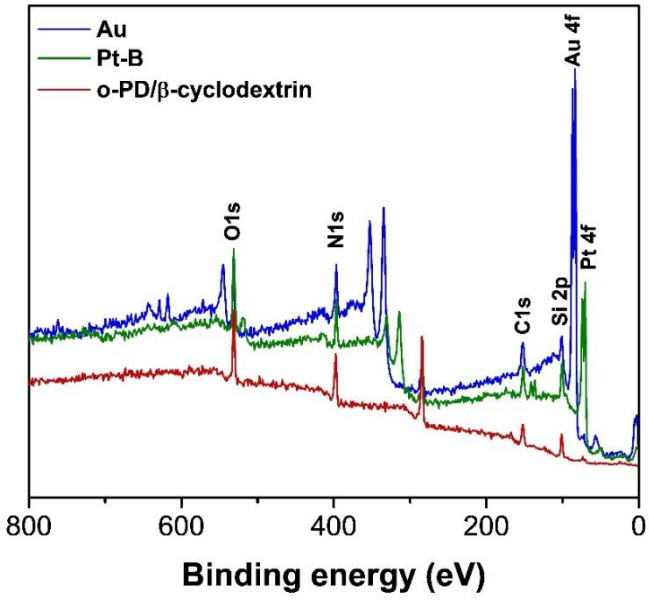

Figure 2.14: *XPS survey scan of clean bare gold (blue); as modified platinum-black (green); and as modified platinum black and after modification with Pt-B, o-phenylenediamine and β-cyclodextrin (red).*

The reduced Pt signal occurs with the introduction of an amine group (C-N) which can be seen in the high resolution scan of the N1s peak at 388.6 eV (see Figure 2.16) and at 286.1 eV in the C1s high resolution spectra. (see Figure 2.17).[40] Whilst this is not representative of the modifications carried out at an ultramicroelectrode, XPS confirmed that electrodeposition was a successful method for modifying evaporated gold electrodes fabricated in a similar manner as the single gold bands. XPS probes the upper 10 nm of the surface; the decrease in Pt signal intensity occurs relative to the introduction of the C-N signal from o-phenylenediamine at 286.1 eV in the C1s high-resolution spectra and at 399.6 eV in the N1s high-resolution spectra (Figure 3C,D), indicating that the o-PD layer had successfully electrodeposited. [47] The XPS measurements confirmed the presence of both Pt-B and o-PD on a larger gold band electrode (fabricated on the silicon substrate).

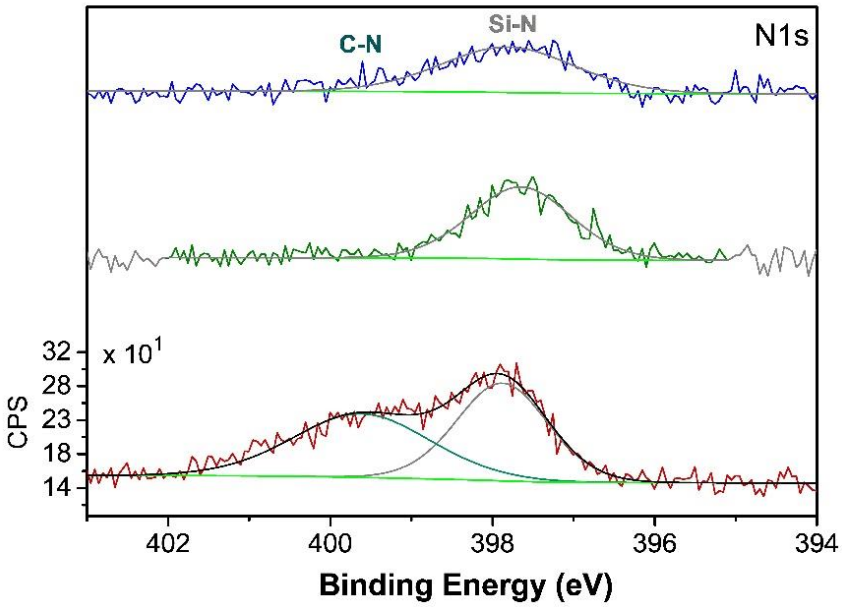

Figure 2.16: *High resolution scans of the N1s.*

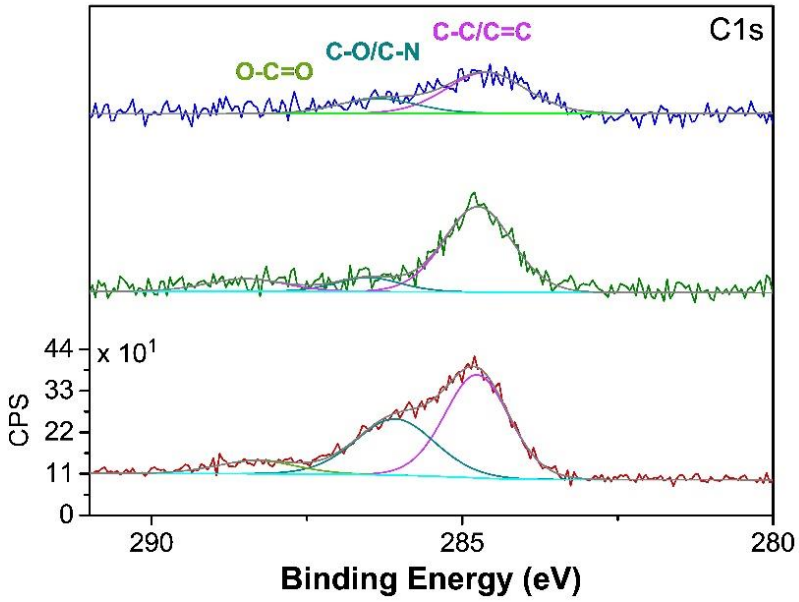

Figure 2.17: *High resolution scans of the C1s peak.*

2.3.2 Glucose detection in phosphate buffers

2.3.2.1 *Calibration*

Linear sweep voltammetry and chronoamperometry measurements were carried out for on-chip glucose measurements in eight predetermined aliquots of glucose (2.5 mM to 15 mM) in a 50 mM PB (pH 7.4). Glucose is oxidized by the entrapped GOx enzyme at the electrode surface generating H_2O_2 and gluconic acid according to the following reaction:

$$O_2 + Glucose \rightarrow Gluconic\ acid + H_2O_2 \qquad (3)$$

The subsequent electro-oxidation of H_2O_2 generated during the enzymatic reaction can be described by the reaction below:

$$H_2O_2 \overset{Pt}{\rightarrow} O_2 + 2H^+ + 2e^- \qquad (4)$$

Figure 2.18 displays linear sweep voltammograms from 0 V to 0.4 V; the current is seen to increase with increasing glucose concentrations in the range of 2.5 mM to 15 mM Sensitivity was determined to be 103.11 μA mM^{-1} cm^{-2}. The theoretical LOD observed was 1.42 mM. Figure 2.19 displays a plot of current versus glucose concentration where a linear increase in current is seen with increasing glucose concentrations

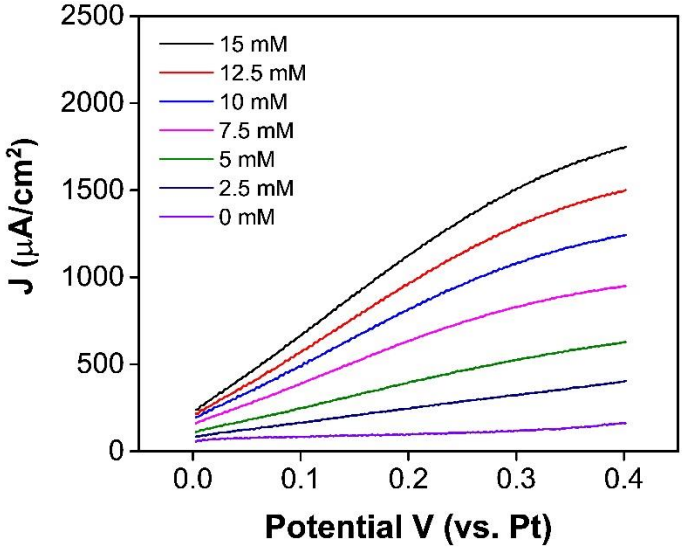

Figure 2.18: *Linear sweep voltammograms at a scan rate of 50 mVs^{-1} from 0 V to 0.4 V in increasing glucose concentrations in 50 mM PB solution (pH 7.4).*

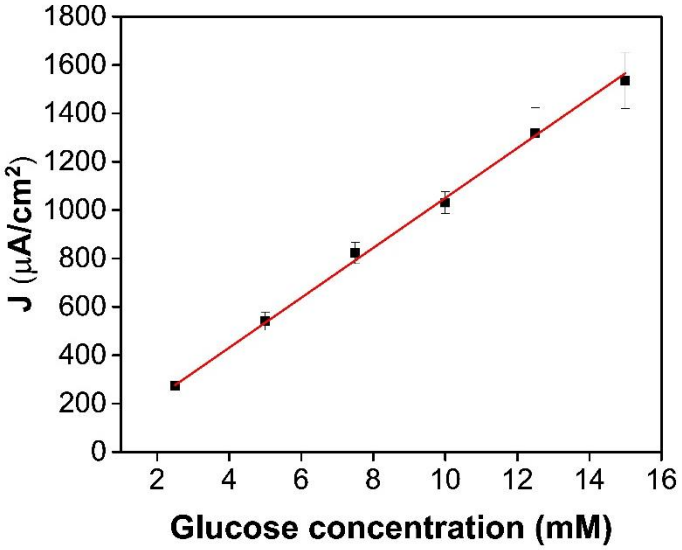

Figure 2.19: *The corresponding calibration obtained at 0.25 V, (Blank background subtracted from each concentration).*

Figure 2.20 displays the chronoamperometric response of the microband at 0.25 V to increasing glucose concentrations. The measurements were conducted for 45 seconds with a quiet time of 10 seconds prior to each scan. A steady-state response was achieved within 10 seconds of applying a potential. A plot of current versus glucose concentration is presented in Figure 2.21.The current was sampled from 40 seconds to 45 seconds by taking an average across 30 data points. This average of the current measured across three

sensors was plotted in the calibration curve. A linear increase in current is observed with increasing glucose concentrations (R^2=0.99). The sensitivity here was determined to be 111.21 µA mM^{-1} cm^{-2} with a theoretical LOD of 0.79 mM.

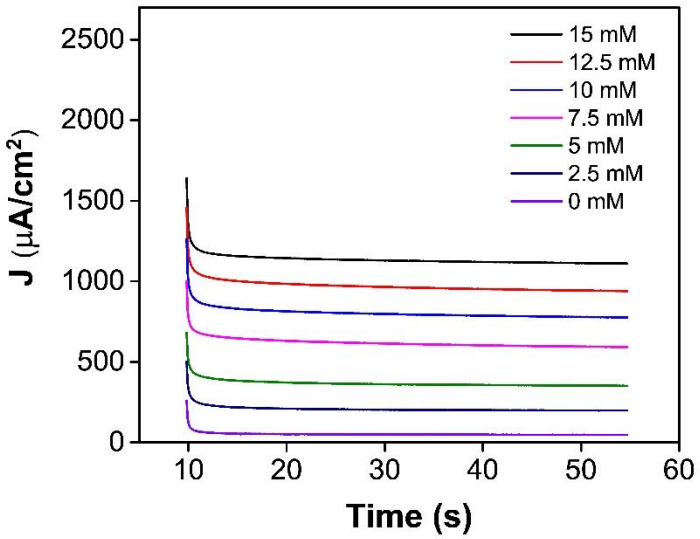

Figure 2.20: *Chronoamperograms obtained for increasing glucose concentrations from 2.5 mM up to 17.5 mM in 50 mM PB (pH 7.4).*

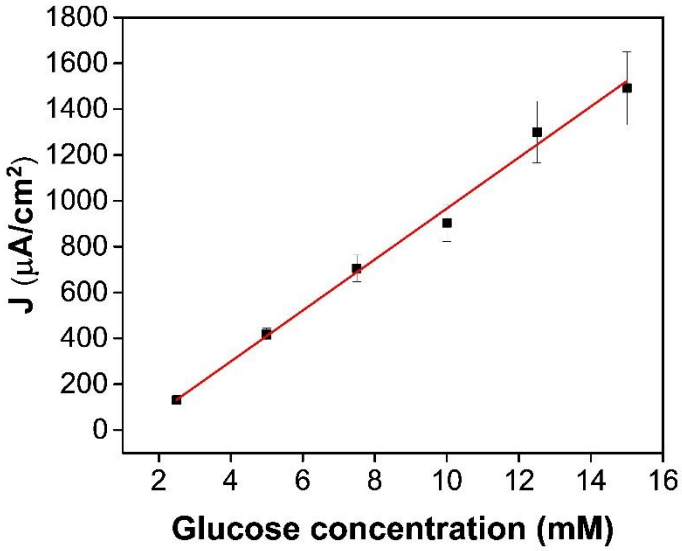

Figure 2.21: *The corresponding calibration curve, (Calibration plot obtained from current sampling time of 30 s at each glucose concentration).*

2.3.2.2 *Selectivity and Stability*

Chronoamperometric measurements were carried out to assess the biosensor selectivity in a 2.5 mM glucose concentration and that of a 2.5 mM glucose solution containing either 0.5 mM L-ascorbic acid, 1 mM fructose, 1 mM maltose, 1 mM uric acid or 0.5 mM

salicylic acid (see Figure 2.22). These concentrations are at the upper end of typical physiological concentrations. The interference effect was calculated using the following equation: $\left[\frac{I_{glucose}}{I_{interference}}\right] * 100$. Where I was sampled at time 30 seconds after the measurement had started for 5 seconds. The results are presented in

Table **2.1**, no obvious change in current was observed (<5 %). These results are attributed to the combination of the o-phenylenediamine electrodeposition which has previously been shown to reduce interference effects by limiting the ability of analytes from reaching the electrode. In addition, the highly charged with 7 – 11 – SO_3^- groups from the anionic sulphonated cyclodextrin have previously been shown to act as a repellent to the ascorbate anion. The results show that the microband sensors are specific to glucose and are not inhibited by the addition of other interfering species which can potentially co-exist within blood. The UME presented here demonstrates selectivity levels comparable to those reported previously for some enzymatic electrochemical glucose sensors.[48,49]

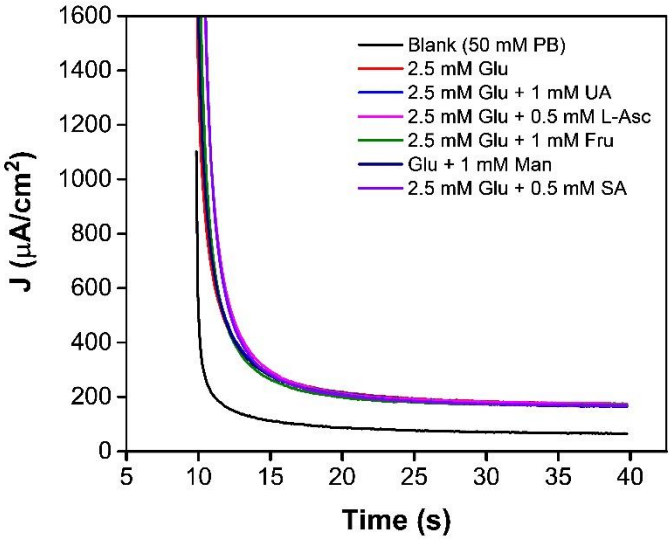

Figure 2.22: *Chronoamperometric response of the on-chip biosensor at 0.25 V to a blank solution (50 mM PB, pH 7.4) to 2.5 mM glucose and to a further separate 5 aliquots of 2.5 mM glucose and other potential interfering species.*

Table 2.1: *Table depicting the current change of interfering species.*

Interfering species	Concentration (mM)	(I/Io * 100)‡
Ascorbic Acid	0.5	100.88 %
Uric Acid	0.5	99.38 %
Salicyclic Acid	0.5	104.44 %
Fructose	1	104.85 %
Mannose	1	104.58 %

After four days of storage in PBS at 4°C, biosensor performance was examined in a 2.5 mM glucose concentration. The sensor demonstrated a sensor recovery value of 93.22% (see Figure **2.23** A), indicating that the enzyme had remained stable over a short time period. Figure **2.23** (B) shows a calibration obtained 1 day after sensor preparation and again 2 days after sensor preparation. Excellent sensor recovery values were determined for three concentrations: 103.4%, 102.0%, and 98.07%, and satisfactory values were determined for the remaining three concentrations: 88.7%, 87.2%, and 87%. For both sets of preliminary stability data, the biosensor demonstrated good short-term stability; however, it must be considered that this is not representative of a comprehensive stability study. Further investigation is necessary to understand the sensor behaviour over time and to determine the long-term storage capabilities.

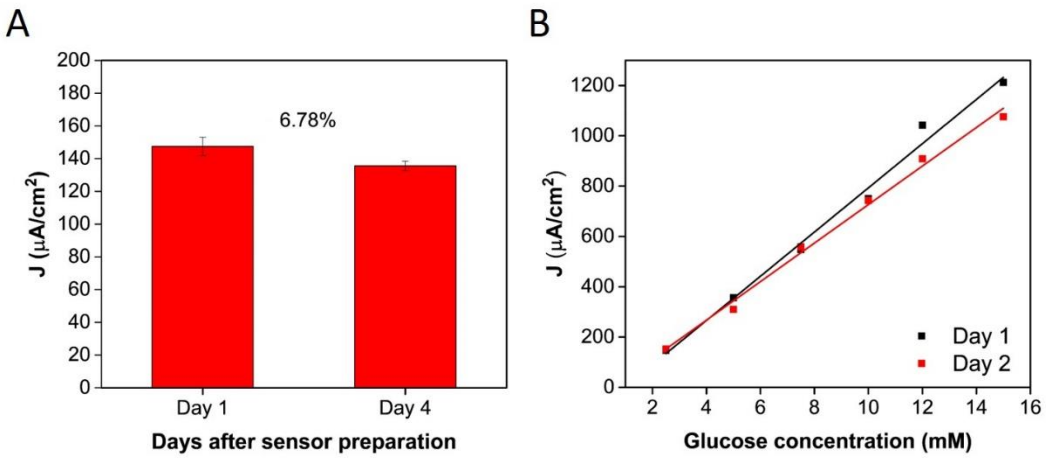

Figure 2.23: *(A) Bar chart depicting the current density measurement for a 2.5 mM concentration measured after 1 day of storage and a 2.5 mM concentration measured 4 days after storage and (B) Calibration curves obtained at the same sensor at Day 1 and again at Day 2 after sensor preparation.*

‡ Where I is the current response of 2.5 mM Glucose in 50 mM PB and Io is the current response of 2.5 mM Glucose and the given concentration of the interferent in 50 mM PB (pH 7.4)

2.3.2.3 *Glucose Detection in foetal bovine serum*

Many studies examine glucose levels in spiked serum samples where serum solutions are diluted in PBS.[50,5142 43] In this study, the electrode performance was examined in 100 % FBS solution to evaluate sensor performance in a more complex biological fluid. A chronoamperometric response was measured for 70 seconds at 0.25 V in FBS, this measurement was then repeated with FBS spiked with 2mM increments of glucose solution (see Figure 2.25). Using standard addition the concentration of the unknown FBS sample was approximated. A background subtraction signal could not be obtained for the calibration, as we did not have FBS of zero glucose concentration. Using Origin, linear regression was applied to determine the x-intercept (-5.49) indicating a glucose concentration of 5.49 mM.[52] The Abbott freestyle optimum neo glucometer confirmed a concentration of 5.07 ± 0.38 mM for n = 10 samples. The increase in concentration determined using the standard addition approach could be a result of the background signal of the FBS. A clear decrease in measured current density was evident (see Figure 2.24) in comparison to the calibration obtained in PBS (Figure 2.21). This is likely to have been a result of the added complexity of the serum. FBS contains lipids, electrolytes, hormones, enzymes, protein and even low levels of antibodies. The reduced sensitivity is likely attributed to non-specific adsorption or precipitation of agents present in the serum onto electrodes. Similar sensitivity changes owing to a change of matrix have been reported by Bollella *et al*., whereby, a microneedle sensor sensitivity determined in buffer was 1473 $\mu A\ cm^{-2}\ mM^{-1}$ and analysis in human serum revealed a sensitivity of $180 \pm 9\ \mu A\ cm^{-2}\ mM^{-1}$.[53] Here, using an integrated on-chip approach, all electrode materials in contact with the serum are subject to potential fouling slowing the movement of glucose to the immobilised glucose oxidase. Despite the decrease in current, a linear response was observed with increasing glucose concentrations up to 17 mM. The results clearly demonstrate that the microband sensors are capable of measuring glucose at physiologically relevant glucose concentrations in complex media solutions. The findings

are of particular significance for point of care applications where specificity, low time-to-results and minimal sample preparation are required to permit early diagnostics.

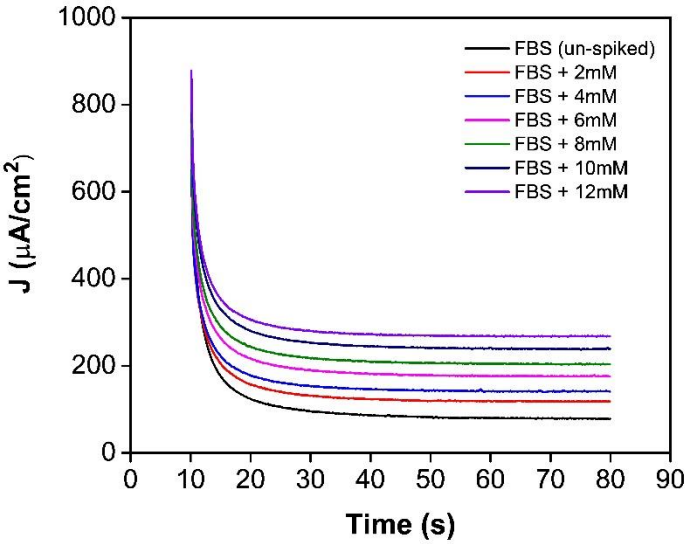

***Figure 2.25**: i-t curves for the chronoamperometric response in 100 % FBS spiked with known concentrations of glucose.*

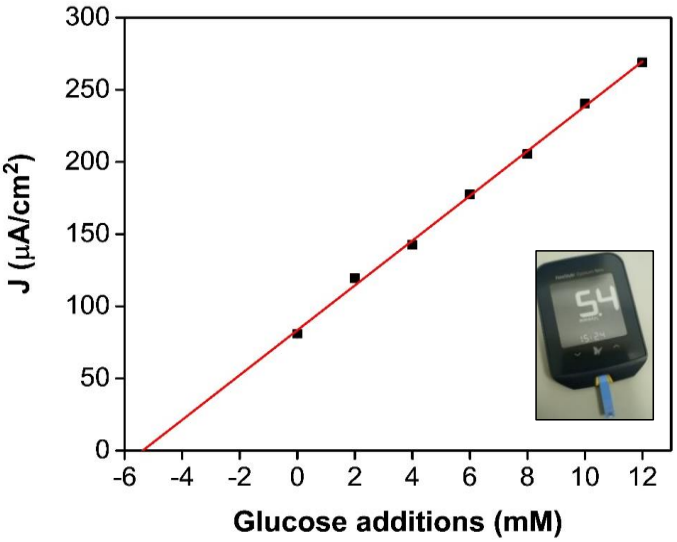

***Figure 2.24**: Corresponding standard addition for figure 2.24, where I was sampled after time 50 seconds.*

2.4 Conclusions and Future Perspectives

This chapter presents a simple two-step electrochemical modification to a single gold microband electrode using the on-chip counter and reference electrodes. The chip used in this work was fabricated with a view to functionalising other electrodes in the future for

multi-analyte detection. SEM images obtained after each modification confirmed a change in surface morphology. EIS measurements carried out in 1 mM FcCOOH confirmed a change in the R_{ct} following each electrode modification step. Glucose detection from 2.5 mM to 15.5 mM was achieved in buffer-based solutions, demonstrating that the electro-polymerisation of the o-PD/β-cyclodextrin/GOx mixture was successful in immobilising the enzyme at the surface of the microband. A number of examples of glucose sensors developed on microelectrodes are presented in Table 2.2. In comparison to many of these, this device offers a lower operating potential owing to the use of the pseudo-reference electrode. The linear detection range is wider and applicable for sensing in bio-fluids such as blood and interstitial fluid.[46] The biosensor reached a steady-state response within 10 seconds of applying a potential. The device demonstrates the potential for mediator-free, on-device electrochemical glucose sensing at the ultramicro scale. Chronoamperometric measurements carried out in 100% FBS confirmed a reduction in sensitivity in comparison to measurements in phosphate-based buffers. Whilst the linear range does not fulfill the entire range required for blood glucose measurements, there is potential for other bio-fluids and diluted media.[47]

Table 2.2: *A comparison of mediator-free miniaturized enzymatic glucose biosensors constructed towards various biomedical sensing applications with the on-chip ultramicroelectrode glucose sensor presented in this work.*

Electrode material*	Linear range	Operating potential	Enzyme immobilization	Sensitivity	Samples tested	Ref.
CFM/Pt-GOx(0.5%)-GA	0-4 mM	0.7 V vs. Ag/AgCl (external RE)	Covalent	0.697 nA mM^{-1} cm^{-2}	Brain slices	
CF-PEDOT-GOx	0.5-15 mM	−0.65 V vs Ag/AgCl (external RE)	Entrapment	8.5 µA mM^{-1} cm^{-2}	PBS	
Pt/PEDGE/BSA-GOx	0-5 mM	0.85 V vs Ag/AgCl (external RE)	Covalent	20.72 pA mM^{-1}	Intracellular	[55]
Pt-B electrode	0.2–43.5 mM	0.7V vs Ag/AgCl (on-device)	Free in solution	Not reported	Serum samples	[56]
Pt/PAA/CS/AuNPs/GOx	0.017–0.81 mM	-0.4V to 0.4 V to vs. Pt (on-device)	Layer by Layer assembly	61.4 µA $mM^{-1}cm^{-2}$	Saliva	[57]
Silver/Nafion/GA-GOx	0-2 mM	0.05 V vs Ag/AgCl (external electrode)	Covalent	1.73 µA mM^{-1}	PBS	[58]
Pt/GA-BSA-GOx/PU/Nafion	0-11 mM	0.5 V vs. IrOx (on-device)	Covalent	1.51 nA mM^{-1}	Intradermal	[59]
GOx-β-cyclodextrin-o-PD/Pt-B/Au	2.5-17 mM	0.25 V vs. Pt (on-device)	Entrapment	111.21 µA mM^{-1} cm^{-2} (Buffer), 15 µA mM^{-1} cm^{-2} (Serum)	Fetal bovine serum	This work

* Abbreviations: CFM: carbon fibre microelectrode, Pt: platinum, GOx: glucose oxidase, GA: glutaraldehyde, CF: carbon fibre, PEDOT: poly (3, 4-ethylenedioxythiophene), PEDGE: poly (ethylene glycol) diglycidyl ether, BSA: bovine serum albumin, PAA: poly (allylamine), CS: chitosan, AuNPs: gold nanoparticles, and PU: polyurethane.

2.5 References

(1) Lisi, F.; Peterson, J. R.; Gooding, J. J. The Application of Personal Glucose Meters as Universal Point-of-Care Diagnostic Tools. *Biosensors and Bioelectronics* **2020**, *148*, 111835. https://doi.org/10.1016/j.bios.2019.111835.

(2) Bobrowski, T.; Schuhmann, W. Long-Term Implantable Glucose Biosensors. *Current Opinion in Electrochemistry* **2018**, *10*, 112–119. https://doi.org/10.1016/j.coelec.2018.05.004.

(3) Teymourian, H.; Barfidokht, A.; Wang, J. Electrochemical Glucose Sensors in Diabetes Management: An Updated Review (2010–2020). *Chem. Soc. Rev.* **2020**, *49* (21), 7671–7709. https://doi.org/10.1039/D0CS00304B.

(4) Corradini, S.; Pilosio, B.; Dondi, F.; Linari, G.; Testa, S.; Brugnoli, F.; Gianella, P.; Pietra, M.; Fracassi, F. Accuracy of a Flash Glucose Monitoring System in Diabetic Dogs. *J Vet Intern Med* **2016**, *30* (4), 983–988. https://doi.org/10.1111/jvim.14355.

(5) Mross, S.; Zimmermann, T.; Zenzes, S.; Kraft, M.; Vogt, H. Study of Enzyme Sensors with Wide, Adjustable Measurement Ranges for in-Situ Monitoring of Biotechnological Processes. *Sensors and Actuators B: Chemical* **2017**, *241*, 48–54. https://doi.org/10.1016/j.snb.2016.10.054.

(6) Cinti, S.; Marrone, R.; Mazzaracchio, V.; Moscone, D.; Arduini, F. Novel Bio-Lab-on-a-Tip for Electrochemical Glucose Sensing in Commercial Beverages. *Biosensors and Bioelectronics* **2020**, *165*, 112334. https://doi.org/10.1016/j.bios.2020.112334.

(7) Artigues, M.; Abellà, J.; Colominas, S. Analytical Parameters of an Amperometric Glucose Biosensor for Fast Analysis in Food Samples. *Sensors* **2017**, *17* (11), 2620. https://doi.org/10.3390/s17112620.

(8) Dung, N. Q.; Duong, T. T. T.; Lam, T. D.; Dung, D. D.; Huy, N. N.; Van Thanh, D. A Simple Route for Electrochemical Glucose Sensing Using Background Current Subtraction of Cyclic Voltammetry Technique. *Journal of Electroanalytical Chemistry* **2019**, *848*, 113323. https://doi.org/10.1016/j.jelechem.2019.113323.

(9) Diouf, A.; Bouchikhi, B.; El Bari, N. A Nonenzymatic Electrochemical Glucose Sensor Based on Molecularly Imprinted Polymer and Its Application in Measuring Saliva Glucose. *Materials Science and Engineering: C* **2019**, *98*, 1196–1209. https://doi.org/10.1016/j.msec.2019.01.001.

(10) Rassas, I.; Braiek, M.; Bonhomme, A.; Bessueille, F.; Raffin, G.; Majdoub, H.; Jaffrezic-Renault, N. Highly Sensitive Voltammetric Glucose Biosensor Based on Glucose Oxidase Encapsulated in a Chitosan/Kappa-Carrageenan/Gold Nanoparticle Bionanocomposite. *Sensors* **2019**, *19* (1), 154. https://doi.org/10.3390/s19010154.

(11) Marquitan, M.; Bobrowski, T.; Ernst, A.; Wilde, P.; Clausmeyer, J.; Ruff, A.; Schuhmann, W. Miniaturized Amperometric Glucose Sensors Based on Polymer/ Enzyme Modified Carbon Electrodes in the Sub-Micrometer Scale. *J. Electrochem. Soc.* **2018**, *165* (12), G3008–G3014. https://doi.org/10.1149/2.0021812jes.

(12) Jędrzak, A.; Rębiś, T.; Klapiszewski, Ł.; Zdarta, J.; Milczarek, G.; Jesionowski, T. Carbon Paste Electrode Based on Functional GOx/Silica-Lignin System to Prepare an Amperometric Glucose Biosensor. *Sensors and Actuators B: Chemical* **2018**, *256*, 176–185. https://doi.org/10.1016/j.snb.2017.10.079.

(13) Kuwahara, T.; Ogawa, K.; Sumita, D.; Kondo, M.; Shimomura, M. Amperometric Glucose Sensing with Polyaniline/Poly(Acrylic Acid) Composite Film Bearing Glucose Oxidase and Catalase Based on Competitive Oxygen Consumption Reactions. *Journal of Electroanalytical Chemistry* **2018**, *811*, 62–67. https://doi.org/10.1016/j.jelechem.2018.01.042.

(14) Morales, M. A.; Halpern, J. M. Guide to Selecting a Biorecognition Element for Biosensors. *Bioconjugate Chem.* **2018**, *29* (10), 3231–3239. https://doi.org/10.1021/acs.bioconjchem.8b00592.

(15) Li, D.; Lin, C.; Batchelor-McAuley, C.; Chen, L.; Compton, R. G. Electrochemical Measurement of the Size of Microband Electrodes: A Theoretical Study. *Journal of Electroanalytical Chemistry* **2019**, *840*, 279–284. https://doi.org/10.1016/j.jelechem.2019.04.006.

(16) Streeter, I.; Fietkau, N.; del Campo, J.; Mas, R.; Mũnoz, F. X.; Compton, R. G. Voltammetry at Regular Microband Electrode Arrays: Theory and Experiment. *J. Phys. Chem. C* **2007**, *111* (32), 12058–12066. https://doi.org/10.1021/jp073224d.

(17) Orozco, J.; Fernández-Sánchez, C.; Jiménez-Jorquera, C. Ultramicroelectrode Array Based Sensors: A Promising Analytical Tool for Environmental Monitoring. *Sensors (Basel)* **2010**, *10* (1), 475–490. https://doi.org/10.3390/s100100475.

(18) Hrapovic, S.; Luong, J. H. T. Picoamperometric Detection of Glucose at Ultrasmall Platinum-Based Biosensors: Preparation and Characterization. *Anal. Chem.* **2003**, *75* (14), 3308–3315. https://doi.org/10.1021/ac026438u.

(19) Nebling, E.; Grunwald, T.; Albers, J.; Schäfer, P.; Hintsche, R. Electrical Detection of Viral DNA Using Ultramicroelectrode Arrays. *Anal. Chem.* **2004**, *76* (3), 689–696. https://doi.org/10.1021/ac0348773.

(20) Lee, J. Y.; Kim, B.-K.; Kang, M.; Park, J. H. Label-Free Detection of Single Living Bacteria via Electrochemical Collision Event. *Sci Rep* **2016**, *6* (1), 30022. https://doi.org/10.1038/srep30022.

(21) Creedon, N.; sayers, R.; O'sullivan, B.; kennedy, emer; Lovera, P.; O'Riordan, A. *Label-Free Impedimetric Nanoband Sensor for Detection of Both Bovine Viral Diarrhoea Virus (BVDV) and Antibody (BVDAb) in Serum*; preprint; Chemistry, 2018. https://doi.org/10.26434/chemrxiv.7326719.v1.

(22) Dawson, K.; Wahl, A.; Murphy, R.; O'Riordan, A. Electroanalysis at Single Gold Nanowire Electrodes. *J. Phys. Chem. C* **2012**, *116* (27), 14665–14673. https://doi.org/10.1021/jp302967p.

(23) Zhao, M.; Gao, Y.; Sun, J.; Gao, F. Mediatorless Glucose Biosensor and Direct Electron Transfer Type Glucose/Air Biofuel Cell Enabled with Carbon Nanodots. *Anal. Chem.* **2015**, *87* (5), 2615–2622. https://doi.org/10.1021/acs.analchem.5b00012.

(24) Chinnadayyala, S. R.; Park, I.; Cho, S. Nonenzymatic Determination of Glucose at near Neutral PH Values Based on the Use of Nafion and Platinum Black Coated Microneedle Electrode Array. *Microchim Acta* **2018**, *185* (5), 250. https://doi.org/10.1007/s00604-018-2770-1.

(25) Urban, S.; Weltin, A.; Flamm, H.; Kieninger, J.; Deschner, B. J.; Kraut, M.; Dittmeyer, R.; Urban, G. A. Electrochemical Multisensor System for Monitoring Hydrogen Peroxide, Hydrogen and Oxygen in Direct Synthesis Microreactors. *Sensors and Actuators B: Chemical* **2018**, *273*, 973–982. https://doi.org/10.1016/j.snb.2018.07.014.

(26) Malitesta, Cosimino.; Palmisano, Francesco.; Torsi, Luisa.; Zambonin, P. Giorgio. Glucose Fast-Response Amperometric Sensor Based on Glucose Oxidase

Immobilized in an Electropolymerized Poly(o-Phenylenediamine) Film. *Anal. Chem.* **1990**, *62* (24), 2735–2740. https://doi.org/10.1021/ac00223a016.

(27) Sasso, S. V.; Pierce, R. J.; Walla, Robert.; Yacynych, A. M. Electropolymerized 1,2-Diaminobenzene as a Means to Prevent Interferences and Fouling and to Stabilize Immobilized Enzyme in Electrochemical Biosensors. *Anal. Chem.* **1990**, *62* (11), 1111–1117. https://doi.org/10.1021/ac00210a004.

(28) Lowry, J. P.; McAteer, Karl.; El Atrash, S. S.; Duff, Adrienne.; O'Neill, R. D. Characterization of Glucose Oxidase-Modified Poly(Phenylenediamine)-Coated Electrodes in Vitro and in Vivo: Homogeneous Interference by Ascorbic Acid in Hydrogen Peroxide Detection. *Anal. Chem.* **1994**, *66* (10), 1754–1761. https://doi.org/10.1021/ac00082a025.

(29) Garjonyte, R.; Malinauskas, A. Amperometric Glucose Biosensor Based on Glucose Oxidase Immobilized in Poly(o-Phenylenediamine) Layer. *Sensors and Actuators B: Chemical* **1999**, *56* (1–2), 85–92. https://doi.org/10.1016/S0925-4005(99)00163-X.

(30) Li, J.; Koinkar, P.; Fuchiwaki, Y.; Yasuzawa, M. A Fine Pointed Glucose Oxidase Immobilized Electrode for Low-Invasive Amperometric Glucose Monitoring. *Biosensors and Bioelectronics* **2016**, *86*, 90–94. https://doi.org/10.1016/j.bios.2016.06.037.

(31) Mousa, H. M.; Aggas, J. R.; Guiseppi-Elie, A. Electropolymerization of Aniline and (N-Phenyl-o-Phenylenediamine) for Glucose Biosensor Application. *Materials Letters* **2019**, *238*, 267–270. https://doi.org/10.1016/j.matlet.2018.12.012.

(32) Mohan, A. M. V.; Windmiller, J. R.; Mishra, R. K.; Wang, J. Continuous Minimally-Invasive Alcohol Monitoring Using Microneedle Sensor Arrays. *Biosensors and Bioelectronics* **2017**, *91*, 574–579. https://doi.org/10.1016/j.bios.2017.01.016.

(33) Ganesana, M.; Trikantzopoulos, E.; Maniar, Y.; Lee, S. T.; Venton, B. J. Development of a Novel Micro Biosensor for in Vivo Monitoring of Glutamate Release in the Brain. *Biosensors and Bioelectronics* **2019**, *130*, 103–109. https://doi.org/10.1016/j.bios.2019.01.049.

(34) Harley, C. C.; Rooney, A. D.; Breslin, C. B. The Selective Detection of Dopamine at a Polypyrrole Film Doped with Sulfonated β-Cyclodextrins. *Sensors and Actuators B: Chemical* **2010**, *150* (2), 498–504. https://doi.org/10.1016/j.snb.2010.09.012.

(35) Barrett, C.; O'Sullivan, F.; Barry, S.; Grygoryev, K.; O'Gorman, D.; O'Mahony, C.; O'Riordan, A. Novel Surface Modified Polymer Microneedle Based Biosensors for Interstitial Fluid Glucose Detection. In *2019 IEEE SENSORS*; IEEE: Montreal, QC, Canada, 2019; pp 1–4. https://doi.org/10.1109/SENSORS43011.2019.8956509.

(36) Dawson, K.; Baudequin, M.; Sassiat, N.; Quinn, A. J.; O'Riordan, A. Electroanalysis at Discrete Arrays of Gold Nanowire Electrodes. *Electrochimica Acta* **2013**, *101*, 169–176. https://doi.org/10.1016/j.electacta.2012.09.105.

(37) Wahl, A.; Barry, S.; Dawson, K.; MacHale, J.; Quinn, A. J.; O'Riordan, A. Electroanalysis at Ultramicro and Nanoscale Electrodes: A Comparative Study. *J. Electrochem. Soc.* **2014**, *161* (2), B3055–B3060. https://doi.org/10.1149/2.010402jes.

(38) Robinson, C.; Creedon, N.; Sayers, R.; Kennedy, E.; O'Riordan, A. Electrochemical Detection of Bovine Immunoglobulins G to Determine Passive

Transfer of Antibodies to Calves. *Anal. Methods* **2020**, *12* (21), 2655–2660. https://doi.org/10.1039/D0AY00194E.

(39) Burke, L. D.; Nugent, P. F. The Electrochemistry of Gold: I the Redox Behaviour of the Metal in Aqueous Media. *Gold Bull* **1997**, *30* (2), 43–53. https://doi.org/10.1007/BF03214756.

(40) Bard, A. J.; Faulkner, L. R. Ch 5 Basic Potential Step Methods. In *Electrochemical Methods: Fundamentals and Applications*; Wiley: New York, 2001; pp 156–225.

(41) Henstridge, M. C.; Compton, R. G. Mass Transport to Micro- and Nanoelectrodes and Their Arrays: A Review. *Chem Record* **2012**, *12* (1), 63–71. https://doi.org/10.1002/tcr.201100032.

(42) Chakraborty, S.; Retna Raj, C. Pt Nanoparticle-Based Highly Sensitive Platform for the Enzyme-Free Amperometric Sensing of H2O2. *Biosensors and Bioelectronics* **2009**, *24* (11), 3264–3268. https://doi.org/10.1016/j.bios.2009.04.015.

(43) Liu, L.; Chen, Y.; Lv, H.; Wang, G.; Hu, X.; Wang, C. Construction of a Non-Enzymatic Glucose Sensor Based on Copper Nanoparticles/Poly(o-Phenylenediamine) Nanocomposites. *J Solid State Electrochem* **2015**, *19* (3), 731–738. https://doi.org/10.1007/s10008-014-2659-9.

(44) Ito, Y.; Okuda-Shimazaki, J.; Tsugawa, W.; Loew, N.; Shitanda, I.; Lin, C.-E.; La Belle, J.; Sode, K. Third Generation Impedimetric Sensor Employing Direct Electron Transfer Type Glucose Dehydrogenase. *Biosensors and Bioelectronics* **2019**, *129*, 189–197. https://doi.org/10.1016/j.bios.2019.01.018.

(45) Rezaei, B.; Boroujeni, M. K.; Ensafi, A. A. Fabrication of DNA, o-Phenylenediamine, and Gold Nanoparticle Bioimprinted Polymer Electrochemical Sensor for the Determination of Dopamine. *Biosensors and Bioelectronics* **2015**, *66*, 490–496. https://doi.org/10.1016/j.bios.2014.12.009.

(46) Rothwell, S. A.; Killoran, S. J.; Neville, E. M.; Crotty, A. M.; O'Neill, R. D. Poly(o-Phenylenediamine) Electrosynthesized in the Absence of Added Background Electrolyte Provides a New Permselectivity Benchmark for Biosensor Applications. *Electrochemistry Communications* **2008**, *10* (7), 1078–1081. https://doi.org/10.1016/j.elecom.2008.05.018.

(47) Layer, R. W. Amines, Aromatic, Phenylenediamines: Amines, Aromatic. In *Kirk-Othmer Encyclopedia of Chemical Technology*; John Wiley & Sons, Inc., Ed.; John Wiley & Sons, Inc.: Hoboken, NJ, USA, 2000; p 1608051412012505.a01. https://doi.org/10.1002/0471238961.1608051412012505.a01.

(48) Chen, X.; Chen, J.; Deng, C.; Xiao, C.; Yang, Y.; Nie, Z.; Yao, S. Amperometric Glucose Biosensor Based on Boron-Doped Carbon Nanotubes Modified Electrode. *Talanta* **2008**, *76* (4), 763–767. https://doi.org/10.1016/j.talanta.2008.04.023.

(49) Chu, X.; Wu, B.; Xiao, C.; Zhang, X.; Chen, J. A New Amperometric Glucose Biosensor Based on Platinum Nanoparticles/Polymerized Ionic Liquid-Carbon Nanotubes Nanocomposites. *Electrochimica Acta* **2010**, *55* (8), 2848–2852. https://doi.org/10.1016/j.electacta.2009.12.057.

(50) Mehmeti, E.; Stanković, D. M.; Chaiyo, S.; Zavasnik, J.; Žagar, K.; Kalcher, K. Wiring of Glucose Oxidase with Graphene Nanoribbons: An Electrochemical Third Generation Glucose Biosensor. *Microchim Acta* **2017**, *184* (4), 1127–1134. https://doi.org/10.1007/s00604-017-2115-5.

(51) Vijayaraj, K.; Hong, S. W.; Jin, S.-H.; Chang, S.-C.; Park, D.-S. Fabrication of a Novel Disposable Glucose Biosensor Using an Electrochemically Reduced Graphene Oxide–Glucose Oxidase Biocomposite. *Anal. Methods* **2016**, *8* (38), 6974–6981. https://doi.org/10.1039/C6AY02032A.

(52) Ellison, S. L. R.; Thompson, M. Standard Additions: Myth and Reality. *Analyst* **2008**, *133* (8), 992. https://doi.org/10.1039/b717660k.
(53) Bollella, P.; Sharma, S.; Cass, A. E. G.; Antiochia, R. Microneedle-Based Biosensor for Minimally-Invasive Lactate Detection. *Biosensors and Bioelectronics* **2019**, *123*, 152–159. https://doi.org/10.1016/j.bios.2018.08.010.
(54) Chen, J.; Zheng, X.; Li, Y.; Zheng, H.; Liu, Y.; Suye, S. A Glucose Biosensor Based on Direct Electron Transfer of Glucose Oxidase on PEDOT Modified Microelectrode. *J. Electrochem. Soc.* **2020**, *167* (6), 067502. https://doi.org/10.1149/1945-7111/ab7e26.
(55) Liao, Q.-L.; Jiang, H.; Zhang, X.-W.; Qiu, Q.-F.; Tang, Y.; Yang, X.-K.; Liu, Y.-L.; Huang, W.-H. A Single Nanowire Sensor for Intracellular Glucose Detection. *Nanoscale* **2019**, *11* (22), 10702–10708. https://doi.org/10.1039/C9NR01997A.
(56) Gu, S.; Lu, Y.; Ding, Y.; Li, L.; Song, H.; Wang, J.; Wu, Q. A Droplet-Based Microfluidic Electrochemical Sensor Using Platinum-Black Microelectrode and Its Application in High Sensitive Glucose Sensing. *Biosensors and Bioelectronics* **2014**, *55*, 106–112. https://doi.org/10.1016/j.bios.2013.12.002.
(57) Zhang, W.; Du, Y.; Wang, M. L. On-Chip Highly Sensitive Saliva Glucose Sensing Using Multilayer Films Composed of Single-Walled Carbon Nanotubes, Gold Nanoparticles, and Glucose Oxidase. *Sensing and Bio-Sensing Research* **2015**, *4*, 96–102. https://doi.org/10.1016/j.sbsr.2015.04.006.
(58) Yang, H.; Rahman, M. T.; Du, D.; Panat, R.; Lin, Y. 3-D Printed Adjustable Microelectrode Arrays for Electrochemical Sensing and Biosensing. *Sensors and Actuators B: Chemical* **2016**, *230*, 600–606. https://doi.org/10.1016/j.snb.2016.02.113.
(59) Ribet, F.; Stemme, G.; Roxhed, N. Ultra-Miniaturization of a Planar Amperometric Sensor Targeting Continuous Intradermal Glucose Monitoring. *Biosensors and Bioelectronics* **2017**, *90*, 577–583. https://doi.org/10.1016/j.bios.2016.10.007.

Chapter 3 Laser scribed graphitic carbon on polyimide substrates, towards bendable enzymatic lactate sensing

3.1 Introduction

Laser scribed graphitic carbon fabrication, first introduced by Lin *et al.* has been demonstrated as a fast, scalable and effective means of constructing electrodes on polymer substrates in comparison with techniques such as screen-printing, metallisation, inkjet printing or extrusion printing processes.[1–3] Laser scribed electrodes have been applied in UV photodetectors, microsupercapacitors, immunosensors and both enzymatic and non-enzymatic biosensors.[4–8] Direct laser scribing can create electrodes and interconnection tracks based on a custom-design using either an infrared or visible laser source. LSG electrodes previously fabricated in Tyndall using a 450 nm laser confirmed improved electrocatalytic performance in comparison to graphite based electrodes fabricated using other visible or infrared lasers.[9] The enhanced electron transfer behaviour is attributed to a highly porous 3D graphitic network containing high surface area edge planes.

This chapter reports on the use of laser scribed graphitic carbon (LSG) electrodes for the construction of an enzymatic lactate sensor with a working range of 0.2 mM to 3 mM, demonstrating potential for hyperlactatemia indication in saliva. Lactate is an indicator of a number of clinical conditions including tissue hypoxia,[10] heart failure,[11] sepsis,[12] and ischemia.[13] Lactate is also an attractive metabolite for human sports performance assessments such as fitness and endurance.[14] Current techniques for blood lactate monitoring in a hospital setting involve extracting blood intravenously and measuring lactate using a blood gas analyser.[15] Other commercial laboratory instruments such as Biosen analyzers and Yellow Spring Instruments (YSI) can quantify lactate from blood, serum and plasma. These bench top approaches are not a straightforward means for monitoring lactate levels over time owing to the need for repeated blood extraction and sample handling.

Electrochemical lactate biosensor developments have predominantly focused on either enzymatic sensing, using lactate oxidase (LOx) or lactate deyhydrogenase (LDH), or non-enzymatic approaches using materials such as metal oxides and conducting polymers for direct lactate detection.[16,17] Non-enzymatic lactate sensing is attractive for low cost and simplified fabrication processes, however, many non-enzymatic approaches have demonstrated detection in basic solutions such as NaOH which are not biological fluids.[18]

Enzymatic biosensors provide high specificity, high sensitivity, quick response times, and direct measurements. Flexible substrates have been used to fabricate a number of lactate sensors for lactate analysis in saliva samples. Petropoulos *et al.* constructed a lactate sensor via screen-printing of a graphite based ink and subsequent modification with prussian blue and a lactate oxidase-nafion layer.[19] Sensor performance studies demonstrated lactate detection between 0.025 mM and 0.25 mM. Cited salivary lactate concentrations reported are approximately 0.1–0.5 mM in healthy individuals at rest but have been reported at higher concentrations of up to 2.5 mM under irregular conditions.[20] Fabrication of working, counter and reference electrodes onto the one platform is pivotal towards producing functional flexible diagnostic biosensor devices. Recently, Marques *et al*. demonstrated electrochemical analysis of ascorbic acid and amoxicillin using a four-electrode configuration, where LSG was used for both the counter and reference electrode.[21]

In this chapter[§], a comparison between the use of a commercial external Ag/AgCl reference electrode, an LSG reference electrode and an Ag/AgCl modified LSG reference electrode was conducted for chronoamperometric lactate measurements. The use of flexible substrates is of interest for the construction of bendable electrodes. Previous studies have documented the effect of bending LSG at both concave and convex curvatures by cycling the electrodes in $[Fe(CN)_6]^{4-}$, whereby, the peak current density between planar, concave and convex stresses was determined to vary by less than 1 %.[3] We explore the potential for chronoamperometric lactate detection using a three-electrode LSG sensor fixed at a bending radius of 7 mm. This work is the first study on scribing a three-electrode configuration on polyimide for bendable lactate sensing.

[§] This work has been published in 'Electrochemical Sensor for Enzymatic Lactate Detection Based on Laser-Scribed Graphitic Carbon Modified with Platinum, Chitosan and Lactate Oxidase.' *Talanta* **2022**, 246, 123492. https://doi.org/10.1016/j.talanta.2022.123492.

3.2 Experimental

3.2.1 Materials, Instrumentation and Software

Polyimide adhesive (0.08 mm) was purchased from Radionics. An Automatic Desktop Laser Engraving Machine was purchased from KK moone. Polyethylene terephthalate films (0.025 mm) were purchased from Goodfellow. Silver paste was purchased from Radionics. Recombinant Lactate Oxidase II from Aerococcus viridans was purchased from Sekisui Ltd. (Lyophilized powder, activity 42.8 U/mg) (UK). Acetic acid was purchased from Fisher Scientific. Phosphate buffered saline, sodium phosphate monobasic, sodium phosphate dibasic, chitosan, potassium ferrocyanide ($K_4[Fe(CN)_6]$), potassium ferricyanide ($K_3[Fe(CN)_6]$), hexachloroplatanic acid, sulfuric acid, l -lactic acid, glucose, uric acid, ascorbic acid acetaminophen and sterile human serum were purchased from Sigma Aldrich. All solutions were prepared with double deionised water with a resistivity of 18.2 MΩ cm. Artificial saliva for medical and dental research was purchased from Pickering Laboratories. Measurements with the Lactate Pro 2 were conducted in the Human Performance Lab, Department of Sport and Physical activity in University College Cork. Unless otherwise stated, electrochemical experiments were performed in a 50 mM phosphate buffer solution (sodium phosphate monobasic and sodium phosphate dibasic) prepared at a pH of 6.7. All electrochemical measurements were carried out with an Autolab electrochemical workstation PGSTAT302N (Metrohm, UK) using the control software NOVA 2.1. Measurements were performed at room temperature within a Faraday Cage (Metrohm). Data curation was carried out using OriginPro software. An electrochemical cell holder was 3D printed using a Form labs 3-D printer. O-rings with a diameter of 7 mm were purchased from duratool to create a seal between the well within the cell holder and the laser scribed electrodes. Crocodile clips and ribbed wires were purchased from Farnell for connection to the potentiostat. A second electrochemical cell holder was also 3D printed with a Form labs 3-D printer for measurements conducted at a fixed bending radius (7 mm).

3.2.2 Electrode fabrication

Polyimide (PI) tape was attached to a cover slip and glass slide to ensure that the PI remains in a planar and rigid configuration during the laser writing process. A 3 W 450 nm laser was used to irradiate the polyimide tape at 30 % laser power producing the porous graphite electrodes on the region of Polyimide covering the cover slip.[**] For measurements conducted at a bending radius of 7 mm, polyethylene terephthalate (PET) films were used in place of the cover slip. Following fabrication, electrodes were rinsed with acetone, DI water, isopropanol and DI water to remove any unwanted deposits from the process. An acrylic nail varnish was applied to the interconnection tracks connecting to the scribed WE, CE and RE to ensure regions exposed within the o-ring were passivated. Silver paste was applied to the regions of the interconnect for contact with crocodile clips.

3.2.3 Sensor preparation and optimisation

Three Pt deposition times, three chitosan concentrations (wt %) and three enzyme concentrations (U) were selected to study potential optimal parameters for the biosensor construction process. The Pt electrodeposition was carried out using amperometry in a solution containing 5 mM H_2PtCl_6 and 0.5 M H_2SO_4 at -0.5 V for 80 seconds against an Ag/AgCl (saturated KCL) RE from CH Instruments and a Pt wire was employed as the CE. Following the Pt electro-deposition, samples were rinsed with DI water and allowed to dry under ambient conditions. A 0.3 wt % chitosan solution was prepared by dissolving chitosan in acetic acid solution (1 wt %) under magnetic stirring for 60 minutes. 6 µl of the chitosan solution was cast on the surface and allowed to dry at room temperature. Aliquots of 2100 U/ml of enzyme were prepared in 50 mM PB solution (pH 6.7) and frozen for use. 6 µl of the enzyme stock were mixed with 24 µl of PB (50 mM, pH 6.7) and 6 µl of the solution was cast on to the surface of the Pt-Chitosan modified electrode. The electrodes were stored overnight at 4 °C in a sealed petri-dish containing lens tissue which had been dampened with ultrapure water. The enzyme mixture was rinsed gently from the surface using 50 mM PB the following day to remove any unbound enzyme.

[**] Laser scribing electrode fabrication was carried out by Mr. Eoghan Vaughan (Tyndall, PhD Student, UCC)

Electrodes were subsequently stored in the fridge with 50 mM PB (pH 6.7) at 4 °C until use.

3.2.4 Characterisation

3.2.4.1 *SEM-EDX*

Scanning electron microscopy images (SEM) and Energy dispersive X-ray analysis (EDX) of the base LSG electrodes, LSG-Pt electrodes and after the chitosan-enzyme casting process was completed with a SEM Quanta 650 Field Emission Gun (FEG) attached with an EDX unit. An accelerating voltage of 10 kV was used for imaging and 20 kV was applied for EDX.

3.2.4.2 *Cyclic Voltammetry*

The working electrode was characterised using cyclic voltammetry (CV) in a 10 mM PBS solution (pH = 7.4) containing 5 mM $K_4[Fe(CN)_6]$ and 5 mM $K_3[Fe(CN)_6]$. CV was performed by cycling the potential from –200 mV to +650 mV versus a Ag/AgCl reference electrode at scan rates of 10 mV/s, 25 mV/s, 50 mV/s, 75 mV/s and 100 mV/s at the bare LSG, Pt modified and CS-LOx modified surface to obtain a plot of peak current versus $v^{1/2}$ for each surface. Nicholsons method was used to determine the heterogeneous electron transfer (HET) rate constant k^0_{app} for each surface where a transfer coefficient $\alpha = 0.5$ and the diffusion coefficients: $[Fe(CN)_6]^{4-/3-}$, $D_0 = 7.63 \times 10^{-6}$ cm^2/s and $D_r = 6.32 \times 10^{-6}$ cm^2/s were assumed.[22]

3.2.5 Electrochemical Analysis

3.2.5.1 *Chronoamperometric lactate detection in phosphate based buffers*

L-lactic acid stock solution was prepared in 50 mM PB (pH 6.7). Buffers were spiked under stirred conditions for chronoamperometric measurements. As-modified electrodes were exposed to aliquots of PB containing lactate concentrations within physiologically relevant levels by dropping 350 µl aliquots into the well of the 3-D cell holder and allowing 30 seconds prior to running a chronoamperometric scan. The solution was

removed and the next concentration was directly added to the electrodes. All data was background subtracted using the values for the phosphate buffer baseline.

3.2.5.2 *Reproducibility, Interference, re-usability and storage*

Reproducibility between modified electrodes was determined by measuring a 1 mM lactate concentration for n = 5 sensors. The re-usability of the biosensor surface was evaluated by measuring 10 subsequent chronoamperometric measurements at 0.4 V for n = 3 samples. In each case, a fresh aliquot of a 1 mM lactate solution was applied to the sensor, the solution was left for 30 seconds prior to running a chronoamperometric scan at 0.4 V for 50 seconds. Five sensors were prepared to assess the storage stability of the LSG-Pt-CS-LOx sensor surface. A calibration was obtained at Day 1, Day 7, Day 14, and Day 30. The sensors were stored at 4°C when not in use with 50 mM PB (pH 6.7) covering the working electrode. The selectivity of the biosensor was studied against a mixture of interfering species that can be found in both saliva and blood. 10 µM acetaminophen, 100 µM Uric acid, 50 µM L-ascorbic acid and 500 µM glucose were assessed with a 0.5 mM lactate concentration in 50 mM PB (pH 6.7). As-modified electrodes were exposed to aliquots of PB containing 0.5 mM lactate with the interfering species by adding 350 µl aliquots onto the chip and allowing 30 seconds prior to running a chronoamperometric scan.

3.2.6 Three electrode configuration

CV was performed at the LSG WE at 100 mV/s in a 10 mM PBS solution (pH = 7.4) containing 5 mM $K_4[Fe(CN)_6]$ and 5 mM $K_3[Fe(CN)_6]$ using a commercial Ag/AgCl RE, an LSG RE and an Ag/AgCl paste modified LSG RE. Chronoamperometry was carried out at the LSG-Pt-CS-LOx WE (n = 3) using each RE. When conducting chronoamperometric measurements with LSG the operating potential was adjusted to 0.2 V owing to the shift in potential observed when connecting LSG as an RE during characterisation. To demonstrate a potential future application, biosensors were prepared to carry out measurements in both sterile human serum and artificial saliva samples spiked with known concentrations of lactate (0.5 mM and 1 mM). The three-LSG electrode configuration was used employing the Ag/AgCl paste modified LSG RE.

3.2.7 Flexibility test

Polyimide adhesive tape was attached to 0.025 mm PET films for measurements carried out at a fixed curvature. The 3-D printed holder was designed to fix the sensor at a bending radius of 7 mm equivalent to a curvature of 0.14 mm^{-1} (see Figure 3.1 A). Screws were inserted into the holder to fix the substrate in place (see Figure 3.1 B). Modified electrodes were exposed to aliquots of 50 mM PB (pH 6.7) containing lactate concentrations within physiologically relevant levels by adding 200 µl of solution into the well at the front of the holder (see Figure 3.1 B). Figure 3.1 C shows the printed holder with LSG based sensor fixed in place. The solution was left for 30 seconds prior to running a 40 second chronoamperometric scan at 0.2 V. The solution was removed and the next concentration was directly added to the electrodes. All data were background subtracted using PB as the blank baseline.

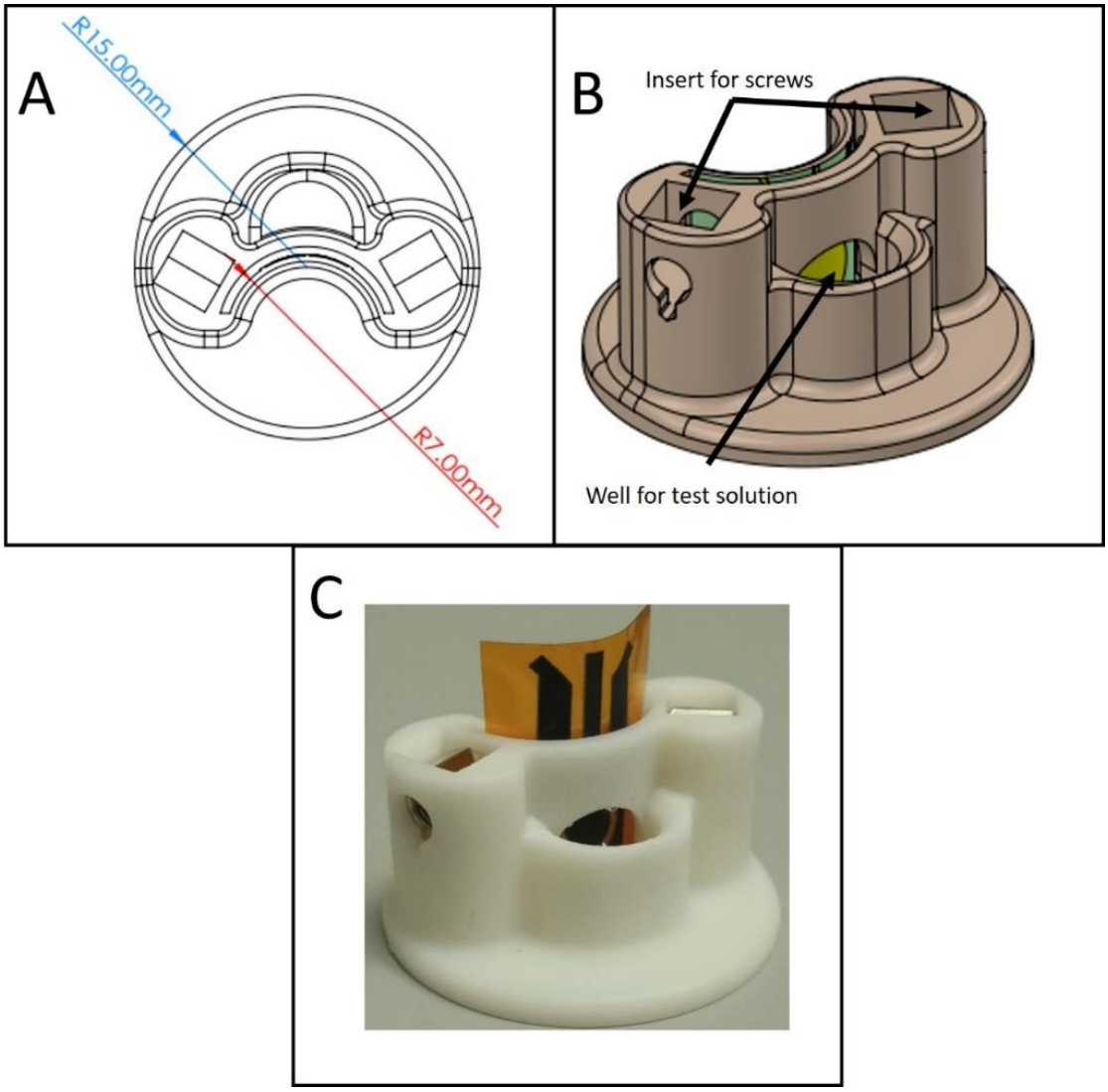

Figure 3.1: *(A) Drawing of a 3D printed holder indicating the bending radius of the insert for the PI-PET film, (B) 3D model of the holder indicating where the screws are inserted to 'fix' the PI-PET film in place.(C) Picture of 3-D printed holder with the sensor in place.*

3.3 Results and Discussion

3.3.1 Electrochemical set-up

Figure 3.2 A displays the 3-D printed holder used to facilitate electrochemical measurements at the LSG WE using an external commercial Ag/AgCl RE and a Pt wire as the CE. A microscopy image of the laser scribed WE,CE and RE are shown in Figure 3.2 B, acrylic varnish was applied to the interconnection tracks to prevent unwanted electrochemical measurements from occurring at regions exposed within the O-ring. For measurements using three-LSG electrodes fabricated on polyimide or Ag/AgCl paste modified LSG, crocodile clips were used to enable connection as displayed in Figure 3.2 C.

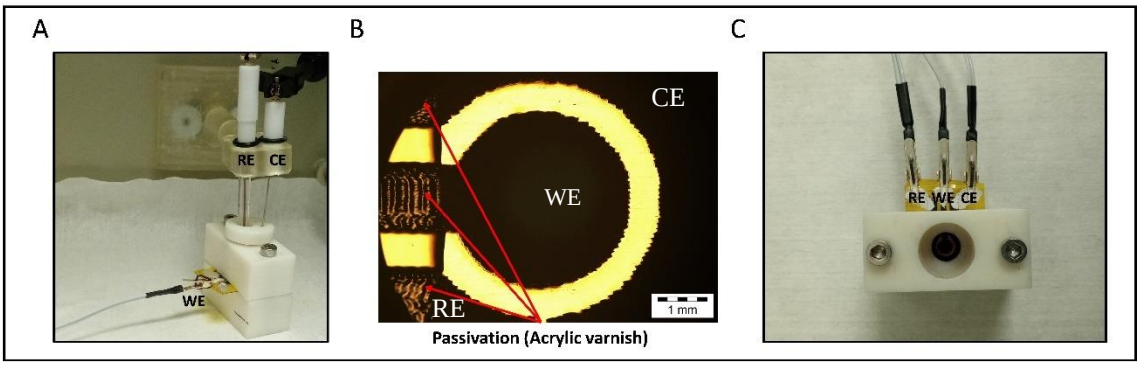

Figure 3.2: *(A) 3-D printed electrochemical cell holder to facilitate electrochemical measurements, (B) Optical microscopy image of the LSG WE and (C) set-up with three-LSG electrode approach.*

3.3.2 Optimisation and Sensor preparation

Figure 3.3 displays a schematic of the modification process used during sensor preparation. Platinum was chosen owing to its catalytic efficiency towards oxidation of H_2O_2.[23] Chitosan is biodegradable, permeable to water, biocompatible and cost effective all of which are favourable characteristics for biosensor construction.[24]

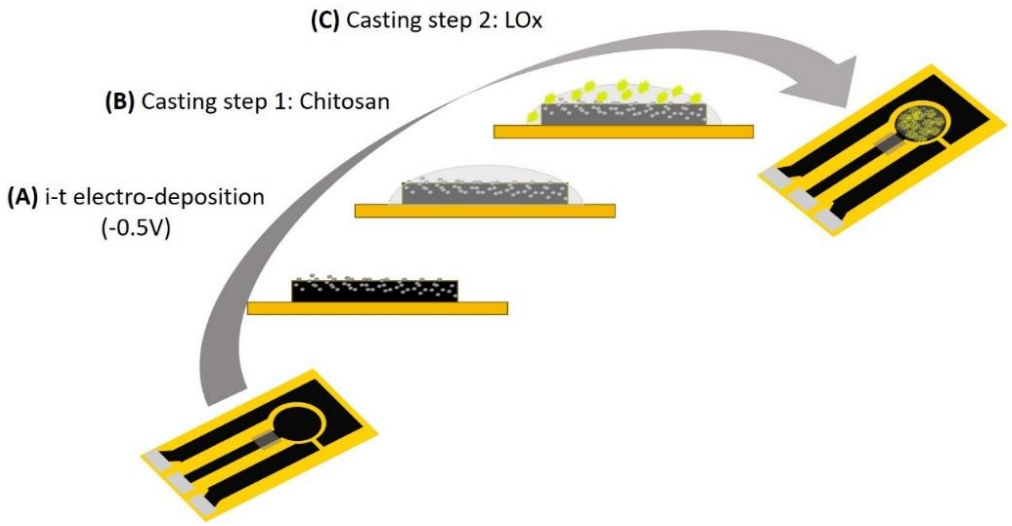

Figure 3.3: *Schematic of modification process including (A) an amperometric Pt deposition for 80 seconds, (B) casting chitosan on to the LSG-Pt electrode and finally (C) casting LOx on to the LSG-Pt-CS electrode.*

Biosensor response to a 1mM lactate concentration was measured at electrodes modified with a Pt electrodeposition time of 40 seconds, 80 seconds and 120 seconds. Chitosan and LOx concentrations were maintained at 0.3 wt % and 2.4 U respectively. Whilst it was expected that a longer deposition time of 120 seconds would provide a higher amperometric response to lactate sensing this was not the case. The increased content of Pt may have covered some of the porous regions of the graphite resulting in a lower quantity of enzyme adsorbing on the surface. An 80 second deposition time was determined to give the optimal response (see Figure 3.4 A). A typical amperometric deposition is displayed in Figure 3.5. Three separate chitosan concentrations were also assessed, 0.1 wt %, 0.3 wt % and 0.6 wt %. A chitosan concentration of 0.3 wt % showed the optimum response to lactate (see Figure 3.4 B). The higher concentration of CS may have resulted in reduced electron or mass transfer/transport, or a decrease in exposed surface area for electron transfer or perhaps a combination of both. In this instance, Pt deposition time was maintained at 80 seconds and the enzyme loading was kept at 2.4 U. Finally, three different concentrations of LOx enzyme were examined. The optimum concentration of enzyme stock was determined to be 2.4 U (Figure 3.4 C). Higher concentrations of enzyme resulted in a lower amperometric response, which could be attributed to the enzyme saturating the LSG-Pt-CS electrode materials resulting in a loss of catalytic activity.

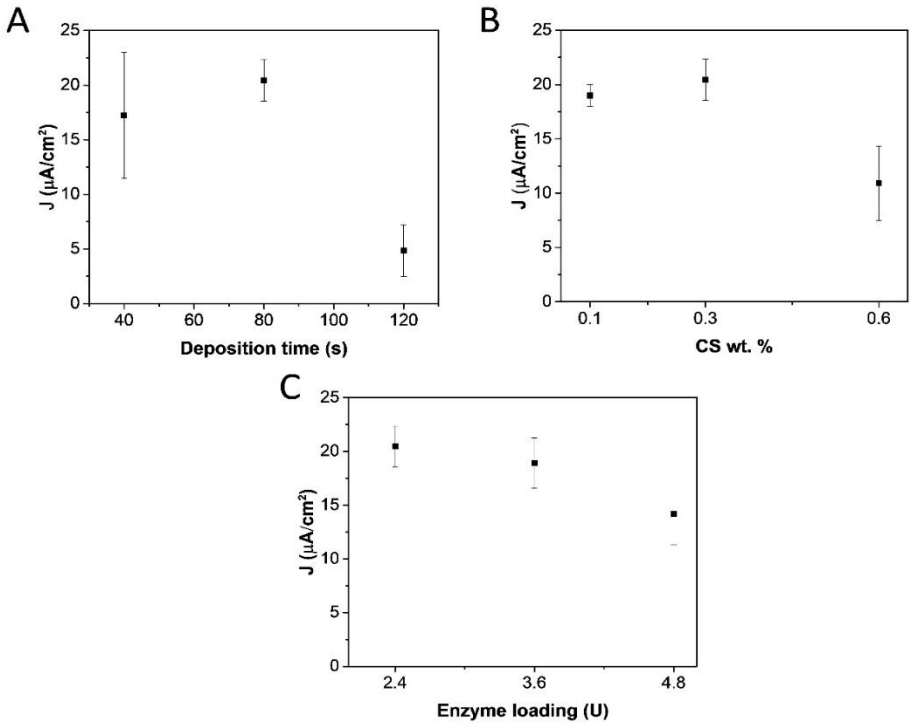

Figure 3.4: *(A) Current density response measured for a 1 mM lactate concentration at an LSG-Pt-CS-LOx electrode whereby amperometric depositions were carried out during 40, 80 and 120 seconds, (B) Current density response measured for a 1 mM lactate concentration at an LSG-Pt-CS-LOx electrode whereby CS loadings were varied by 0.1, 0.3 and 0.6 wt % (C) Current density response measured for a 1mM lactate concentration at an LSG-Pt-CS-LOx electrode whereby the enzyme concentrations studied were 2.4 U, 3.6 U and 4.8 U.*

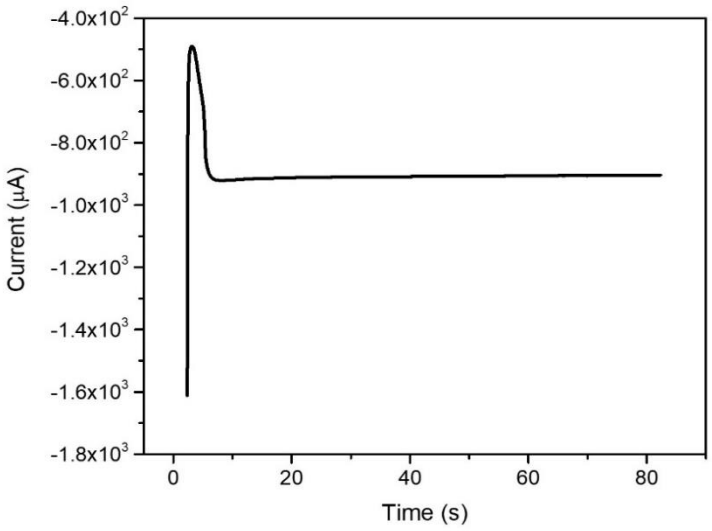

Figure 3.5: *Typical amperometric depsosition carried out at -0.5 V for 80 seconds using an external Ag/AgCl RE and a Pt wire.*

The surface morphology of the scribed graphitic surface is displayed in Figure 3.6 A. Following electrodeposition SEM images confirmed that Pt particulates are present on the 3-D network (Figure 3.6 B and C). Similarly, following the two-step casting process, a clear change in surface morphology is visible owing to the introduction of the chitosan-lactate oxidase organic layer (Figure 3.6 D). The EDX spectra shown in Table 3.1 confirms that prior to electrodeposition carbon accounts for 100 % of the species. Following the amperometric electrodeposition 5.46 wt % of Pt is introduced, following casting steps with CS and LOx a further decrease in C is visible with the introduction of species present in the buffer solution (Na, P and O) used to prepare stocks of chitosan and lactate oxidase.

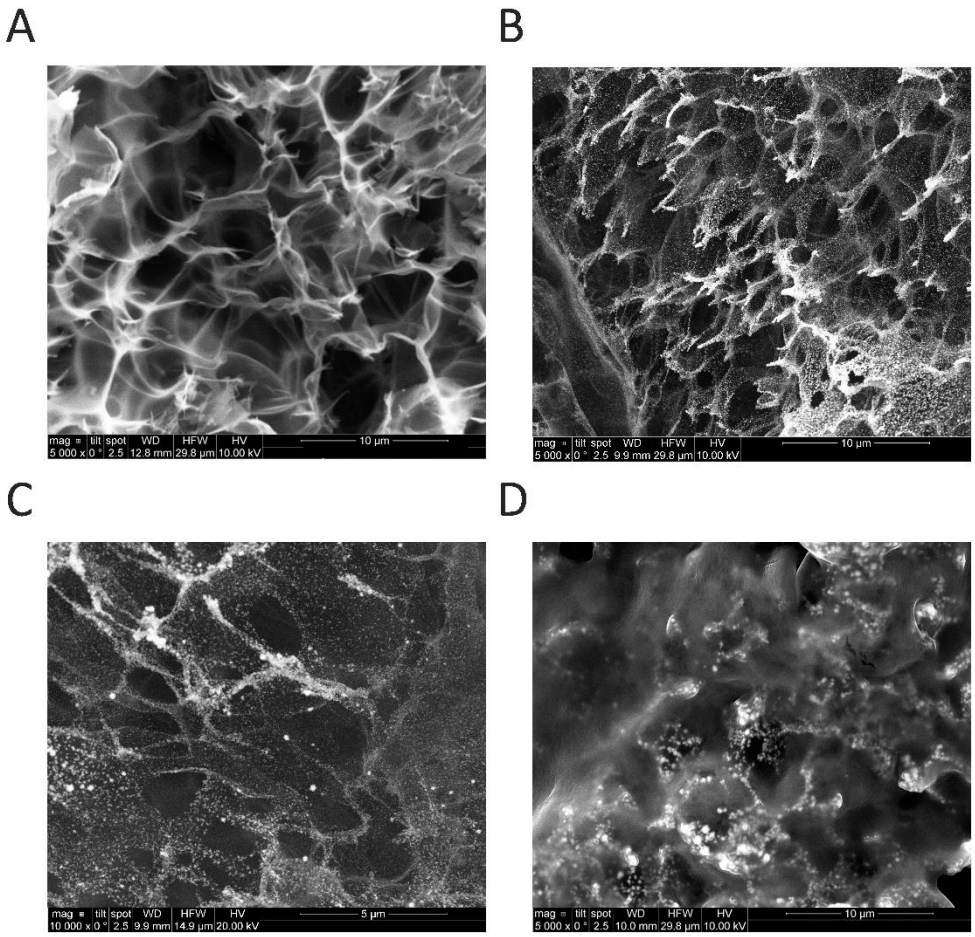

Figure 3.6: *Scanning electron micrograph obtained at 10 kV at (A) the LSG surface (5000x) (B) after an amperometric platinum electrodeposition at -0.5 V for 80 seconds (5000x) (C) after an amperometric platinum electrodeposition at -0.5 V for 80 seconds (10000x) and (C) after the two step casting process with chitosan and lactate oxidase, overnight storage and rinsing (5000x).*

Table 3.1: *Energy dispersive X-ray analysis at each modification step of the biosensor construction process.*

Electrode	C	Pt	Na	P	O
			(%)		
LSG	100	0	0	0	0
LSG-Pt	94.54	5.46	0	0	0
LSG-Pt-CS-LOx	58.79	5.84	5.40	3.92	26.04

Figure 3.7 displays CVs carried out in 5 mM $K_4[Fe(CN)_6]$ and 5 mM $K_3[Fe(CN)_6$ at various scan rates (10 mV/s to 100 mV/s) at the fabricated (A) LSG WE , (B) the Pt modified LSG electrode and (C) the CS-LOx modified surface to assess for changes in electrochemical behaviour. The electroactive surface area of the LSG and LSG-Pt electrodes were determined using Randles-Sevcik equation:

$$I_p = 2.69 \times 10^5 A D^{1/2} n^{3/2} v^{1/2} C$$

Where n is the number of electrons (n = 1), A is the electroactive surface area (cm^2), D is the diffusion coefficient of the redox probe (6.70×10^{-6} cm^2 s^{-1}), C is the concentration of the electrolyte solution (10 mM), υ is the scan rate (V s^{-1}), Ip is the peak oxidation current (mA). The bare LSG electroactive area determined was 0.11 cm^2. For the Pt modified LSG this was found to be 0.15 ± 0.01 cm^2. The platinum modification results in a slightly larger surface area for electron transfer. The area measured for the CS-LOx modified surface was 0.21 ± 0.04 cm^2.

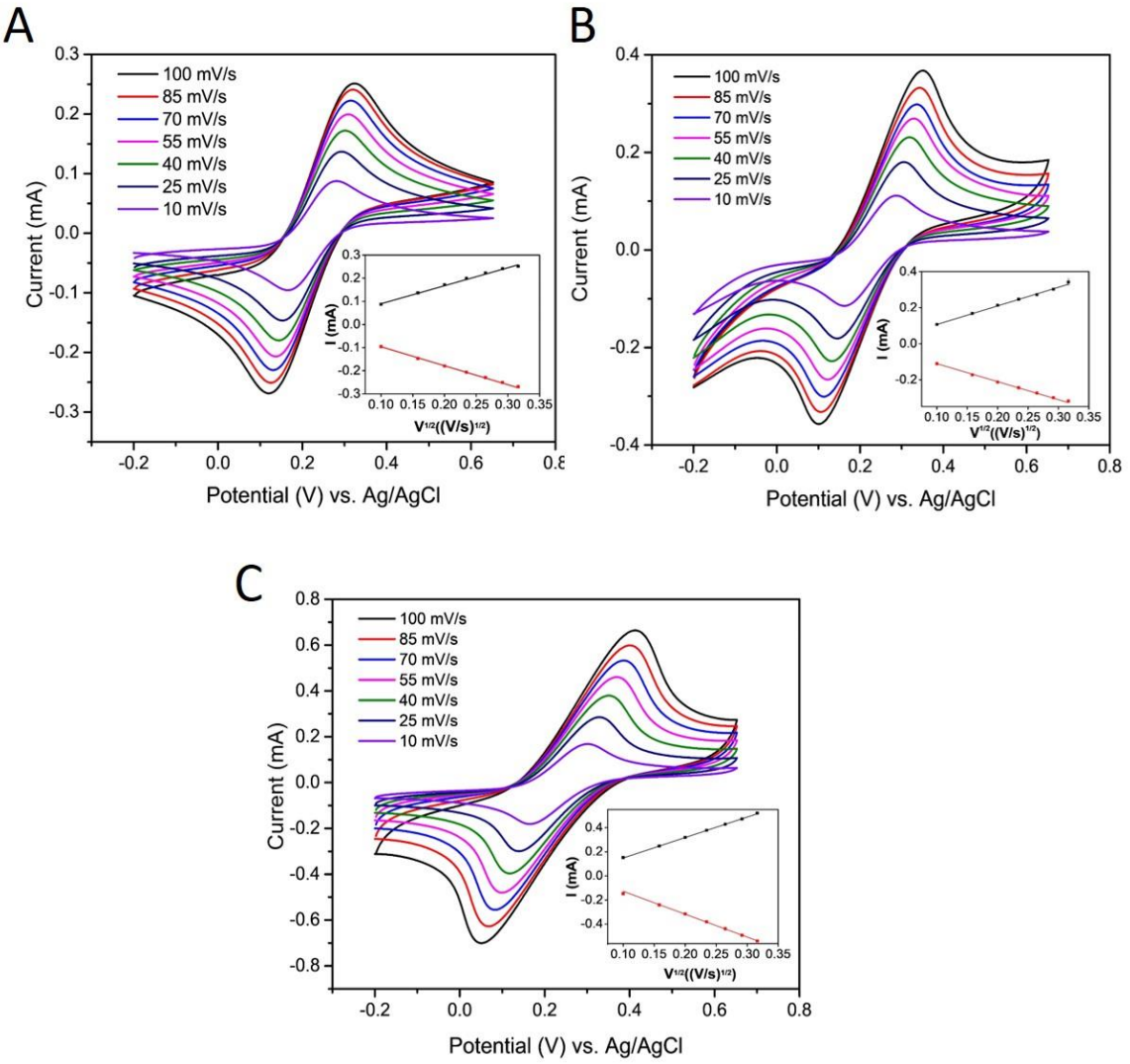

Figure 3.7: *Cyclic voltammograms carried out at (A) LSG (B) LSG modified with Pt (C) LSG modified with Pt and CS-LOx in a 5 mM $[Fe(CN)_6]^{3-/4-}$ in 0.01M PBS (inset: peak oxidation and reduction values vs square root of potential scan rate).*

Figure 3.8 A displays a plot of peak separation versus $v^{½}$. The peak separation was found to increase following the chitosan-LOx modification. The k^0_{app} determined for the CS-LOx modified surface was 8.9 x 10^{-4} cm/s, 10 times lower than that of the LSG and LSG-Pt electrode which were 1.07 x 10^{-2} cm/s and 1.05 x 10^{-2} cm/s respectively. This may have resulted from higher iR or potentially a lower electroactive area or potentially as a result of the slower electron transfer process that exists following the CS-LOx modification (see Figure 3.8 B).

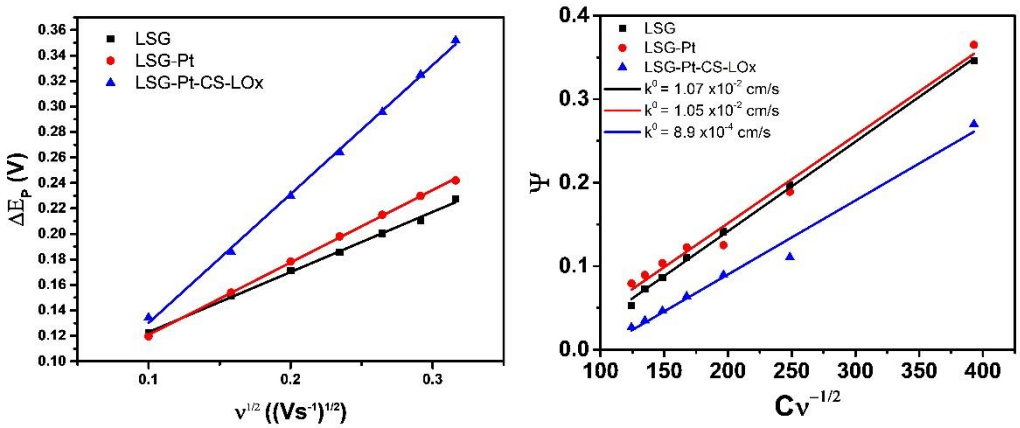

Figure 3.8: *(A) Peak separation and (B) HET rate constant comparison.*

An operating potential of 0.4 V was applied at the LSG-Pt-CS-LOx electrodes in various L-lactate concentrations. Figure 3.9 displays the typical chronoamperometric measurements obtained at each concentration with a 10 second quiet time and a 30 second measurement. The mean current response for n = 3 biosensors during the 30 to 40 second sampling time (as indicated by the grey region in figure 3.9) was used to plot the calibration curve displayed in Figure 3.10 showing a linear region between 0.2 mM and 3 mM with a correlation coefficient of 0.999. The sensor sensitivity was 35.8 μA/mM/cm^2.

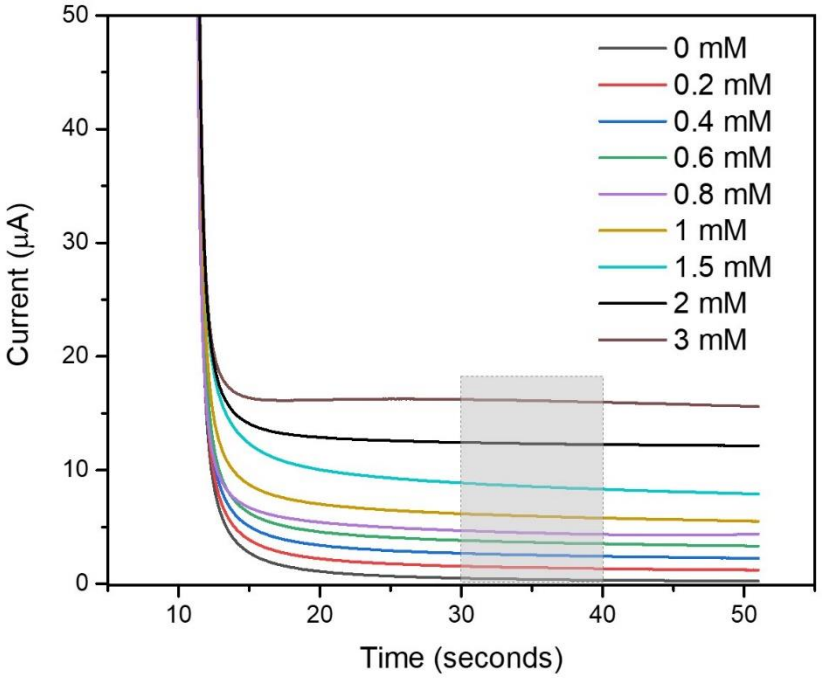

Figure 3.9: *Chronoamperometric measurements carried out at 0.4 V at the LSG-Pt-CS-LOx electrode.*

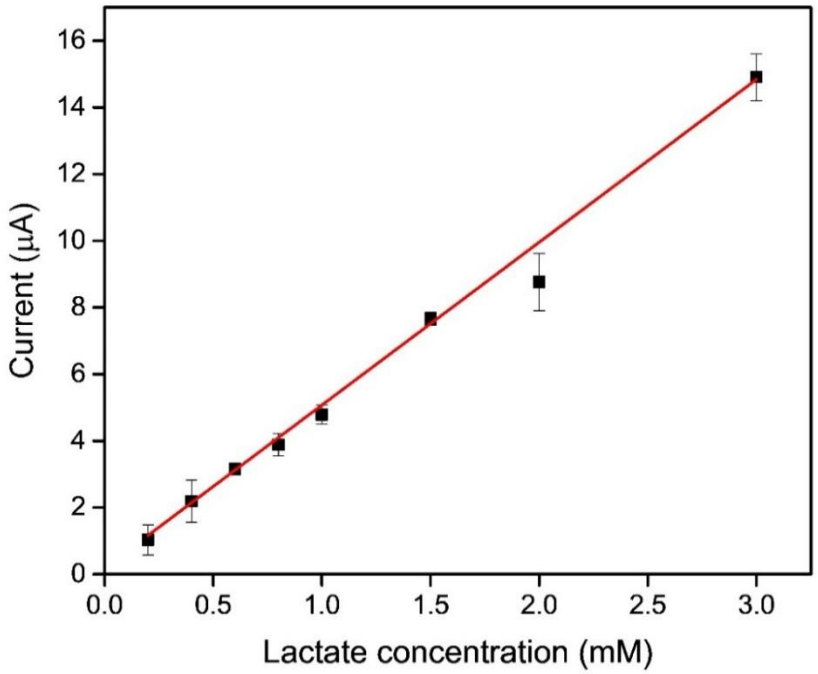

Figure 3.10: *Calibration constructed from the chronoamperometric scans in Lactate obtained for n=3 LSG-Pt-CS-LOx biosensors.*

3.3.3 Reproducibility, stability and selectivity

The relative standard deviation (RSD) determined between the mean current obtained for a 1 mM lactate concentration using n = 5 biosensors was 2.7 % (Figure 3.11 A). The stability of the LSG-Pt-CS electrode was measured by conducting repeated chronoamperometric measurements using n = 3 electrodes (Figure 3.11 B). Each sensor could run up to 10 measurements maintaining an RSD of less than 5 % between each 0.5 mM lactate concentration. Going beyond 10 measurements resulted in an increased RSD (> 10 %) between the mean current response.

A one month shelf life test was conducted to assess sensor performance after 1 day, 1 week, 2 weeks and 1 month of storage (Figure 3.11 C) at 4 °C, while the WE was covered with 0.05 M PB. No decrease in sensor sensitivity was observed after 30 days of storage. The sensitivity changed by 4.9 μA/mM/cm^2, 4.2 μA/mM/cm^2 and 9.1 μA/mM/cm^2 after 7, 14 and 30 days of storage respectively. The change may be attributed to the removal of chitosan from the electrode surface exposing more Pt for H_2O_2 oxidation. Despite an increased RSD between current response at Day 1 and Day 30, the calibration demonstrates linear detection for up to 2 mM indicating that the LOx enzyme had remained stable in the presence of the LSG-Pt-CS electrode modifications, which can be attributed to the biocompatibility of the electrode materials.

The interference effect of other potential oxidising species that can be present in saliva was assessed using chronoamperometry in a 0.25 mM lactate concentration containing either 0.05 mM glucose, 0.1 mM uric acid, 0.1 mM paracetamol or 0.05 mM L-ascorbic acid. The sensor was selective towards lactate in the presence of glucose and L-ascorbic acid with a change in sensor response of 1.4 % and 2.1 % respectively. However, the sensor response in the presence of paracetamol and uric acid resulted in change in sensor response greater than 20 % (see Figure 3.11 D). Further work on the development of a permselective membrane could eliminate the effects of potential oxidising interfering species.

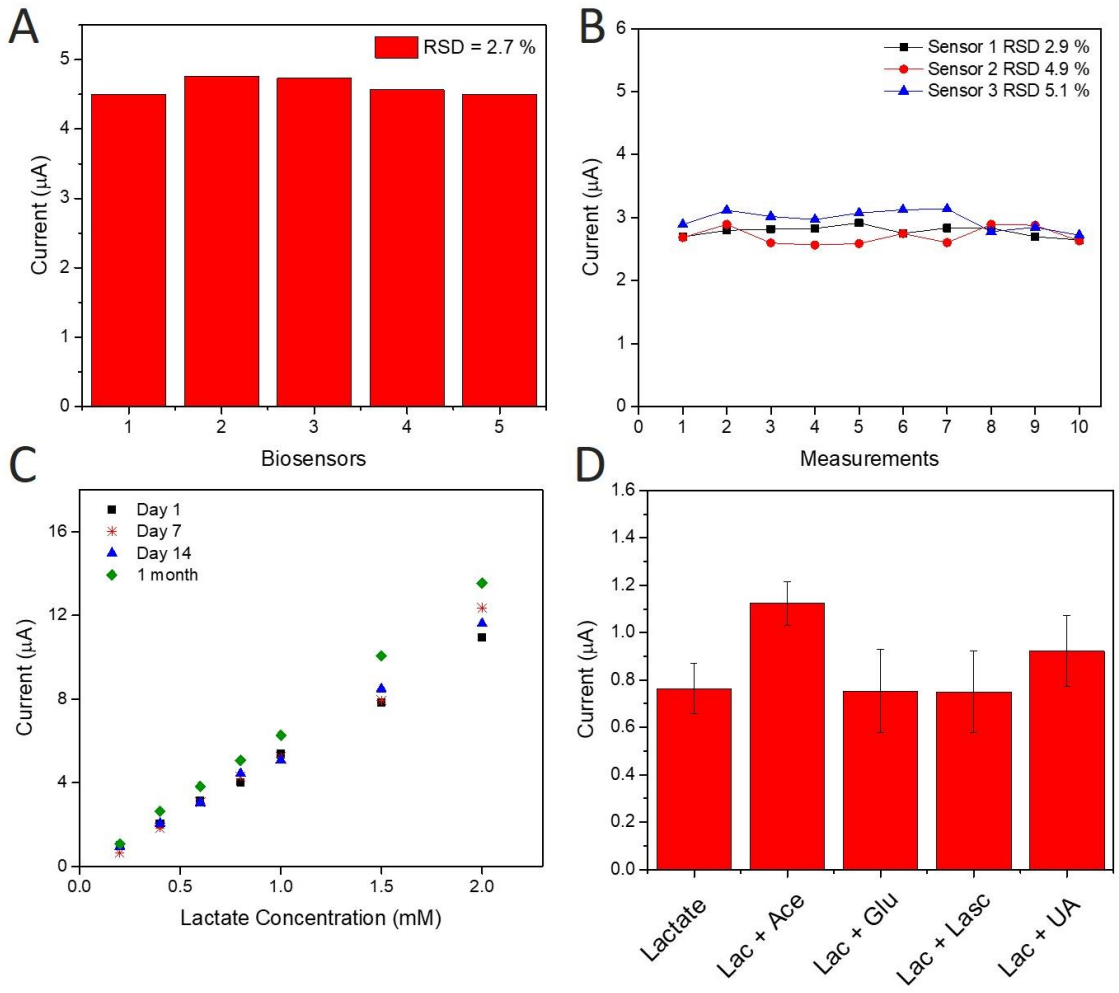

***Figure 3.11**: (A) Bar chart depicting the current response of the LSG-Pt-CS-LOx electrode to 1 mM Lactate concentration for n=5 Biosensors, (B) Scatter plot of 10 amperometric measurements obtained at 0.5 mM for n=3 Biosensors, (C) Calibration plots obtained after biosensor storage for 1, 7, 14 and 30 days and (D) Bar chart depicting selectivity measurements to a 0.25 mM Lactate concentration.*

3.3.4 Three-electrode configuration

LSG and LSG modified with Ag/AgCl paste were studied as pseudo-REs. The Ag/AgCl paste was painted over the LSG RE carefully with a small paint brush ensuring the whole electrode was covered in the paste. Figure 3.12 displays eight CV measurements carried out using the LSG RE. Both the anodic and cathodic peak potentials between eight consecutive sweeps varied by 1 mV. The average anodic and cathodic peak currents determined were 210.6 ± 3.9 µA and −220 ± 2 µA. The inset of Figure 3.12 displays the anodic peak potential region of the CV where the shift in peak potential can be observed. Figure 3.13 shows eight CV measurements carried out with the Ag/AgCl paste modified

LSG RE. The anodic and cathodic peak potentials did not differ between measurements (see inset of Figure 3.13). The average anodic and cathodic peak currents were 197.8 ± 0.6 µA and −203.7 ± 0.2 µA.

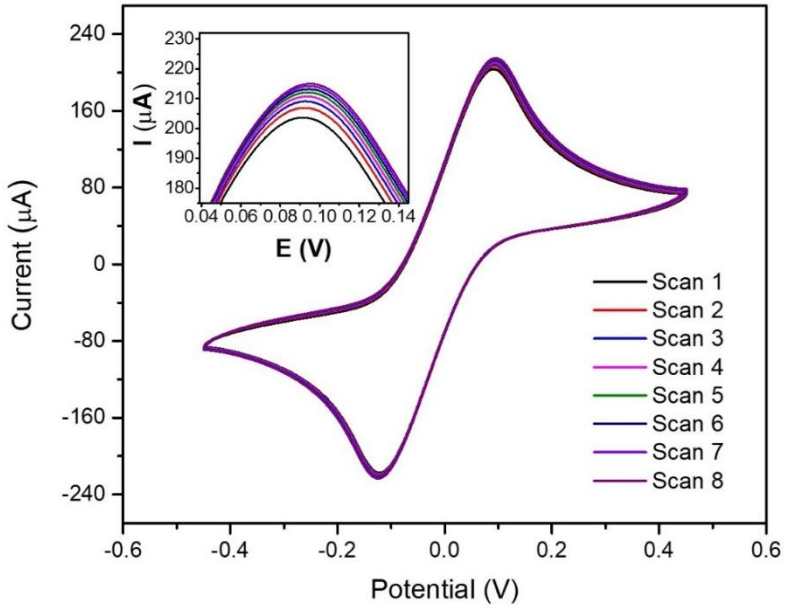

Figure 3.12: *CV (8 cycles) at the LSG WE in 0.1 M PBS (pH 7.4) containing 5 mM $K_4Fe(CN)_6/K_3Fe(CN)_6$) versus an LSG RE, inset displays anodic peak currents*

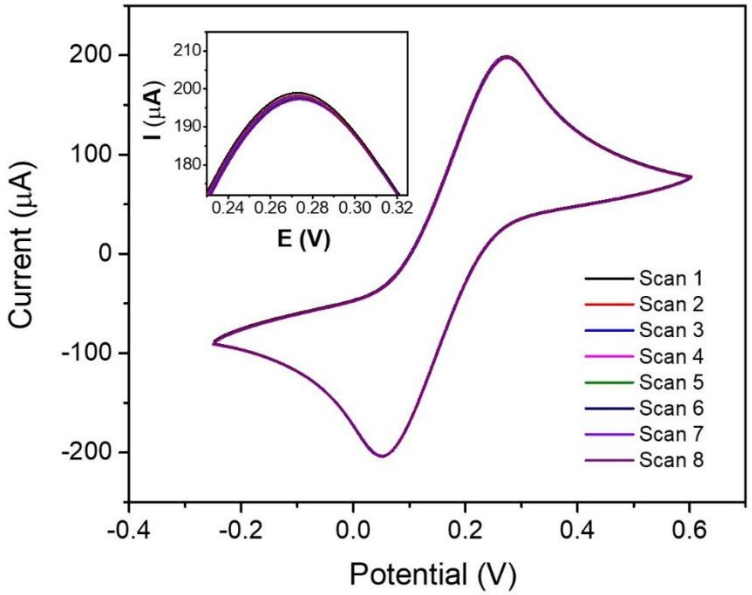

Figure 3.13: *CV (8 cycles) at the LSG WE in 0.1 M PBS (pH 7.4) containing 5 mM $K_4Fe(CN)_6/K3Fe(CN)_6$) versus an Ag/AgCl modified LSG RE, inset displays anodic peak currents*

Figure 3.14 shows CV measurements carried out using an external commercial Ag/AgCl RE (Blue), the LSG RE (Wine) and the Ag/AgCl paste modified LSG RE (Green). A peak potential shift of -0.173 V was observed between the external Ag/AgCl RE and the LSG RE. A minor peak potential shift of 6 mV was observed between the Ag/AgCl paste modified LSG and the external RE which may result from the chloride ion concentration in the phosphate buffered saline. LSG was also investigated as a CE and was found to behave similarly to the Pt wire (Figure 3.16). Chronoamperometric measurements were carried out using each RE at the LSG-Pt-CS-LOx biosensor. Figure 3.15 displays the corresponding calibrations for the three-LSG lactate sensing approach (green) overlaid with the calibrations obtained with an Ag/AgCl modified LSG RE (blue) and the use of an external RE Ag/AgCl (red). The working linear range was the same for each of the calibrations, and all calibrations demonstrated good linearity with a squared correlation coefficient, $R^2 > 0.99$. The standard deviation between the sensitivities of each calibration was determined to be ±2.3 μA/mM/cm^2.

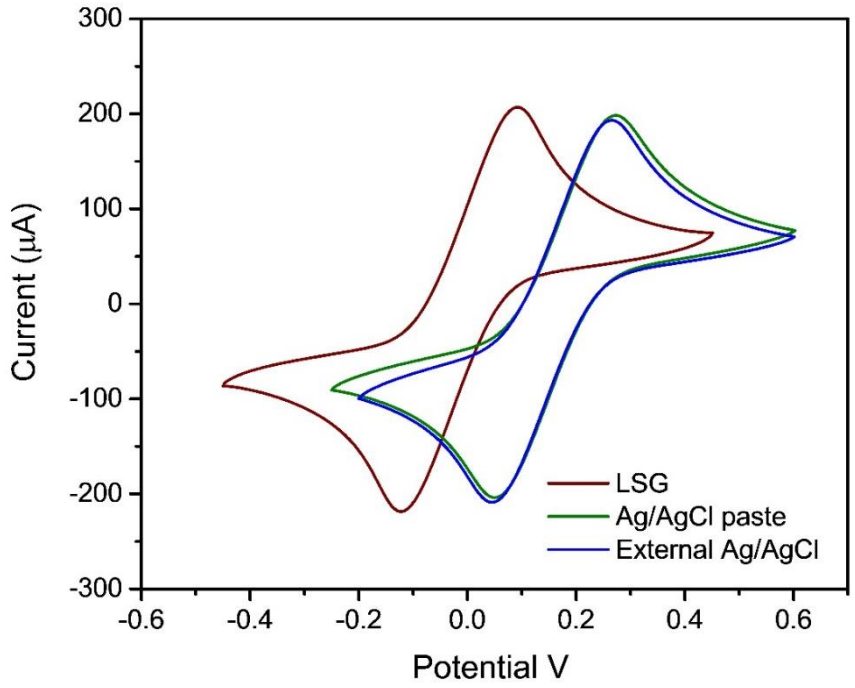

Figure 3.14: *Cyclic voltammetry carried out at 100 mV/s at the LSG WE using an external Ag/AgCl (Blue), the LSG RE (wine) and the Ag/AgCl paste modified LSG (green).*

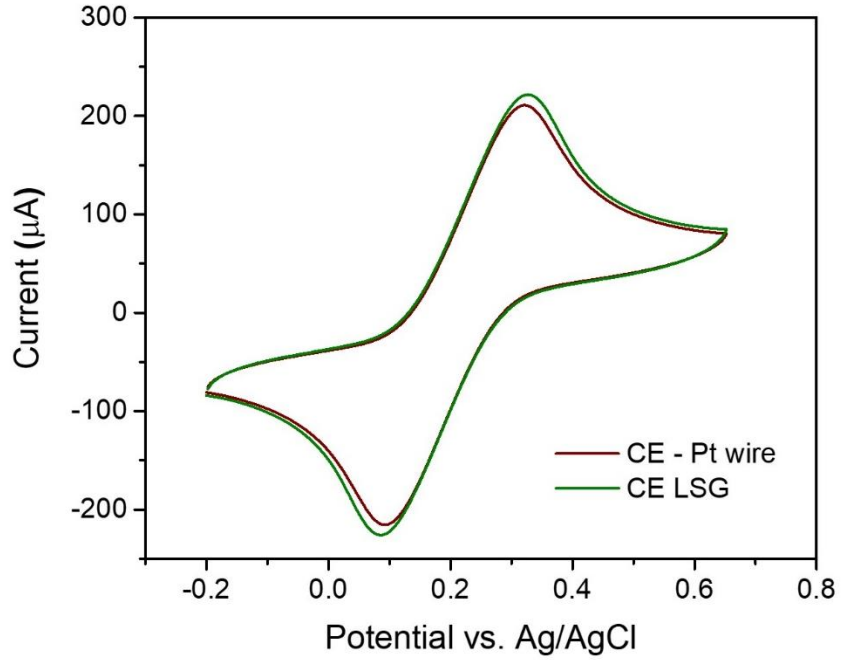

Figure 3.16: *Cyclic voltammetry carried out at 100 mV/s at the LSG WE using* a Pt wire (green) and LSG as a CE (red)

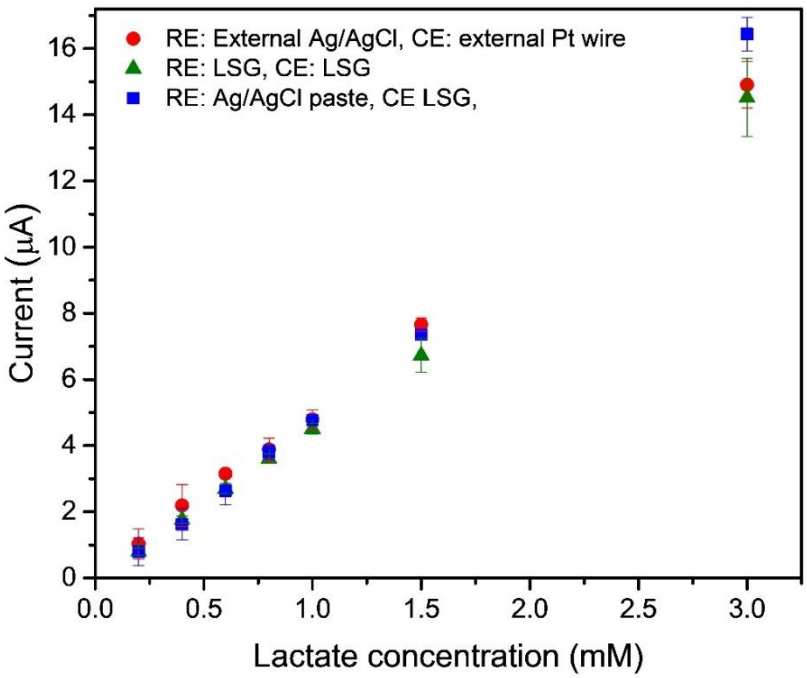

Figure 3.15: *Corresponding calibration graphs obtained for chronoamperometric lactate measurements employing 1. The external Ag/AgCl RE (0.4V) and Pt wire CE (red), 2. LSG as both an RE and CE (green) (0.2V) and 3. Ag/AgCl paste modified on LSG (0.4V) (blue) with the LSG CE.*

3.3.5 Bent Configuration

Chronoamperometry was used to assess the functionality of the LSG-Pt-CS-LOx biosensors whilst they were fixed at a curvature of 0.14 mm^{-1} (an equivalent bending radius of 7 mm). Figure 3.17 displays the calibration response obtained for the planar polyimide sensor (K = 0 mm^{-1}) attached to a rigid glass substrate overlaid with the calibration response obtained when the sensor was fabricated on polyimide attached to flexible PET substrates (K = 0.14 mm^{-1}). The calibration obtained whilst the sensor was fixed in a bent state showed a sensitivity 2.37 $\mu A/mM/cm^2$ higher than that of measurements obtained at the planar substrate. For concentrations lower than 1.5 mM the RSD was less than 5 % and for the 3 mM concentrations the RSD increased to 7.5%. This was the case for both planar and bent electrode configurations. These results demonstrate the potential for integration or attachment of the LSG flexible PI-PET substrates onto devices/components. Similar observations have been reported by Nayak *et al.* where LSG modified with Pt nanoparticles demonstrated stable redox currents during CV measurements in 10 mM $K_3Fe[CN]_6$ whilst the WE was fixed at a bending radius of 15 mm, 13 mm and 11 mm.[25]

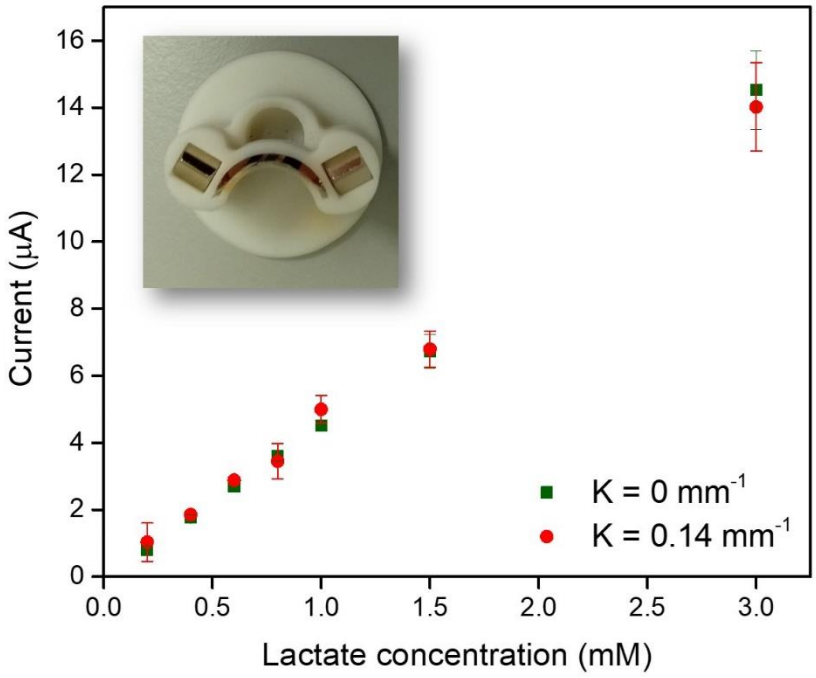

Figure 3.17: *Corresponding calibration graphs obtained for chronoamperometric lactate measurements carried out at K = 0.14 mm^{-1} and K= 0 mm^{-1} using LSG as a CE and RE.*

3.3.6 Sensor performance in artificial saliva and diluted human serum

The LSG-Pt-CS-LOx sensor was used to measure lactate levels in artificial saliva and sterile human serum samples spiked with known lactate concentrations. Artificial saliva samples were spiked with 0.5 mM and 1 mM lactate concentrations. Sterile human serum was diluted in 0.05 M PB (1:10) and subsequently spiked with 0.5 mM and 1 mM Lactate concentrations. The current response was measured at + 0.4 V vs. Ag/AgCl (paste). The corresponding current value was background subtracted using a baseline value for un-spiked artificial saliva and un-spiked human serum. The current was then substituted into the calibration curve to obtain the corresponding concentration i.e. concentration measured. This was generated using the 'find X from Y' function in Origin. The concentration determined by the LSG-Pt-CS-LOx sensor in each sample is tabulated in Table 3.2 along with the spiked concentrations and calculated sensor recovery values. A calibrated Lactate Pro 2 analyser was used to validate the LSG lactate biosensor. The spiked artificial saliva and diluted human serum solutions were added near the window of the lactate strip using a micropipette. For each concentration, the Lactate Pro 2 measured a higher concentration than the known spiked concentration. This increase may be attributed to deviations from the device instructions for use (IFU). Firstly, pipetting solution to the window entry point may have caused inaccurate measurements as the IFU indicated "Accurate test results will not be obtained if you apply your blood to the check window directly". Another challenge was that, typically, for blood lactate measurements, a lancet is applied to the skin and blood is tested directly after puncturing the skin, "For accurate test results, touch the test strip to your blood immediately after puncturing". Here, both the artificial saliva and diluted human serum test solutions are exposed to air for a period of time prior to conducting the measurement. In artificial saliva spiked with 0.5 mM, the sensor recovery value was 124%. Artificial saliva contains sodium carboxymethyl cellulose used to increase the viscosity of the solution. The higher sensor recovery observed may be a result of reduced sensor accuracy for lower lactate concentrations in this media by comparison to the buffer solutions used to prepare the calibration. In the solution spiked with 1 mM lactate the sensor recovery value determined was 102%. In diluted human serum, the sensor recovery values determined were between 94 and 102%. These results indicate that the use of LSG as a CE and Ag/AgCl paste as an RE is viable for the measurement of lactate levels in diluted human serum and artificial saliva.

Table 3.2: *Amperometric detection using the three-electrode configuration on polyimide using artificial saliva and sterile human serum spiked with 0.5 mM and 1 mM Lactate concentrations.*

Real Sample	Spiked concentration	Concentration measured	% Sensor Recovery	Lactate Pro 2 measurement
Artificial Saliva (n=3)	0.5 mM	0.63 mM ± 0.04 mM (n=3)	124 %	0.61 ± 0.06 mM (n=5)
Artificial Saliva (n=3)	1 mM	1.03 ± 0.06 mM (n=3)	102 %	1.56 ± 0.048 mM (n=5)
Human serum diluted in (10 % Buffer (n=3)	0.5 mM	0.47 ± 0.09 mM (n=3)	94 %	0.72 ±0.074 mM (n=5)
Human serum diluted in (10 % Buffer (n=3)	1 mM	1.01 ± 0.15 mM (n=3)	101 %	1.74 ± 0.12 mM (n=5)

3.3.7 Comparison of the LSG lactate sensor with other flexible lactate biosensors

Table 3.3 presents the sensor performance of several flexible lactate sensors for comparison with the performance of the LSG-Pt-CS-LOx biosensor presented in this chapter. In comparison to techniques listed below, LSG on flexible polyimide offers a low cost approach to fabricating a flexible lactate sensor. Our working linear range exceeds that of a previous lactate sensors reported for saliva analysis on screen printed flexible substrates. The sensor sensitivity values are comparable or improved in comparison to those presented in **Table 3.3**. Furthermore, we demonstrated sensor functionality in a flexible/bent state whereby the mean current values measured for each concentration within the calibration curve varied by less than 8 %.

Table 3.3: *A comparison of the flexible LSG lactate sensor with other lactate sensors constructed on flexible substrates.*

Electrode	Linear range	Operating technique and parameters	Immobilisation strategy	Sensitivity	LOD	Ref.
CZO film/FePt NPs	0.2-5 mM	±3 V	N/A	25.32 mV/mM	3.1±0.3 mM	[26]
C/AgNWs/MIP	10^{-3} mM to 100 mM	DPV	Non-enzymatic	-	0.22 µM	[27]
GMOC-LOx	0-10 mM	0.1 V (PB) 0.3 V (Artificial Sweat)	Cast and dried under vacuum	36.2 µA/cm^2/mM	0.3 mM	[28]
C/PB/LOx /ETH 500-PVC-DOS	1-50 mM	-50 mV	Casting	-9.4 nA/mM	0.1 mM	[29]
Au/PB-Carbon/PPY/LOx	0-1 mM & 1-6mM	−50 mV	Electro-polymerisation	−5.70 and −1.78 nA/mM	-	[30]
Au/ZnO-LOx	0-100 mM	10 mV (EIS)	Dithiobis succinimidyl propionate (linker chemistry)	8.3% mM^{-1}	-	[31]
Au/PB/LOx/CS	0-30 mM	−0.1 V	Casting	19.13 µA/mM cm^2 14.6 µA/mM cm^2 (in artificial sweat)	0.137 mM	[32]
PET/Au/ZnO-NFs/LOx	1-20 mM	0.239 V (EIS)	Electrostatic physical adsorption	11.76 µA/decade/cm^2	1.26 nM	[33]
Ag NPs/NiO NPs/Polyurethane (PU)	0-3 mM	OCP	Non-enzymatic	8.86 nA/mM/mm^2	0.38 mM	[34]
C/PB/LOx/Nafion	0.025 mM–1.5 mM	−50 mV vs. the internal Ag pseudo reference electrode.	Casting (Adsoption)	Not reported	0.01 mM	[19]
Pt/LOD	0–1.5 mM but logarithmic up to 70 mM	+650 mV	Immobilised via covalent cross-linking with BSA and GA	Not reported	0.2 mM	[35]
Au/TTF/CNT/LOx-CS-CNT	1-24 mM	0 V	Casting	68 µA /mM/ cm^2	-	[36]
LSG/Pt/CS/LOx	**0.2-3mM**	**0.4 V vs. Ag/AgCl (0.2 V vs. LSG)**	**Casting / adsorption**	**39.3 µA/mM/cm^2**	**0.12 mM**	**This work**

3.4 Conclusion

This chapter reports on the use of direct laser scribing as a low cost, precise and reproducible method of fabricating bendable enzymatic lactate sensors. A customized three-electrode design on polyimide tape was achieved using a 450 nm laser-scribing fabrication process. The LSG WE was modified via a Pt electrodeposition followed by casting chitosan and lactate oxidase on the surface. Chronoamperometric lactate detection was achieved within a working linear range of 0.2 mM to 3 mM, with a limit of detection of 0.12 mM.

The biosensor demonstrated excellent reproducibility with an RSD of less than 5 % for n = 5 sensors. Working stability was demonstrated by obtaining 10 successive measurements over n = 3 sensors. No decrease in current response was evident when calibrating a biosensor that had been stored for up to 30 days.

To investigate the efficacy of both LSG and Ag/AgCl modified LSG, chronoamperometric lactate detection was carried out with both REs for comparison to a commercial Ag/AgCl RE. Both LSG and Ag/AgCl paste modified LSG demonstrated functionality similar to the external RE.

No noticeable change in signal response was observed whilst the flexible polyimide substrates were fixed at a curvature, K = 0.14 mm^{-1} in comparison to the calibration obtained at a curvature of K = 0 mm^{-1}, signifying opportunities for sensor attachment or integration with oral-care products such as mouth swabs and mouth guards.

Challenges in sensor selectivity were observed for this combination of electrode materials in the presence of both acetaminophen and uric acid. For use-case scenarios, involving whole biological fluids further work would be required for the integration of an additional membrane/perm-selective layer to limit interference effects. For a potential future application, sterile human serum spiked with 0.5 mM and 1 mM of lactate were analysed with the three-electrode sensor. The biosensor measured 0.47 mM and 1.01 mM respectively. In the case of artificial saliva spiked with 0.5 mM and 1 mM of lactate the measured concentrations were by 0.63 mM and 1.03 mM respectively.

3.5 References

(1) Lin, J.; Peng, Z.; Liu, Y.; Ruiz-Zepeda, F.; Ye, R.; Samuel, E. L. G.; Yacaman, M. J.; Yakobson, B. I.; Tour, J. M. Laser-Induced Porous Graphene Films from Commercial Polymers. *Nat Commun* **2014**, *5* (1), 5714. https://doi.org/10.1038/ncomms6714.

(2) Tian, H.; Yang, Y.; Xie, D.; Cui, Y.-L.; Mi, W.-T.; Zhang, Y.; Ren, T.-L. Wafer-Scale Integration of Graphene-Based Electronic, Optoelectronic and Electroacoustic Devices. *Sci Rep* **2015**, *4* (1), 3598. https://doi.org/10.1038/srep03598.

(3) Nayak, P.; Kurra, N.; Xia, C.; Alshareef, H. N. Highly Efficient Laser Scribed Graphene Electrodes for On-Chip Electrochemical Sensing Applications. *Adv. Electron. Mater.* **2016**, *2* (10), 1600185. https://doi.org/10.1002/aelm.201600185.

(4) Lei, Y.; Alshareef, A. H.; Zhao, W.; Inal, S. Laser-Scribed Graphene Electrodes Derived from Lignin for Biochemical Sensing. *ACS Appl. Nano Mater.* **2020**, *3* (2), 1166–1174. https://doi.org/10.1021/acsanm.9b01795.

(5) Prabhakaran, A.; Nayak, P. Surface Engineering of Laser-Scribed Graphene Sensor Enables Non-Enzymatic Glucose Detection in Human Body Fluids. *ACS Appl. Nano Mater.* **2020**, *3* (1), 391–398. https://doi.org/10.1021/acsanm.9b02025.

(6) Soares, R. R. A.; Hjort, R. G.; Pola, C. C.; Parate, K.; Reis, E. L.; Soares, N. F. F.; McLamore, E. S.; Claussen, J. C.; Gomes, C. L. Laser-Induced Graphene Electrochemical Immunosensors for Rapid and Label-Free Monitoring of *Salmonella Enterica* in Chicken Broth. *ACS Sens.* **2020**, *5* (7), 1900–1911. https://doi.org/10.1021/acssensors.9b02345.

(7) Li, Y.; Zhang, Y.; Chen, Z.; Li, Q.; Li, T.; Li, M.; Zhao, H.; Sheng, Q.; Shi, W.; Yao, J. Self-Powered, Flexible, and Ultrabroadband Ultraviolet-Terahertz Photodetector Based on a Laser-Reduced Graphene Oxide/$CsPbBr_3$ Composite. *Photon. Res.* **2020**, *8* (8), 1301. https://doi.org/10.1364/PRJ.395090.

(8) Kim, M.; Gu, M. G.; Jeong, H.; Song, E.; Jeon, J. W.; Huh, K.-M.; Kang, P.; Kim, S.-K.; Kim, B. G. Laser Scribing of Fluorinated Polyimide Films to Generate Microporous Structures for High-Performance Micro-Supercapacitor Electrodes. *ACS Appl. Energy Mater.* **2021**, *4* (1), 208–214. https://doi.org/10.1021/acsaem.0c02096.

(9) Vaughan, E.; Larrigy, C.; Burke, M.; Sygellou, L.; Quinn, A. J.; Galiotis, C.; Iacopino, D. Visible Laser Scribing Fabrication of Porous Graphitic Carbon Electrodes: Morphologies, Electrochemical Properties, and Applications as Disposable Sensor Platforms. *ACS Appl. Electron. Mater.* **2020**, *2* (10), 3279–3288. https://doi.org/10.1021/acsaelm.0c00612.

(10) Bakker, J.; Nijsten, M. W.; Jansen, T. C. Clinical Use of Lactate Monitoring in Critically Ill Patients. *Ann Intensive Care* **2013**, *3* (1), 12. https://doi.org/10.1186/2110-5820-3-12.

(11) Zymliński, R.; Biegus, J.; Sokolski, M.; Siwołowski, P.; Nawrocka-Millward, S.; Todd, J.; Jankowska, E. A.; Banasiak, W.; Cotter, G.; Cleland, J. G.; Ponikowski, P. Increased Blood Lactate Is Prevalent and Identifies Poor Prognosis in Patients with Acute Heart Failure without Overt Peripheral Hypoperfusion. *Eur J Heart Fail* **2018**, *20* (6), 1011–1018. https://doi.org/10.1002/ejhf.1156.

(12) Gernardin, G.; Pradier, C.; Tiger, F.; Deloffre, P.; Mattei, M. Blood Pressure and Arterial Lactate Level Are Early Indicators of Short-Term Survival in Human

Septic Shock. *Intensive Care Med* **1996**, *22* (1), 17–25. https://doi.org/10.1007/BF01728326.

(13) Brillantino, A.; Iacobellis, F.; Renzi, A.; Nasti, R.; Saldamarco, L.; Grillo, M.; Romano, L.; Castriconi, M.; Cittadini, A.; De Palma, M.; Scaglione, M.; Di Martino, N.; Grassi, R.; Paladino, F. Diagnostic Value of Arterial Blood Gas Lactate Concentration in the Different Forms of Mesenteric Ischemia. *Eur J Trauma Emerg Surg* **2018**, *44* (2), 265–272. https://doi.org/10.1007/s00068-017-0805-7.

(14) Bonaventura, J. M.; Sharpe, K.; Knight, E.; Fuller, K. L.; Tanner, R. K.; Gore, C. J. Reliability and Accuracy of Six Hand-Held Blood Lactate Analysers. *J Sports Sci Med* **2015**, *14* (1), 203–214.

(15) Wolf, A.; Renehan, K.; Ho, K.; Carr, B.; Chen, C.; Cornell, M.; Ye, M.; Rojas-Peña, A.; Chen, H. Evaluation of Continuous Lactate Monitoring Systems within a Heparinized In Vivo Porcine Model Intravenously and Subcutaneously. *Biosensors* **2018**, *8* (4), 122. https://doi.org/10.3390/bios8040122.

(16) Heo, S. G.; Yang, W.-S.; Kim, S.; Park, Y. M.; Park, K.-T.; Oh, S. J.; Seo, S.-J. Synthesis, Characterization and Non-Enzymatic Lactate Sensing Performance Investigation of Mesoporous Copper Oxide (CuO) Using Inverse Micelle Method. *Applied Surface Science* **2021**, *555*, 149638. https://doi.org/10.1016/j.apsusc.2021.149638.

(17) Choi, Y. M.; Lim, H.; Lee, H.-N.; Park, Y. M.; Park, J.-S.; Kim, H.-J. Selective Nonenzymatic Amperometric Detection of Lactic Acid in Human Sweat Utilizing a Multi-Walled Carbon Nanotube (MWCNT)-Polypyrrole Core-Shell Nanowire. *Biosensors* **2020**, *10* (9), 111. https://doi.org/10.3390/bios10090111.

(18) Kim, S.; Kim, K.; Kim, H.-J.; Lee, H.-N.; Park, T. J.; Park, Y. M. Non-Enzymatic Electrochemical Lactate Sensing by NiO and Ni(OH)2 Electrodes: A Mechanistic Investigation. *Electrochimica Acta* **2018**, *276*, 240–246. https://doi.org/10.1016/j.electacta.2018.04.172.

(19) Petropoulos, K.; Piermarini, S.; Bernardini, S.; Palleschi, G.; Moscone, D. Development of a Disposable Biosensor for Lactate Monitoring in Saliva. *Sensors and Actuators B: Chemical* **2016**, *237*, 8–15. https://doi.org/10.1016/j.snb.2016.06.068.

(20) Schabmueller, C. G. J.; Loppow, D.; Piechotta, G.; Schütze, B.; Albers, J.; Hintsche, R. Micromachined Sensor for Lactate Monitoring in Saliva. *Biosensors and Bioelectronics* **2006**, *21* (9), 1770–1776. https://doi.org/10.1016/j.bios.2005.09.015.

(21) Marques, A. C.; Cardoso, A. R.; Martins, R.; Sales, M. G. F.; Fortunato, E. Laser-Induced Graphene-Based Platforms for Dual Biorecognition of Molecules. *ACS Appl. Nano Mater.* **2020**, *3* (3), 2795–2803. https://doi.org/10.1021/acsanm.0c00117.

(22) Nicholson, R. S. Theory and Application of Cyclic Voltammetry for Measurement of Electrode Reaction Kinetics. *Anal. Chem.* **1965**, *37* (11), 1351–1355. https://doi.org/10.1021/ac60230a016.

(23) Hall, S. B.; Khudaish, E. A.; Hart, A. L. Electrochemical Oxidation of Hydrogen Peroxide at Platinum Electrodes. Part II: Effect of Potential. *Electrochimica Acta* **1998**, *43* (14–15), 2015–2024. https://doi.org/10.1016/S0013-4686(97)10116-5.

(24) Petrucci, R.; Pasquali, M.; Scaramuzzo, F. A.; Curulli, A. Recent Advances in Electrochemical Chitosan-Based Chemosensors and Biosensors: Applications in Food Safety. *Chemosensors* **2021**, *9* (9), 254. https://doi.org/10.3390/chemosensors9090254.

(25) Yoon, H.; Nah, J.; Kim, H.; Ko, S.; Sharifuzzaman, M.; Barman, S. C.; Xuan, X.; Kim, J.; Park, J. Y. A Chemically Modified Laser-Induced Porous Graphene Based Flexible and Ultrasensitive Electrochemical Biosensor for Sweat Glucose Detection. *Sensors and Actuators B: Chemical* **2020**, *311*, 127866. https://doi.org/10.1016/j.snb.2020.127866.

(26) Nien, Y.-H.; Kang, Z.-X.; Su, T.-Y.; Ho, C.-S.; Chou, J.-C.; Lai, C.-H.; Kuo, P.-Y.; Lai, T.-Y.; Dong, Z.-X.; Chen, Y.-Y.; Huang, Y.-H. Investigation of Flexible Arrayed Lactate Biosensor Based on Copper Doped Zinc Oxide Films Modified by Iron–Platinum Nanoparticles. *Polymers* **2021**, *13* (13), 2062. https://doi.org/10.3390/polym13132062.

(27) Lin, K.-C.; Muthukumar, S.; Prasad, S. Flex-GO (Flexible Graphene Oxide) Sensor for Electrochemical Monitoring Lactate in Low-Volume Passive Perspired Human Sweat. *Talanta* **2020**, *214*, 120810. https://doi.org/10.1016/j.talanta.2020.120810.

(28) Shitanda, I.; Mitsumoto, M.; Loew, N.; Yoshihara, Y.; Watanabe, H.; Mikawa, T.; Tsujimura, S.; Itagaki, M.; Motosuke, M. Continuous Sweat Lactate Monitoring System with Integrated Screen-Printed MgO-Templated Carbon-Lactate Oxidase Biosensor and Microfluidic Sweat Collector. *Electrochimica Acta* **2021**, *368*, 137620. https://doi.org/10.1016/j.electacta.2020.137620.

(29) Xuan, X.; Pérez-Ràfols, C.; Chen, C.; Cuartero, M.; Crespo, G. A. Lactate Biosensing for Reliable On-Body Sweat Analysis. *ACS Sens.* **2021**, *6* (7), 2763–2771. https://doi.org/10.1021/acssensors.1c01009.

(30) Park, J.; Sempionatto, J. R.; Kim, J.; Jeong, Y.; Gu, J.; Wang, J.; Park, I. Microscale Biosensor Array Based on Flexible Polymeric Platform toward Lab-on-a-Needle: Real-Time Multiparameter Biomedical Assays on Curved Needle Surfaces. *ACS Sens.* **2020**, *5* (5), 1363–1373. https://doi.org/10.1021/acssensors.0c00078.

(31) Bhide, A.; Lin, K.-C.; Muthukumar, S.; Prasad, S. On-Demand Lactate Monitoring towards Assessing Physiological Responses in Sedentary Populations. *Analyst* **2021**, *146* (11), 3482–3492. https://doi.org/10.1039/D1AN00455G.

(32) Wang, R.; Zhai, Q.; An, T.; Gong, S.; Cheng, W. Stretchable Gold Fiber-Based Wearable Textile Electrochemical Biosensor for Lactate Monitoring in Sweat. *Talanta* **2021**, *222*, 121484. https://doi.org/10.1016/j.talanta.2020.121484.

(33) Alam, F.; Jalal, A. H.; Forouzanfar, S.; Karabiyik, M.; Rabiei Baboukani, A.; Pala, N. Flexible and Linker-Free Enzymatic Sensors Based on Zinc Oxide Nanoflakes for Noninvasive L-Lactate Sensing in Sweat. *IEEE Sensors J.* **2020**, *20* (10), 5102–5109. https://doi.org/10.1109/JSEN.2020.2968278.

(34) Huang, Y.-S.; Chen, K.-Y.; Cheng, Y.-T.; Lee, C.-K.; Tsai, H.-E. An Inkjet-Printed Flexible Non-Enzymatic Lactate Sensor for Clinical Blood Plasma Test. *IEEE Electron Device Lett.* **2020**, *41* (4), 597–600. https://doi.org/10.1109/LED.2020.2973343.

(35) Tur-García, E. L.; Davis, F.; Collyer, S. D.; Holmes, J. L.; Barr, H.; Higson, S. P. J. Novel Flexible Enzyme Laminate-Based Sensor for Analysis of Lactate in Sweat. *Sensors and Actuators B: Chemical* **2017**, *242*, 502–510. https://doi.org/10.1016/j.snb.2016.11.040.

(36) Payne, M. E.; Zamarayeva, A.; Pister, V. I.; Yamamoto, N. A. D.; Arias, A. C. Printed, Flexible Lactate Sensors: Design Considerations Before Performing On-Body Measurements. *Sci Rep* **2019**, *9* (1), 13720. https://doi.org/10.1038/s41598-019-49689-7.

Chapter 4 Additive manufacturing of electrochemical sensors: Fabrication, characterisation and electrochemical analysis

4.1 Introduction

The use of conventional fabrication techniques is not always feasible or cost-effective for the fabrication or integration of electrodes with 3-D devices. Electrode fabrication on 3D constructs such as probes, deflated balloons, catheter devices etc. remains an interesting manufacturing challenge specifically with respect to fabricating reproducible electrodes on devices. One approach towards addressing this is the fabrication of flexible electrodes for subsequent integration with devices. An example of this can be seen in Figure 4.1, where Park *et al.* fabricated a flexible three-electrode sensor configuration using photolithography, electron beam evaporation and lift-off methods. The electrodes were applied to a 1.2 mm diameter biopsy needle to demonstrate conductivity, pH and glucose detection.[1]

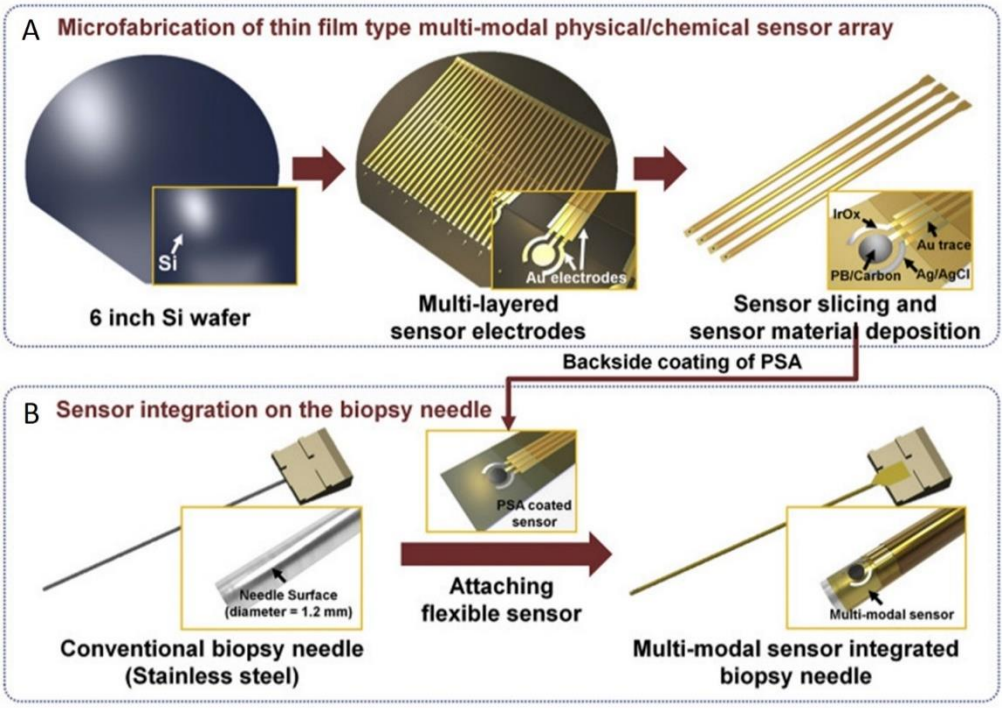

***Figure 4.1**: Fabrication of a biopsy needle integrated with a multi-modal physical/chemical sensor array (A) fabrication process of biosensor electrodes for multi-modal physical/chemical sensor array and (B) integration process of the multi-modal physical/chemical sensor array onto the surface of biopsy needle. (Taken from[1])*

Another approach to consider is the use of autonomous additive printing techniques to dispense conductive inks on to flexible substrates for subsequent attachment with 3D structures. Additive printing technologies have provided distinct advantages for prototyping multidimensional structures for applications such as medical devices, aerospace components and electronics.[2–4] Typically, a design concept is prepared using a

CAD software such as SolidWorks, that is then converted in to an appropriate file format compatible with the printer software.[5,6] Components are usually manufactured based on a defined layering deposition process. Examples of additive printing methods include powder-based, lamination, visible or UV polymerisation and extrusion.[7,8] Among these, extrusion printing has contributed to the fabrication of electrodes for electrochemical sensors.[9–12] Figure 4.2 A displays a simple representation of a conventional fabrication process involving photolithography, electron beam evaporation and lift-off processes for comparison to Figure 4.2 B depicting a schematic for an additive printing method, which is autonomous, efficient, results in less waste material and requires less equipment.[7,13]

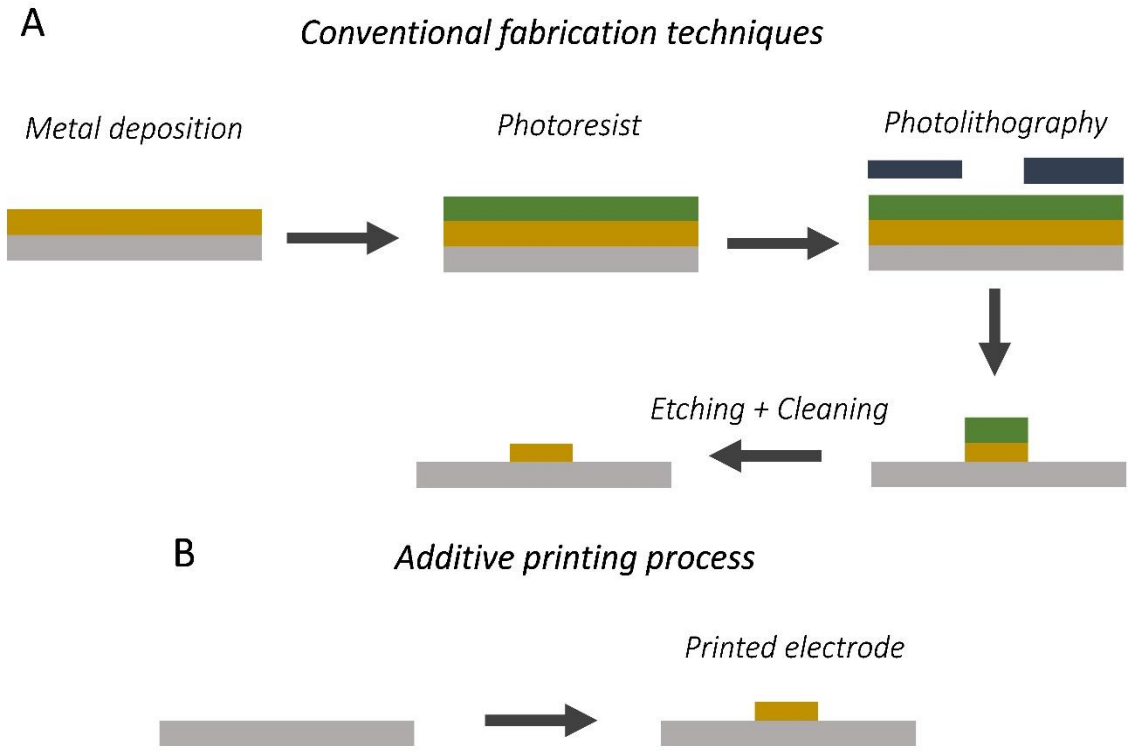

Figure 4.2: *Schematic representing (A) conventional electrode fabrication processes versus (B) additive printing methods. (Adapted from [14])*

Circuit boards can already be printed or rapid prototyping with devices such as the Voltera V-One (shown in Figure 4.3 A). This device is an extrusion-printing tool that directly writes on to substrates using a simple syringe/plunger set-up. It has been used to print radiofrequency electronics and antenna, supercapacitors, nanowire electronics for pressure sensing, chemo-resistive patterned electrodes for the detection of volatile compounds, FET ionic sensors, digital microfluidic sensors. More recently, it has been investigated to fabricate electrodes for electrochemical applications.[10,14–19] This chapter aims to examine the potential for using a using a low cost resource PCB printer for the

additive fabrication of flexible electrodes (Figure 4.3 B and C) with a view to hybrid device-sensor applications. The objectives for this chapter are outlined below:

1. Design and print electrodes using gold-thermoplastic inks onto a low cost flexible substrate
2. Determine the variation in geometrical properties between electrodes printed using the same print parameters and curing time
3. Electrochemically characterise the electrodes
4. Characterise the electrode morphology and composition
5. Assess the stability of the flexible electrodes during an electrochemical measurement whilst fixed at a specific curvature
6. Examine the effect of applying a stress on electrodes before conducting an electrochemical measurements
7. Demonstrate sensor performance using lactate oxidase as a model enzyme for lactate detection.

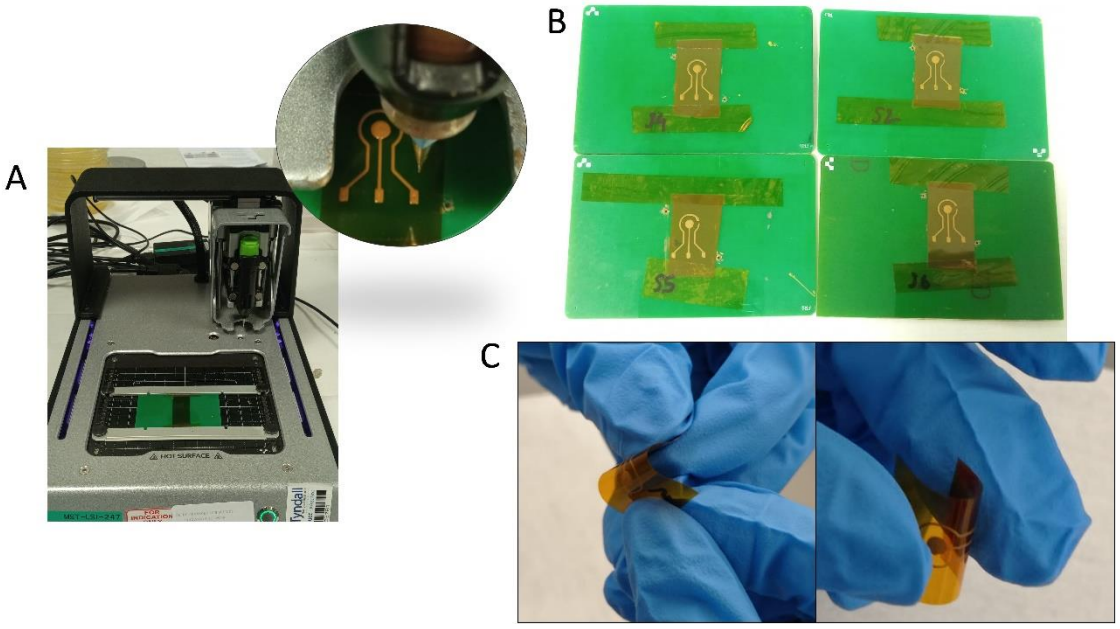

Figure 4.3: *(A) Image of the Voltera printer and a close up image of the dispenser nozzle nozzle tip after completion of a print, (B) Electrodes printed on to polyimide substrates attached to the PCB FR1 boards (C) Image of printed electrodes.*

4.2 Experimental

4.2.1 Materials and Apparatus

Polyimide (Kapton) films (50µm thickness) and silver paste were procured from Radionics RS (Dublin, Ireland). Gold polymer paste ink (C2041206P2) and platinum polymer paste ink (C2050804P9) were purchased from Sun chemical (New Jersey, US). A stretchable encapsulant PE773 stretchable was purchased from DuPont™. The Voltera V-one dispense printer, FR1 substrates (Printed circuit board substrate) and 150-micron nozzles were obtained from Voltera (Kitchener, ON, Canada). An electrochemical cell holder was 3D printed using a Formlabs 3-D printer with standard white resin, also purchased from Formlabs (Massachusetts, United States). O-rings with a diameter of 7 mm were acquired from Radionics to create a seal between the well within the electrochemical cell holder and the dispense printed electrodes (DPE). Screen-printed gold electrodes were purchased from DropSens Asturias, Spain. Acetic acid was purchased from Fisher Scientific (Massachusetts, United States). Phosphate buffered saline tablets (PBS 10 mM, pH 7.4), sodium phosphate monobasic, sodium phosphate dibasic, chitosan, potassium ferrocyanide ($K_4[Fe(CN)_6]$), potassium ferricyanide ($K_3[Fe(CN)_6]$), hexamineruthenium (III) chloride $(Ru(NH_3)_6)^{3+}$, chloroplatanic acid, sulfuric acid and L-lactic acid were acquired from Sigma Aldrich (Arklow, Ireland). Recombinant lactate oxidase II from Aerococcus viridans (lyophilized powder, activity 42.8 U/mg) was obtained from Sekisui Ltd, (Maidstone, United Kingdom). Crocodile clips and ribbed wires were obtained from Farnell (Dublin, Ireland). All solutions were prepared using deionised water with a resistivity of 18.2 MΩ cm^{-1}. Data was plotted and analysed using Origin 2016 Pro software.

4.2.2 Electrode fabrication

A Voltera V-one dispense printer was used to fabricate gold disc WEs with a specified diameter of 2.5 mm, an Au CE and a Pt RE with a specified width of 0.25 mm in addition to interconnection tracks and contact pads by direct extrusion printing on to 50 µm thickness polyimide films. The electrode design (see Figure 4.4 (a)) was prepared in Altium designer software and exported as a Gerber file (GTL). The Voltera V-one software was used to drive the print by following a series of steps:

1. In the Voltera software ink list, the conductor ink with properties close to that of the gold polymer paste was selected (Figure 4.4 (b)), which determines the printing parameters (see Table 4.1).
2. The Gerber file was loaded into the Voltera V-one software.
3. Alignment holes were drilled into the FR1 PCB board using the two circles within the Gerber file at either side of the three electrodes.
4. Polyimide was attached within the alignment markers using kapton tape. Figure 4.4 (c) shows the board clamped to the printer, with polyimide attached within the alignment markers.
5. Probing and alignment was then carried out; the probe (see Figure 4.4 (d)) created an outline of the print to confirm that the design is within the polyimide substrate boundaries. The alignment markers can be seen in the image to the right of the probe as the smaller blue circles. The probe creates a height map of the substrate by probing at each of the regions on the substrate marked with the larger blue circles. If the surface height across the substrate has varied the print will not proceed.
6. After the probing step, the ink cartridge within the dispense holder was mounted on to the V-one printer. Prior to proceeding with a print, both a priming step and a qualitative calibration step are required. The priming step involved turning a gear on the dispense holder until the ink flows from the nozzle. Once ink flow is successful, the gear is turned back ¼ of a step to prevent flow until the ink cartridge is set up and the print is initiated. If the priming step is not carried out correctly, i.e. if the gear on the nozzle is not turned back, once a print is initiated, the piston will exert a larger amount of pressure on the ink. Another issue can be the height of the nozzle from the board, if the probing step is not carried out correctly, and the nozzle is too close to the substrate larger traces such as the example shown in Figure 4.4 e with the red x. Prior to each print, a visual inspection is carried out. If larger quantities of ink are dispensed, the print can be cleaned with acetone and the priming step is repeated by turning the gear of the dispenser back to ensure that ink is not flowing from the nozzle. If no improvements are observed, increasing the height of the nozzle from the substrate can help to achieve a print similar to that with the green tick in figure 4.4 e. If both the priming step and adjusting the height did not result in improvements the print is cleaned and the probing and alignment steps were repeated.

7. Once the calibration step was complete, the print was initiated. The Voltera used a 3-axis motion control system and a positioning resolution of 1 µm; the inks were printed using a dispenser tip with a 150-µm inner nozzle diameter.

Once the prints were complete (Figure 4.4 (f)) the electrodes were cured for 30 minutes at 80 °C as indicated in the instructions for the polymer paste inks.

The WE interconnection tracks were passivated using a stretchable encapsulant that was cured for 10 minutes at 100 °C to prevent electrochemical reactions from occurring at the WE connection track exposed within the diameter of the o-ring. Silver paste was applied to the contact pads using a paintbrush to prevent scratching/contact pad removal during connection with the crocodile clips for electrochemical measurements.

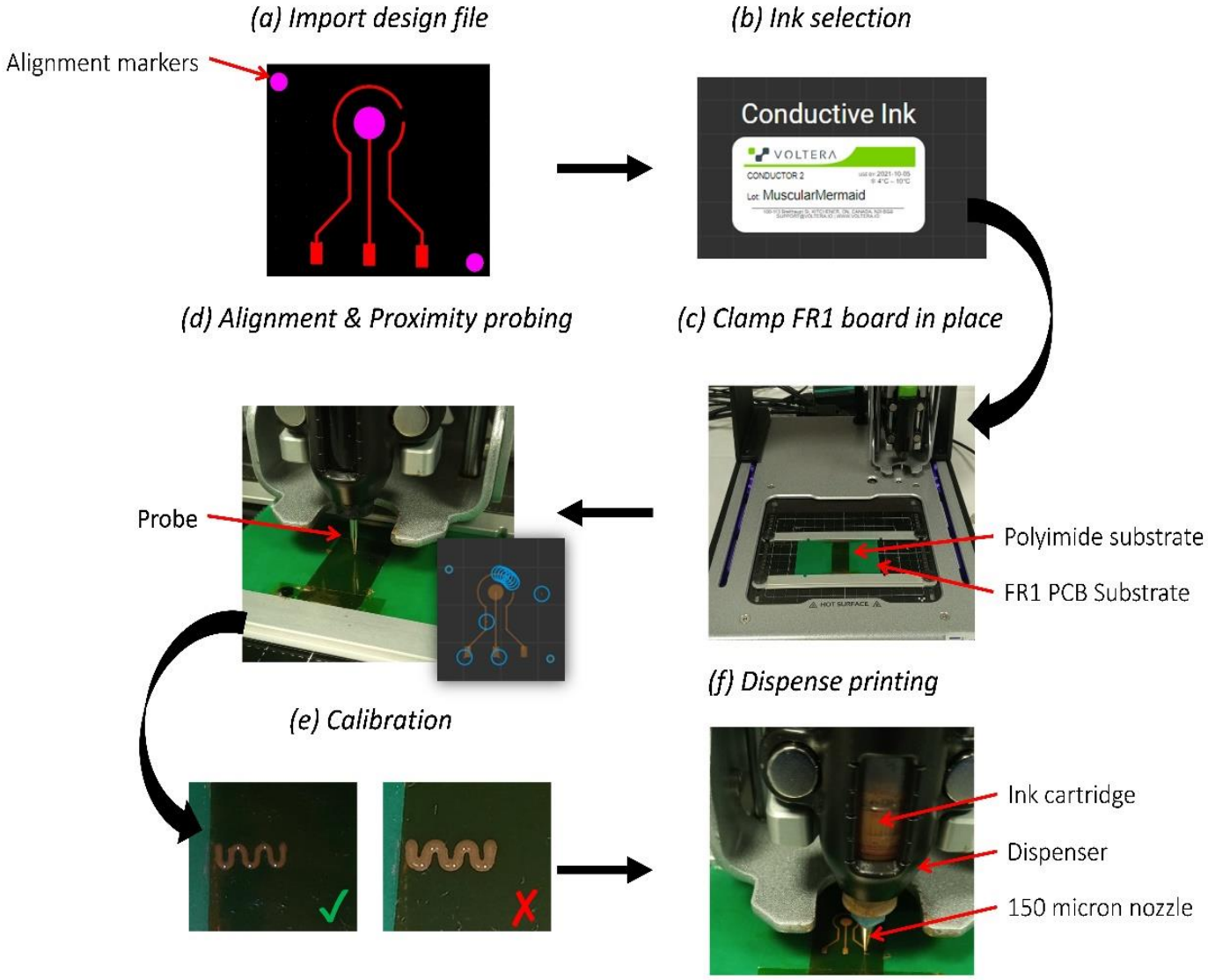

Figure 4.4: *Voltera V-one aligned printing process for the preparation of dispense printed gold electrodes, interconnection tracks and contact pads.*

Table 4.1: *Table of print parameters, their description as defined by Voltera and the settings used during the print.*

Parameter	Description	Setting
Pass spacing	The minimum center-to-center distance between two adjacent printed lines	0.15 mm
Dispensing Height	Distance between the nozzle tip and the substrate	0.10 mm
Feedrate	Speed of dispenser during printing	500 mm/min
Kick	Stroke Length of the piston within the dispenser (how much pressure is applied)	0.35 mm
Trim Length	The maximum distance the dispenser will travel before initiating a 'kick'	50 mm
Trace penetration	Distance a trace travels in to a feature (contact pad/electrode)	0.15 mm
Anti-stringing distance	Distance travelled during print before travelling backwards to break any potential 'stringing' effects	0.1 mm
Soft start ratio/soft stop ratio	These parameters are use to compensate for the delay between when pressurisation begins and when the flow rate reaches the correct level to initiate printing	0.1 mm/0.15 mm
Rheological set point	How the printer compensates for the flow rate over time. For high-viscosity compressible fluids (like the conductive ink or solder paste), this parameter is increased if the flow rate is decreasing over time.	0.16 mm

4.2.3 Characterisation

3D microscopy images were obtained using a Keyence VHX2000 system that can cover magnification ranges of x1 and x1000. The Quanta 650 Scanning electron microscope (SEM) was used to obtain images and energy dispersive X-ray analysis (EDX) mapping of the printed electrodes. XPS measurements were carried out in the University of Limerick using the Kratos AXIS ULTRA spectrometer for the quantification of elements present in the printed electrode. The detection limit of the XPS is < 0.1 atomic %, any elements not detected may be absent or below the detection limit of the XPS. The analysis area is approximately 1 mm^2 and the depth of analysis is approximately 10 nm. The parameters used were as follows: Sample Temperature: 20-30 ^oC, X-Ray Gun: mono Al K_a 1486.58 eV; 150 W (10 mA, 15kV), Pass Energy: 160 eV for survey spectra and 20 eV for narrow regions, Step: 1.0 eV (survey), 0.05 eV (regions), Dwell: 50ms (survey), 100 ms (regions), Sweeps: survey (~3), narrow regions (2-10), Calibration: the C 1s line at 284.8 eV was used as charge reference. Spectra were collected in the direction normal to the surface.

4.2.4 Electrochemical Analysis

4.2.4.1 *Electrochemical characterisation*

All electrochemical measurements were carried out using an Autolab potentionstat PGSTAT302N electrochemical workstation (Metrohm Ltd, Utrecht, The Netherlands) controlled by the Autolab NOVA software. All experiments were performed at room temperature using a Faraday Cage (Metrohm, Cheshire, UK). A three-electrode cell was used for electrochemical characterisation, the printed Au disc electrode was used as a WE versus an Ag/AgCl RE (saturated KCL) and an external Pt CE. Potentiodynamic cycling in 0.5 M H_2SO_4 from -200 mV to 1600 mV at 100 mVs^{-1} was performed for up to 18 cycles to clean the electrodes. The electrochemical behaviour of the Au polymer ink WE was studied using two different redox probes. Cyclic voltammetry (CV) was carried out in 5 mM $[Fe(CN)_6]^{4-/3-}$ in a 10 mM PBS solution (pH, 7.4). This process was repeated in 5 mM $[Ru(NH_3)_6]^{3+}$ in a 10 mM PBS solution (pH, 7.4). An external Ag/AgCl RE and a Pt wire CE were used for this. Cyclic voltammetry (CV) was also carried out at various scan rates (10, 25, 50, 75 and 100 mV s^{-1}) on a commercial screen printed electrode in a 10 mM PBS solution (pH, 7.4) containing 5 mM $[Fe(CN)_6]^{4-/3-}$ at a potential window of -300 mV to 500 mV for comparison to the dispense printed WEs at -400 mV to 800 mV. For experiments using the three-electrode configuration, the cell consisted of a 2.5 mm diameter dispense printed Au WE, a dispense printed Au CE electrode and a dispense printed Pt electrode as the pseudo-reference. Electrodes were characterised in 5 mM $[Fe(CN)_6]^{4-/3}$ prepared in 10 mM PBS (pH 7.4) using CV performed at a potential window of -600 mV to 600 mV at 100 mVs^{-1} versus the Pt printed pseudo-reference electrode.

4.2.4.2 *Electrode stability*

Electrode stability was assessed by bending the sensor at a bending radius of approximately 4 mm in one direction (convex) and then in the other direction (concave). After every 10 bending cycles (where one cycle refers to bending in one direction) a CV was measured in 10 mM PBS solution (pH, 7.4) containing 5 mM $[Fe(CN)_6]^{4-/3-}$. This was repeated for up to 200 cycles. Electrodes were also fixed at a bending radius of 7 mm for comparison to electrodes in a planar configuration (curvature = 0 mm bending radius). Both configurations were also assessed using CV in 5 mM $[Fe(CN)_6]^{4-/3-}$ in a 10 mM PBS solution (pH, 7.4) at 100 mV/s.

4.2.4.3 *Feasibility for lactate detection at dispense printed electrodes*

Pt electrodepositions were carried out using amperometry in a solution containing 5 mM H_2PtCl_6 and 0.5 M H_2SO_4 at -0.5 V for 300 seconds against an Ag/AgCl RE (CH instruments), and a Pt wire (CH instruments) was used as the CE. Following the Pt electrodeposition, the sample was rinsed with DI water and allowed to dry under ambient conditions. A 0.3 wt. % chitosan solution was prepared by dissolving chitosan in acetic acid solution (1 wt. %) under magnetic stirring for 1 hour. The chitosan solution was cast onto the electrodes and allowed to dry under ambient conditions. 24 µl of a BSA stock solution (10 mg/ml) prepared in 10 mM PBS (pH 7.4) was mixed with 6 µl from the enzyme stock solution (2000 U/ml). 6µl of the final solution was cast on to the surface of the CS-Pt modified DPE, and allowed to dry under ambient conditions before being stored overnight at 4 °C. Electrodes were rinsed gently with 50 mM PB solution to remove any unadsorbed enzyme and were stored in the fridge with 50 mM PB (pH 6.7) at 4°C when not in use. L-lactic acid stock solution was prepared in 50 mM PB (pH 6.7). Buffer was spiked under stirred conditions for chronoamperometric measurements. As-modified electrodes were exposed to aliquots of PB containing titrated lactate concentrations within physiologically relevant levels by dropping 350 µl aliquots into the well of the 3-D cell holder and allowing 30 seconds prior to running a chronoamperometric scan. The solution was then removed, and the next concentration was directly added to the electrodes. All data were background subtracted using the phosphate buffer baseline measurements.

4.3 Results

4.3.1 Characterisation – 3D microscopy and SEM

4.3.1.1 Reproducibility of dispense printing

The weight of the polyimide strips attached to the FR1 substrate was measured before and after dispensing. The weight of dispensed ink measured for n = 8 working electrodes was 8.1 mg ± 1.3 mg (RSD = 16%). The diameter of the WE was determined using 3-D microscopy dimensional measurements (see Figure 4.5 A) This was used to obtain an approximate surface area of 0.059 cm^2 ± 0.003 cm^2 (RSD 5%). The printed WE diameter was approximately 0.2 mm larger than the diameter specified in the design file imported into the Voltera software (2.5 mm). This increase was attributable to the ink spreading during the 30 minutes curing process. The width of the interconnection track was also measured across three points on the track for n = 8 samples as displayed in Figure 4.5 A, the average width measured was 0.43 mm ± 0.07 mm (RSD = 15.6 %). Since the Voltera V-one does not control the height of the extruded material, DPEs were cross-sectioned by cutting them with a scissors at a distance from the region of interest. They were then positioned in a cylindrical mould such that the region of interest could be reached through the bottom face of the cylindrical mould. The samples were held in position in the mould using a specimen mounting clip which is purpose-designed for this task. The mould was then filled with a standard mounting resin used for the metallographic preparation of samples. This is a two-part resin (resin & hardener) which is transparent and cures in 8 hours at ambient temperature. The cured sample was then de-mounted from the mould and ground & polished (using progressively finer grades of paper / polish) until the region of interest was reached. The final polishing stage was done with a 1µm diamond grit suspension. The cross sections were then used to obtain dimensional measurements with the SEM. A coating thickness of 0.10 mm ± 0.01 mm (RSD = 13.1%) was measured. (see Figure 4.5 B).

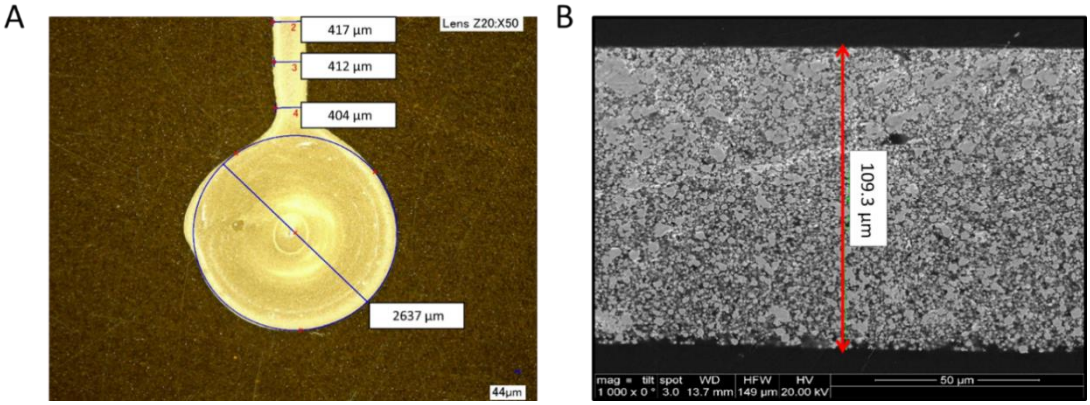

Figure 4.5: *(A) 3D- microscopy image of Au WE with diameter and interconnection track width measurements (B) SEM cross section analysis displaying a width measurement.*

4.3.2 Electrochemical analysis

CV in 0.5 M H_2SO_4 was carried out to clean the electrode surface (see Figure 4.6) for a sample CV). In this example, gold oxide was formed at 1.20 V (vs. Ag/AgCl). On the reverse sweep, a reduction peak can be seen at 0.83 V resulting from the gold oxide removal. This behaviour was not consistent from sample to sample.[20] During the cleaning

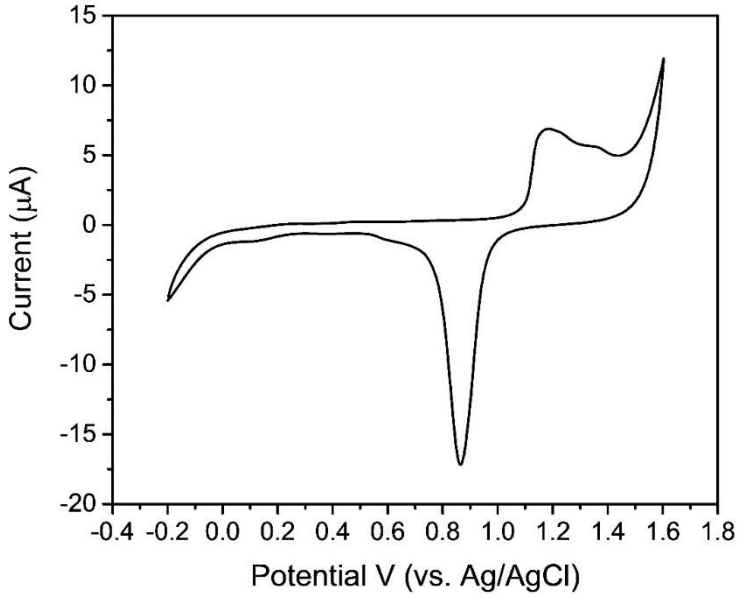

Figure 4.6: *Sample potentiodynamic cycling in 0.1 M H_2SO_4 from -0.2 V to 1.6 V at 100 mV/s.*

step in H_2SO_4 a decrease of charge was observed between scan 1 and that of scan 18. Electrodes produced using the same fabrication process exhibited variations in both oxidation and reduction behaviour during potentiodynamic cycling in 0.5 M H_2SO_4. As can be seen in Figure 4.7, for sensor 1 (S1) (blue), a broad oxidation peak was observed at 1.12V, while two reduction peaks can be seen at 0.91 V and 0.64 V. This reduction behaviour is not indicative of the typical behaviour of gold in H_2SO_4.[21] For S2 (red), a broad oxidation peak was present at 1.20 V and again two reduction peaks were noted at 0.90 V and 0.70 V. Finally, for S3 two oxidation peaks were present at 1.12 V and 1.20 V and two reduction peaks were visible at 0.91 V and 0.76 V. Clear variations in electrochemical behaviour existed between electrodes fabricated using the same printing fabrication process and parameters. The presence of additional peaks may be attributed to the thermoplastic resin mixture, or perhaps the presence of oxygen. Different Au crystal faces exposed could also result in additional peaks being present, however, confirmation would require further investigation.

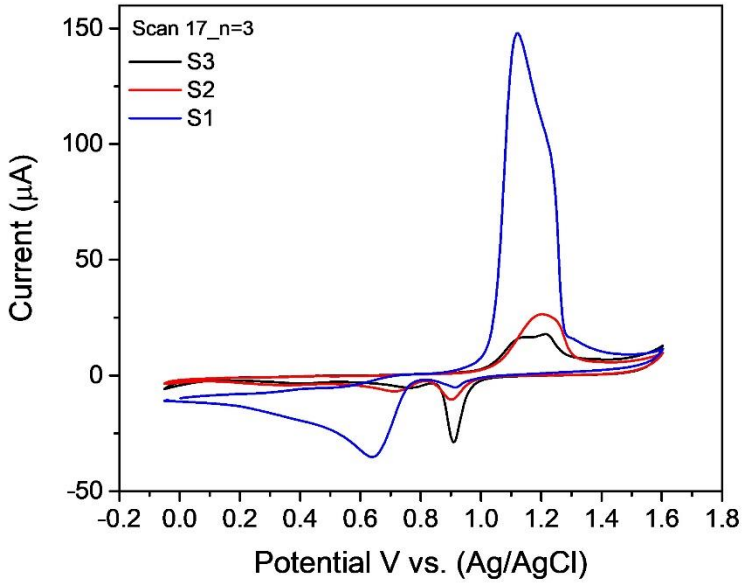

Figure 4.7: *Potentiodynamic cycling in 0.5 M H_2SO_4 from -0.2 V to 1.6 V at 100 mV/s at n =3 WE (CE: Pt wire).*

To further examine the electrochemical performance of dispense printed electrodes, CV was carried out in two redox mediators: 5 mM $[Ru(NH_3)_6]^{3+}$ (outer sphere redox mediator) and 5 mM $[Fe(CN)_6]^{4-/3-}$ (inner sphere redox mediator). Figure 4.8 A displays the CV plots measured in $[Ru(NH_3)_6]^{3+}$ at scan rates of 10 mV/s to 1000 mV/s. A linear

relationship between the peak current and the square root of the scan rate was observed with correlation coefficients of 0.97 and 0.98 for the peak oxidation and reduction reactions respectively (Figure 4.8 B). An overlay of n = 3 CVs obtained at 100 mV/s is exhibited in Figure 4.9. At 100 mV/s, the average peak separation determined for the bare dispense printed electrode was 92.0 mV ± 4.2 mV above the theoretical ΔEp (59 mV) for a one-electron reversible reaction. This is attributed to both IR drop and slower kinetics occurring at the conductive ink electrode. Peak anodic currents had a relative standard deviation of 6.2 %.

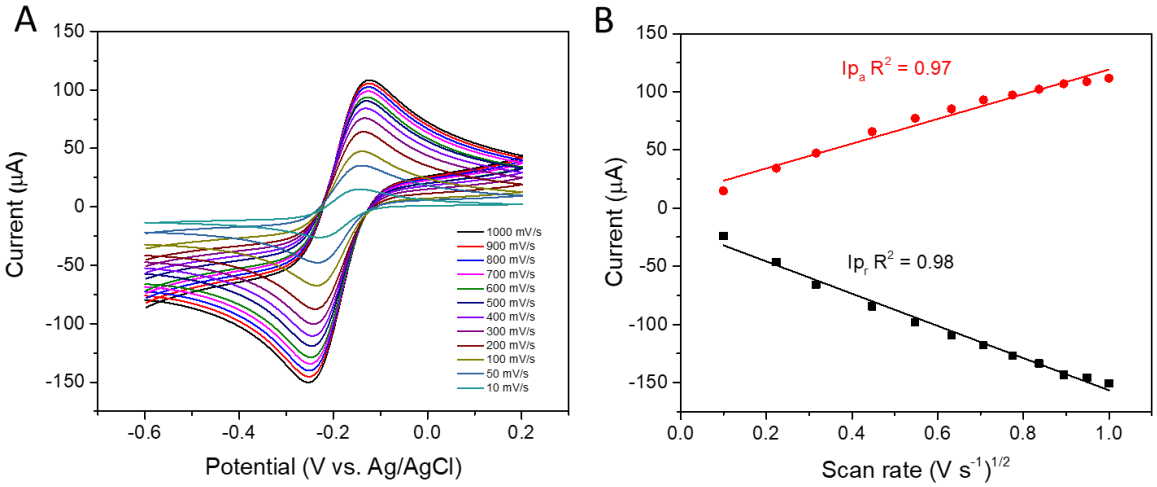

Figure 4.8: *(A) CVs on a dispense printed Au electrode at increasing scan rates (10 mV/s up to 1000 mV/s) in 5 mM $[Ru(NH_3)_6]^{3+}$ (B) Corresponding plot of peak current vs. $v^{1/2}$.*

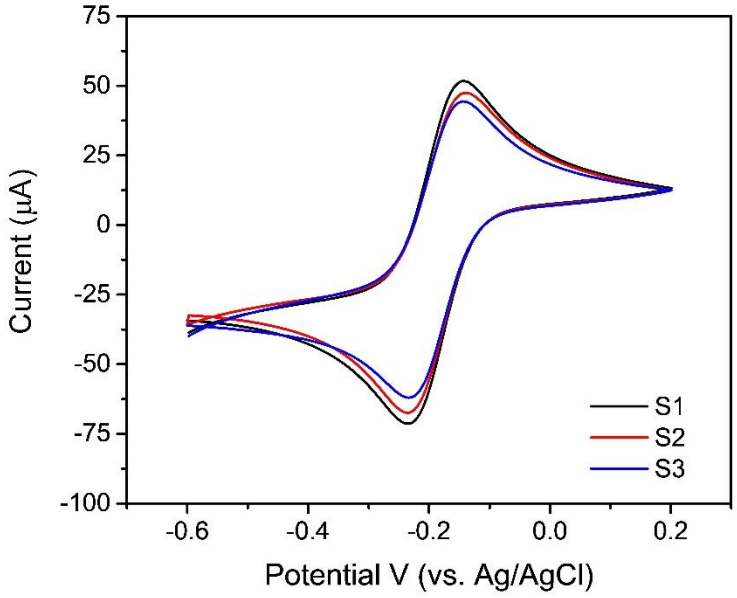

Figure 4.9: *CVs measured on three dispense printed Au electrodes at 100 mV/s in 5 mM $[Ru(NH_3)_6]^{3+}$ made up in 10 mM PBS (pH 7.4).*

Figure 4.10 A displays the CV plots measured in $[Fe(CN)_6]^{4-/3-}$ at scan rates of 10 mV/s to 1000 mV/s. Again, a linear relationship exists between the peak oxidation and reduction currents and the square root of the scan rate (Figure 4.10 B). These results indicate that fast electron transfer can occur at the printed electrode structures; however, a larger variation in ΔEp was observed at 100 mV/s with an average ΔEp of 163 mV ± 38 mV. Figure 4.11 illustrates a clear difference between CV measurements carried out at n = 3 DPEs as peak currents had a relative standard deviations of 26.8%. The ferro/ferricyanide redox probe has however been described as a non-ideal system due to challenges with decomposition and adsorption which may be contributing to these variations. [22]

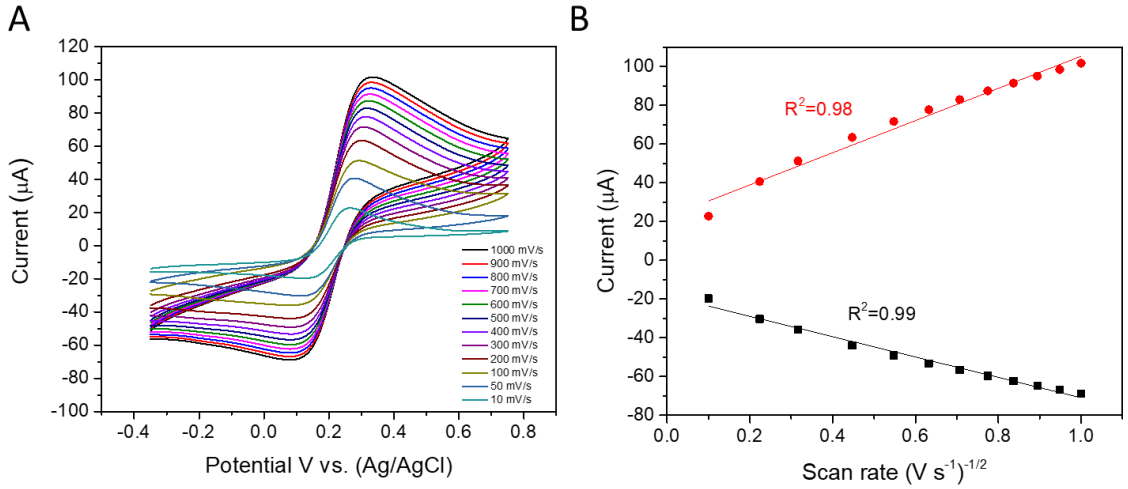

Figure 4.10: *(A) CVs measured on a dispense printed Au electrode at increasing scan rates (10 mV/s up to 1000 mV/s) in 5 mM $[Fe(CN)_6]^{4-/3-}$ (B) Corresponding plot of peak current vs. $v^{1/2}$.*

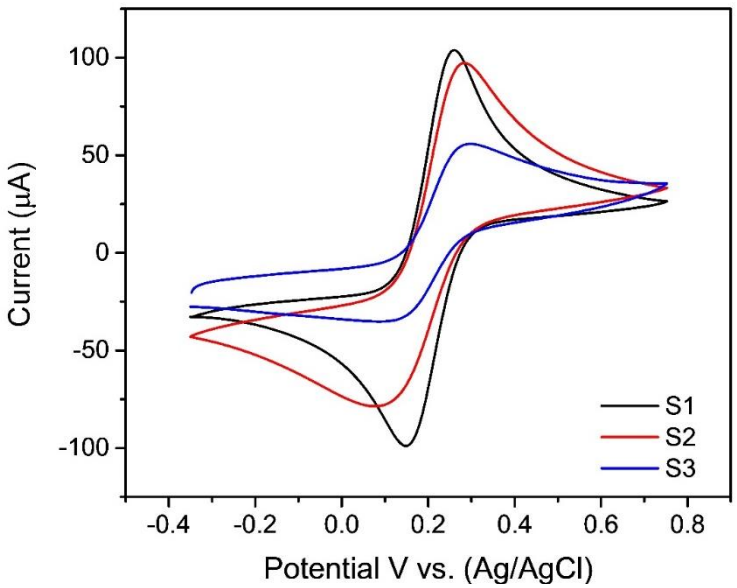

Figure 4.11: *CVs measured on three dispense printed Au electrodes at 100 mV/s in 5 mM $[Fe(CN)_6]^{4-/3-}$ made up in 10 mM PBS (pH 7.4).*

Au screen printed electrode (1.6 mm diameter) was assessed in 5 mM $[Fe(CN)_6]^{4-/3-}$ for comparison to a dispense printed Au electrode. The electrochemical behaviour of a commercial Au screen printed electrode was assessed in 5 mM $[Fe(CN)_6]^{4-/3-}$ for comparison to a dispense printed Au electrode. Figure 4.12 A displays CVs at various scan rates at the Au SPE. The CVs exhibit reversible behaviour, which results in increasing peak currents with increasing scan rates. For the dispense printed electrodes, the redox behaviour is quasi-reversible, again, resulting in increasing anodic peak currents with increasing scan rates (see Figure 4.12 B). At 100 mV/s, the peak current for the dispense printed electrode is 4.61 µA in comparison to the Au SPE, which, at

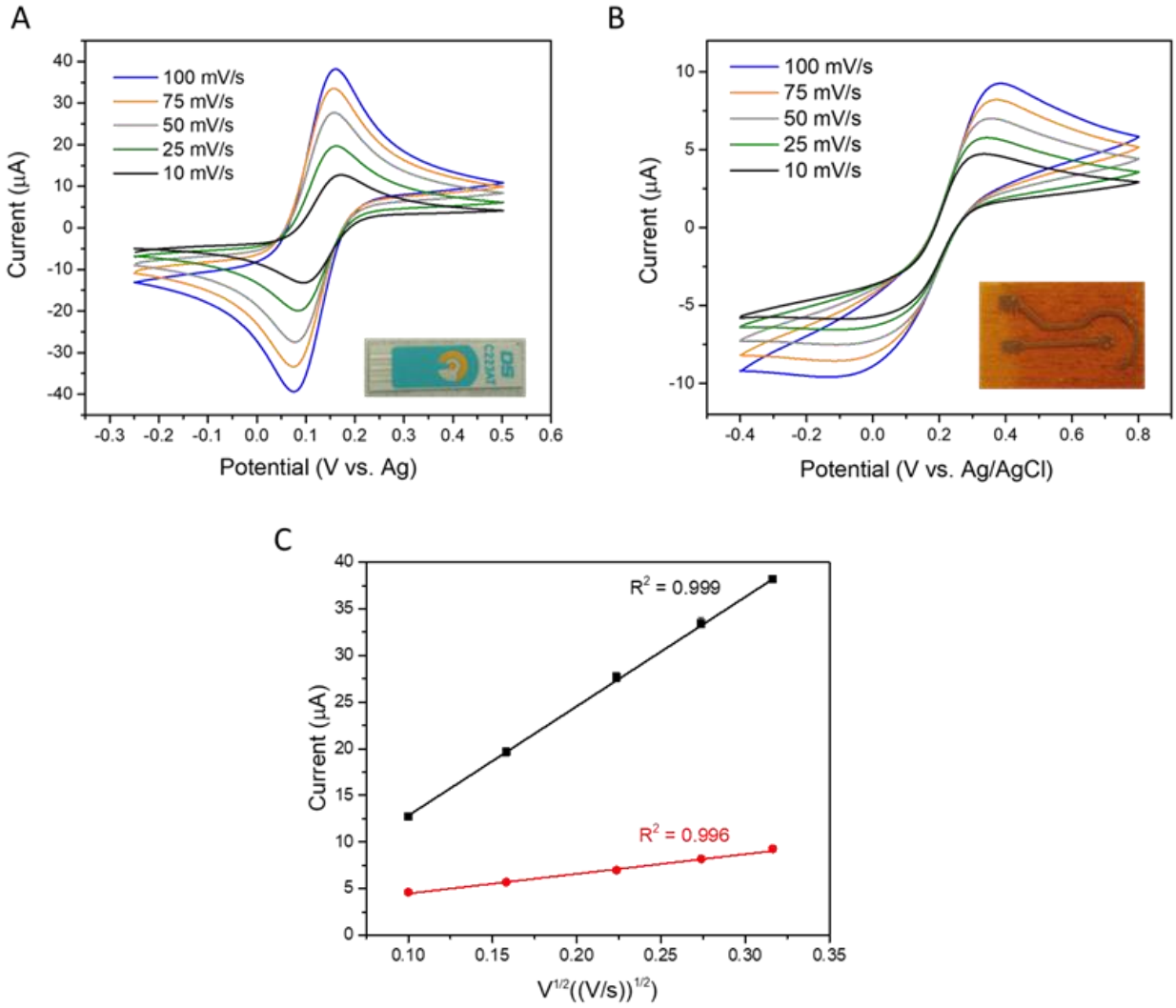

Figure 4.12: *A CVs obtained at various scan rates (10 mV/s, 25 mV/s, 50 mV/s, 75 mV/s and 100 mV/s) in a 5 mM ($K_4[Fe(CN)_6]$) and 5 mM $K_3[Fe(CN)_6]$ made up in 10 mM PBS (pH 7.4) using a commercial Au screen printed electrode (1.6 mm diameter), B CVs obtained at various scan rates at a dispense printed Au electrode (1.4 mm diameter) C Over lay of anodic peak currents for the Au SPE (black) and Au DPE (red).*

100 mV/s has a peak current of 12.72 µA. Figure 4.12 C shows a plot of peak current versus the square root of the scan rate for both electrodes. It is evident that the currents are higher for the commercial SPE. Although the geometric area is similar, the measured electroactive area of exposed metallic gold structures present on the dispense printed electrode is lower than that of the commercial SPE. Based on issues seen with the inner-sphere redox probe this experiment could be repeated with ruthenium to assess if kinetics are having an effect.

4.3.2.1 *Three-electrode configuration*

Au polymer paste ink and Pt polymer paste ink were also dispense printed onto the polyimide substrate to fabricate a CE and RE respectively. Figure 4.13 displays an Au WE and CE dispense printed on to the polyimide sheet. The CE had an increase in track width at the point where the nozzle finished dispensing. Excluding this region, the average width measured over multiple electrodes (n = 6) across the connection track was 480.0 ± 29.5 µm.

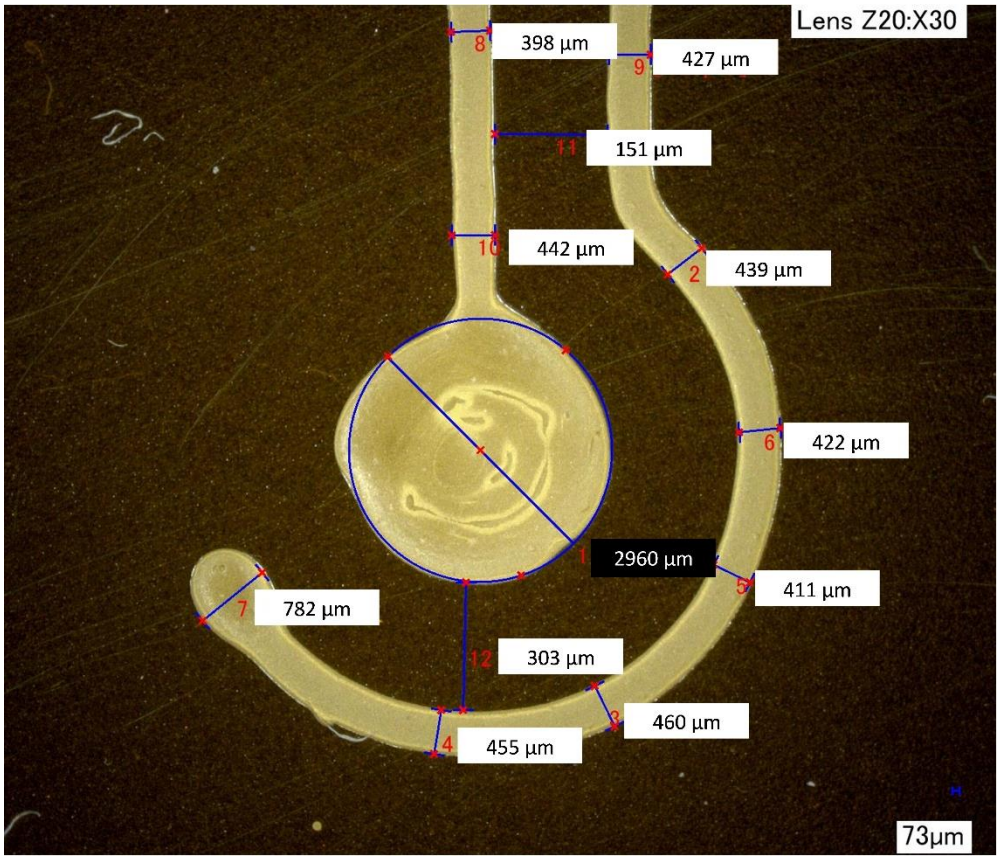

***Figure 4.13**:3D- microscopy image of dispense printed electrodes (Au WE and CE) including the WE diameter, and interconnection track width measurements and CE width measurements.*

Figure 4. **14** displays dispense printed 3 electrode. The Pt polymer paste RE after dispensing and curing was determined to have a width of 593.8 ± 83.4 µm

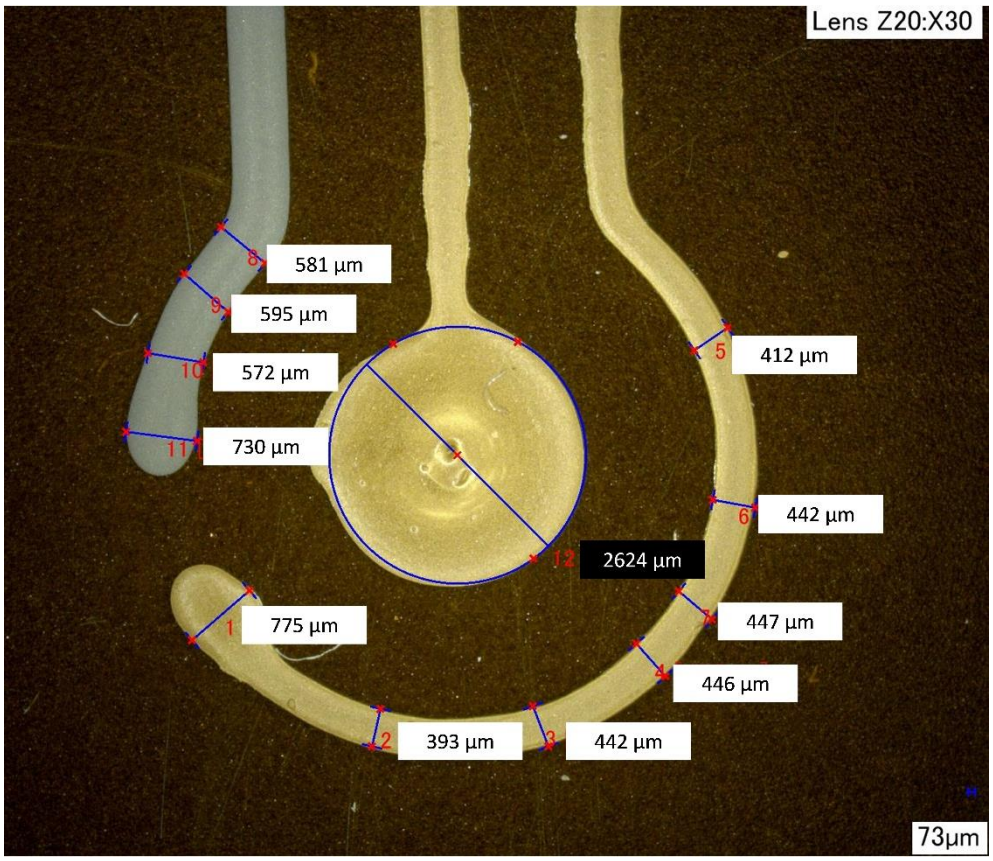

Figure 4. 14: *3D- microscopy image of dispense printed electrodes (Au WE and CE, Pt RE) including the WE diameter and CE and RE width measurements.*

Figure 4.15 displays eight CVs recorded at 100 mV/s using the three dispense printed electrode set-up. An Ip potential shift of –27mV was observed between scan 1 and scan 8. CVs recorded at 100 mV/s at "three-electrode" dispense printed electrodes Figure 4.16 displayed similar variations to measurements carried out with a conventional RE and CE

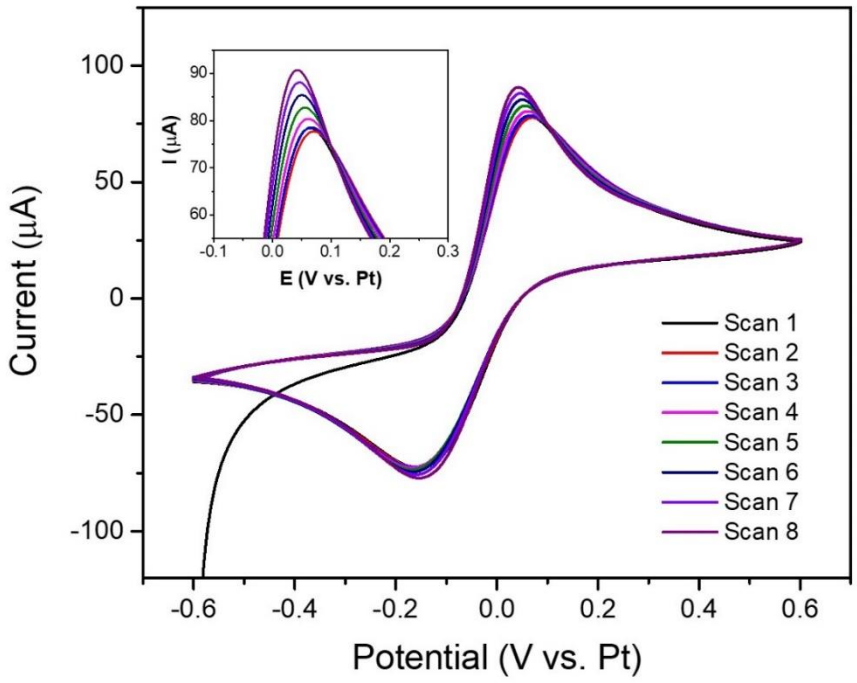

***Figure 4.15**: Eight CV scans measured using three-dispense printed electrodes (WE & RE – Au polymer paste, RE – Pt polymer paste) at 100 mV/s in 5 mM $[Fe(CN)_6]^{4-/3-}$ made up in 10 mM PBS (pH 7.4).*

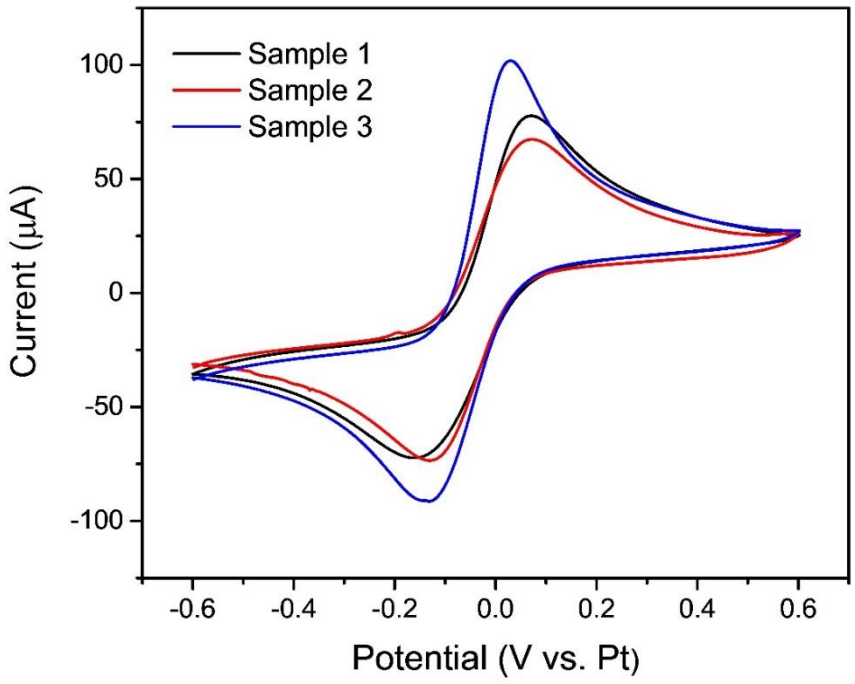

***Figure 4.16:** CVs measured using three-dispense printed electrodes (WE & RE – Au polymer paste, RE – Pt polymer paste) at 100 mV/s in 5 mM $[Fe(CN)_6]^{4-/3-}$ made up in 10 mM PBS (pH 7.4) (figure shows scan 2).*

4.3.2.2 *Morphology and compositional analysis – SEM, EDX mapping, and XPS*

The surface morphology of the dispense printed WEs were studied using SEM. Figure 4.17 shows a SEM image of the Au WE (10000x) obtained after curing. Au particles can be seen across the WE surface. Upon closer inspection, it is clear that the distribution of the Au particles is not uniform across the electrode. Increasing the magnification to 40,000x displays what appears to be partially exposed regions of Au particles and regions that look to be covered/entrapped (see Figure 4.18). This material is likely the thermoplastic component of the gold polymer paste ink.

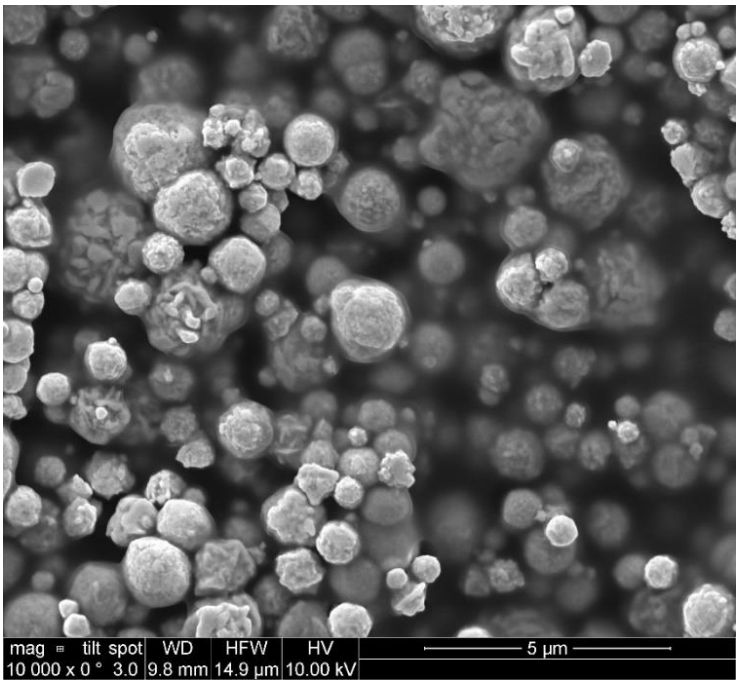

Figure 4.17: *SEM image (10000x) depicting surface morphology of the Au printed particles after curing.*

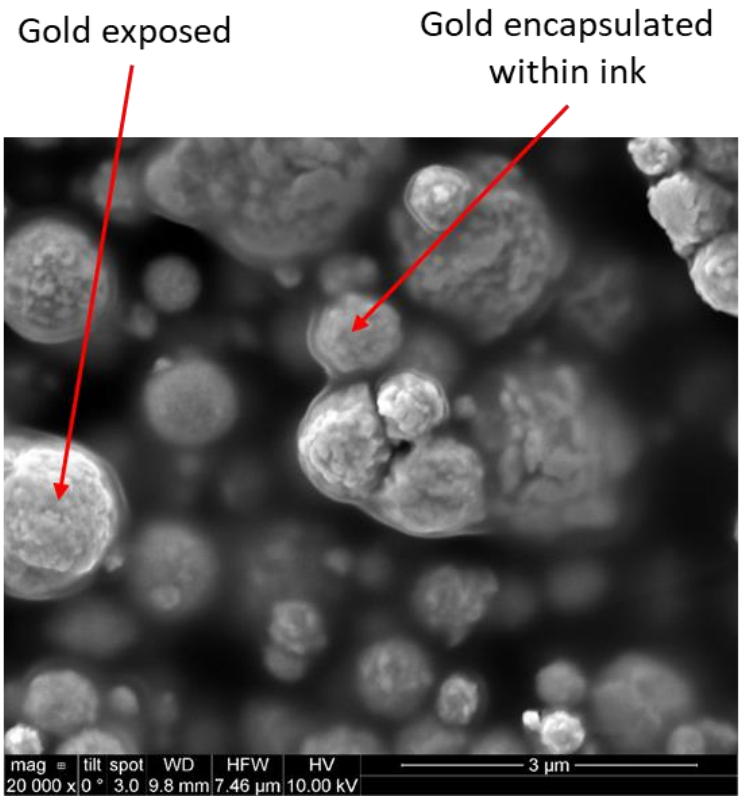

Figure 4.18: *SEM image (40000x) depicting regions of exposed Au and regions covered in organic/polymer paste.*

The Voltera V-one dispensed Au ink in a circular motion starting from the edge of the WE diameter until it reached the centre. Figure 4.19 A shows a low magnification SEM image on which the spiral path taken by the printing nozzle is visible. EDX mapping was carried out to assess for changes in Au content between a region at the centre of a printed spiral (Figure 4.19 B) and a region at the edge of a spiral line print (Figure 4.19 C). The weights % of Au is found to decrease in the region at the edge of a spiral line. XPS analysis was carried out for spectroscopic surface characterisation of the ink. Figure 4.20 displays the measured XPS survey scan of the dispense printed electrode surface confirming the presence of gold, carbon and oxygen. Surprisingly only 3.26 at.% Au was determined. Converting this to weight % gives 33 wt. % which is lower than what was observed with EDX, however, as mentioned in chapter 2 XPS analyses the upper nanometre layers. The conductive ink is cured over a 30 minute period whereby the gold ink may be settling. If this is the case, the upper surface layer would have more thermoplastic resin.

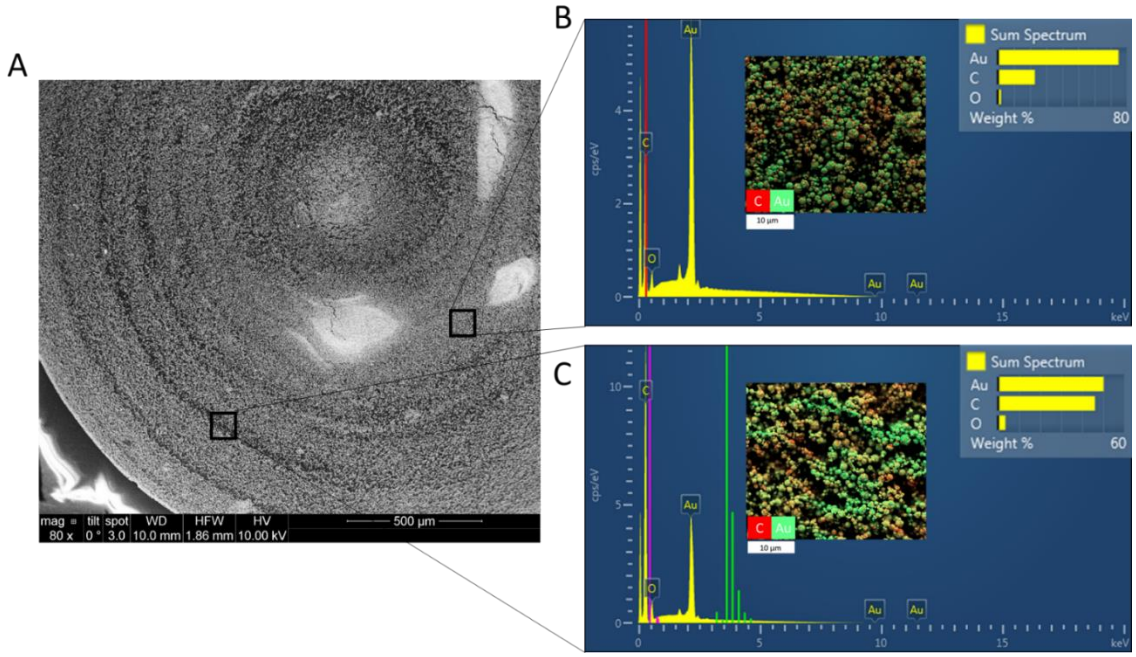

Figure 4.19: *(A) Electron microscopy image of the Au electrode (B) EDX mapping spectra obtained at the centre of a print spiral (C) EDX mapping spectra obtained at the edge of a print spiral.*

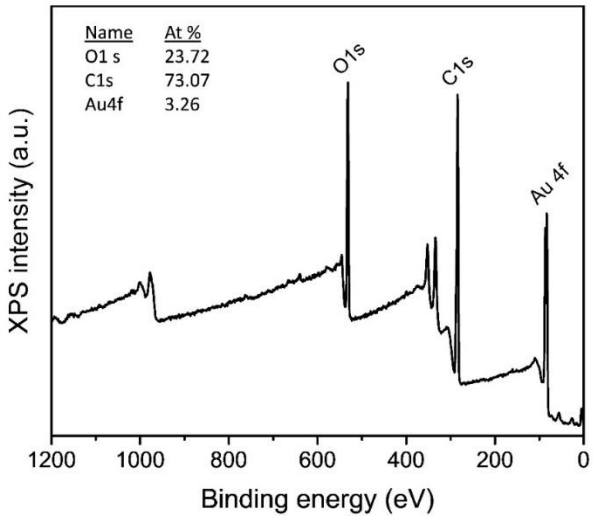

Figure 4.20: *XPS spectrum of dispense printed Au electrode.*

High resolution spectra were also acquired, Figure 4.21 A displays two distinguishing peaks at 84.7 eV for Au 4f (7/2) and at 87.4 eV for Au 4f (5/2) confirming the presence of Au structures. The C1s spectrum was de-convoluted into three main peaks at binding

energies of 284.8 eV, which was assigned to C=C, 286.1 eV for C-O and 288.0 eV which was assigned to O-C=O (Figure 4.22 B). High resolution spectra of the O1s peak revealed three main peaks at 531.9 eV, 533.4 eV and 535.2 eV which were assigned to C=O, O-C=O and adsorbed H_2O respectively (Figure 4.21 C). The XPS results corroborate the SEM and EDX data, as images had revealed that many Au particles were covered or partially exposed. Both SEM and XPS results reveal that the electrode surface is not rich in clean exposed gold metallic structures, which we believe results in variable electrochemical measurements during standard characterization. That being said the peak

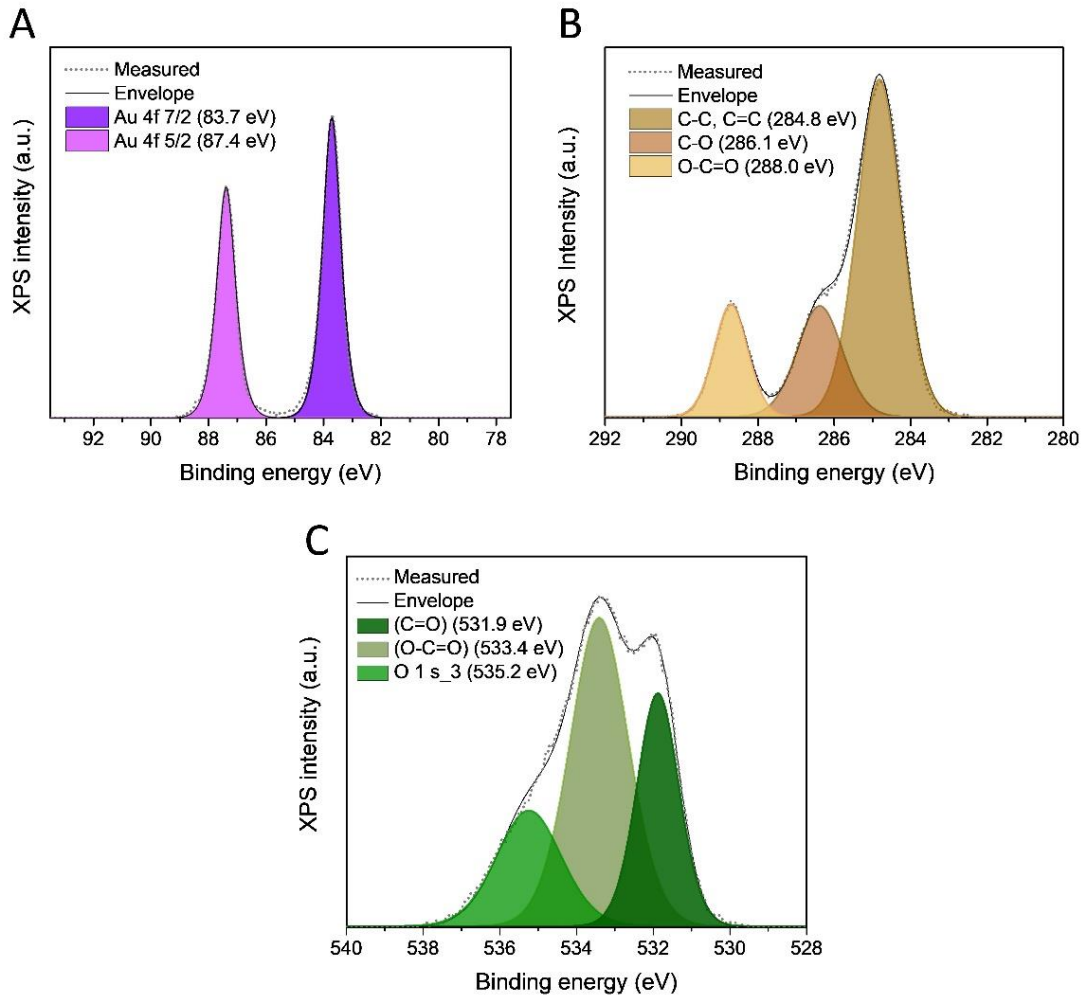

Figure 4.21: *High-resolution XPS spectra for (A) Au 4f spectra of Au polymer paste, (B) C1s spectra of Au polymer paste and (C) O1s spectra of Au polymer paste.*

anodic currents for the measurements in ruthenium had showed a good relative standard deviation of 6.2 % between electrodes.

4.3.2.3 *Electrode stability*

Figure 4.22 A exhibits CVs recorded in $[Fe(CN)_6]^{4-/3-}$ prepared in 10 mM PBS (pH 7.4) prior to and after bending the substrate. Polyimide substrates were bent at an approximate bending radius of 4-5 mm forwards (concave) and again at the same bending radius

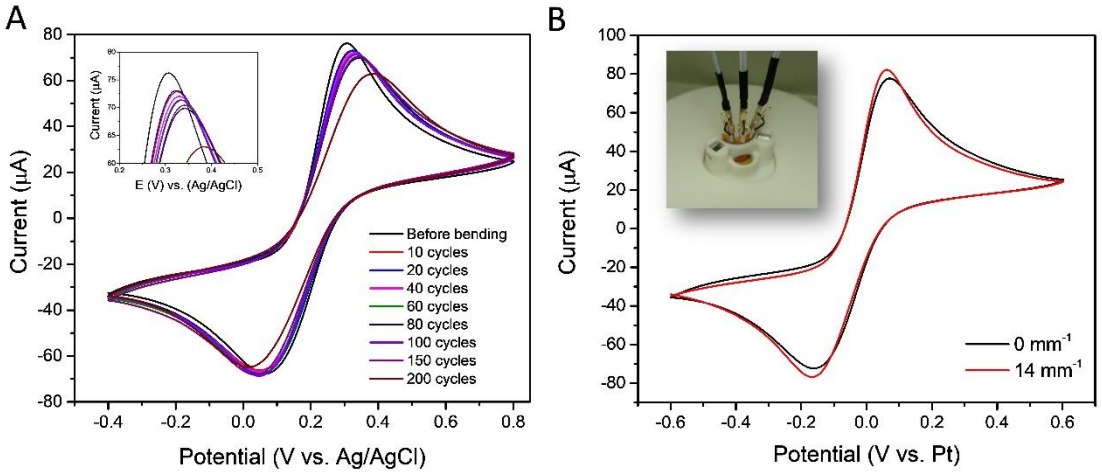

Figure 4.22: *(A) CVs measured at dispense printed Au electrodes at 100 mV/s in 5 mM $[Fe(CN)_6]^{4-/3-}$ made up in 10 mM PBS (pH 7.4) before and after bending the electrode at an approximate bending radius of 4mm-5mm (B) CVs measured at dispense printed Au electrodes at 100 mV/s in 5 mM $[Fe(CN)_6]^{4-/3-}$ made up in 10 mM PBS (pH 7.4) versus the Pt printed pseudo RE and the Au printed CE.*

backwards (convex) 10 times (10 cycles) before conducting another measurement. This process was repeated for 200 bending cycles. Figure 4.22 B displays an overlay of CVs measured in 5 mM $[Fe(CN)_6]^{4-/3-}$ prepared in 10 mM PBS (pH 7.4) at the three-electrode configuration whilst fixed at a bending radius of 7 mm (red) and in a planar (unbent) configuration (black) (owing to challenges observed with reproducibility this was demonstrated using the same electrode).

4.3.2.3.1 Lactate sensor demonstration

The surface morphology of the working electrode preparation steps was examined using SEM. Figure 4.23 A displays the printed Au working electrode and Figure 4.23 B shows the surface morphology after a 300 second platinum electrodeposition, showing complete coverage of the printed ink. Figure 4.23 C shows the electrode following casting with chitosan where the platinum particles were no longer clearly visible, and Figure 4.23 D presents an SEM obtained after casting the BSA-LOx mixture where an amorphous layer of BSA is clearly visible on the surface.

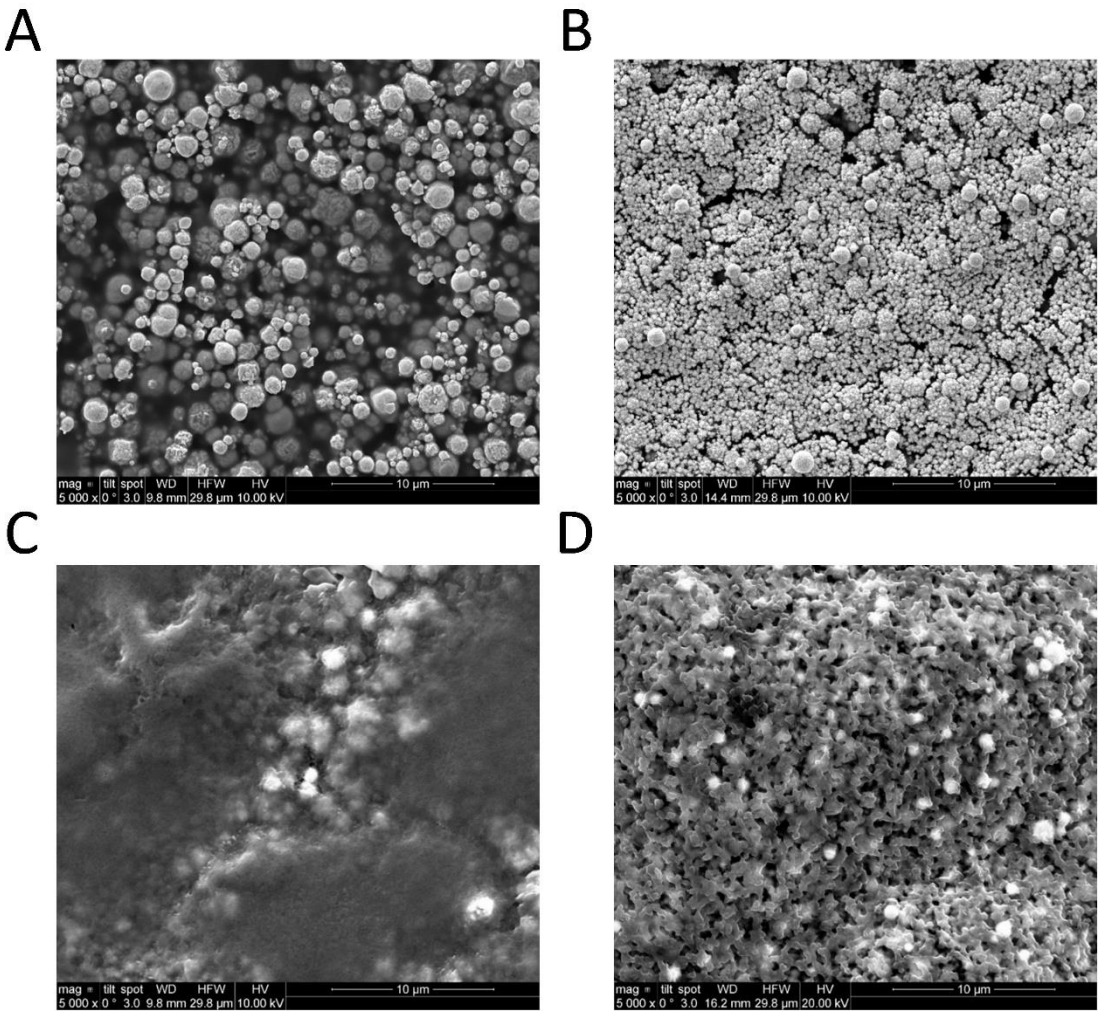

Figure 4.23:*SEM images of (A) Au DPE (B) Pt modified DPE (C) Pt/CS modified DPE (D) BSA-LOx/CS/Pt modified DPE.*

Figure 4.24 displays the chronoamperometric response to lactate at + 0.4 V. The chronoamperometric measurements were studied in response to increasing concentrations of lactate in 50 mM PB (pH 7.4) in an unstirred environment. The Au/Pt/CS/LOx-BSA electrodes reached relatively stable currents 10 seconds after the measurement started. The current measured after 30 seconds was used to prepare the calibration curve. Figure 4.25 shows the corresponding calibrations obtained for n = 3 biosensors for lactate sensing. A linear range is visible between 0.2 mM and 1.0 mM for all sensors, however clear variation exists between the currents measured for n = 3 samples with an RSD of >25% for each of the concentrations measured.

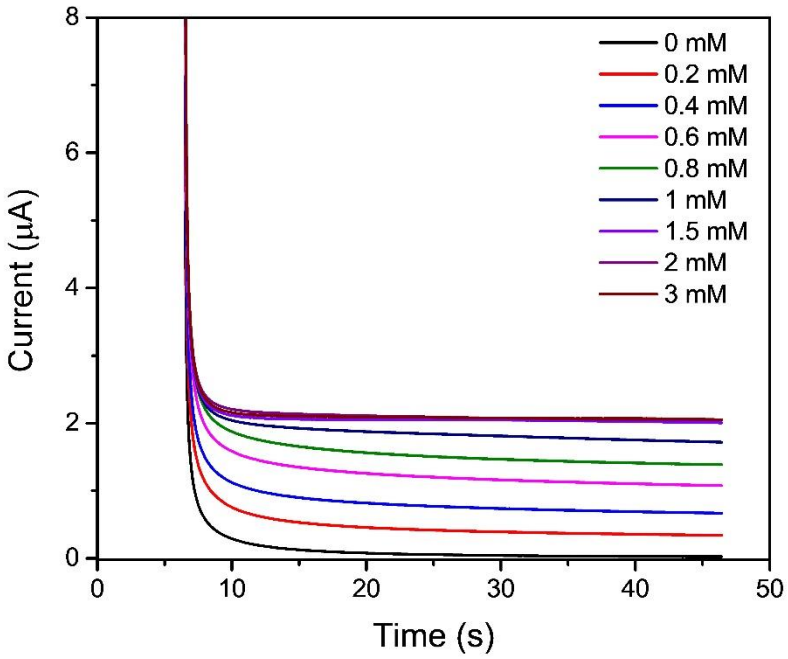

Figure 4.24: *Chronoamperometric responses of increasing concentrations of lactate from 0 to 3 mM* $E_{applied}$ *= + 0.4V (vs. Ag/AgCl).*

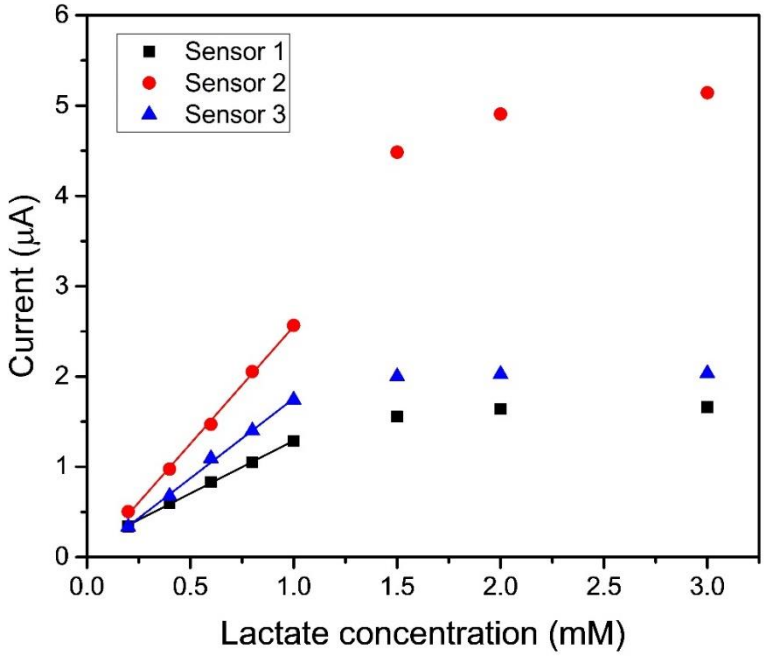

Figure 4.25: *Calibration plot for n = 3 samples, based on sampling the current at 30 seconds.*

Using the diameter measurement obtained with the 3D microscope to measure an approximate geometric area for each of the samples, a plot of current density versus lactate concentration (for concentrations within the linear range) is displayed in Figure 4.26. A sensitivity value of 19.5 μA/mM/cm^2 was determined for sensor 1, 43.4 μA/mM/cm^2 for sensor 2 and 29.5 μA/mM/cm^2 for sensor 3. Indeed variations in exposed gold can result in variable platinum electrodepositions. However, further analysis on electrodes in H_2O_2 would help to confirm if the variation is a result of electrode area variations or kinetics.

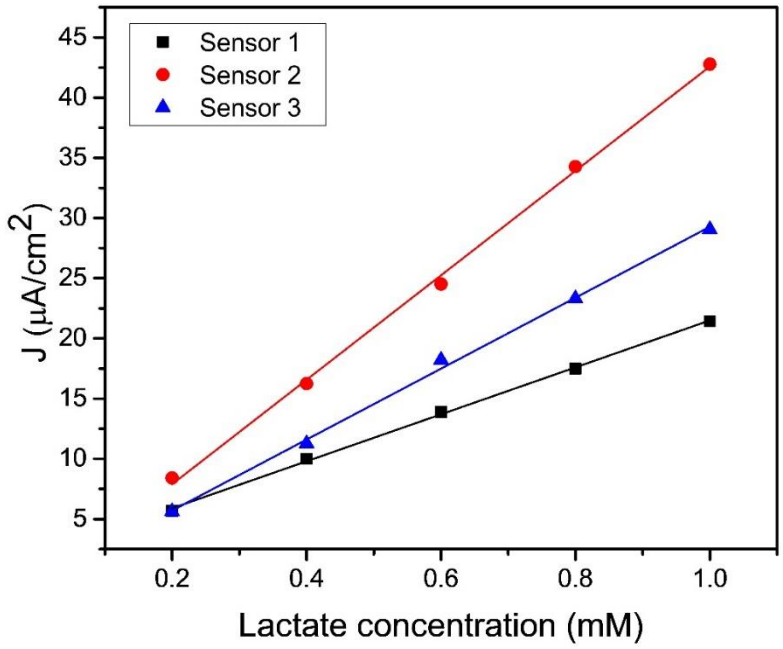

Figure 4.26: *Plot of current density (J) versus Lactate concentration (mM) for concentrations within the linear range of the calibration.*

4.4 Discussion

Additive printing methods have introduced many opportunities for researchers to develop customisable electrochemical sensing devices without the need for multiple processing steps and unnecessary waste material. However, each technique is not without challenges. Table 4.2 details examples of additive printing tools used to fabricate electrodes for electrochemical sensor applications. To date, many publications of 3-D printed electrochemical sensor platforms have focused on printing carbon-based electrodes using fused deposition modelling (FDM). Like the Voltera V-one, FDM is an extrusion-based printer used to deposit thermoplastic inks. Differing from the Voltera V-one FDM dispenses material in a semi molten state through a heated nozzle. Once a layer is printed, the material solidifies on the printer bed via an air cooler attached to the extruder. Subsequently, the next layer is deposited by lowering the printer stage.[23] Similar to the Voltera V-one, FDM print resolution depends on the nozzle diameter. Nassar *et al.* reported an FDM print with a trace width of 230 µm when printing with a 250 µm nozzle.[24] In this work, using a 150 µm nozzle, the trace width of the gold polymer paste interconnects was 430 µm ± 70 µm (RSD = 15.6 %), approximately 200 µm larger than the Altrium design. However, since the minimum trace width for the Voltera V-one is claimed to be 200 µm, optimising parameters (e.g. curing time and temperature, ink composition) may be one approach to obtaining dimensions closer to that of the Altrium design (within the limits of the printer specification). Despite this, the WE diameter measurements were reproducible with an average diameter of 2.74 mm ± 0.07 mm. By contrast to extrusion based printing, the inkjet printer can achieve feature sizes of less than 50 µm.[25] The average coating thickness of the Voltera printed electrodes was 0.101 mm ± 0.013 mm while Inkjet can facilitate a coating thickness of less than 1 µm. In this work, we examined the potential for fabricating flexible electrodes from gold polymer paste inks using the Voltera-V one extrusion printer. Another printing tool creating interest is the Aerosol Jet Printer. This is a non-contact direct printing tool that uses a pneumatic or ultrasonic atomizer to generate an aerosol from liquid inks. One of the major opportunities with Aerosol jet printing is the ability to print electrodes directly onto 3-D surfaces, while Inkjet, FDM and the Voltera V-one are limited to printing on flat surfaces. Like inkjet and extrusion printing, aerosol jet printers offer mask-less fabrication and less material waste during printing. While aerosol jet printers offer higher resolution prints with feature sizes as low as 10 µm they are more costly than the Voltera V-one. Whilst

we are seeing the use of AJPs in research, the number of reports of electrochemical biosensors constructed from aerosol jet printed electrodes are limited.‡‡

In this work, we examined the electrochemical behaviour between dispense printed electrodes after conducting an electrochemical clean in 0.5 M H_2SO_4. Unmodified electrode performance varied from sensor to sensor in a common redox probe (5 mM $[Fe(CN)_6]^{4-/3-}$) as seen in Figure 4.11. The flexible electrodes remained attached to the polyimide substrates after repeated bending, in addition they continued to operate during electrochemical characterisation measurements. Similar behaviour was observed between CVs carried out on a single sensor in a planar/flat configuration and in a fixed bent configuration as was shown in Figure 4.22 B. These results indicate good electrode stability. Electrodes modified with Pt/CS/BSA and LOx showed good linear behaviour within a lactate concentration range of 0.2 mM to 1 mM lactate. Despite this, the reproducibility between the sensors was poor. This is likely a result of inhomogeneous exposure of gold from electrode to electrode. Starting with a reproducible electrode surface is a key factor to building a successful biosensor. Alternative cleaning or activation steps have been reported as a means of improving the electrode performance by removal of the thermoplastic material at the electrode surface.[26] Richter *et al.* for example have reported an improvement in current response and peak separation after chemical and electro-chemical activation with 0.5 M NaOH.[9] Another approach reported by Pereira *et al.* involved the use of O_2 plasma to activate the 3D-printed carbon-black-polylactic acid electrode. This activation step resulted in an increase in both electroactive area and sensor sensitivity.[27] Immersion in dimethylformamide (DMF) for 10 minutes has also been shown to enhance the electrochemical response of 3D printed graphene/polylactic acid electrodes. DMF dissolves the upper polymer layer exposing graphene flakes in the composite matrix.[28] Additional reports on electrochemical activation steps can be found in a review article by Cardoso *et al.*[7]

‡‡ A web of science search result for aerosol jet printed electrochemical biosensors yielded 7 results.

Table 4.2: *Examples of additive printer tools used to fabricate electrodes for electrochemical sensor applications.*

Printing technique	Printer tool	Material printed	Electrochemical technique	WE dimensions	Target	Ref
Extrusion	Voltera V-one	(Ag) conductive ink	CV	-	Urea	[19]
Extrusion	FDM TRIBLAB printer	carbon-loaded polylactic acid (PLA)	LSV & Chronoamperometry	<8 mm	Caffeine & Glucose	[29]
Extrusion	3D pen	Carbon back-PLA	SWV and DPV	-	Dopamine	[27]
Ink-jet	Fujifilm DIMATIX Materials Printer Dmp-283	Enzyme layer (Ink 1), GLA layer (Ink 2) and nafion layer (Ink 3)	Chronoamperometry	N/A	Phosphate	[30]
Aerosol Jet printing	AJ 300, Optomec Inc.	Nanoparticle Ag ink and Loctite 3105	Chronoamperometry	30 µM	H_2O_2 and Glucose	[31]
Extrusion	Voltera V-one	Gold polymer paste ink	Chronoamperometry	2.5 mm	Lactate	This work

4.5 Conclusions

In summary, this chapter has investigated a 3-D extrusion printing tool for the fabrication of electrodes for electrochemical analysis applications. The Voltera V-one system was used to construct flexible conductive electrodes using gold-thermoplastic inks. The geometrical reproducibility of the printed electrodes was assessed using 3-D microscopy and SEM. Dimensional measurements determined an average WE area of 0.06 cm^2 ± 0.003 cm^2 (RSD 5%). Cross sectional SEM analysis determined an electrode height 0.1 mm ± 0.013 mm (RSD=13.1%).

Potentiodynamic cycling in 0.5 M H_2SO_4 revealed variable behaviour between electrodes during acid cleans. Electrochemical characterisation in two common redox probes $[Ru(NH_3)_6]^{3+}$ and $[Fe(CN)_6]^{4-/3-}$ demonstrated fast electron transfer behaviour, CVs in $[Ru(NH_3)_6]^{3+}$ demonstrated good reproducibility with an average Ipa of 0.44 ± 0.027 µA and an average peak separation of 92 eV ± 4.2eV at 100 mV/s. On the other hand, large variability was observed between CVs obtained with n = 3 electrodes in $[Fe(CN)_6]^{4-/3-}$,the average Ipa current was 0.72 ± 0.19 µA and the average ΔEp was 163 mV ± 38 mV. This probe is more useful if you want to measure analytes that undergo slow (inner-sphere) electron transfer.Inconsistencies during standard electrochemical characterisation procedures indicated poor reproducibility between electrodes fabricated using the same printing and curing steps.

A commercial screen-printed electrode was assessed for comparison to a dispense printed electrode in 5 mM $[Fe(CN)_6]^{4-/3-}$. Fully reversible behaviour was revealed for the commercial dropsens electrode in comparison to dispense printed electrodes, which demonstrated quasi-reversible behaviour. Higher anodic and cathodic peak currents were observed at commercial SPEs. The reduced peak currents are likely a result of the smaller surface area of metallic gold structures present on the DPE.

Owing to variations observed during routine electrochemical characterisation, further analysis was carried out to better understand the surface morphology and composition of the DPEs. SEM revealed that the electrode surface consisted of portions of Au particles above the thermoplastic material and other Au particles appeared entrapped underneath it. EDX mapping recognised variations in Au surface coverage at different locations of the electrode. XPS results confirmed 73.0 at.% of Carbon was present at the electrode surface and just 3.3 at.% of Au was present. These results support the SEM images,

indicating that a large portion of the outer electrode surface (upper 10 nm) was the thermoplastic material.

The variability observed between electrodes is likely attributed to variations in the quantity of gold ink dispensed between prints and to differences in 'exposed metallic regions' between the electrodes. The volume of dispensed ink during each print could not be controlled using this printer; furthermore, the calibration step did not enable precision between prints. As a low cost PCB printer, precision will not match that of high cost, more complex equipment such as the LPKF multi-layer PCB manufacturing platform or the Optomec aerosol jet printer. Despite this, further work could be conducted to better understand the optimum dispense printer parameters while taking ink properties into consideration. Studying varied ink formulations, curing times and temperatures in addition to chemical and/or electrochemical cleaning procedures could help to identify conditions that may improve both reproducibility between prints and the electrode performance. Despite challenges observed, a number of clear achievements were met. The thermoplastic resin adhered well to the polyimide (as material remained attached during bending measurements) and electrochemical characterisation in $[Fe(CN)_6]^{4-/3-}$ was demonstrated for both a planar and "flexed/bent" arrangement. Furthermore, a dispense printed electrode was modified to demonstrate lactate detection as a potential proof of concept sensor.

4.6 References

(1) Park, J.; Jeong, Y.; Kim, J.; Gu, J.; Wang, J.; Park, I. Biopsy Needle Integrated with Multi-Modal Physical/Chemical Sensor Array. *Biosensors and Bioelectronics* **2020**, *148*, 111822. https://doi.org/10.1016/j.bios.2019.111822.

(2) Liu, G.; He, Y.; Liu, P.; Chen, Z.; Chen, X.; Wan, L.; Li, Y.; Lu, J. Development of Bioimplants with 2D, 3D, and 4D Additive Manufacturing Materials. *Engineering* **2020**, *6* (11), 1232–1243. https://doi.org/10.1016/j.eng.2020.04.015.

(3) Blakey-Milner, B.; Gradl, P.; Snedden, G.; Brooks, M.; Pitot, J.; Lopez, E.; Leary, M.; Berto, F.; du Plessis, A. Metal Additive Manufacturing in Aerospace: A Review. *Materials & Design* **2021**, *209*, 110008. https://doi.org/10.1016/j.matdes.2021.110008.

(4) Goh, G. L.; Zhang, H.; Chong, T. H.; Yeong, W. Y. 3D Printing of Multilayered and Multimaterial Electronics: A Review. *Adv. Electron. Mater.* **2021**, *7* (10), 2100445. https://doi.org/10.1002/aelm.202100445.

(5) Ruan, X.; Wang, Y.; Cheng, N.; Niu, X.; Chang, Y.; Li, L.; Du, D.; Lin, Y. Emerging Applications of Additive Manufacturing in Biosensors and Bioanalytical Devices. *Adv. Mater. Technol.* **2020**, *5* (7), 2000171. https://doi.org/10.1002/admt.202000171.

(6) O'Neil, G. D. Toward Single-Step Production of Functional Electrochemical Devices Using 3D Printing: Progress, Challenges, and Opportunities. *Current*

Opinion in Electrochemistry **2020**, *20*, 60–65. https://doi.org/10.1016/j.coelec.2020.02.023.

(7) Cardoso, R. M.; Kalinke, C.; Rocha, R. G.; dos Santos, P. L.; Rocha, D. P.; Oliveira, P. R.; Janegitz, B. C.; Bonacin, J. A.; Richter, E. M.; Munoz, R. A. A. Additive-Manufactured (3D-Printed) Electrochemical Sensors: A Critical Review. *Analytica Chimica Acta* **2020**, *1118*, 73–91. https://doi.org/10.1016/j.aca.2020.03.028.

(8) Silva, A. L.; Salvador, G. M. da S.; Castro, S. V. F.; Carvalho, N. M. F.; Munoz, R. A. A. A 3D Printer Guide for the Development and Application of Electrochemical Cells and Devices. *Front. Chem.* **2021**, *9*, 684256. https://doi.org/10.3389/fchem.2021.684256.

(9) Richter, E. M.; Rocha, D. P.; Cardoso, R. M.; Keefe, E. M.; Foster, C. W.; Munoz, R. A. A.; Banks, C. E. Complete Additively Manufactured (3D-Printed) Electrochemical Sensing Platform. *Anal. Chem.* **2019**, *91* (20), 12844–12851. https://doi.org/10.1021/acs.analchem.9b02573.

(10) Hassan, K.; Tung, T. T.; Stanley, N.; Yap, P. L.; Farivar, F.; Rastin, H.; Nine, M. J.; Losic, D. Graphene Ink for 3D Extrusion Micro Printing of Chemo-Resistive Sensing Devices for Volatile Organic Compound Detection. *Nanoscale* **2021**, *13* (10), 5356–5368. https://doi.org/10.1039/D1NR00150G.

(11) Crapnell, R. D.; Bernalte, E.; Ferrari, A. G.-M.; Whittingham, M. J.; Williams, R. J.; Hurst, N. J.; Banks, C. E. All-in-One Single-Print Additively Manufactured Electroanalytical Sensing Platforms. *ACS Meas. Au* **2021**, acsmeasuresciau.1c00046. https://doi.org/10.1021/acsmeasuresciau.1c00046.

(12) Foster, C. W.; Elbardisy, H. M.; Down, M. P.; Keefe, E. M.; Smith, G. C.; Banks, C. E. Additively Manufactured Graphitic Electrochemical Sensing Platforms. *Chemical Engineering Journal* **2020**, *381*, 122343. https://doi.org/10.1016/j.cej.2019.122343.

(13) Hamzah, H. H.; Shafiee, S. A.; Abdalla, A.; Patel, B. A. 3D Printable Conductive Materials for the Fabrication of Electrochemical Sensors: A Mini Review. *Electrochemistry Communications* **2018**, *96*, 27–31. https://doi.org/10.1016/j.elecom.2018.09.006.

(14) Jalouli, A.; Khuje, S.; Sheng, A.; Islam, A.; Di Luigi, M.; Petit, D.; Li, Z.; Zhuang, C.-G.; Kester, L.; Armstrong, J.; Yu, J.; Ren, S. Flexible Copper–Graphene Nanoplates on Ceramic Supports for Radiofrequency Electronics with Electromagnetic Interference Shielding and Thermal Management Capacity. *ACS Appl. Nano Mater.* **2021**, *4* (11), 11841–11848. https://doi.org/10.1021/acsanm.1c02415.

(15) Seol, M.-L.; Nam, I.; Ribeiro, E. L.; Segel, B.; Lee, D.; Palma, T.; Wu, H.; Mukherjee, D.; Khomami, B.; Hill, C.; Han, J.-W.; Meyyappan, M. All-Printed In-Plane Supercapacitors by Sequential Additive Manufacturing Process. *ACS Appl. Energy Mater.* **2020**, *3* (5), 4965–4973. https://doi.org/10.1021/acsaem.0c00510.

(16) Khuje, S.; Sheng, A.; Yu, J.; Ren, S. Flexible Copper Nanowire Electronics for Wireless Dynamic Pressure Sensing. *ACS Appl. Electron. Mater.* **2021**, acsaelm.1c00905. https://doi.org/10.1021/acsaelm.1c00905.

(17) Bao, C.; Kaur, M.; Kim, W. S. Toward a Highly Selective Artificial Saliva Sensor Using Printed Hybrid Field Effect Transistors. *Sensors and Actuators B: Chemical* **2019**, *285*, 186–192. https://doi.org/10.1016/j.snb.2019.01.062.

(18) Min, X.; Bao, C.; Kim, W. S. Additively Manufactured Digital Microfluidic Platforms for Ion-Selective Sensing. *ACS Sens.* **2019**, *4* (4), 918–923. https://doi.org/10.1021/acssensors.8b01689.

(19) Roy, D.; Singh, P.; Halder, S.; Chanda, N.; Mandal, S. 3-D Printed Electrode Integrated Sensing Chip and a PoC Device for Enzyme Free Electrochemical Detection of Blood Urea. *Bioelectrochemistry* **2021**, *142*, 107893. https://doi.org/10.1016/j.bioelechem.2021.107893.

(20) Scanlon, M. D.; Salaj-Kosla, U.; Belochapkine, S.; MacAodha, D.; Leech, D.; Ding, Y.; Magner, E. Characterization of Nanoporous Gold Electrodes for Bioelectrochemical Applications. *Langmuir* **2012**, *28* (4), 2251–2261. https://doi.org/10.1021/la202945s.

(21) Burke, L. D.; Nugent, P. F. The Electrochemistry of Gold: I the Redox Behaviour of the Metal in Aqueous Media. *Gold Bull* **1997**, *30* (2), 43–53. https://doi.org/10.1007/BF03214756.

(22) Dumitrescu, I.; Unwin, P. R.; Macpherson, J. V. Electrochemistry at Carbon Nanotubes: Perspective and Issues. *Chem. Commun.* **2009**, No. 45, 6886. https://doi.org/10.1039/b909734a.

(23) Browne, M. P.; Novotný, F.; Sofer, Z.; Pumera, M. 3D Printed Graphene Electrodes' Electrochemical Activation. *ACS Appl. Mater. Interfaces* **2018**, *10* (46), 40294–40301. https://doi.org/10.1021/acsami.8b14701.

(24) Nassar, H.; Dahiya, R. Fused Deposition Modeling-Based 3D-Printed Electrical Interconnects and Circuits. *Advanced Intelligent Systems* **2021**, *3* (12), 2100102. https://doi.org/10.1002/aisy.202100102.

(25) Seifert, T.; Sowade, E.; Roscher, F.; Wiemer, M.; Gessner, T.; Baumann, R. R. Additive Manufacturing Technologies Compared: Morphology of Deposits of Silver Ink Using Inkjet and Aerosol Jet Printing. *Ind. Eng. Chem. Res.* **2015**, *54* (2), 769–779. https://doi.org/10.1021/ie503636c.

(26) Pumera, M. Three-Dimensionally Printed Electrochemical Systems for Biomedical Analytical Applications. *Current Opinion in Electrochemistry* **2019**, *14*, 133–137. https://doi.org/10.1016/j.coelec.2019.02.001.

(27) Pereira, J. F. S.; Rocha, R. G.; Castro, S. V. F.; João, A. F.; Borges, P. H. S.; Rocha, D. P.; de Siervo, A.; Richter, E. M.; Nossol, E.; Gelamo, R. V.; Muñoz, R. A. A. Reactive Oxygen Plasma Treatment of 3D-Printed Carbon Electrodes towards High-Performance Electrochemical Sensors. *Sensors and Actuators B: Chemical* **2021**, *347*, 130651. https://doi.org/10.1016/j.snb.2021.130651.

(28) Manzanares Palenzuela, C. L.; Novotný, F.; Krupička, P.; Sofer, Z.; Pumera, M. 3D-Printed Graphene/Polylactic Acid Electrodes Promise High Sensitivity in Electroanalysis. *Anal. Chem.* **2018**, *90* (9), 5753–5757. https://doi.org/10.1021/acs.analchem.8b00083.

(29) Katseli, V.; Economou, A.; Kokkinos, C. Single-Step Fabrication of an Integrated 3D-Printed Device for Electrochemical Sensing Applications. *Electrochemistry Communications* **2019**, *103*, 100–103. https://doi.org/10.1016/j.elecom.2019.05.008.

(30) Bai, Y.; Guo, Q.; Xiao, J.; Zheng, M.; Zhang, D.; Yang, J. An Inkjet-Printed Smartphone-Supported Electrochemical Biosensor System for Reagentless Point-of-Care Analyte Detection. *Sensors and Actuators B: Chemical* **2021**, *346*, 130447. https://doi.org/10.1016/j.snb.2021.130447.

(31) Yang, H.; Rahman, M. T.; Du, D.; Panat, R.; Lin, Y. 3-D Printed Adjustable Microelectrode Arrays for Electrochemical Sensing and Biosensing. *Sensors and Actuators B: Chemical* **2016**, *230*, 600–606. https://doi.org/10.1016/j.snb.2016.02.113.

Chapter 5 Summary and Future perspectives

5.1 Summary

The work described within this thesis involved the characterisation and development of three separate platforms for electrochemical sensor applications. This section aims to provide a combined summary of each chapter in addition to proposing future directions for each body of work.

In chapter 2 the fabrication and characterisation of gold ultramicroband electrodes fabricated on silicon substrates was described. CVs obtained at the bare gold electrodes in 1 mM FcCOOH demonstrated steady state behaviour with the on-chip Pt RE and Au CE. The electrode was modified via two electrodeposition steps, firstly to coat the electrode with platinum black followed by the electropolymerization of glucose oxidase as a model enzyme within a mixture of an o-phenylenediamine and ß-cyclodextrin. Both modifications were carried out with the on-chip CE and RE requiring low volumes of solution during biosensor construction. The enzymatic-based ultramicroband biosensor demonstrated a linear response to glucose from 2.5–15 mM, using both linear sweep voltammetry and chronoamperometric measurements in buffer-based solutions. The biosensor performance was examined in 30 µl volumes of fetal bovine serum. Whilst a reduction in the sensor sensitivity was evident within 100% serum samples (compared to buffer media), the UME demonstrated linear glucose detection with increasing glucose additions, from approximately 5 mM to 17 mM, showing their potential for analysis in more complex media environments. Although the linear dynamic range does not fulfil the entire physiological range required for blood glucose measurements, there is clear potential for analysis in bio-fluids and diluted bio-fluids.

Chapter 3 focused on the use of laser scribed graphite electrodes for enzymatic lactate detection on a flexible platform. LSG fabrication is a cost effective means of producing flexible electrodes in a timely manner. Flexible electrodes are valuable to the future of electrochemical sensing owing to their potential to be integrated with arbitrary surfaces such as wearable platforms and probes. Three-LSG electrodes were fabricated onto polyimide substrates using a 450 nm laser. Functionalisation of the LSG WE was carried out via an electrodeposition and two casting steps. The resulting biosensor demonstrated chronoamperometric lactate detection within a linear range of 0.2 mM to 3 mM, with a limit of detection of 0.11 mM. The biosensor revealed a sensitivity of 35.8 µA/mM/cm^2

and excellent reproducibility (RSD <5 %, n = 5), comparable to that of commercial biosensors and exceeding that of recently reported flexible lactate sensors. The working stability was demonstrated by obtaining 10 successive measurements over n = 3 sensors, which had RSD values of 2.9 % 4.9 % and 5.1 %. Both LSG and Ag/AgCl paste modified LSG demonstrated functionality similar to an external Ag/AgCl RE for chronoamperometric lactate measurements, furthermore, substrates bent at a fixed curvature K = 0.14 mm^{-1} displayed similar functionality to measurements carried out with a flat sensor. We propose that this platform could be advanced for applications requiring bent or flexible packaging of biosensors for example application onto a curved section of a mouthguard. This flexible sensor has also demonstrated potential as a low-cost diagnostic platform for saliva or diluted serum analysis. Sterile human serum spiked with lactate at concentrations of 0.5 mM and 1 mM was measured and determined to be 0.47 mM and 1.01 mM respectively. Similarly spiked lactate concentrations of 0.5 mM and 1 mM in artificial saliva were determined to be 0.63 mM and 1.03 mM.

Chapter 4 explored the potential for utilising a low-cost PCB printer to fabricate flexible electrodes for electrochemical sensor applications. Electrodes were dispense printed from a thermoplastic gold resin for the WE and CE and a thermoplastic platinum mixture for the RE. Dimensional measurements revealed an average WE area of 0.06 cm^2 ± 0.003 cm^2 (RSD = 5 %) and an electrode height of 0.1 mm ± 0.013 mm (RSD = 13.1 %). Electrochemical characterisation of the dispense printed electrodes revealed inconsistencies in electrochemical performance between sensors fabricated under the same set of conditions. SEM and XPS data revealed that the electrode surface was partially covered with the thermoplastic resin. Poor reproducibility is likely attributed to variations in the quantity of polymer covering the gold surface, in addition to the heterogeneity of the gold particles dispersed in the ink. The flexible gold electrodes were modified with platinum, chitosan, BSA and lactate oxidase for the chronoamperometric measurement of lactate. Each calibration curve showed a linear region in the range of 0.2 mM to 1 mM, however, poor reproducibility was observed between calibrations.

5.2 Future Perspectives

5.2.1 Silicon Platform

To determine the viability of the ultramicroband glucose sensor, future experiments would be needed to assess the long-term storage stability in addition to conducting measurements over longer periods of time. Preliminary storage results revealed that after two days of storage in PBS, the sensor recovery decreased to approximately 87 % for three out of six concentrations measured. A sensor applied to measure one concentration, when re-measured after four days of storage at 4°C was found to have a sensor recovery of 93 %. SEM imaging could be used to determine the effects of repeated electrochemical measurements on electrode stability. The resulting calibration obtained from chronoamperometric measurements carried out in foetal bovine serum showed a decrease in sensor sensitivity. To realise the use of this single UME on-chip, glucose sensor assessment of diluted real samples could be a next step towards validating the sensor performance. The end goal for this platform is a multi-parametric sensing device capable of measuring biomarker levels in bio-fluids.

As detailed in chapter 2, the silicon chip platform consists of 6 WEs and the on-chip CE and RE. One challenge faced by this device during experimentation was the ability to functionalise each electrode on the one device in the same manner. While electrodepositing the o-PD/β-cyclodextrin/GOx layer at WE 1 for 20 minutes, WE 2 to WE 6, the CE and RE remain in contact with the solution. Adsorption of species from solutions on to electrodes during experimental procedures can lead to partial passivation. Micro-fluidic developments would help to facilitate functionalisation of electrodes without potential adsorption or fouling of species from solutions onto the remaining WEs. Furthermore, incorporating microfluidics with six separate channels could allow for electrochemical analysis at each WE. The Pt pseudo RE should be characterised within the matrix of interest i.e. PBS and Foetal bovine serum.

5.2.2 LSG platform

Future work on the LSG platform should focus on improving the robustness of LSG electrodes and investigating their biocompatibility. Laser scribed graphite can be easily removed from the substrate upon mechanical scraping, which is not desirable for either

wearable or *in-vivo* applications. This challenge could be addressed by coating the electrodes with a protective layer. Comparative studies on the application of membranes such as polyurethane, PVC, PEDOT, hydrogels etc. could be helpful towards identifying suitable materials to improve the robustness of LSG sensors.

Since LSG is of growing interest for wearable sensors, assessing biocompatibility, skin irritation and toxicity is essential. Preliminary studies, conducted by collaborators, using normal human dermal fibroblast cells growing in contact with the LSG electrodes showed good cell viability after 72 hours. Additional biocompatibility studies should be carried out to identify potential adverse effects of LSG when in contact with biological tissues.

Advanced instrumentation is another interesting avenue to consider, specifically for wearable platforms since they require compact electronics. Whilst the majority of lab based research is conducted with a bench top potentiostat, a faraday cage and a computer, handheld devices are being built and configured to conduct specific electrochemical techniques. Figure 5.1 shows an image of the LSG sensor connected to a compact potentiostat built in-house in Tyndall which can conduct both CV and Chronoamperometry. Assessing the electrochemical performance of LSG sensors using compact potentiostats is an essential next step for the development of these devices as wearables or portable sensors.

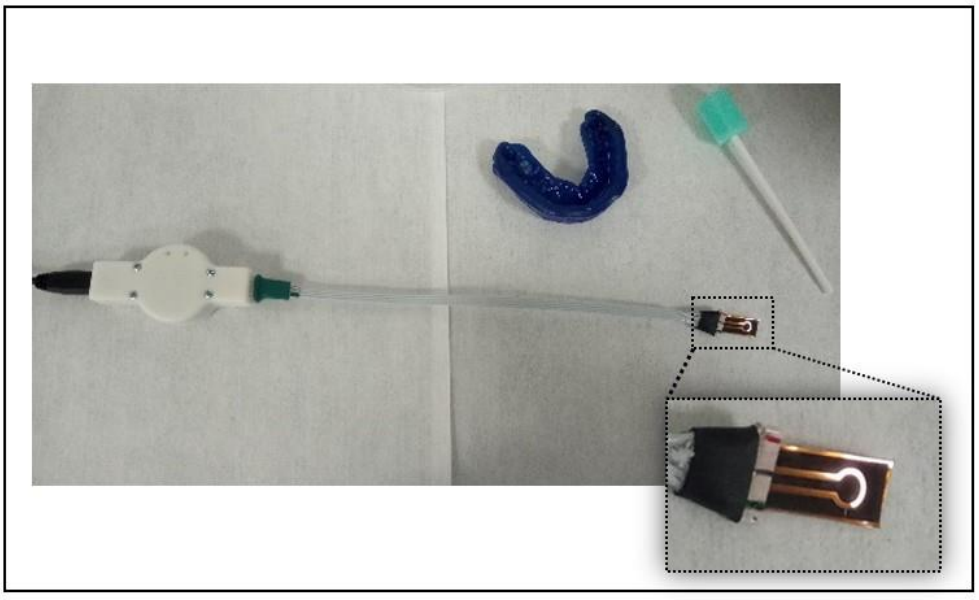

Figure 5.1: *Picture of a miniaturised potentiostat connected to the LSG electrodes.*

Specific to the study outlined in chapter 3, sensor selectivity was challenged when assessing the use of the LSG-Pt-CS-LOx biosensor in buffer based media spiked with

interfering species. Including an additional membrane layer such as PVC could be examined. Whilst membranes have been shown to reduce sensor sensitivity, additional coating layers can offer a mechanism to prevent oxidation of electroactive species.

Finally, the fabrication of the reference electrode was not ideal. Indeed the Ag/AgCl paste was applied manually to the LSG RE electrode with a paint brush which is not a scalable fabrication method. Alternative fabrication methods, such as screen printing or dispense printing the Ag/AgCl RE could be explored. Finally the LSG quasi-RE should be characterised within each matric of interest i.e. PBS, Saliva and Human male serum.

5.2.3 Dispense printed electrodes

PCB printing offers a cost effective method of fabricating electrodes at the lab scale, however, since the Voltera V-one software parameters are limited, a number of alternative approaches could be assessed to improve the reproducibility between prints. Curing temperature, curing time and the application of an activation clean using NaOH and/or DMF are some examples of potential strategies to investigate with the commercial gold polymer paste inks. The dispense printed pseudo-RE requires further testing to assess its stability. Printing Ag/AgCl in place of Pt is another potential approach to consider. Fabrication of varied electrode dimensions, dual electrodes and printing onto alternative substrates are also potential avenues to explore. **Figure 5.2** A shows the electrode design that was used in chapter 4 (number 1), examples of alternative designs are also shown (number 2, 3 and 4). Number 2 is a dual electrode design, number 3 is a WE with a diameter of 1000 microns and number 4 is a WE with a diameter of 500 microns. Figure 5.2 B shows the design of electrode number 1, but printed on PET instead of polyimide. From a broader perspective, with improvements to the base electrode layers, the application of flexible electrodes onto 3-D devices such as a probe to assess electrochemical performance would be an interesting next step. Again the quasi-reference electrode should be characterised in each matrix of interest.

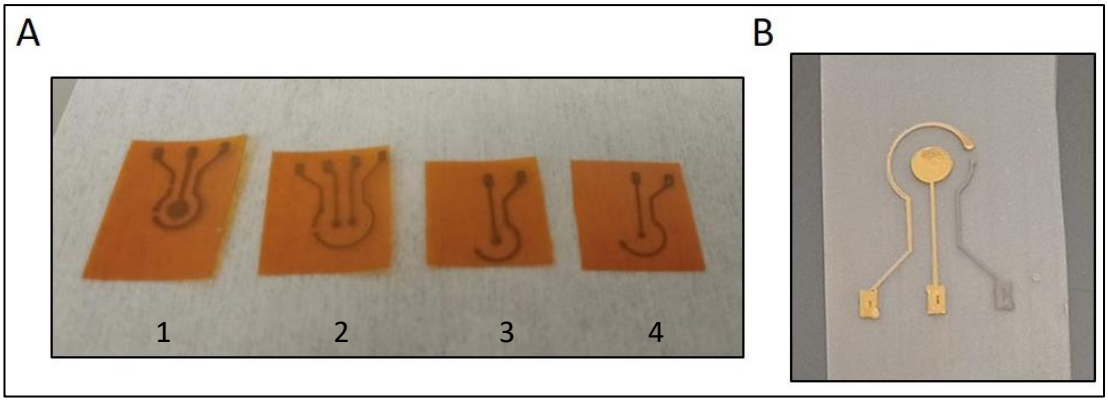

Figure 5.2: *(A) Pictures of test prints, from left to right: a WE diameter 2500 µm, a dual WE configuration, a WE diameter 1000 µm and a WE diameter of 500 µm and (B) a test print of gold polymer paste ink as a WE and CE and Pt polymer paste ink as the pseudo-RE on PET material.*

Appendices

A.1: Peer reviewed publications

1. **Madden, J.**; Vaughan, E.; Thompson, M.; O' Riordan, A.; Galvin, P.; Iacopino, D.; and Rodrigues Teixeira, S.; "Electrochemical sensor for enzymatic lactate detection based on laser-scribed graphitic carbon modified with platinum, chitosan and lactate oxidase", *Talanta*, **2022**, 246, 123492. https://doi.org/10.1016/j.talanta.2022.123492.
2. **Madden, J.**; Barrett, C.; Laffir, F.R.;Thompson, M.; Galvin, P and O' Riordan, A.; "On-Chip Glucose Detection Based on Glucose Oxidase Immobilized on a Platinum-Modified, Gold Microband Electrode", *Biosensors*, **2021**, 11 (8), 249. https://doi.org/10.3390/bios11080249.
3. **Madden, J.**; Thompson, M.; O' Mahony, C.; O' Riordan, A.; and Galvin, P, "Biosensing in dermal interstitial fluid using microneedle based electrochemical devices", *Sensing and Bio-sensing Research*, **2020,** 29, 100348. https://doi.org/10.1016/j.sbsr.2020.100348.

A.2 Publication in preparation

1. **Madden, J**.; Teixeira, S. and Galvin, P. "Fabrication and characterisation of electrodes using a low cost additive PCB printer tool for electrochemical sensing applications", **2022,** In Preparation.

A.2: Presentations, Conferences and Workshops

1. Madden J. (2021) "Development of electrochemical biosensors on macro and microelectrodes towards medical/diagnostic applications", To research and innovation team in West Pharma (9-Nov-18) – Oral presentation

2. Madden, J. (2020) 'Biosensing in Dermal Interstitial Fluid using Microneedle based Electrochemical devices, To research and innovation team in West Pharma - Oral presentation
3. Madden et. al (2019) 'Modification of ultra-microelectrodes on chip for enzymatic glucose sensing, Royal society of chemistry analytical research forum, London – Poster Presentation
4. Madden, J. (2019) "Modifications to ultramicroelectrdoes for glucose detection", Student satellite ISE symposium, University of Limerick – Oral Presentation
5. Madden et. al (2018) 'Electrochemical sensing on single microband electrodes towards near-patient diagnostic applications', IEEE NANO, Cork – Poster Presentation
6. Madden et. al (2017)**:** "Microneedles for Glucose Sensing", Skin Wearables, Dublin – Poster presentation
7. Madden J. (2016): "Continuous Microneedle-Based Glucose Sensing", Augmented Human Behaviour, Dublin – Poster Presentation

A.3: Demonstrations, Public engagement & Training

1. Training and mentoring an FYP student for 6 months
2. Demonstrations to Transition year and 1st year Engineering UCC students
3. Various Demonstrations @ public engagement events
    - Carnival of Science 2019 – Fitzgeralds Park, Cork
    - Science Week 2018 – Neptune Stadium, Cork
    - Inspiring women in STEM (IWISH) 2018 – City Hall, Cork
    - Tyndall Culture night 2017 – Tyndall National Institute, Cork